YANGNIAN WU

SYNTHESIS AND ANALYSIS OF REACTIONLESS SPATIAL PARALLEL MECHANISMS

Thèse

présentée

à la Faculté des études supérieures

de l'Université Laval

pour l'obtention

du grade de Philosophiae Doctor (Ph.D.)

Département de génie mécanique

FACULTÉ DES SCIENCES ET DE GÉNIE

UNIVERSITÉ LAVAL

QUÉBEC

APRIL 2003

Abstract

A mechanism is said to be reactionless if, for any motion of the mechanism, there is no reaction force and moment at its base or supporting structure at all times. A systematic study of the synthesis and kinematic analysis of reactionless spatial multi-degree-of-freedom parallel mechanisms is performed in this thesis.

Firstly, a new kind of 3-DOF parallel mechanism referred to as a parallelepiped mechanism is proposed and a practical design is implemented. The 3-DOF parallelepiped mechanisms are dynamically balanced using counterweights and counter-rotations and are used as legs to synthesize multi-degree-of-freedom parallel mechanisms. Reactionless spatial 6-DOF parallel mechanisms are obtained by dynamically balancing each detached leg mechanism independently based on an algorithm using point masses to replace a moving platform. The dynamic simulation software ADAMS was used to simulate the motion of the mechanisms and to verify that the mechanisms are reactionless at all times and for arbitrary trajectories.

Next, the synthesis of novel reactionless spatial 3-DOF and 6-DOF mechanisms without separate counter-rotations, using four-bar linkages is addressed in this thesis. Based on the conditions of dynamic balancing of a single planar four-bar linkage moving in the plane, the spatial problem is shown to be equivalent to ensuring that the inertia tensor of reactionless four-bar linkages remains constant when the planar mechanism(s) is(are) moving. The reactionless conditions for planar four-bar linkages undergoing spatial motion are first given. A mechanism composed of a pair of connected reactionless four-bar linkages with constant inertia tensor is constructed. Then, a reactionless spatial 3-DOF mechanism is synthesized using four-bar linkages and further serves as a leg

to synthesize a reactionless 6-DOF parallel mechanism.

Finally, the kinematic analyses including the inverse and direct kinematics as well as the determination of singularity loci and workspace of both the 3-DOF leg mechanisms and the 6-DOF parallel mechanisms proposed in this thesis are solved. The Jacobian matrices of the mechanisms associated with different actuation schemes are derived. Geometrical algorithms, discretization methods or analytic methods are proposed for the determination of the workspace and singularity analysis for the mechanisms. Finally, the graphical representations that show the relationship between the singularity loci and the constant-orientation workspace of the proposed mechanisms are given.

Reactionless spatial multi-degree-of-freedom mechanisms have great potential applications such as space robots, telescope mirror mechanisms and some industrial high speed devices. All the results of kinematic analysis will be of great help during the design process and for the control of these mechanisms.

_____   _____

Yangnian Wu   Clément M. Gosselin

Résumé

Un mécanisme est dit équilibré dynamiquement si, pour n'importe quel mouvement dudit mécanisme, il n'y a aucune réaction en termes de forces et de moments sur la structure de support. Une étude systématique portant sur la synthèse et l'analyse cinématique de mécanismes parallèles spatiaux à plusieurs degrés de liberté (DDL) et équilibrés dynamiquement est réalisée dans cette thèse.

Premièrement, un nouveau type de mécanisme parallèle à trois DDL, désigné comme "parallélépipède mécanique", est proposé ainsi que sa réalisation pratique. Ce parallélépipède mécanique à trois DDL est équilibré dynamiquement en utilisant des contrepoids et contre-rotations, puis utilisé comme patte pour synthétiser des mécanismes parallèles à degrés de liberté multiples. En effet, des mécanismes parallèles spatiaux à six DDL équilibrés dynamiquement peuvent être obtenus en combinant des pattes indépendamment équilibrées grâce à un algorithme qui remplace la plate-forme mobile par des masses ponctuelles équivalentes. Des simulations dynamiques utilisant le logiciel ADAMS ont été réalisées pour vérifier l'équilibrage dynamique des mécanismes en tout temps et quelle que soit la trajectoire de la plate-forme.

Ensuite, la synthèse de nouveaux mécanismes spatiaux équilibrés dynamiquement à trois et six DDL, sans contre-rotations séparées, mais basée sur des mécanismes à quatre barres, est présentée dans cette thèse. Basée sur les conditions d'équilibrage dynamique d'un mécanisme à quatre barres se déplaçant dans le plan, l'extension au cas spatial est montrée équivalente à assurer que la matrice d'inertie de ces mécanismes à quatre barres reste constante lors du mouvement. Conséquemment, les conditions d'équilibrage dynamique des mécanismes à quatre barres lors de mouvements spatiaux

sont présentées en premier lieu. Un mécanisme composé d'une paire de mécanismes à quatre barres à matrice d'inertie constante est proposé. Ensuite, un mécanisme spatial à trois DDL est synthétisé, basé sur les mécanismes à quatre barres précédemment trouvés, ce mécanisme est utilisé comme patte pour un mécanisme parallèle à six DDL.

Finalement, l'analyse cinématique des mécanismes à trois et six DDL discutés précédemment, incluant la résolution des problèmes géométriques directs et inverses ainsi que l'étude des singularités, est présentée. Les matrices jacobiennes associées aux différentes possibilités d'actionnement des mécanismes sont aussi présentées. Les algorithmes géométriques, les méthodes analytiques et de discrétisation, sont proposés afin de déterminer l'espace de travail ainsi que les singularités des mécanismes correspondants. Enfin, les représentations graphiques établissant la relation entre lieux de singularité et espace de travail à orientation constante sont présentées.

Les mécanismes spatiaux à degrés de liberté multiples équilibrés dynamiquement ont un grand potentiel d'application dans des domaines variés, tels que la robotique spatiale, les mécanismes d'orientation de miroirs de télescopes ainsi que certains systèmes industriels à grandes vitesses. Tous les résultats de l'analyse cinématique seront d'un grand secours lors de la conception mais aussi pour le contrôle de ces mécanismes.

<div style="display:flex; justify-content:space-between;">

_____

Yangnian Wu

_____

Clément M. Gosselin

</div>

iv

Foreword

I am very much obliged to my supervisor Prof. Clément Gosselin for his invaluable supervision, tremendous support, continuous encouragements and critical review of the manuscript. Throughout the thesis research, I've been inspired by his rich ideas and have benefited so much from his comprehensive expertise in robotics and mechanisms.

I am also grateful to Prof. Just Herder of Delft University of Technology for his valubale suggestions and detailed remarks in the prereview and the modification of the final version of my thesis. Furthermore, I thank Prof. Meyer Nahon of McGill University and Prof. Benoît Levesque for the examination of my thesis and for their precious comments.

Special thanks are also due to all the members of the Robotics Laboratory for their help and friendship as well as for their contributions to creating the most pleasing working atmosphere ever enjoyed and never forgotten by all the people who stayed there for a while. In particular, I would like to thank Boris Mayer St-Onge for his help in using the laboratory facilities and Thierry Laliberté, Simon Foucault, Pierre-Luc Richard, Mathieu Myrand for the CAD models of the mechanisms and Lionel Birglen for the French translation and Dimiter Zlatanov, Xianwen Kong, Ilian Bonev and Bruno Monsarrat for helpful discussions.

I am greatly indebted to my wife, Ling Cao, for her understanding and constant support without any complaint since we got married. Thanks also go to my daughter, Qianqian Wu, with whom, I could not afford much time in the evenings.

Contents

List of Tables

List of Figures

Chapter 1

Introduction

1.1 Motivation

Parallel mechanisms are defined as architectures in which the moving payload is connected to the fixed base by multiple kinematic chains. Each chain can be considered as one mechanism and is a system with several links, joints and a base (see for instance Figure 1.1).

As compared with serial mechanisms, parallel mechanisms are characterized by low moving inertia, high stiffness, high dexterity, compact size and high power to weight ratio and hence they can be controlled with a high bandwidth. Therefore, they are especially suitable for applications requiring large load capacity or high speed and accuracy. Parallel mechanisms have received considerable attention by both researchers

Figure 1.1: Flight simulator (courtesy of CAE Electronics).

and manufacturers over the past thirty years. The first device based on a parallel mechanism designed by Gwinnett was filed for a patent in 1928. Gough (1962) was the first to invent and build the popular octahedral hexapod as a tire testing machine (Bonev, 2003). This original architecture was put into practice in flight simulators (Figure 1.1) in the 1970's and still remains the most popular and best studied parallel mechanism. Since the 1980's, more and more researchers have focused on parallel mechanisms or manipulators. So far, parallel mechanisms are used in a number of applications in machine tools, medical robots, alignment devices (Figure 1.3(b)), haptic devices, coordinate measuring machines and so on (Kong, 2002).

Parallel mechanisms are excellent candidates for advanced robotic applications. However, similarly to other robotic devices, they exert forces and moments on their base (frame) while moving, causing vibration and associated noise, wear, fatigue as well as disturbances in the supporting structure of the mechanism (Ricard and Gosselin, 2000). These reaction forces and moments, the so-called shaking forces and shaking moments, are undesirable in many applications.

In space robotics (Figure 1.2), manipulators are mounted on free-floating bodies such as a spacecraft, a space vehicle, a satellite, or a space-station. Hence, any motion of the manipulator has some dynamic effect on the free-floating base, by virtue of the principle of conservation of momentum and angular momentum, and the position and orientation of the spacecraft will be disturbed (Dubowsky, 1991; Papadopoulos, 1991). Very often this is not acceptable because, for instance, the orientation of the solar
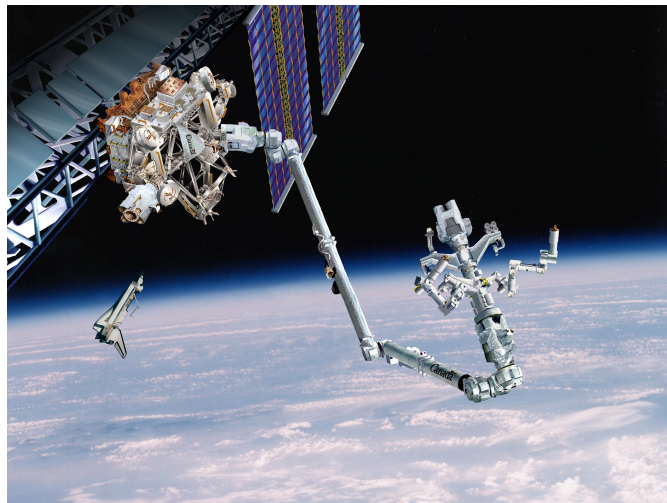
Figure 1.2: Space robots (courtesy of MD Robotics).

panels or of the communications antennae should not change. To preserve the proper position and orientation of the spacecraft, stabilizing systems like control rockets or inertial reaction wheels are generally used. However, the operations of these systems consume energy in space (Legnani et al., 1999).

In certain telescopes (Figure 1.3), a secondary mirror is used both for correcting the tracking error of the telescope and for chopping for infrared observation. The tracking error sources of the telescope are the control errors of the telescope control system, the deflection of the telescope structure induced by gravity and wind and the atmospheric image motion. All these disturbances do not have a specified direction and vary continuously. Hence, the use of parallel mechanisms (Figure 1.3(b)) to move the secondary mirror of a telescope at high frequencies may excite the structure of telescope and make things worse.

Especially in micro and nano mechatronics (such as in microassembly machines), vibration amplitudes may readily reach the order of magnitude of the required positioning resolution. Also in larger-scale precision devices and in systems with delicate equilibrium, shaking forces and moments can rapidly become dominant (Herder, 2003).

In order to eliminate the undesired shaking forces and moments, reactionless mechanisms have been proposed or developed for some applications (see Section 1.2 for a literature overview). A mechanism is said to be *reactionless* or *dynamically balanced* or *completely balanced* if, for any motion of the mechanism, there is no reaction force

(a) Hubble space telescope
(courtesy of NASA).

(b) Active secondary mirror
(courtesy of IPA).

Figure 1.3: Telescope mechanisms.

and moment at its base or supporting structure at all times. This property is crucial for space robotics to preserve the momentum of the moving base and for telescopes to avoid exciting the structure of the telescope while moving the secondary mirror at high frequencies. In industrial applications involving high-speed motions, eliminating or reducing the reactions on the base of the robot would also significantly improve the general performance by reducing vibrations and thereby improving the accuracy. Therefore, the development of reactionless parallel mechanisms for these potential applications motivates our research. In this thesis, the synthesis and analysis of reactionless spatial multi-degree-of-freedom parallel mechanisms are studied systematically.

1.2 Methodology and Literature Review

1.2.1 Dynamic balancing

For a system with constant mass, the resultant of the external forces acting on the system equals the time rate of change of the linear momentum of the system, while the resultant of the external moments with respect to a fixed point O (or the center

of mass of the system) equals the time rate of change of the angular momentum about the same point (Meriam and Kraige, 1993), namely,

$$\Sigma \mathbf{F} = m\dot{\mathbf{v}} \tag{1.1}$$

$$\Sigma \mathbf{M} = \dot{\mathbf{h}} \tag{1.2}$$

where $\Sigma \mathbf{F}$ is the resulting external force, m is the total mass, $\mathbf{v}$ is the velocity of the center of mass of the system, $\Sigma \mathbf{M}$ is the resulting external moment about a fixed reference point O and $\mathbf{h}$ is the total angular momentum of the system about the same point.

The opposites of the terms on the righthand side of eqs. (1.1) and (1.2) are actually the so-called shaking force and shaking moment respectively due to the moving masses and inertia. Clearly, from eq. (1.1) and (1.2), if the linear momentum ($m\mathbf{v}$) and the total angular momentum ($\mathbf{h}$) of the system remain constant for any motion at all times the shaking force and shaking moment will vanish. Usually, the state of rest will be included in the possible motions of the mechanism, in which case both linear and angular momentum are zero. Therefore, in practical situations, the conditions for dynamic balance are that for all motions of the mechanism the center of mass of the system should remain stationary and the total angular momentum must be zero at all times. The strategy for eliminating the shaking force is referred to as *(shaking) force balancing* while the strategy for eliminating the shaking moment is referred to as *(shaking) moment balancing*. The combination of force and moment balancing is referred to as *dynamic balancing*.

Hence, two constraints have to be satisfied for a mechanism to be reactionless, namely, the center of mass of the mechanism should remain fixed (stationary) and the total angular momentum must remain constant (zero) with respect to a fixed point at all times for arbitrary trajectories of the end-effector (Ricard and Gosselin, 2000), i.e.,

$$\frac{d\mathbf{r}}{dt} = 0 \tag{1.3}$$

$$\frac{d\mathbf{h}_o}{dt} = 0 \tag{1.4}$$

where $\mathbf{r}$ is the position vector of the center of mass and $\mathbf{h}_o$ is the total angular momentum of the mechanism relative to a fixed point O. Equations (1.3) and (1.4) are necessary and sufficient conditions for a mechanism to be dynamically balanced, i.e., reactionless. More specifically, eq. (1.3) implies force balancing whereas eq. (1.4) implies

moment balancing. Apparently, dynamic balancing includes both force balancing and moment balancing. All the force balancing, moment balancing and dynamic balancing approaches in the literature are based on these fundamental equations.

Note that in the context of dynamic balancing, in general, no other external forces than gravity and no other moments than the actuator torques on the system are considered. Dynamic balancing is associated with inertia forces other than gravity. Hence, "no reaction force" in the definition of *reactionless* in the present thesis actually implies no reaction force other than gravity. Yet, the definition is the real case in space (zero gravity). Additionally, eqs. (1.1) and (1.2) are only applicable to a system with constant mass, hence, any change in platform (or end-effector) mass (e.g., picking up an object) will deteriorate the dynamic balance. This problem is beyond the scope of our work.

As compared with dynamically balanced mechanism, a mechanism is said to be *statically balanced* if every possible configuration of the mechanism is a static equilibrium configuration. Hence, no actuator forces or torques are required to maintain the mechanism in any configuration (Herder, 2003). Two static balancing methods, namely, using counterweights and using springs, are often used. Clearly, a mechanism with a stationary global center of mass (force balanced) has constant gravitational potential energy (statically balanced). Hence, force balancing implies static balancing, however, static balancing does not imply force balancing. Although using springs is a good solution to statically balance mechanisms without great increase of the mass of the system, there still exist reaction forces on the base, in other words, springs do not contribute to force balancing. Therefore, we cannot obtain reactionless mechanisms using springs. A large number of statically balanced or gravity compensated mechanisms, serial manipulators and multi-degree-of-freedom parallel manipulators have been developed or presented in the literature. Since static balancing is not the subject of this thesis, we do not review more about this issue here. The readers can refer to the theses of Herder (2001) and Wang (1998) as well as their long lists of references. Figure 1.4 shows the prototype of a statically balanced 6-DOF parallel manipulator using springs (Gosselin et al., 1999).

The balancing of mechanisms has been an important research topic for several decades (e.g., Berkof and Lowen, 1969; Lowen et al., 1983; Dresig et al., 1998; Arakelian and Smith, 1999; Kochev, 2000). Extensive studies on the balancing of planar linkages and some research works related to the complete balancing of spatial linkages with only

Figure 1.4: Statically balanced parallel manipulator (from Gosselin et al., 1999).

one degree of freedom have been presented in the literature.

In order to completely force balance mechanisms it must be possible to make the global center of mass of the mechanisms stationary. This is usually accomplished by the addition of counterweights or internal mass redistribution. Of course, adding a duplicate mechanism to the initial mechanism is a primary but sometimes efficient approach for this purpose. Several methods have been applied for the complete force balancing of mechanisms. Most of them originate from two methods, namely the *method of linearly independent vectors* and the *complex mass method*. The method of linearly independent vectors was proposed by Berkof and Lowen (1969) for four-bar and six-bar linkages, implying that the masses of arbitrarily shaped links can be redistributed in such a way that the total center of mass becomes stationary. Tepper and Lowen (1972) subsequently generalized this method and presented a theorem — *"Contour theorem"*, i. e., from each link there is a contour to the ground by way of revolutes only —to determine whether or not a linkage can be fully force balanced by the addition of counterweights or redistribution of link masses, as well as the minimum number of counterweights of the linkages. Using this method, Bagci (1982) presented the force balancing of planar 4-bar, 6-bar and 8-bar linkages with *force transmission irregularities* — with multiple sliding pairs — by adding appropriate balancing idler loops. Kaufman and Sandor (1971) extended the method of linearly independent vectors to the force balancing of spatial linkages. Later, Kochev (1987) applied this approach to both planar and spatial linkages and Yu (1987a, 1988) for spatial linkages. The method proposed by Walker and Oldham (1978, 1979) based on the concept of mass replacement and mass flow was

called the complex mass method by Lowen et al. (1983) and extended by Chen (1984) to balance spatial linkages and by Ye and Smith (1994) to completely balance planar linkages using an equivalence by which a complex planar linkage can be converted into a number of simple equivalent sub-linkages and cranks. It was also further improved by Yao and Smith (1993) for the force balancing of planar linkages using a step-by-step balancing procedure based on a mass flow diagram. Kong and Yang (1998) proposed a mass moment substitution method by which the formulation of the conditions for complete shaking force balancing of the spatial linkages can be reduced to the mass moment substitution of binary links, ternary links, quaternary links, dyads and spatial serial open chains.

The first general approach for full force balancing of spatial linkages was presented by Kaufman and Sandor (1971) and Chen (Chen 1984). They generalized the method of linearly independent vectors (Berkof, 1969) by replacing the complex vector with algebraic operators of a more general form. Compared to these methods, Kochev (1987) has developed another general method in which local coordinate systems and only Cartesian coordinates are used to simplify the balancing equations and which is applicable to more types of linkages and provides fewer sufficient shaking force balancing conditions. Yu has performed the complete shaking force and shaking moment balancing of spatial linkages like the Bennett, RSCR and RRRSR (1987a) and partial dynamic balancing of the RSS'R spatial linkage (1987b) by adding dyads between linkages. He also obtained complete shaking force and shaking moment balancing of spatial irregular force transmission mechanisms such as RSPC and RRCRC mechanism by using dyads and triads (1988). However, all the spatial linkages mentioned here have only one degree of freedom.

In the literature, partial dynamic balancing, where at least some shaking forces or shaking moments remain after balancing, were presented for some planar and spatial mechanisms (Berkof and Lowen, 1971; Smith, 1975; Huang and Liu, 1986; Yu, 1987b). Yet, this is not the subject of this thesis.

Some authors have addressed the trajectory planning of manipulators in order to generate reactionless trajectories or minimize disturbances (Dubowsky and Torres, 1991; Papadopoulos and Dubowsky, 1991; Papadopoulos and Abu-Abed, 1996; Legnani et al., 1999; Kochev, 1990b). However, the approaches based on trajectory planning are only suitable for some special applications. Agrawal and Shirumalla (1995) presented

a scheme for motion planning of a dual-arm free-floating planar manipulator where one arm is commanded to perform desired tasks while the other provides compensating motions to keep the base inertially fixed.

Using the aforementioned approaches for force balancing, dynamically balanced mechanisms have been achieved and presented. Most of the authors in the literature on dynamic balancing have used additional counter-rotations — counter-rotating inertial elements designed to balance the shaking moments of the mechanisms — such as fixed-axis-inertia counterweights, planetary-gear-train or toothed-belt inertia counterweights (Huang and Liu, 1986; Gao 1989, 1991; Ye and Smith 1994; Arakelian and Smith, 1999; Esat and Bahai, 1999), additional balancing links (dyads, triads, idler loops, etc.)(Bagci 1982, 1992; Yu 1987a, 1988) and symmetrically arranged identical mechanisms (Kochev 2000) or active control of counter-rotation (Kochev, 1992a) or using redundant actuation (Angeles et al., 1992). However, adding counter-rotations to a mechanism increases its complexity and can reduce its practicality significantly, especially in multi-degree-of-freedom systems.

The four-bar linkage is a relatively simple and common element in machines. Almost half of all researchers in the field of balancing have been focusing on this kind of mechanism. The complete shaking force and shaking moment balancing of four-bar linkages have been achieved by using separate counter-rotations such as fixed-axis-inertia counterweights (Berkof, 1973), idler loops (Bagci, 1982), planetary-gear-train-inertia counterweights (Gao, 1990), toothed belts (Esat and Bahai, 1999) or noncircular gearset inertia-counterweights (Kochev, 1992). Ricard and Gosselin (2000) have also focused on the four-bar linkage and obtained the complete balancing of the linkage in the plane as a set of constraints on the geometric and inertial parameters of the links but without separate counter-rotations. These dynamically balanced four-bar linkages have been stacked up to synthesize reactionless planar 3-DOF parallel mechanisms (Ricard and Gosselin 2000) and reactionless spatial 3-DOF parallel mechanisms (Vollmer and Gosselin, 2000; Gosselin et al., 2003). However, since the reactionless four-bar linkages are balanced only in the plane, the stacked reactionless mechanisms — used as legs to synthesize planar or spatial 3-DOF mechanisms — can only move in the plane. Hence, these reactionless four-bar linkages cannot be directly used to synthesize reactionless spatial 6-DOF mechanisms. As we mentioned above, it is impossible to further moment balance the statically balanced 6-DOF parallel manipulator (Figure 1.4) to finally obtain a reactionless 6-DOF parallel mechanism. Foucault and Gosselin (2002)

Figure 1.5: Prototype of a reactionless planar 3-DOF parallel mechanism (from Foucault and Gosselin, 2002).

dynamically balanced five-bar mechanisms — with parallelogram architecture — using counterweights and counter-rotations (e.g., fixed-axis-inertia counterweights) and used them as legs to build a reactionless 3-DOF parallel manipulator (Figure 1.5). However, it is obvious that we cannot use these dynamically balanced five-bar mechanisms to construct spatial reactionless parallel mechanism with more than three degrees of freedom.

In summary, as emerges from the literature, the dynamic balancing of spatial multi-degree-of-freedom parallel manipulators or mechanisms has received virtually no attention due to the complexity of this problem. To the best of our knowledge, only a reactionless 3-DOF spatial parallel mechanism has been presented in the literature (Vollmer and Gosselin, 2000; Gosselin et al., 2002).

1.2.2   Kinematic Analysis

The kinematic analysis of parallel mechanisms including inverse and direct (or forward) kinematics, workspace and singularity analyses are important issues in the context of design and control of the mechanisms.

Computing the set of actuated joint coordinates from the set of Cartesian pose (position and orientation) of the end-effector is referred to as *inverse kinematics*. Since

the trajectories of the mechanism are usually given in the Cartesian space while the actuators are mounted at joints, the solution of the inverse kinematics is necessary for controlling a manipulator.

Computing the set of Cartesian pose of the end-effector from the set of actuated joint coordinates is referred to as *direct (or forward) kinematics*. As opposed to the serial manipulators, the inverse kinematics of parallel mechanisms are simple, while their direct kinematics are very complex especially for 6-DOF parallel mechanisms. Fortunately, the direct kinematics of different types of parallel manipulators is often similar. In other words, the direct kinematics of a new parallel mechanism can be often found to be equivalent to that of some existing mechanisms as we will discuss in Section 4.4 (Merlet 1992a; Nanua *et al.* 1990; Ebert-Uphoff and Gosselin 1998).

The *workspace* of a manipulator is defined as the set of Cartesian poses that the end-effector of the manipulator can reach. The workspace determines the volume or hyper-volume in which the manipulator can perform tasks. It is well known that parallel manipulators have a rather limited and complex workspace. As the *complete workspace* of a 6-DOF parallel manipulator is a six-dimensional highly coupled entity which is practically impossible to visualize, algorithms for various subsets of it have been proposed. The most common subset is the *constant-orientation workspace* (Merlet, 1994) which is the set of permissible positions for a point of the moving platform while the platform is kept at a constant orientation (Bonev, 2002a). Two kinds of major approaches — *discretization* algorithms (Benea, 1996; Wang, 1998) and geometric methods (Gosselin, 1990; Gosselin et al., 1992; Merlet, 1994; Bonev and Gosselin, 2002) have been proposed for the determination of the workspace of different parallel mechanisms. The philosophy of discretization algorithm (or numerical algorithm) consists roughly in discretizing the three-dimensional space, solving the inverse kinematic problem at each point, verifying the constraints that limit the workspace and searching for the boundaries of the workspace. Although such discretization algorithms are very slow and require large amounts of memory and disk space for storing the computed data, they are used by most researchers and can be applied to any type of architecture. On the contrary, the geometric methods based on the explicit expressions of all constraints that limit the workspace are fast and accurate and very useful during the design stage. However, it is very difficult or impossible to determine the workspace for some complex parallel mechanisms using geometric methods (Bonev, 2002a).

The *kinematic singularity* in a parallel mechanism is defined as configurations in which the end-effector gains or loses one or more degrees of freedom instantaneously and therefore the manipulator becomes uncontrollable. The singularity loci, which are obtained as curves or surfaces in the Cartesian space, are of great interest in the context of design since they can be used to verify whether or not the singularities will be avoided later on for a given application.

Gosselin and Angeles (1990) have shown that singularities of closed-loop mechanisms can be systematically classified in three main groups. The first type of singularity corresponds to a configuration in which the end-effector loses one or more degrees of freedom and lies at a deadpoint and on the boundaries of the workspace of the manipulator. The second type of singularity corresponds to a configuration in which the end-effector gains one or more degrees of freedom (i.e., the end-effector is movable when all the input joints are locked) and lies at a deadpoint and inside the workspace. The third type of singularity corresponds to configurations in which a finite motion of the end-effector is possible even if the actuated joints are locked or where a finite motion of the actuated joints produces no motion of the end-effector. This kind of singularity, also called architecture singularity, can occur only when some special conditions on the parameters of a manipulator are satisfied. This classification has been complemented in Ma and Angeles (1991) and further refined in Zlatanov et al. (1994; 1995).

The singularity analysis of type I of a parallel mechanism is the same as that of serial mechanisms. The singularity of type III could be avoided by proper choice of the kinematic parameters. However, the singularity analysis of type II of a parallel mechanism is usually very complex. It is difficult to analyze and has received much attention from many researchers over the past two decades. Two main approaches have been proposed for the singularity analysis of type II of parallel mechanism, namely, the algebraic method based on the determinant of the Jacobian matrix from the velocity equation of the manipulator and the method based on line geometry or screw theory. Analytical expressions describing the singularity loci of planar and spherical parallel manipulators and the Gough-Stewart platform have been obtained by the algebraic method (Gosselin and Angeles, 1990; Gosselin and Sefrioui, 1992; Sefrioui and Gosselin, 1995; Collins and McCarthy, 1998; Mayer St-Onge and Gosselin, 2000). It is very useful to obtain analytical expressions for the singularity loci to generate graphical representations in the workspace in a context of analysis and design. However, such expressions are very difficult or impossible to obtain for some parallel mechanisms with

more than three degrees of freedom or with complex leg mechanisms since the corresponding closed-form expressions of the determinant of the Jacobian matrices include both Cartesian and joint coordinates. After substituting the active and passive joint coordinates with Cartesian coordinates using the equations of the inverse kinematics problem, the closed-form expression of the corresponding determinant is of very complex form or does not exist. Then, the method based on line geometry or screw theory — with similar principle for both methods — has been proposed for the singularity analysis of complex spatial parallel mechanisms (Merlet, 1988; 1989; 1992b; Mouly and Merlet, 1992; Collins and Long, 1994; Notash, 1998; Monsarrat and Gosselin, 2001). Apparently, a numerical method — as used in the determination of the workspace — can be used to determine the singularity locus on which the determinant of the Jacobian matrix is zero for any kind of mechanisms.

1.3   Objectives of the Thesis Research

In order to meet the requirements of advanced robotic applications like space robotics or telescope mechanisms, the development of reactionless spatial multi-degree-of-freedom mechanisms or manipulators — having up to 6-DOF — has become an attractive research subject in the field of parallel mechanisms. Hence, a systematic study of the synthesis and analysis of reactionless spatial multi-degree-of-freedom parallel mechanisms is performed in this thesis. Our research has three main goals.

The first goal of our research is to propose a simple but suitable spatial 3-DOF mechanism which can be dynamically balanced and then use it as legs to synthesize reactionless 6-DOF parallel mechanisms. A new 3-DOF parallel mechanism referred to as a parallelepiped mechanism is presented. A general dynamic balancing approach using counterweights and counter-rotations is used for dynamically balancing this new kind of leg mechanism. Finding out the dynamic equivalence between point masses and moving platform in space will enrich the strategy of using point masses to replace a moving platform. This strategy greatly simplifies the dynamic balancing of spatial multi-degree-of-freedom parallel mechanisms.

The second objective of this thesis is to obtain dynamically balanced four-bar linkages which can move spatially (out of the plane) as the extension of the reactionless

four-bar linkages in the plane (Ricard and Gosselin, 2000) and then use these four-bar linkages to synthesize reactionless spatial 3-DOF and 6-DOF mechanisms without separate counter-rotations.

For novel manipulators, it is necessary to find the inherent characteristics of the mechanisms in the context of design and control of the mechanisms. Thus, the kinematic analysis including inverse kinematics, determination of workspace and singularity analysis of the 3-DOF leg mechanisms and 6-DOF parallel mechanisms are the third aim of this thesis. The suitable approaches discussed in the preceding section for the kinematic analysis will be used for the corresponding mechanisms proposed in this thesis.

1.4   Organization of the Thesis

The present thesis consists of two main parts covering Chapters 2–6. The first part (Chapters 2–4) starts with the geometric description of the presented mechanisms, continues with the kinematic analysis, and ends with the dynamic balancing. The second part (Chapters 5–6) takes a different order. Since the architecture and balancing conditions of the spatial mechanisms are obtained through systematic extension by way of stacking dynamically balanced units, this type synthesis approach is completed first. Subsequently, the kinematic analysis of the resulting mechanisms is presented.

In Chapter 2, a novel 3-DOF parallel mechanism referred to as a parallelepiped mechanism is proposed. Two types of actuation schemes of the mechanism are considered. The kinematic analysis including the inverse and direct kinematics as well as the determination of singularity loci and workspace for the two actuation types of the mechanism is solved. A geometrical algorithm and a discretization method are used for the determination of the workspace of the mechanism.

In Chapter 3, the design and dynamic balancing of parallelepiped mechanisms are addressed. At the beginning of this chapter, the dynamic balancing of general parallelepiped mechanisms is discussed. Then, practical implementations of the parallelepiped mechanisms for both types of actuation schemes are presented. The balancing equations are derived by imposing that the center of mass of the mechanism is fixed and

that the total angular momentum is constant (zero) with respect to a fixed point. Optimization is performed to determine the counterweights and counter-rotations based on the balancing conditions. The dynamic simulation software ADAMS is used to simulate the motion of the 3-DOF parallelepiped mechanisms and to verify the reactionless property of the dynamically balanced mechanisms.

In Chapter 4, the synthesis, kinematic analysis and dynamic balancing of 6-DOF parallel mechanisms using parallelepiped mechanisms are dealt with. The Jacobian matrices of the mechanisms associated with different actuation schemes are derived. A geometrical algorithm and a discretization method are used for the determination of the workspace for the mechanisms using two different cases of the leg mechanism introduced in Chapter 2. The graphical representations that show the relationship between the singularity loci and the constant-orientation workspace of the mechanisms are given. Finally, the dynamic equivalence between a moving platform and three point masses will be discussed and the dynamic balancing of the 6-DOF parallel mechanisms are addressed.

In Chapter 5, the synthesis of novel reactionless spatial 3-DOF and 6-DOF mechanisms without separate counter-rotations, using four-bar linkages is presented. A general planar four-bar linkage is first considered in order to obtain the conditions for its spatial dynamic balancing. Based on the conditions of dynamic balancing of a planar four-bar linkage, it is shown that the spatial problem is equivalent to ensuring that the inertia tensor of planar reactionless four-bar linkages remains constant while the linkages are undergoing spatial motion. Then, the reactionless conditions for planar four-bar linkages moving spatially are derived and reactionless spatial 3-DOF mechanisms using four-bar linkages without separate counter-rotations are synthesized. Finally, the latter mechanisms are used to synthesize 6-DOF reactionless mechanisms which do not involve separate counter-rotations.

In Chapter 6, the inverse kinematics and singularity analysis of the reactionless 6-DOF parallel mechanism using four-bar linkages synthesized in Chapter 5 are presented. Three types of actuation schemes of the mechanism are considered. The Jacobian matrix of the mechanism is first derived. The Grassmann line geometry method is then used to determine the conditions associated with the singular configurations. Finally, the graphical representations that show the singularity loci and the constant-orientation workspace of the mechanism using a geometrical algorithm and a discretization method

are given.

Finally, a summary of the results obtained in this thesis and some discussion as well as directions on future research work are given in Chapter 7.

Chapter 2

Kinematic Analysis of Spatial 3-DOF Parallelepiped Mechanisms

In this chapter, the mechanical architecture and kinematic analysis of a novel 3-DOF parallel mechanism referred to as a parallelepiped mechanism are first presented. Two types of actuation schemes of the mechanism are considered. The inverse and direct kinematic problems of these two instances of the mechanism are solved. The expressions of the singularity loci and their graphical representation are obtained. Finally, geometrical algorithms and discretization methods are used for the determination of the workspace for the two cases of the mechanism.
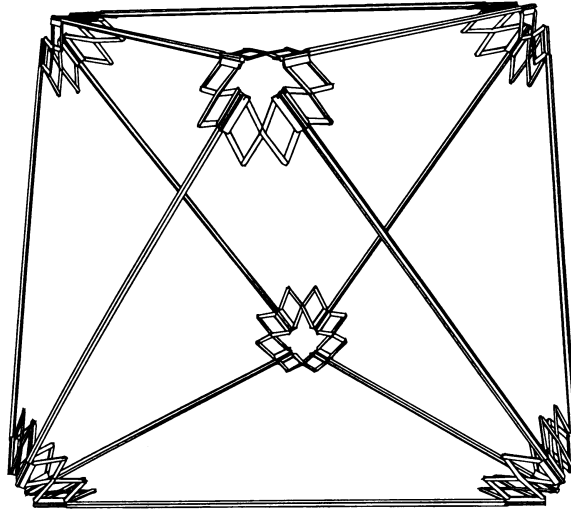
Figure 2.1: An octahedral truss (Hamlin and Sanderson, 1994).

2.1   Introduction

Parallel mechanisms or manipulators have received much attention over the last 30 years. Several kinds of 3-DOF parallel manipulators have been presented for different applications in the literature (Clavel, 1988; Lee and Shah, 1988; Gosselin and Angeles, 1989; Di Gregorio and Parenti-Castelli, 1998; Siciliano, 1999; Tsai and Joshi, 2000). Furthermore, in order to design light mechanisms with high stiffness, deformable trusses have also been contemplated (Reinholtz and Gokhale, 1987; Arun et al., 1990; Salerno and Reinholtz, 1994; Hertz and Hughes, 1994). Deformable trusses are akin to parallel mechanisms. However, they are generally built by assembling deformable 1-dof modules in series, thereby augmenting the complexity and degrading the stiffness. Hamlin and Sanderson (1994) have addressed the synthesis of an octahedral truss (Figure 2.1) using offset hinges as concentric multilink spherical joints at each vertex of the mechanism.

As we mentioned in Chapter 1, the major objective of this thesis is to develop reactionless multi-degree-of-freedom parallel mechanisms. We will first search for 3-DOF mechanisms which can be dynamically balanced. Then, we will construct 6-DOF reactionless manipulators or mechanisms using these 3-DOF dynamically balanced mechanisms as legs. Foucault and Gosselin (2002) have presented a planar 3-DOF reactionless parallel mechanism using the legs of the planar five-bar parallelogram linkages
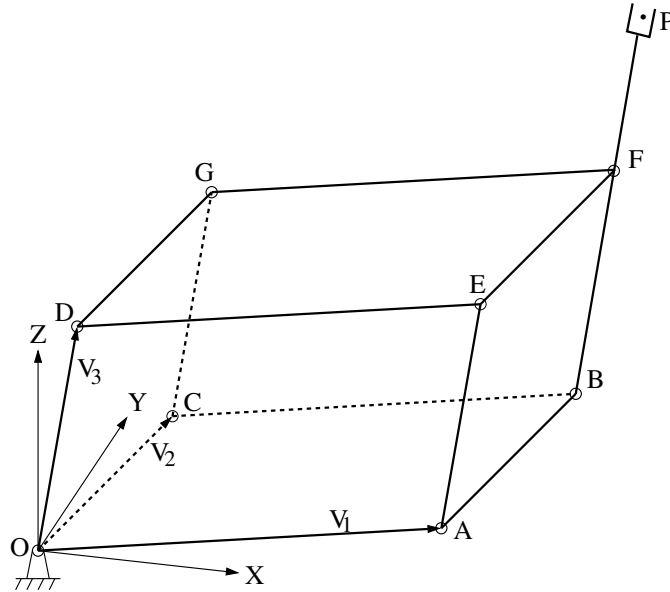
Figure 2.2: 3-DOF parallelepiped mechanism.

(Figure 1.5). If we append additional segments that move out of the plane of the parallelogram linkage, a novel spatial 3-DOF parallel mechanism referred to as a parallelepiped mechanism is obtained, that is first presented in this chapter. After describing the design techniques, the kinematic analysis including the inverse and direct kinematics as well as the determination of singularity loci and workspace of the mechanisms will be solved. Simulation tools for demonstrating the characteristics of the 3-DOF parallelepiped mechanisms will also be developed.

2.2   Geometric Description

A schematic representation of a 3-DOF parallelepiped mechanism is shown in Figure 2.2. Point P is the end-effector and is located on link BFP. The mechanism consists of a parallelepiped with 6 faces. The parallelepiped can be deformed with the faces remaining planar and with opposite faces remaining parallel, while providing three degrees of freedom, and can therefore be used to position point P in space. The three edges attached to the ground and denoted by V_1, V_2 and V_3 respectively are actuated using fixed revolute actuators. The following groups of links have equal length, namely: $OA = CB = GF = DE, OC = AB = EF = DG, OD = AE = BF = CG$. All the opposite links remain parallel throughout the motion, i.e., $OA \parallel CB \parallel GF \parallel DE, OC \parallel$
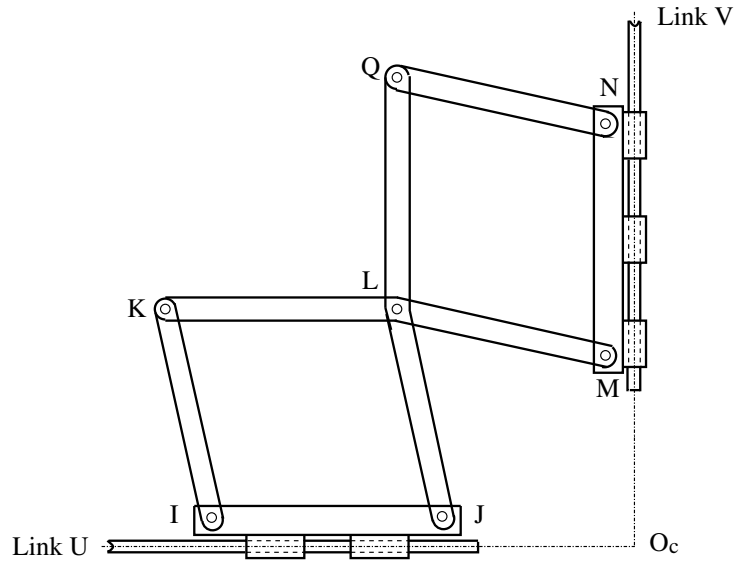
Figure 2.3: An offset planar hinge (Hamlin and Sanderson, 1994).

$AB \parallel EF \parallel DG$ and $OD \parallel AE \parallel BF \parallel CG$.

This mechanism may be considered as a "truly parallel" deformable truss, i.e., a multi-dof truss-type mechanism in which all actuators are mounted in parallel.

Several feasible designs of the parallelepiped mechanism have been investigated. A simple implementation is to use an offset planar hinge (Hamlin and Sanderson, 1994) at each corner of the 6 faces of the mechanism (or at any two of the three corners at each vertex of the parallelepiped). The offset planar hinge (Figure 2.3) is a Watt I type mechanism with two straight brackets (IK, NQ), two identical bent brackets (KLM, JLQ), and two leaves (IJ, MN). Each leaf can rotate around the corresponding link (or pin) of the parallelepiped. Moreover, $IJ = KL = LQ = MN$, $IK = JL = ML = NQ$, and the offsets of the leaf pivots relative to their leaf axes are the same. By suitable design of the parameters of the hinge mechanism, the intersection point O_c of the two leaf axes becomes the center of rotation for the links U and V while moving. Hence, the three adjacent links can rotate about the vertex center point at each vertex of the parallelepiped as a spherical joint while the faces of the parallelepiped remain planar.

Another feasible design of the parallelepiped mechanism is shown in Figure 2.4. Each of the faces (e.g. face $OAED$) is a planar $4R$ parallelogram mechanism. The 6 parallelograms are attached to each other at the vertices of the parallelepiped. More specifically, each pair of adjacent parallelograms is connected by a revolute joint with
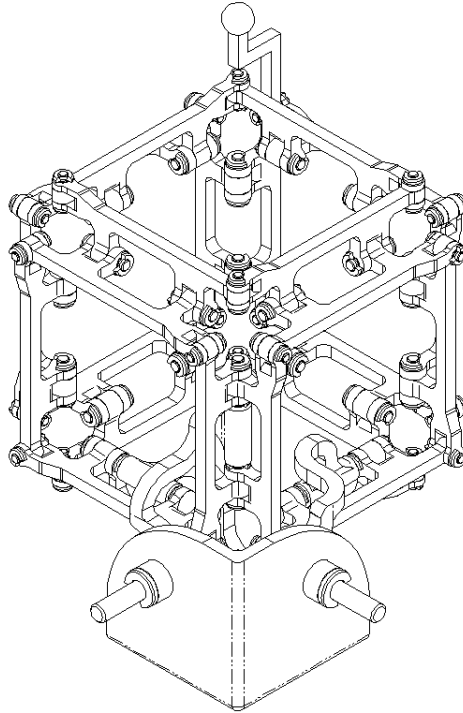
Figure 2.4: CAD model of a feasible design of the parallelepiped mechanism (courtesy of Thierry Laliberté and Mathieu Myrand).

intersecting axes. Hence the parallelepiped can be deformed with the faces remaining planar and with opposite faces remaining parallel. Notice that all the axes of the revolute joints at a given vertex intersect at the vertex center point at all times.

The fixed coordinate frame is denoted as $OXYZ$ and is attached to the base. Two types of actuation schemes of the mechanism designated as Case I and Case II respectively (Figure 2.5 and Figure 2.6) are considered in the present work. In Case I, V_1 and V_2 rotate around the Z axis and V_3 around the X axis, while in Case II, V_1, V_2 and V_3 rotate around the Y, Z and X axes respectively.

2.3 Inverse Kinematics

In parallelepiped mechanisms (Figure 2.2), let the Cartesian coordinates of P be (x, y, z) expressed in the fixed frame. Moreover, let l_1, l_2 and l_3 be the lengths of the three edges (V_1, V_2 and V_3 respectively) of the parallelepiped mechanism and let l_e be the
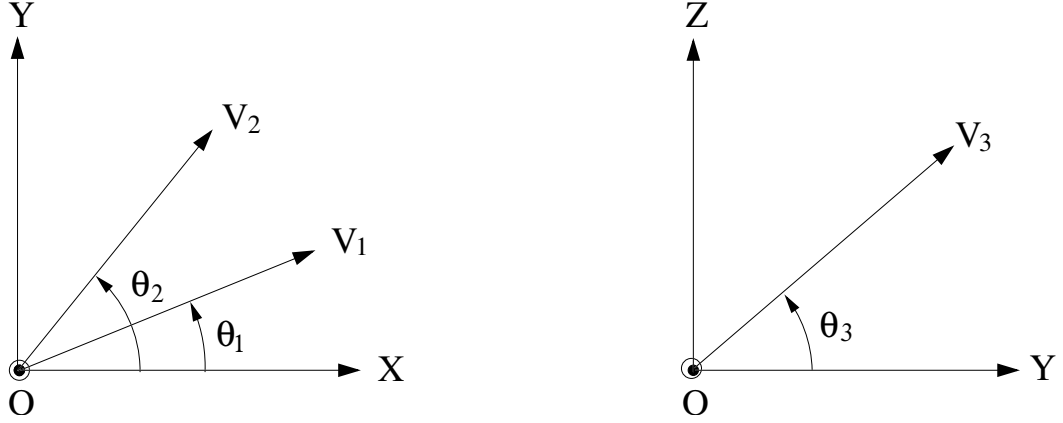
Figure 2.5: The first type of actuation of the parallelepiped mechanism (Case I).
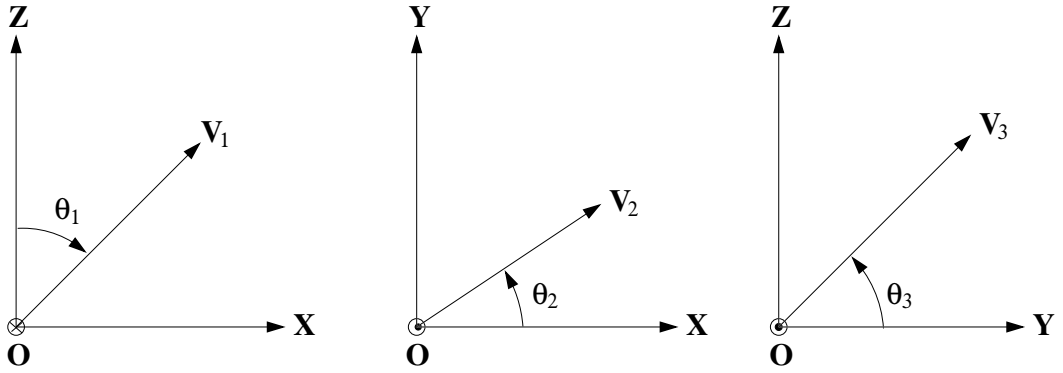
Figure 2.6: The second type of actuation of the parallelepiped mechanism (Case II).

length of the extended part of link BF attached to the end-effector. The definitions of the actuated joint coordinates $(\theta_1, \theta_2, \theta_3)$ are shown in Figures 2.5 and 2.6.

2.3.1 Case I

The position of the end-effector can be written as

$$\mathbf{p} = l_1\mathbf{e}_1 + l_2\mathbf{e}_2 + (l_3 + l_e)\mathbf{e}_3 \tag{2.1}$$

where

$$\mathbf{e}_1 = \begin{bmatrix} \cos\theta_1 \\ \sin\theta_1 \\ 0 \end{bmatrix}, \quad \mathbf{e}_2 = \begin{bmatrix} \cos\theta_2 \\ \sin\theta_2 \\ 0 \end{bmatrix}, \quad \mathbf{e}_3 = \begin{bmatrix} 0 \\ \cos\theta_3 \\ \sin\theta_3 \end{bmatrix} \tag{2.2}$$

Hence,

$$\mathbf{p} = \begin{bmatrix} l_1 \cos\theta_1 + l_2 \cos\theta_2 \\ l_1 \sin\theta_1 + l_2 \sin\theta_2 + (l_3 + l_e)\cos\theta_3 \\ (l_3 + l_e)\sin\theta_3 \end{bmatrix} = \begin{bmatrix} x \\ y \\ z \end{bmatrix} \tag{2.3}$$

From the above equation, two solutions for θ_3 — obtained from the z component — and four solutions for θ_1 and θ_2 are obtained.

For the velocity analysis, the differentiation of eq. (2.3) with respect to time yields

$$\dot{\mathbf{p}} = \mathbf{J}\dot{\boldsymbol{\theta}} \tag{2.4}$$

where $\mathbf{J}$ is the Jacobian matrix, which can be written as follows

$$\mathbf{J} = \begin{bmatrix} -l_1 \sin\theta_1 & -l_2 \sin\theta_2 & 0 \\ l_1 \cos\theta_1 & l_2 \cos\theta_2 & -(l_3 + l_e)\sin\theta_3 \\ 0 & 0 & (l_3 + l_e)\cos\theta_3 \end{bmatrix} \tag{2.5}$$

Hence the actuated joint velocities can be obtained by solving the linear system of equations given in eq. (2.4).

An example is now given in order to illustrate the inverse kinematics and velocity analysis of the mechanism. Let

$$l_1 = 100, \ l_2 = 100, \ l_3 = 100, \ l_e = 50$$

where the lengths are in millimeters. Let the end-effector trace a planar circle with a radius of 20 mm, centered at $(0, 35, 0)$ and located in a plane parallel to the XZ plane, i.e., the parametric equations of the trajectory can be written as, for $0 \leq t \leq 2\pi$,

$$\begin{aligned} x &= 20 \cos t \\ z &= 20 \sin t \\ y &= 35 \end{aligned}$$

The actuated joint coordinates and velocities for the first actuator are plotted in Figure 2.7.
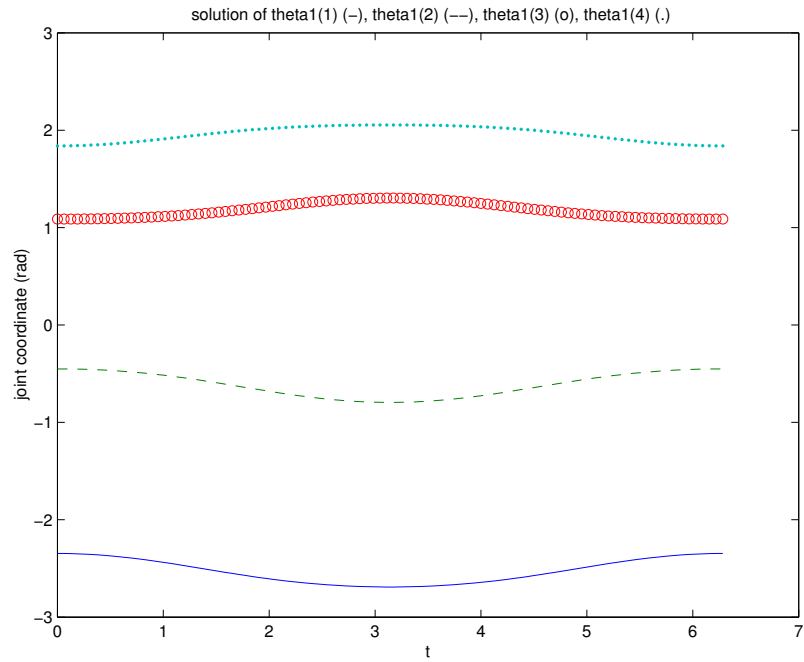
(a) Four solutions for θ_1
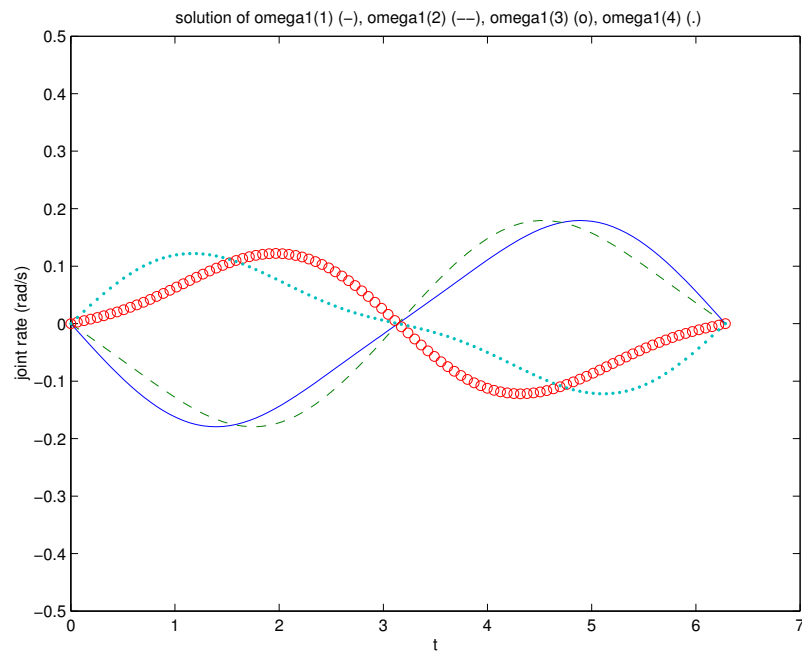
(b) Four solutions for $\dot{\theta}_1$

Figure 2.7: First set of actuated joint coordinates and velocities (Case I).

2.3.2 Case II

For Case II, one has

$$
\mathbf{e}_1 = \begin{bmatrix} \sin\theta_1 \\ 0 \\ \cos\theta_1 \end{bmatrix}, \ \mathbf{e}_2 = \begin{bmatrix} \cos\theta_2 \\ \sin\theta_2 \\ 0 \end{bmatrix}, \ \mathbf{e}_3 = \begin{bmatrix} 0 \\ \cos\theta_3 \\ \sin\theta_3 \end{bmatrix} \tag{2.6}
$$

and hence eq. (2.1) leads to

$$
\mathbf{p} = \begin{bmatrix} l_1\sin\theta_1 + l_2\cos\theta_2 \\ l_2\sin\theta_2 + (l_3 + l_e)\cos\theta_3 \\ l_1\cos\theta_1 + (l_3 + l_e)\sin\theta_3 \end{bmatrix} = \begin{bmatrix} x \\ y \\ z \end{bmatrix} \tag{2.7}
$$

The Jacobian matrix is written as

$$
\mathbf{J} = \begin{bmatrix} l_1\cos\theta_1 & -l_2\sin\theta_2 & 0 \\ 0 & l_2\cos\theta_2 & -(l_3 + l_e)\sin\theta_3 \\ -l_1\sin\theta_1 & 0 & (l_3 + l_e)\cos\theta_3 \end{bmatrix} \tag{2.8}
$$

From eq. (2.7), the actuated joint coordinates can be obtained by solving a univariate 8th-order polynomial equation. Consequently, the inverse kinematics leads to a maximum of eight real solutions in this case. This result is readily obtained by applying elimination between the three equations. The actuated joint coordinates and velocities for the first actuator of the same example as Case I are plotted in Figure 2.8. In this example, only four of the solutions are real.

2.4 Direct Kinematics

For given actuated joint coordinates (θ_1, θ_2 and θ_3), the Cartesian coordinates can be calculated from eq.(2.3) and (2.7) for Case I and Case II respectively. The solution is unique and straightforward.
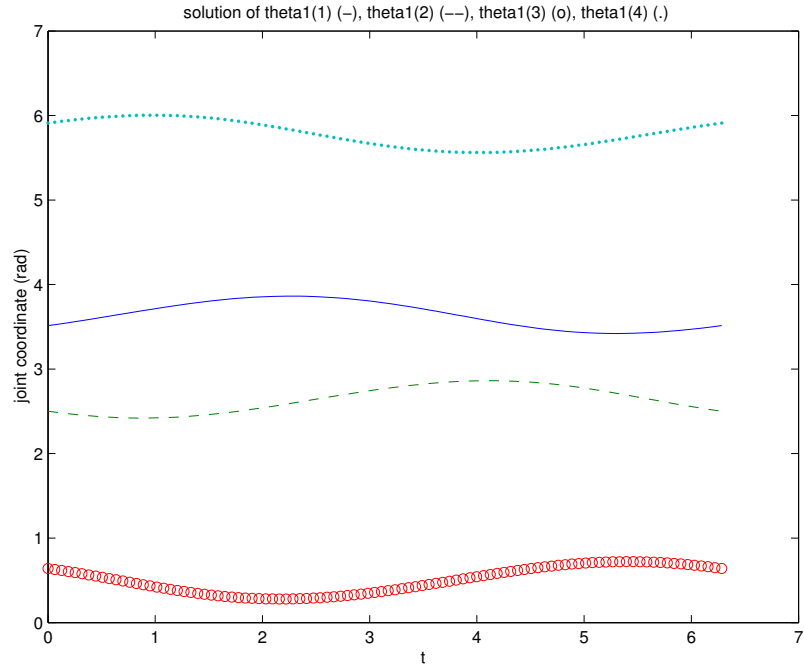
(a) Four solutions for θ_1
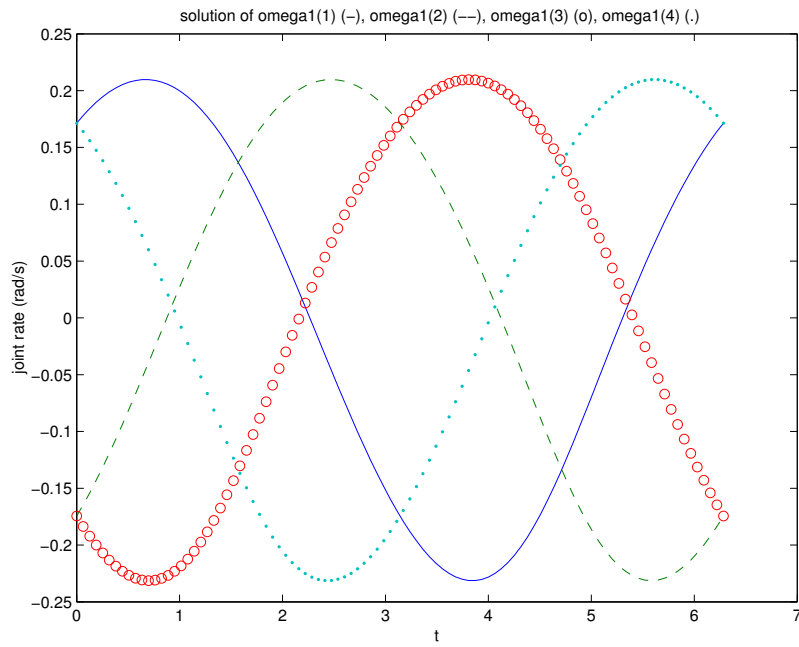
(b) Four solutions for $\dot{\theta}_1$

Figure 2.8: First set of actuated joint coordinates and velocities (Case II).
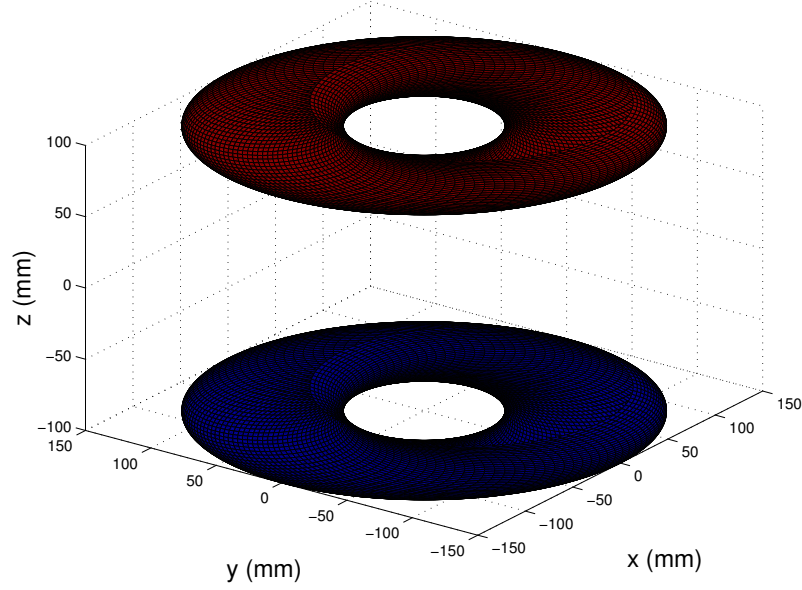
Figure 2.9: Singularity surface for Case I ($\theta_3 = \pm\frac{\pi}{2}$)

2.5 Singularity Analysis

The singularity loci can be obtained using the expression of the determinant of the Jacobian matrix, a quantity which is known to vanish in singular configurations, i.e.,

$$\det(\mathbf{J}) = 0 \tag{2.9}$$

Hence, for Case I, substituting eq. (2.5) into eq. (2.9) leads to

$$\cos\theta_3 \sin(\theta_2 - \theta_1) = 0 \tag{2.10}$$

i.e.,

$$\cos\theta_3 = 0 \tag{2.11}$$

or

$$\sin(\theta_2 - \theta_1) = 0 \tag{2.12}$$

From eq. (2.11), over the interval $]-\pi, \pi]$, one has

$$\theta_3 = \pm\frac{\pi}{2} \tag{2.13}$$

From eq. (2.12), one has

(a) Singularity surface

(b) z = 0 mm

(c) y = 40 mm

(d) x = 140 mm
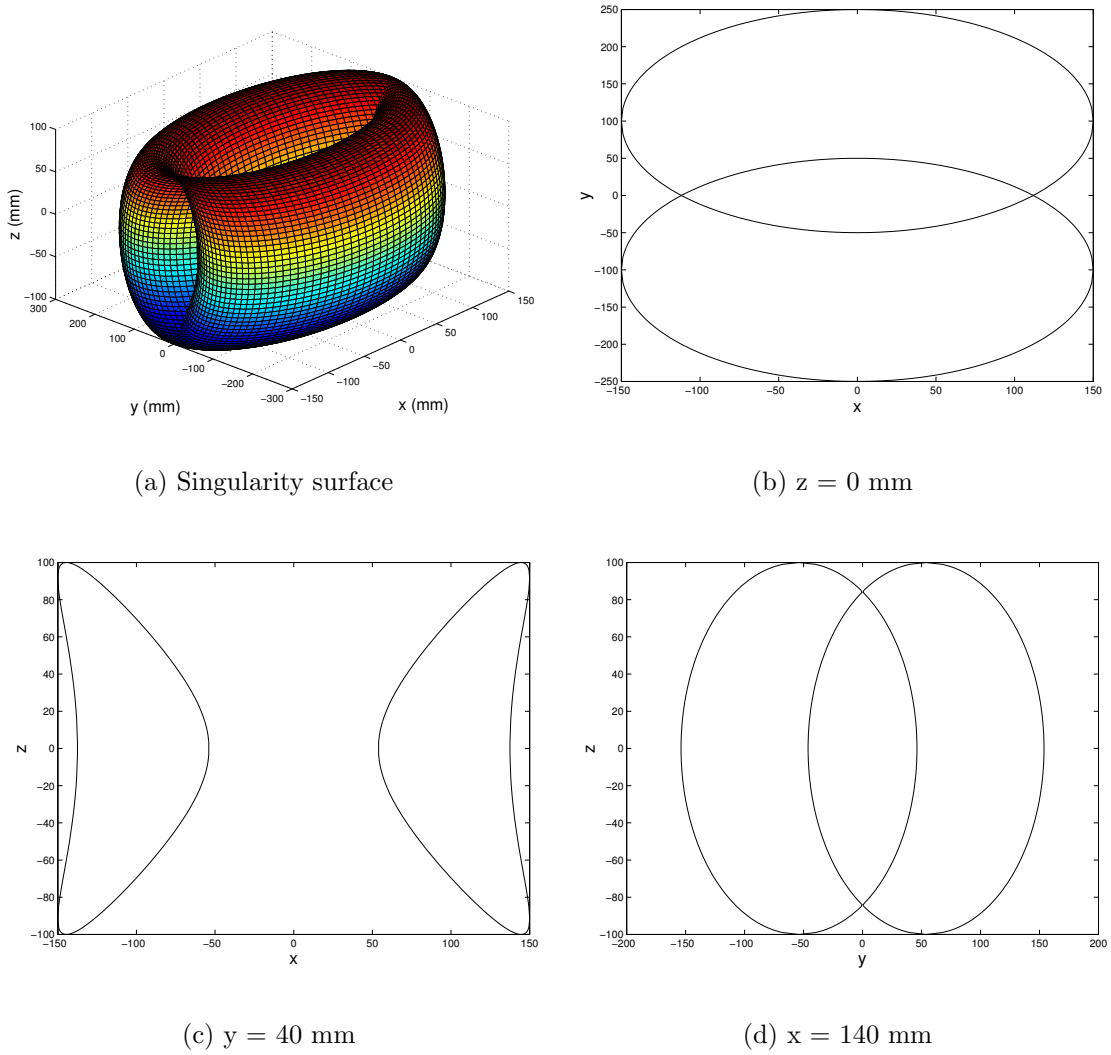
Figure 2.10: Singularity surface and its sections for Case I $(\theta_2 = \theta_1)$

$$\theta_2 = \theta_1 \tag{2.14}$$

or

$$\theta_2 = \pi + \theta_1 \tag{2.15}$$

For simplicity and generality, the joint limits and mechanical interferences of the mechanism are ignored for the determination of the singularity loci and workspace in this thesis. A mechanism with the lengths of $100\,mm$ for l_1 and $50\,mm$ for l_2, l_3 and l_e respectively is taken as an example.

The condition $(\theta_3 = \pm\frac{\pi}{2})$ means that the first zones of singularity in Cartesian space are two annular zones parallel to the xy plane — each of which is enclosed by two concentric circles with the outer and inner radii of $(l_1 + l_2)$ and $(l_1 - l_2)$ (link OA and OC are collinear but in the same and opposite direction) respectively.

The latter conditions $(\theta_2 = \theta_1$ and $\theta_2 = \pi + \theta_1)$ express that link OA and OC are collinear, the vertex B moves consequently on circles in the xy plane, centered at the origin but with radii of $(l_1 + l_2)$ and $(l_1 - l_2)$ respectively. Hence, the corresponding singularity surfaces are formed by a circle — parallel to the yz plane and with a radius of $(l_3 + l_e)$ — the center of which traces circles of radius $(l_1 + l_2)$ and $(l_1 - l_2)$ respectively. The surface obtained by sweeping a circle $\mathcal{C}$, while its center moves on the track circle $\mathcal{K}$ and the plane of the circle $\mathcal{C}$ remains parallel to the plane $\mathcal{F}$ perpendicular to the plane of $\mathcal{C}$ is a quartic surface and is referred to as a *Bohemian dome* (Weisstein, 2002; Bonev and Gosselin, 2002). Both singularity surfaces corresponding to eqs. (2.14) and (2.15) are Bohemian domes. In order to better demonstrate the singularity surfaces, different sections are also obtained. The singularity surfaces and their sections associated with the conditions $\theta_2 = \theta_1$ and $\theta_2 = \pi + \theta_1$ for the example mechanism are shown in Figure 2.10 and Figure 2.11 respectively.

For Case II, substituting eq. (2.8) into eq. (2.9) leads to

$$\cos\theta_1 \cos\theta_2 \cos\theta_3 - \sin\theta_1 \sin\theta_2 \sin\theta_3 = 0 \tag{2.16}$$

Equation (2.16) corresponds to a surface in joint space (Figure 2.12). From eq. (2.7) and eq. (2.16), the singularity surface and its sections for different values of z in Cartesian space can be also obtained as demonstrated in Figure 2.13.

(a) Singularity surface

(b) $z = 0$ mm

(c) $x = 40$ mm

(d) $y = 140$ mm
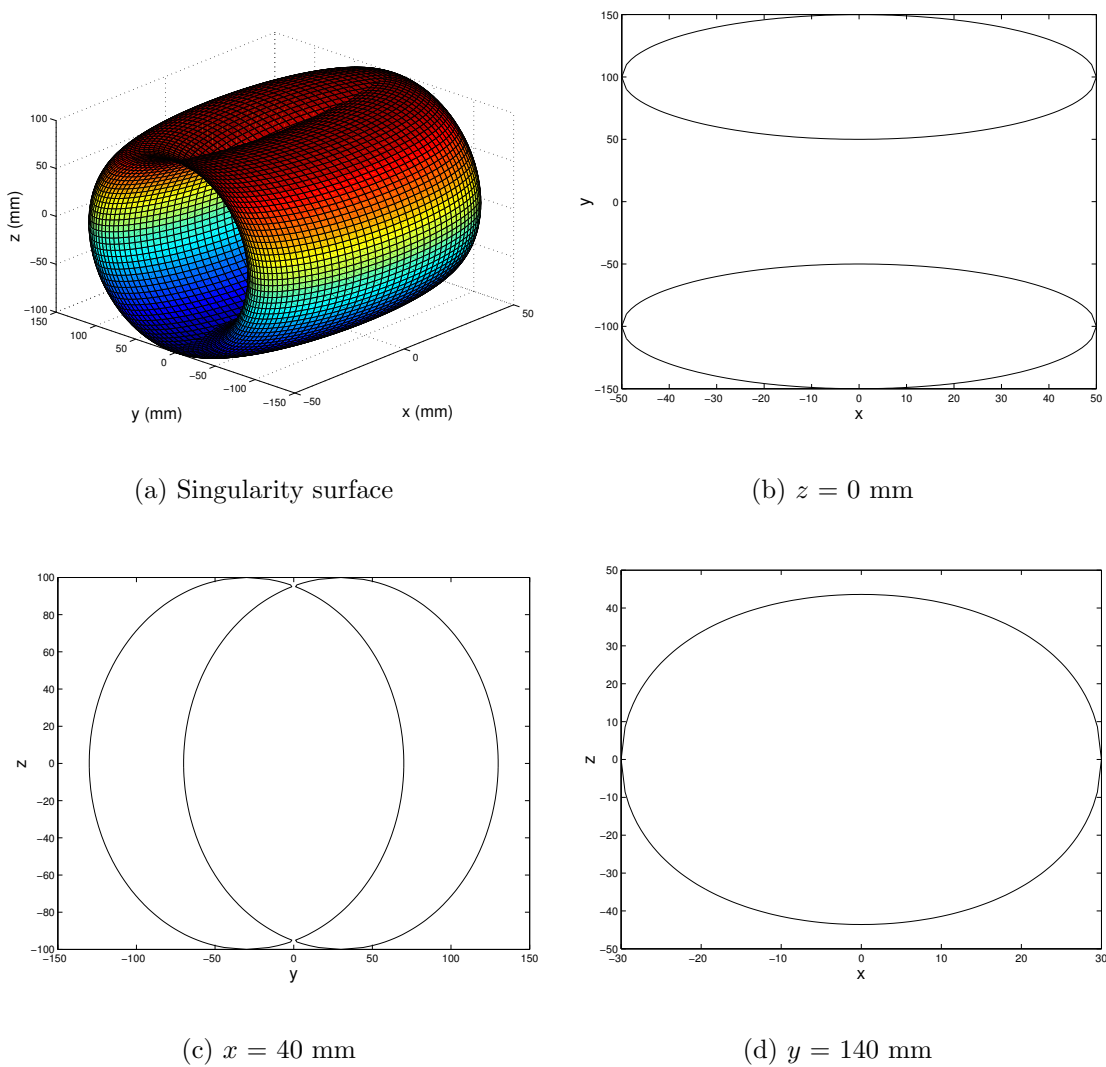
Figure 2.11: Singularity surface and its sections for Case I $(\theta_2 = \pi + \theta_1)$
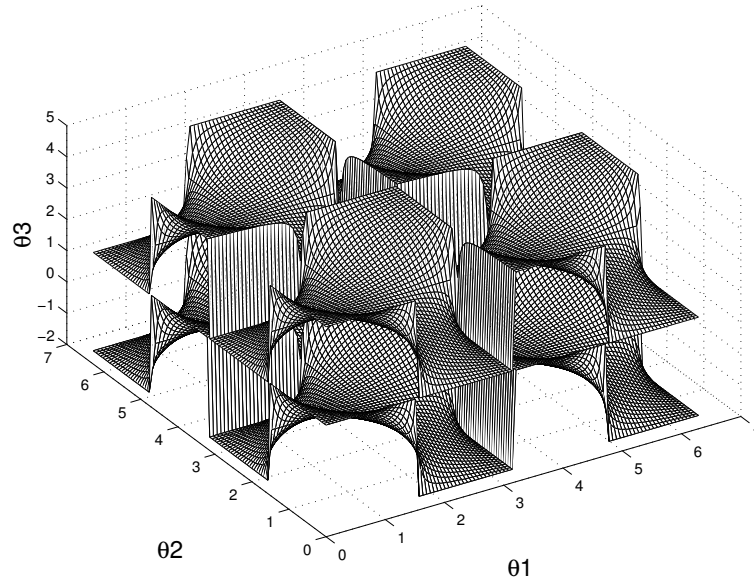
Figure 2.12: Singularity surface in joint space (Case II)

2.6   Workspace

For Case I, it is found by inspection that the three kinds of singularity surfaces corresponding to the three conditions presented above define the top and bottom, outer and inner boundaries of the workspace, respectively. Since the cross-section of the singularity surface for a given z is defined by two circles (Figure 2.10), the cross-section of the workspace on planes parallel to the xy plane can be obtained by the intersection of regions bounded by circles. The resulting workspace and its boundaries for the example mechanism are finally shown in Figure 2.14.

For Case II, it is very difficult to determine the workspace by a geometrical method. A discretization algorithm is therefore used for this case (Bonev, 2002a). Finally, the workspace and its boundary for the example mechanism are demonstrated in Figure 2.15 and 2.16. The workspace includes the space between the outer and inner boundaries as well as two lines from point $(0, 0, 14)$ to point $(0, 0, 187)$ and from point $(0, 0, -14)$ to point $(0, 0, -187)$ respectively.

Naturally, the workspace of the parallelepiped mechanism will decrease if the joint limits and mechanical interferences of the mechanism are considered. However, a workspace optimization with these constraints can be undertaken to meet the require-
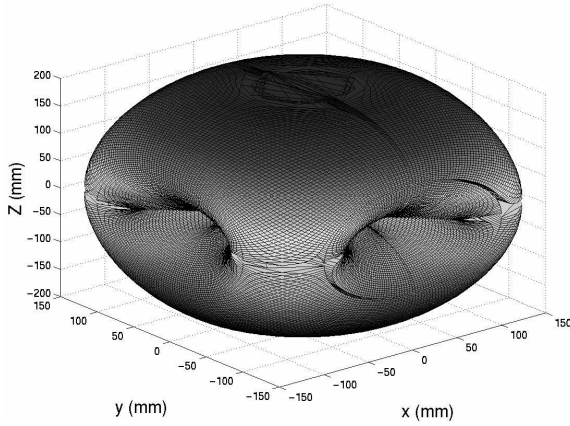
(a) Singularity surface
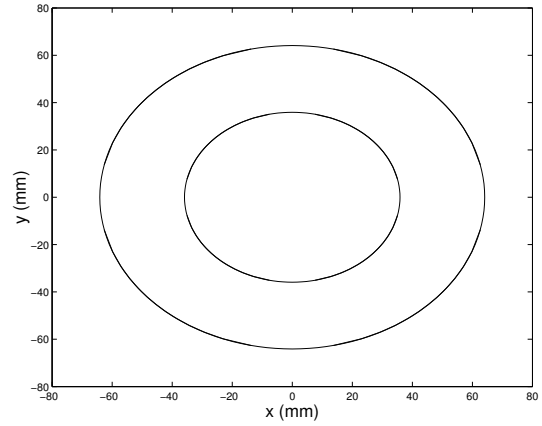
(b) $z = 199$ mm
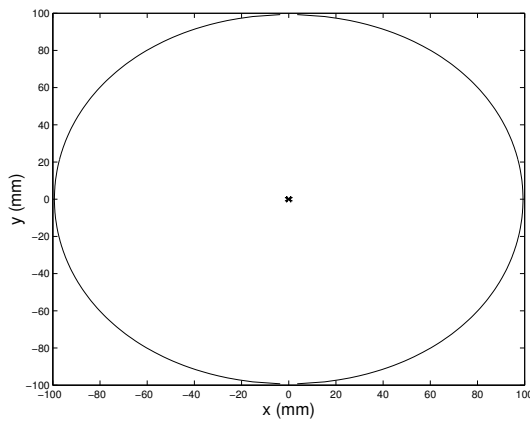
(c) $z = 187$ mm
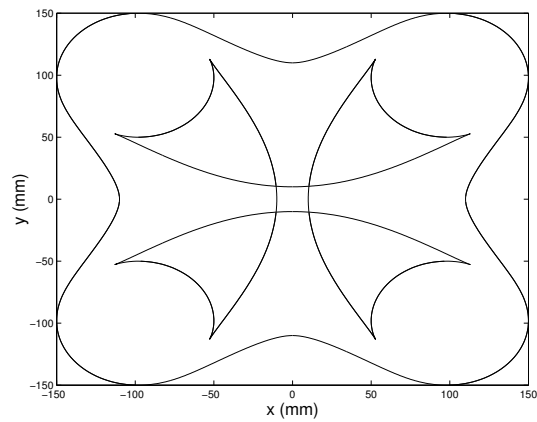
(d) $z = 20$ mm

Figure 2.13: Singularity surface and its sections for different values of z in Cartesian space (Case II).
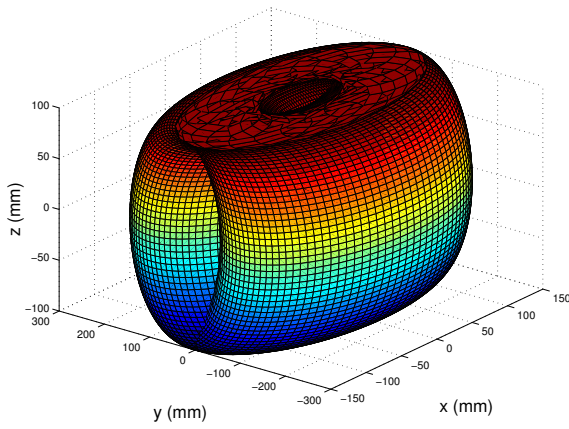
(a) Workspace
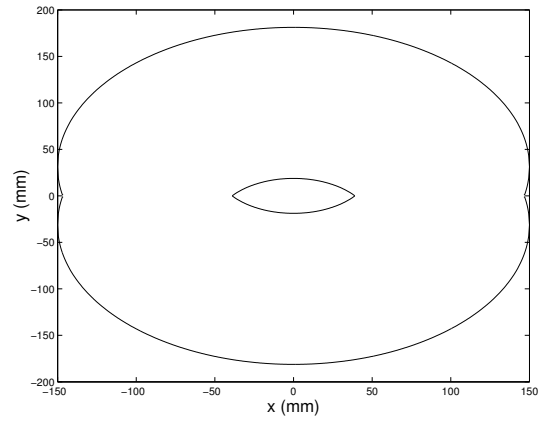
(b) $z = 95$ mm
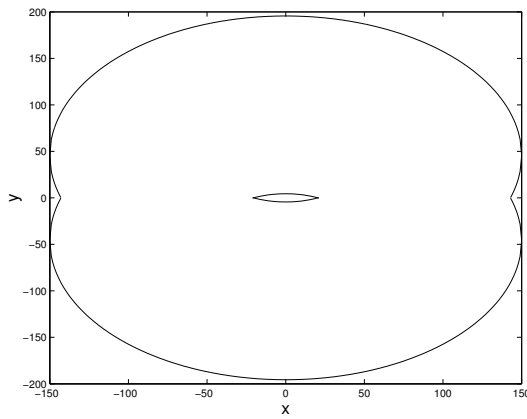
(c) $z = 89$ mm
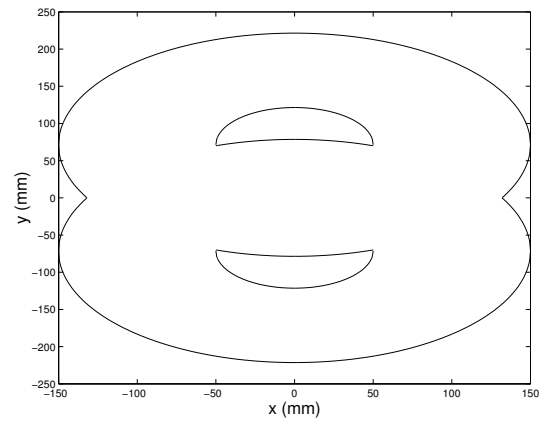
(d) $z = 70$ mm
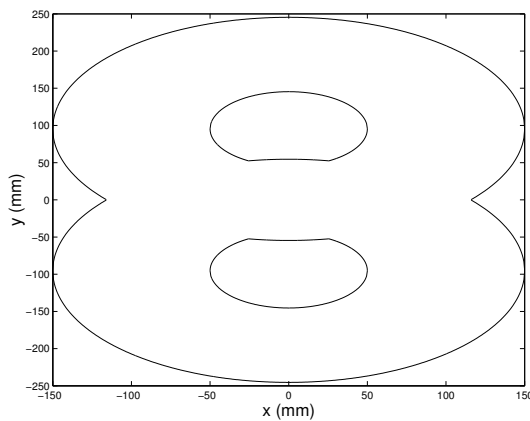
(e) $z = 30$ mm
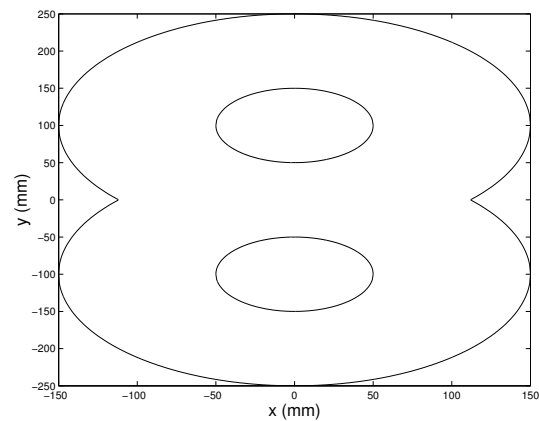
(f) $z = 0$ mm

Figure 2.14: Workspace and its boundaries for different values of z (Case I).
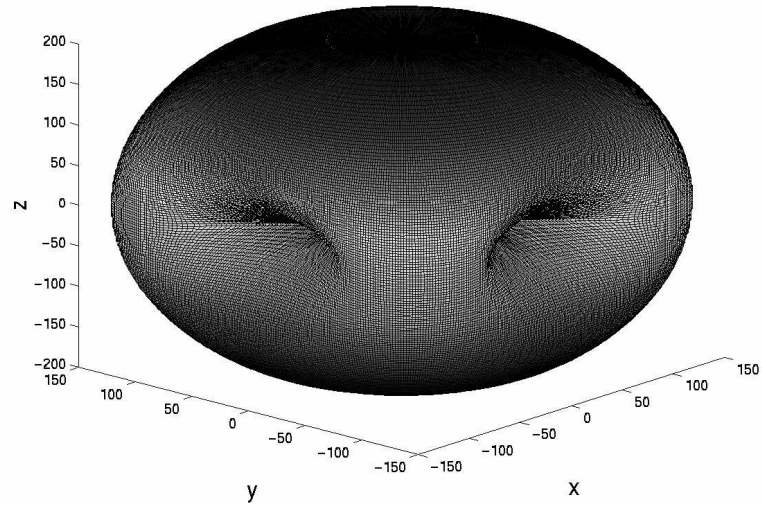
(a) Workspace
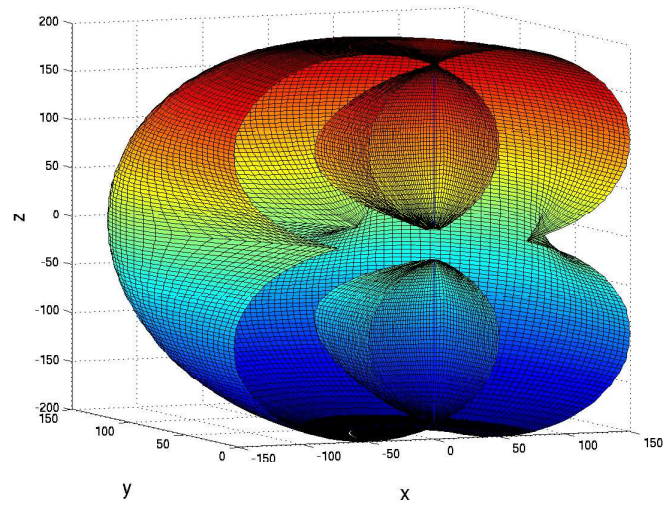
(b) Half section of the workspace

Figure 2.15: Workspace (Case II).
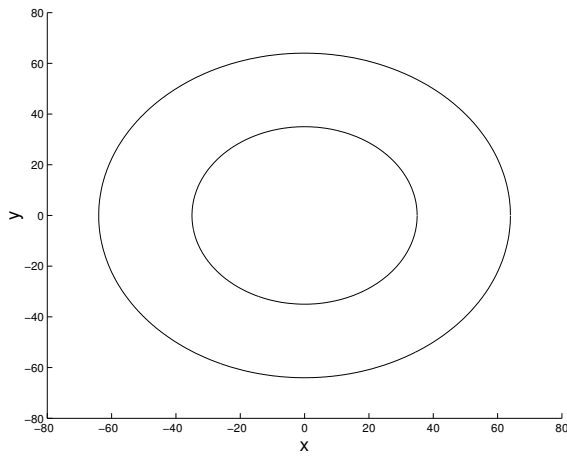
(a) $z = 199$ mm
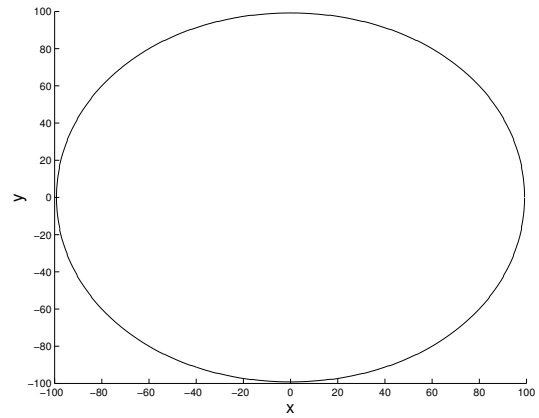
(b) $z = 187$ mm
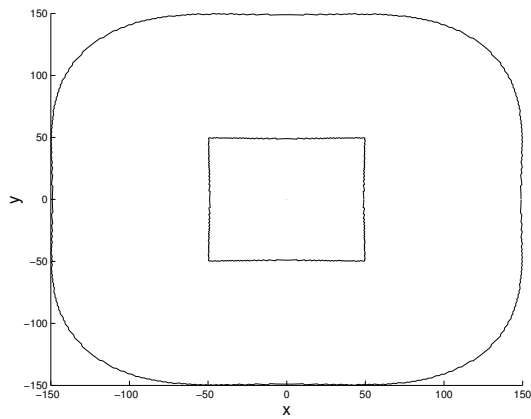
(c) $z = 90$ mm
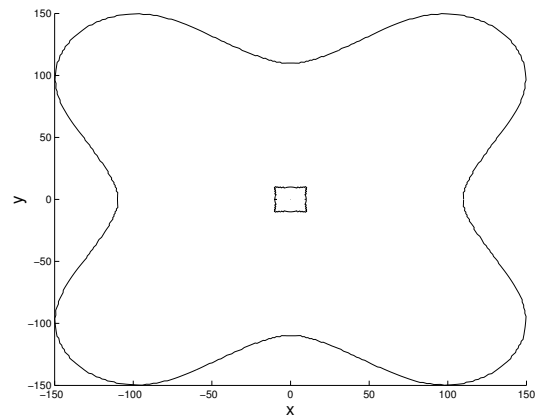
(d) $z = 20$ mm
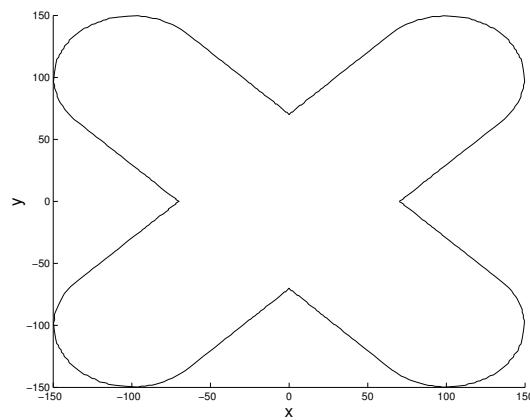
(e) $z = 0$ mm

Figure 2.16: Boundary of the workspace for different values of z (Case II).
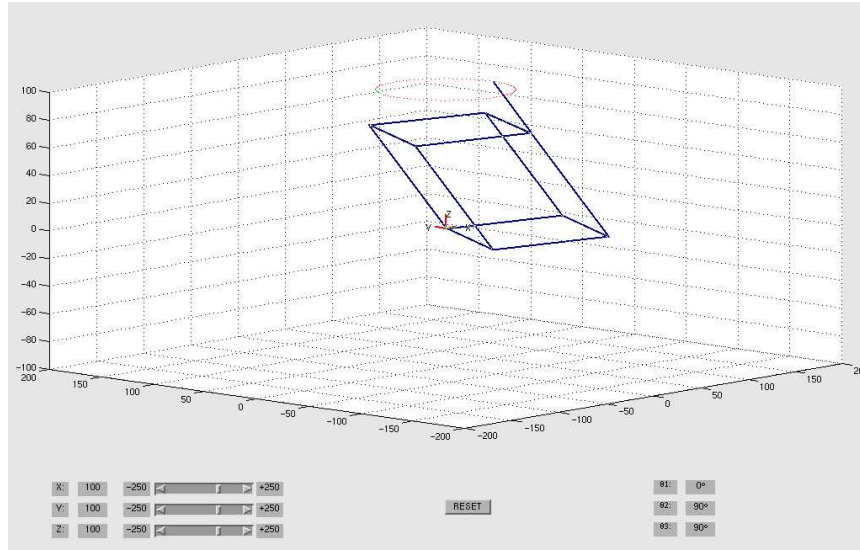
Figure 2.17: Simulation tools for parallelepiped mechanisms.

ments of practical applications (Masory and Wang, 1992).

From the above kinematic analysis, we find that a 3-DOF parallelepiped mechanism may be regarded as a three-link serial chain, in the sense that the kinematic analyses of the two kinds of mechanisms are completely the same. At the same time, only the parallelepiped mechanism may be considered as a multi-dof truss-type parallel mechanism in which all actuators are mounted in parallel on the base. The mechanism has then lower inertia and a higher stiffness as compared to the three-link serial chain where two of the three actuators are mounted on the moving links.

2.7 Development of Simulation Tools for 3-DOF Parallelepiped Mechanisms

In order to simulate the kinematics of 3-DOF parallelepiped mechanisms, simulation tools have been developed using Matlab on the basis of the kinematic analysis mentioned above. These tools allow the kinematic simulation of the mechanism for any given trajectory and show the position of the mechanism and the actuated joint coordinates for any interactively given set of Cartesian coordinates (see Figure 2.17).

2.8   Conclusion

The mechanical architecture and kinematic analysis of a novel 3-DOF parallel mechanism referred to as a parallelepiped mechanism are first presented in this chapter. Two types of actuation schemes of the mechanism are considered. The inverse and direct kinematic problems associated with the two cases of the mechanism have been solved. The expressions of the singularity loci and their graphical representations have been obtained. A geometrical algorithm and a discretization method are respectively used for the determination of the workspace for the two cases of the mechanism. Simulation tools for demonstrating the characteristics of the 3-DOF parallelepiped mechanisms have also been developed. All the results will be provided as guides for the future design of the mechanisms. Furthermore, the 3-DOF parallelepiped mechanisms will be used as legs to synthesize 6-DOF dynamically balanced parallel mechanisms.

Chapter 3

Dynamic Balancing of Spatial 3-DOF Parallelepiped Mechanisms

In this chapter, the design and dynamic balancing of parallelepiped mechanisms are addressed. Two types of actuation schemes of the mechanism are considered. The balancing equations are derived by imposing that the center of mass of the mechanism is fixed and that the total angular momentum is constant with respect to a fixed point. Optimization is performed to determine the counterweights and counter-rotations based on the balancing conditions. The dynamic simulation software ADAMS is used to simulate the motion of the 3-DOF parallelepiped mechanisms and to verify that the mechanisms are reactionless at all times and for arbitrary trajectories. At the beginning of this chapter, the dynamic balancing of general parallelepiped mechanisms is discussed. Then, practical implementations of the parallelepiped mechanisms for both types of actuation schemes are presented. Dynamic balancing conditions for the practical mechanisms are derived and simulation using ADAMS is performed. Several numerical examples of reactionless 3-DOF parallelepiped mechanisms are given. It is shown that 3-DOF parallelepiped mechanisms can be completely balanced.

3.1   Introduction

As discussed in Section 1.2, two constraints have to be satisfied for a mechanism to be reactionless, namely, the center of mass of the mechanism should remain fixed and the total angular momentum must remain constant (zero) with respect to a fixed point at all times for arbitrary trajectories of the end-effector. Equations (1.3) and (1.4) are necessary and sufficient conditions for a mechanism to be dynamically balanced, i. e., reactionless.

Since a reactionless 6-DOF parallel manipulator using parallelepiped mechanisms will be constructed in the next chapter, a point mass is here considered at the end-effector of the 3-DOF parallelepiped mechanism. Indeed, the 6-DOF manipulator will be composed of three legs connecting the base to a common thin platform. Each of the three legs will be a parallelepiped mechanism. The mass and inertia of the platform will be distributed among the attachment points of the legs and replaced by three point masses m_p. In the next chapter, the dynamic equivalence between a platform and three point masses will be discussed in detail.

In this chapter, in order to facilitate understanding the phenomenon of dynamic balancing and some related issues, the dynamic balancing of elementary links is introduced first. The dynamic balancing of a 3-DOF parallelepiped mechanism with a point mass at the end-effector is then addressed.

3.2   Dynamic Balancing of Elementary Links

A single pivoted link with mass m_b and center of mass at a distance r_b from pivot O is shown in Figure 3.1. Clearly, a shaking force for any motion, and a shaking moment will act on the frame whenever the link accelerates or decelerates. The shaking force can be eliminated by adding an appropriate counterweight m_c at the extension part of the link to make the linear momentum constant, i.e., the total center of mass is made stationary at the pivot. The shaking moment can be eliminated by adding a separate counter-rotation (e.g., a fixed-axis-geared inertia counterweight in Figure 3.1) with inertia I_c (or effective inertia I_{cr} with respect to pivot O, i.e., $I_{cr} = i_z I_c$ where i_z is

the gear ratio) rotating in the opposite direction of the link to make the total angular momentum constant (zero). Hence, from eqs. (1.3) and (1.4), two sufficient conditions for dynamic balancing of the link can be written as follows:

$$m_b r_b = m_c r_c \tag{3.1}$$

$$I_{cr} = m_b(k_b^2 + r_b^2) + m_c r_c^2 \tag{3.2}$$

where k_b is the radius of gyration of the link with respect to its center of mass.

Under the above conditions, the system will be dynamically balanced, i.e., there is no shaking force and shaking moment on the base. From eqs. (1.1) and (1.2), clearly, the resulting external force and moment are zero. If we consider the whole balanced system as a system isolated from the frame, the external forces and moment are the joint forces ($\mathbf{F}_{bx}, \mathbf{F}_{by}, \mathbf{F}_{cx}, \mathbf{F}_{cy}$) and the actuator driving torque $\mathbf{T}_d$ acting on the system (the tooth force on counter-rotation which generates forces on joints is an internal force). Although the directions of the forces and torque depend on which motion is applied, the zero reaction force and moment on the base always come from: $F_{bx} = F_{cx}, F_{by} = F_{cy}$ and $T_d = dF_{cx}$ (d is the distance between the two joints) and their opposite directions. In other words, the reactions of the individual joint forces act on the frame and constitute a moment to cancel the actuator reaction torque for any motion. Note that in a real prototype the actuator inertia must be taken into account which in fact can be part of the link inertia or the counter-rotation inertia depending on the mounting of the actuator.

Stacking two such links can form a planar two-link open chain (Figure 3.2(a)). The dynamic balancing can be obtained by adding two counterweights and two counter-rotations. Moreover, using two of these chains as legs can synthesize a dynamically balanced five-bar linkage with a special architecture of the parallelogram which allows simplification: instead of four, now three counterweights are used by optimization, and instead of four, only two counter-rotations are sufficient (equal angular velocity of opposite links)(Figures 3.2(b) and 1.5). Two actuators and two counter-rotations can be mounted on the base such that the moving mass and inertia of the system can be reduced.

Finally, a 3-DOF parallelepiped mechanism emerges from appending the third segments that move out of the plane of the planar five-bar parallelogram linkage. Three actuators and three counter-rotations are all mounted on the base.
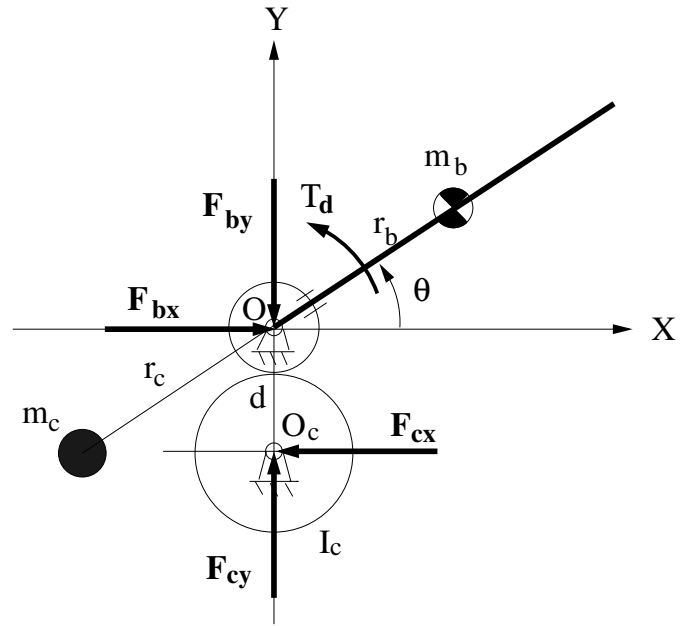
Figure 3.1: Dynamic balancing of a single link.

(a)   (b)
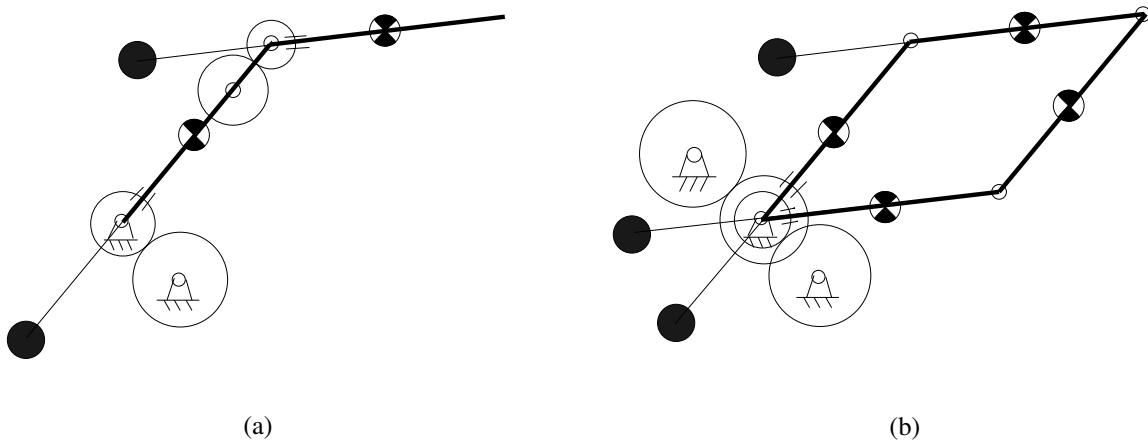
Figure 3.2: Dynamic balancing of elementary links: (a) a planar two-link open chain, (b) a five-bar linkage with parallelogram architecture.
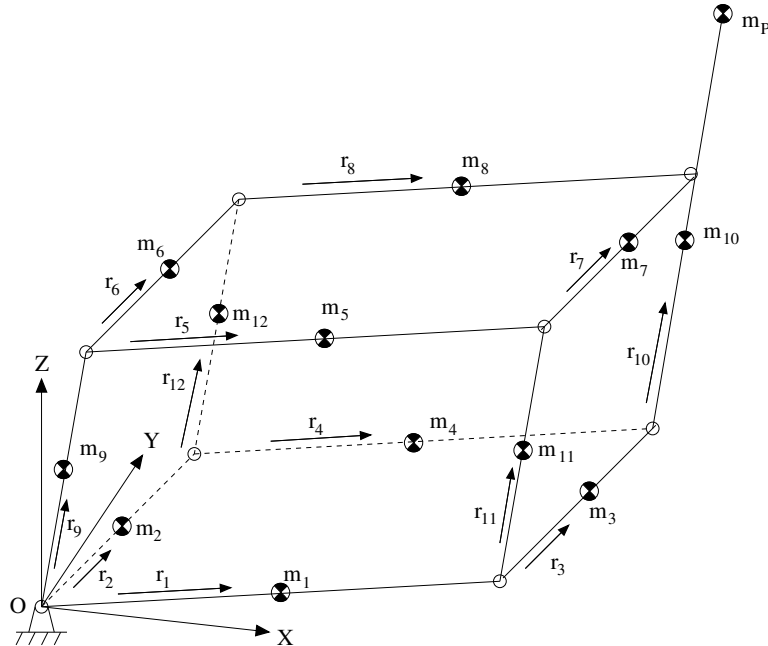
Figure 3.3: Schematic representation for the determination of the balancing conditions.

3.3 Conditions for the 3-DOF Parallelepiped Mechanisms to be Reactionless

A schematic representation for the determination of the balancing conditions for parallelepiped mechanisms is shown in Figure 3.3 (three counter-rotations are not shown on the figure). The center of mass of each edge of the parallelepiped mechanism is assumed to be located on the axis of the corresponding edge. The fixed coordinate frame $OXYZ$ as well as the unit vectors $\mathbf{e}_1, \mathbf{e}_2$ and $\mathbf{e}_3$ are defined as in Section 2.2.

From Figure 3.3, the position vector of the global center of mass of the parallelepiped mechanism, noted $\mathbf{r}$, can be written as

$$
\begin{aligned}
M\mathbf{r} = {} & m_1 r_1 \mathbf{e}_1 + m_2 r_2 \mathbf{e}_2 + m_3(l_1\mathbf{e}_1 + r_3\mathbf{e}_2) + m_4(l_2\mathbf{e}_2 + r_4\mathbf{e}_1) + m_5(l_3\mathbf{e}_3 + r_5\mathbf{e}_1) + \\
& m_6(l_3\mathbf{e}_3 + r_6\mathbf{e}_2) + m_7(l_1\mathbf{e}_1 + l_3\mathbf{e}_3 + r_7\mathbf{e}_2) + m_8(l_3\mathbf{e}_3 + l_2\mathbf{e}_2 + r_8\mathbf{e}_1) + \\
& m_9 r_9 \mathbf{e}_3 + m_{10}(l_1\mathbf{e}_1 + l_2\mathbf{e}_2 + r_{10}\mathbf{e}_3) + m_{11}(l_1\mathbf{e}_1 + r_{11}\mathbf{e}_3) + \\
& m_{12}(l_2\mathbf{e}_2 + r_{12}\mathbf{e}_3) + m_p(l_1\mathbf{e}_1 + l_2\mathbf{e}_2 + (l_3 + l_e)\mathbf{e}_3) \quad (3.3)
\end{aligned}
$$

where r_i is the distance from a vertex to the center of mass of link i, as indicated on the figure, m_p is the point mass located at point P and m_i is the mass of the ith link of the mechanism, as indicated in Figure 3.3, and vectors $\mathbf{e}_i$ are as defined in eqs. (2.2)

and (2.6). Moreover, M is the total mass of the mechanism, i. e.,

$$M = \sum_{i=1}^{12} m_i + m_p \qquad (3.4)$$

Collecting terms in eq. (3.3), one obtains

$$M\mathbf{r} = (m_1 r_1 + m_3 l_1 + m_4 r_4 + m_5 r_5 + m_7 l_1 + m_8 r_8 + m_{10} l_1 + m_{11} l_1 + m_p l_1)\mathbf{e}_1 +$$
$$(m_2 r_2 + m_3 r_3 + m_4 l_2 + m_6 r_6 + m_7 r_7 + m_8 l_2 + m_{10} l_2 + m_{12} l_2 + m_p l_2)\mathbf{e}_2 +$$
$$(m_5 l_3 + m_6 l_3 + m_7 l_3 + m_8 l_3 + m_9 r_9 + m_{10} r_{10} + m_{11} r_{11} + m_{12} r_{12} + m_p(l_3 + l_e))\mathbf{e}_3$$
$$(3.5)$$

From eqs. (1.3) and (3.5), a set of sufficient conditions for force balancing of the mechanism can be written as follows:

$$m_1 r_1 + m_4 r_4 + m_5 r_5 + m_8 r_8 + (m_3 + m_7 + m_{10} + m_{11} + m_p)l_1 = 0 \qquad (3.6)$$

$$m_2 r_2 + m_3 r_3 + m_6 r_6 + m_7 r_7 + (m_4 + m_8 + m_{10} + m_{12} + m_p)l_2 = 0 \qquad (3.7)$$

$$(m_5 + m_6 + m_7 + m_8)l_3 + m_9 r_9 + m_{10} r_{10} + m_{11} r_{11} + m_{12} r_{12} + m_p(l_3 + l_e) = 0 \quad (3.8)$$

Moreover, for case I, the angular momentum of the mechanism can be written as

$$\mathbf{h}_o = \sum_{i=1}^{12} (\mathbf{h}_{gi} + \mathbf{r}_{gi} \times m_i \dot{\mathbf{r}}_{gi}) + \mathbf{r}_p \times m_p \dot{\mathbf{r}}_p - I_{cr1} \dot{\theta}_1 \mathbf{u}_1 - I_{cr2} \dot{\theta}_2 \mathbf{u}_2 - I_{cr3} \dot{\theta}_3 \mathbf{u}_9 \qquad (3.9)$$

where $\mathbf{r}_p$ is the position vector of point P, I_{cri} is the inertia of the counter-rotation connected to the ith actuator — which is added to dynamically balance the mechanism — and $\mathbf{r}_{gi}$ is the position vector of the center of mass of the ith link. Vector $\mathbf{h}_{gi}$ is the angular momentum of the ith link with respect to its center of mass, i.e,

$$\mathbf{h}_{gi} = m_i k_i^2 \dot{\theta}_i \mathbf{u}_i, \quad i = 1, \ldots, 12 \qquad (3.10)$$

where k_i is the radius of gyration of the ith link with respect to its center of mass and, for Case I,

$$\dot{\theta}_i = \dot{\theta}_1, \ \mathbf{u}_i = [0, 0, 1]^T, \quad i = 1, 4, 5, 8;$$
$$\dot{\theta}_i = \dot{\theta}_2, \ \mathbf{u}_i = [0, 0, 1]^T, \quad i = 2, 3, 6, 7;$$
$$\dot{\theta}_i = \dot{\theta}_3, \ \mathbf{u}_i = [1, 0, 0]^T, \quad i = 9, 10, 11, 12$$

The components of $\mathbf{h}_o$ can then be written as

$$h_{ox} = A(\sin\theta_1\cos\theta_3\dot{\theta}_3 - \cos\theta_1\sin\theta_3\dot{\theta}_1) + B(\sin\theta_2\cos\theta_3\dot{\theta}_3 - \cos\theta_2\sin\theta_3\dot{\theta}_2) + F\dot{\theta}_3 \tag{3.11}$$

$$h_{oy} = -A(\sin\theta_1\sin\theta_3\dot{\theta}_1 + \cos\theta_1\cos\theta_3\dot{\theta}_3) - B(\sin\theta_2\sin\theta_3\dot{\theta}_2 + \cos\theta_2\cos\theta_3\dot{\theta}_3) \tag{3.12}$$

$$h_{oz} = A(\sin\theta_1\cos\theta_3\dot{\theta}_1 - \cos\theta_1\sin\theta_3\dot{\theta}_3) + B(\sin\theta_2\cos\theta_3\dot{\theta}_2 - \cos\theta_2\sin\theta_3\dot{\theta}_3) +$$
$$C\cos(\theta_2 - \theta_1)(\dot{\theta}_1 + \dot{\theta}_2) + D\dot{\theta}_1 + E\dot{\theta}_2 \tag{3.13}$$

where

$$A = m_5 l_3 r_5 + m_7 l_1 l_3 + m_8 l_3 r_8 + m_{10} l_1 r_{10} + m_{11} l_1 r_{11} + m_p l_1 (l_3 + l_e) \tag{3.14}$$

$$B = m_6 l_3 r_6 + m_7 l_3 r_7 + m_8 l_2 l_3 + m_{10} l_2 r_{10} + m_{12} l_2 r_{12} + m_p l_2 (l_3 + l_e) \tag{3.15}$$

$$C = m_3 l_1 r_3 + m_4 l_2 r_4 + m_7 l_1 r_7 + m_8 l_2 r_8 + m_{10} l_1 l_2 + m_p l_1 l_2 \tag{3.16}$$

$$D = (m_3 + m_7 + m_{10} + m_{11} + m_p) l_1^2 + m_1(k_1^2 + r_1^2) + m_4(k_4^2 + r_4^2) +$$
$$m_5(k_5^2 + r_5^2) + m_8(k_8^2 + r_8^2) - I_{cr1} \tag{3.17}$$

$$E = (m_4 + m_8 + m_{10} + m_{12} + m_p) l_2^2 + m_2(k_2^2 + r_2^2) + m_3(k_3^2 + r_3^2) +$$
$$m_6(k_6^2 + r_6^2) + m_7(k_7^2 + r_7^2) - I_{cr2} \tag{3.18}$$

$$F = (m_5 + m_6 + m_7 + m_8) l_3^2 + m_p(l_3 + l_e)^2 + m_9(k_9^2 + r_9^2) +$$
$$m_{10}(k_{10}^2 + r_{10}^2) + m_{11}(k_{11}^2 + r_{11}^2) + m_{12}(k_{12}^2 + r_{12}^2) - I_{cr3} \tag{3.19}$$

From eqs. (1.4) and (3.11–3.13), a set of sufficient conditions for moment balancing of the mechanism can be written as $A = B = C = D = E = F = 0$, i. e.,

$$m_5 l_3 r_5 + m_7 l_1 l_3 + m_8 l_3 r_8 + m_{10} l_1 r_{10} + m_{11} l_1 r_{11} + m_p l_1 (l_3 + l_e) = 0 \tag{3.20}$$

$$m_6 l_3 r_6 + m_7 l_3 r_7 + m_8 l_2 l_3 + m_{10} l_2 r_{10} + m_{12} l_2 r_{12} + m_p l_2 (l_3 + l_e) = 0 \tag{3.21}$$

$$m_3 l_1 r_3 + m_4 l_2 r_4 + m_7 l_1 r_7 + m_8 l_2 r_8 + m_{10} l_1 l_2 + m_p l_1 l_2 = 0 \tag{3.22}$$

$$(m_3 + m_7 + m_{10} + m_{11} + m_p) l_1^2 + m_1(k_1^2 + r_1^2) + m_4(k_4^2 + r_4^2) +$$
$$m_5(k_5^2 + r_5^2) + m_8(k_8^2 + r_8^2) - I_{cr1} = 0 \tag{3.23}$$

$$(m_4 + m_8 + m_{10} + m_{12} + m_p) l_2^2 + m_2(k_2^2 + r_2^2) + m_3(k_3^2 + r_3^2) +$$
$$m_6(k_6^2 + r_6^2) + m_7(k_7^2 + r_7^2) - I_{cr2} = 0 \tag{3.24}$$

$$(m_5 + m_6 + m_7 + m_8) l_3^2 + m_p(l_3 + l_e)^2 + m_9(k_9^2 + r_9^2) +$$
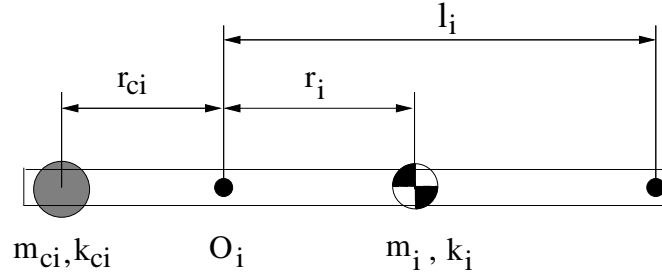
Figure 3.4: Counterweight on the link.

$$m_{10}(k_{10}^2 + r_{10}^2) + m_{11}(k_{11}^2 + r_{11}^2) + m_{12}(k_{12}^2 + r_{12}^2) - I_{cr3} = 0 \qquad (3.25)$$

Hence, any mechanism of type I satisfying eqs. (3.6–3.8) as well as eqs. (3.20–3.25) will be reactionless. Moreover, from eqs. (3.5) and (3.11–3.13), it is found that the global center of mass of the mechanism will be fixed at the origin O of the coordinate frame (i. e., $\mathbf{r} = 0$) and the angular momentum of the mechanism relative to the fixed point O will be zero (i. e., $\mathbf{h}_o = 0$) under the above dynamic balancing conditions.

For case II, the same conditions of static and dynamic balancing are obtained following the same procedure as in Case I. This confirms that the balancing conditions are not dependent on the actuation schemes.

3.4   Optimization

From the equations obtained above for the static and dynamic balancing of the mechanisms it is clear that there exist infinitely many solutions to the equations and that a direct determination of the variables — the masses and positions of counterweights and the magnitude of the counter-rotations — is not straightforward. In other words there are infinitely many reactionless mechanisms available for a given geometry of the parallelepiped mechanisms. Hence, optimization is used in order to obtain better solutions for the counterweights and counter-rotations. The objective of the optimization is to minimize the masses of the counterweights and to locate the center of mass of each link as close as possible to the geometric center of the link. Two different types of objective functions have been used for the optimization of the parallelepiped mechanisms,

namely

$$\min F = \eta_1 \sum_{i=1}^{12}(r_i - 0.5l_i)^2 + \eta_2 \sum_{i=1}^{12} m_i \tag{3.26}$$

or

$$\min F = \sum_{i=1}^{12} m_{ci} r_i^2 \tag{3.27}$$

where η_1 and η_2 are weighting coefficients and m_{ci} is the mass of the counterweight added on the ith link while m_i is the mass of link i including the counterweight (Fig. 3.4). The optimization is subject to the constraint conditions (3.6–3.8) and (3.20–3.22). The masses m_{ci} and positions r_{ci} of counterweights are selected as the variables of the optimization. The resulting mass m_i, position of center of mass r_i and radius of gyration k_i of the ith link can be calculated from the link parameters and the mass and position of the added counterweight on the link (Fig. 3.4) on the assumption of uniform link with a linear density ρ_l (namely, the mass of the origin link is equal to $l_i\rho_l$). The two objectives of the optimization are chosen to minimize the counterweight of a link and to force the resulting center of mass of the link as close as possible to the joint O_i no matter whether the counterweight is located on the original part or extension part of the link, hence to minimize the momentum of the link with respect to the reference point O of the system, finally to minimize the required counter-rotations. This is the optimization of a constrained nonlinear multivariable function. Hence, the function *constr* of the mathematical software Matlab is used for this purpose. This function uses the Sequential Quadratic Programming (SQP) in addition to checking the positivity of the Hessian of the Lagrangian at each major iteration. Since *constr* may only give local solutions, different initial values given randomly were used for the optimization and the best solution was chosen as the optimization result. T he counter-rotations are computed, a posteriori, upon convergence to a solution, by substituting the optimum solution into eqs. (3.23–3.25) and solving for I_{cri}.

An example of optimization is now given. The geometry of the mechanism has been chosen such that

$$l_1 = l_2 = l_3 = 200 \ mm, \ l_e = 100 \ mm, \ m_p = 0.05 \ kg$$

$$\rho_l = 0.211272 \ kg/m$$

and an optimization has been performed using the objective function of eq. (3.27). Since *constr* may only give local solutions, different initial values have been used for

Table 3.1: A numerical example of reactionless spatial 3-DOF parallelepiped mechanism.

Link i	m_i (kg)	r_i (mm)	k_i (mm)
1	1.2437	-92.3	40.3
2	1.0619	-91.0	43.2
3	0.0424	100.0	57.7
4	0.4499	-78.8	62.7
5	0.0424	100.0	57.7
6	0.5105	-81.3	59.4
7	0.0424	100.0	57.7
8	0.0424	100.0	57.7
9	1.2439	-92.3	40.3
10	0.0636	150.0	86.6
11	0.5105	-81.3	59.4
12	0.0424	100.0	57.7
	I_{cr1} $(kgmm^2)$	I_{cr2} $(kgmm^2)$	I_{cr3} $(kgmm^2)$
	46700	43000	50300

the optimization and the best solution was chosen as the optimization result as shown in Table 3.1.

The reactionless example mechanism is represented schematically in Figure 3.5. The three counter-rotations are connected to the actuated bars by transmissions and the magnitudes of the counter-rotations with respect to corresponding axes must be I_{cr1}, I_{cr2} and I_{cr3}.

3.5   Verification of the Reactionless Property

The verification of the reactionless property is performed using the dynamic simulation software ADAMS. For the above example mechanism, simulation models for Case I and Case II respectively are built using ADAMS (Figure 3.6). In the simulation modeling, the joints are defined using revolute joints or spherical joints. However, in order to sim-
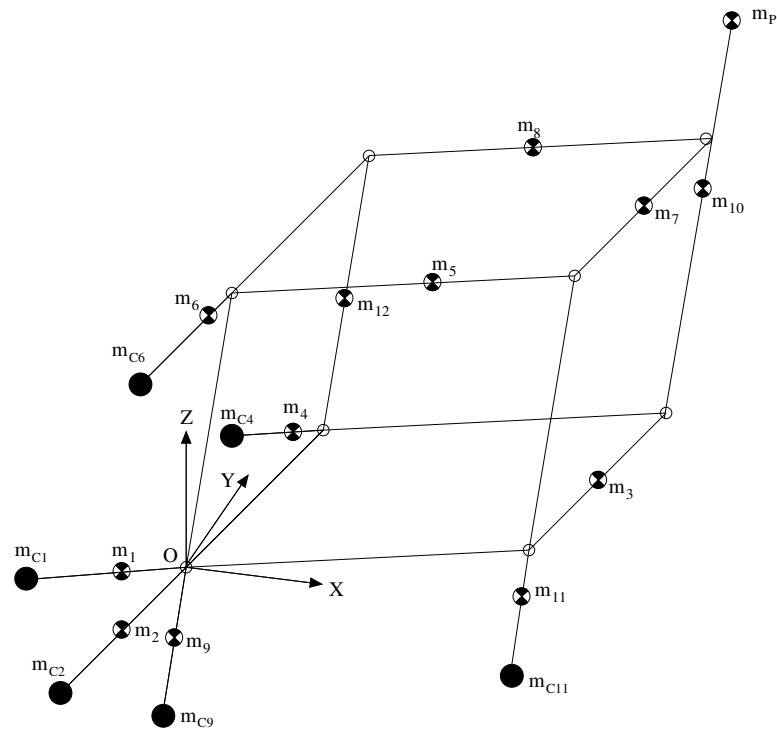
(a) Arrangement of the counterweights.
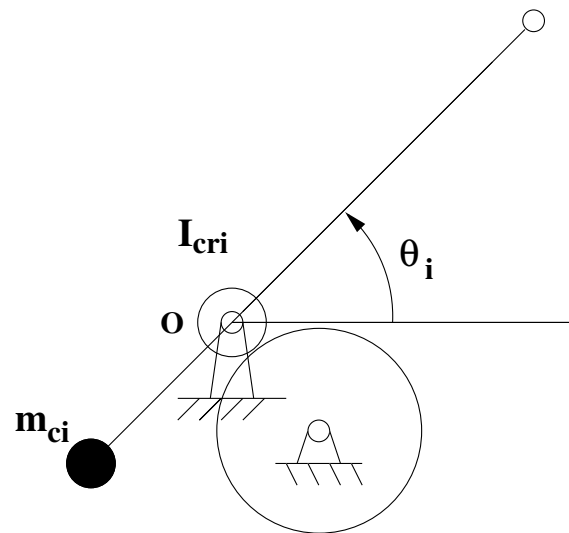
(b) Arrangement of the counter-rotations.

Figure 3.5: Schematic presentation of an example of dynamic balancing.
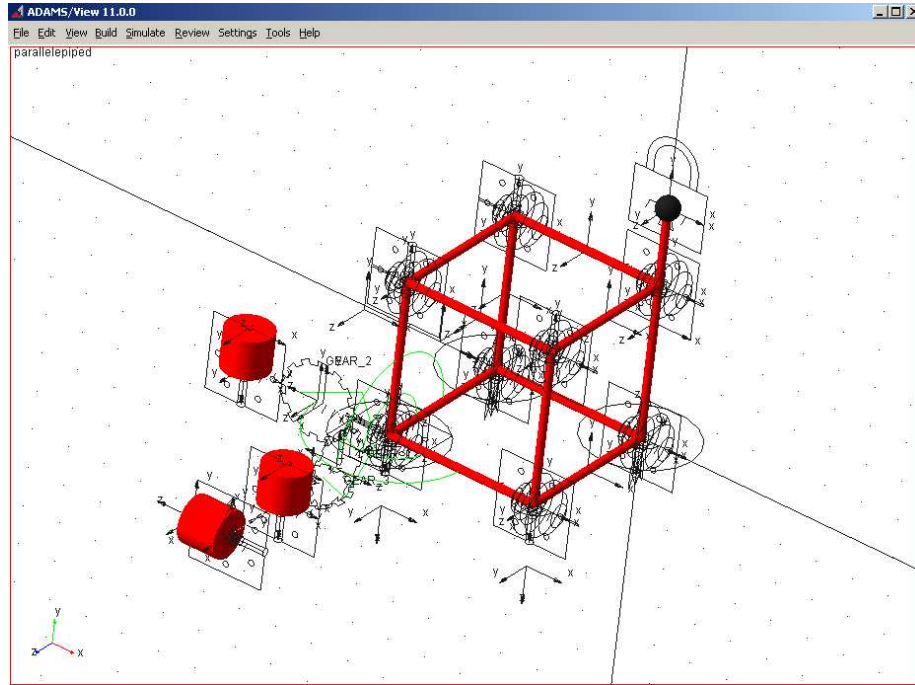
(a) Case I
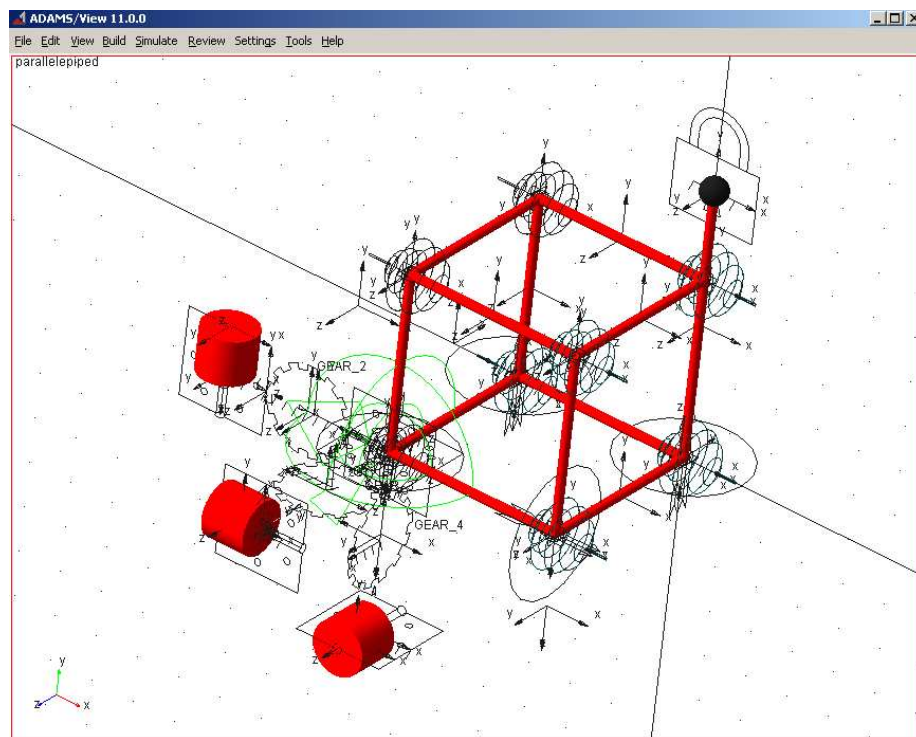
(b) Case II

Figure 3.6: Simulation of 3-DOF parallelepiped mechanisms using ADAMS.
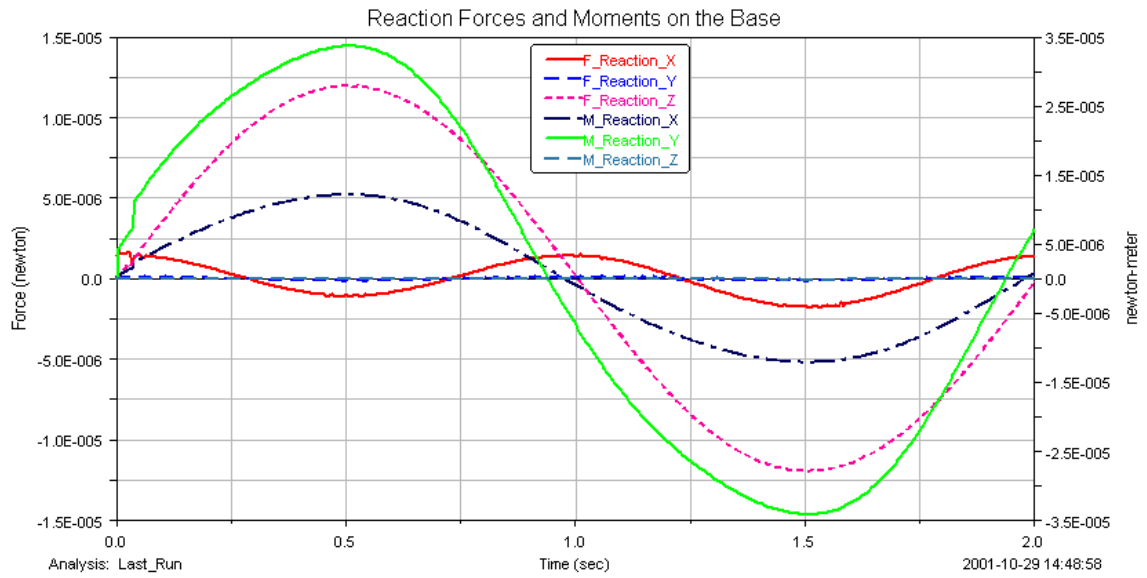
(a) Reaction forces and moments on the base.
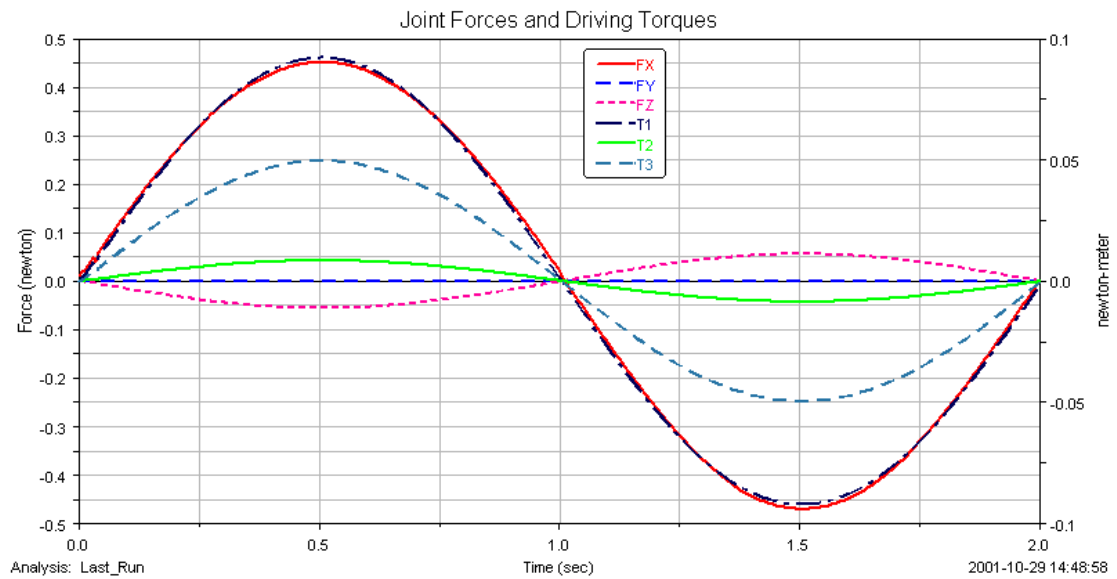
(b) Joint forces and driving torques.

Figure 3.7: Verification of the reactionless property of 3-DOF parallelepiped mechanisms (Case I).
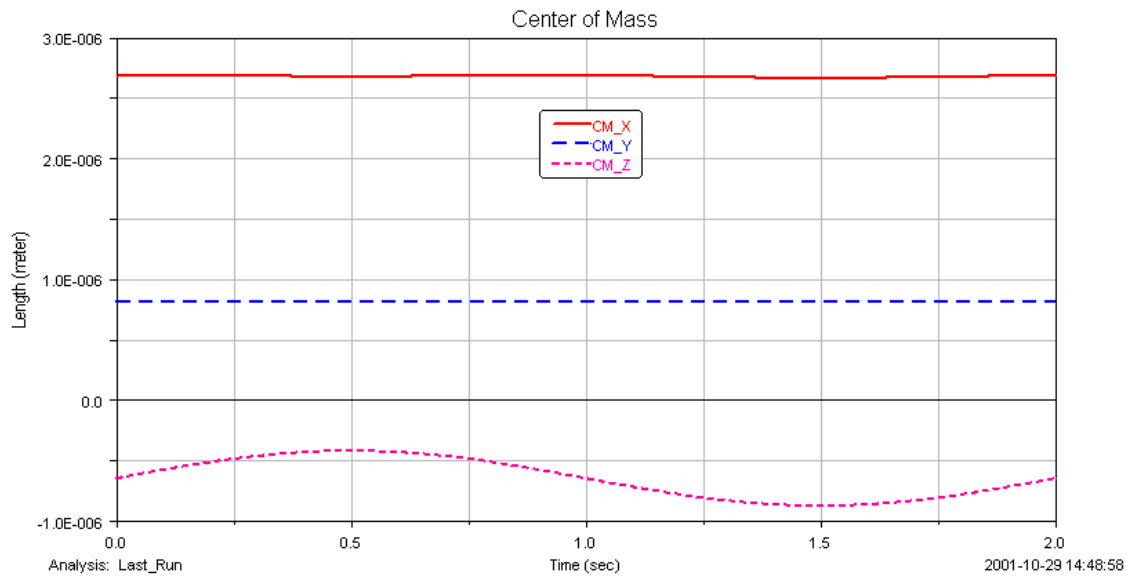
Figure 3.8: Verification of the property of fixed center of mass.
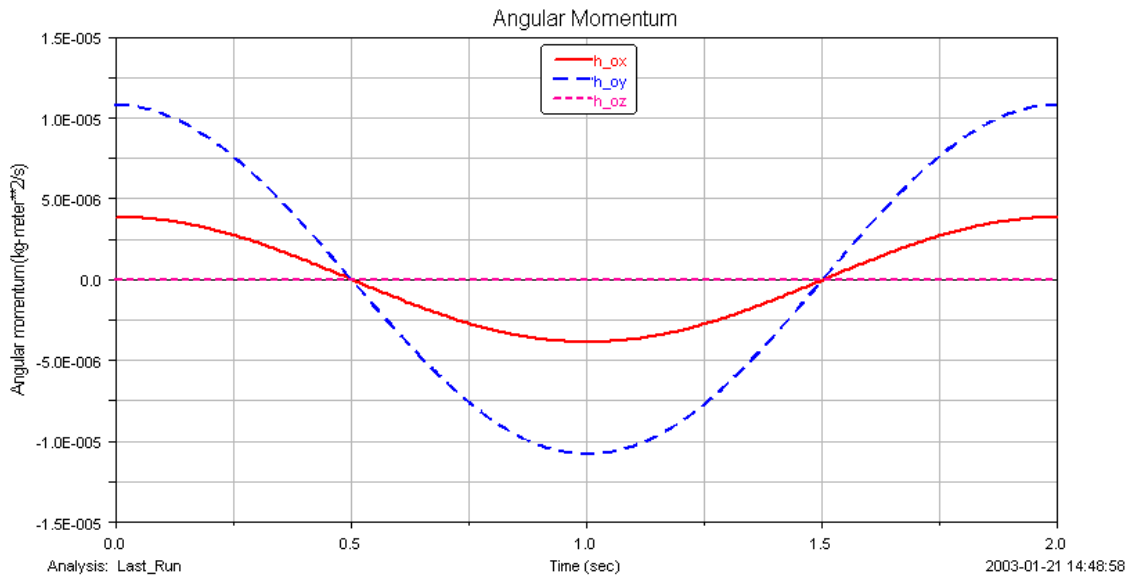
Figure 3.9: Verification of the property of constant angular momentum.
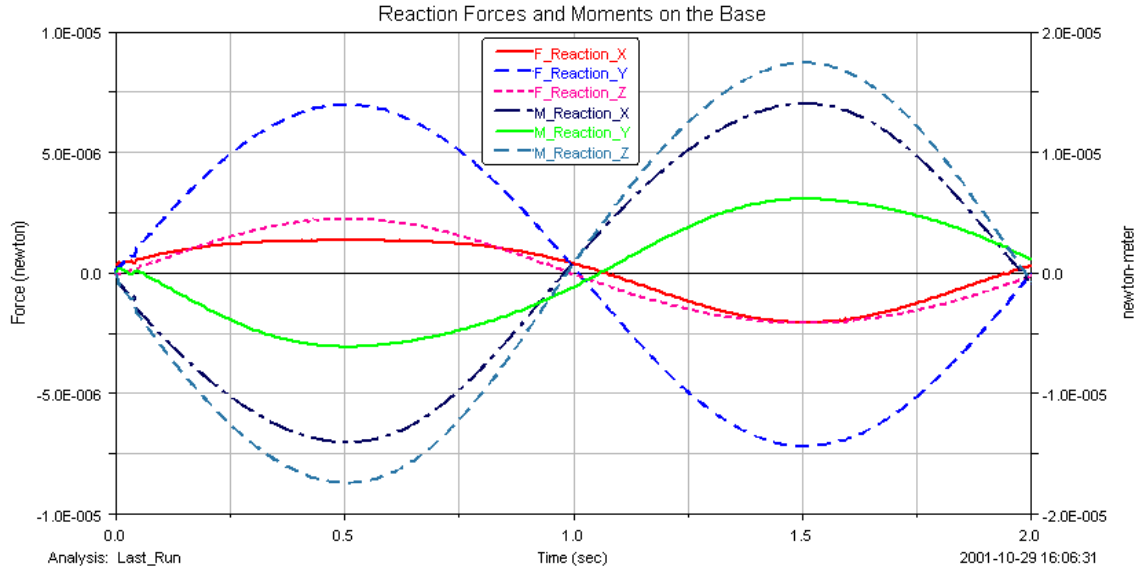
Figure 3.10: Verification of the reactionless property of 3-DOF parallelepiped mechanisms (Case II).

ulate the real motion of the mechanism, some constraints — parallelism between the bars — are also imposed. It has been found that this does not affect the resulting reaction forces and moments on the base in the simulation. The mass, center of mass and moments of inertia of each link which actually include the properties of corresponding counterweights are specified interactively. The three cylinders —with certain moments of inertia and defined as counter-rotations — are fixed on the base and connected respectively to the actuated links by gears. The effective inertia of the counter-rotations with respect to corresponding axes must be equal to the required values.

Simulations have been performed for several arbitrary trajectories. The global reaction forces and moments on the base as well as the forces on the joint connecting the first link with the base and the driving torques of the three actuators for the Case I are illustrated in Figure 3.7. The results clearly demonstrate that the resulting reaction forces and moments on the base are very small compared to the joint forces and driving torques (with a ratio of 10^{-4} to 10^{-5}). Additionally, Figure 3.8 and 3.9 show that the center of mass of the mechanism is fixed and the angular momentum of the mechanism is constant (zero). Indeed, all the non-zero results obtained are most likely due to small modeling errors arising from the limited number of digits used in ADAMS for the parameters.

For the example mechanism of Case II, similar results have been obtained. The reaction forces and moments on the base are illustrated in Figure 3.10.

Hence, it is clearly shown that the 3-DOF parallelepiped mechanisms can be completely balanced. In other words, there are no reaction forces and moments on the base at all times and for arbitrary trajectories.

3.6 A Practical Implementation of 3-DOF Parallelepiped Mechanisms

3.6.1 Description of the Mechanisms

As mentioned before, several feasible designs can be proposed for the parallelepiped mechanisms (Figure 2.2). Moreover, it is found that half of the parallelepiped mechanism — with three instead of six faces — has the same function as the parallelepiped. The CAD models and schematic representations of a practical implementation of the parallelepiped mechanisms for Case I and Case II are shown in Figure 3.11 and Figure 3.12 respectively.

In Case I, the bottom face consists of a planar 5-bar linkage connected by revolute joints. The offset in the linkage is designed for the mounting of the two actuators which drive the edges V_1 and V_2 (Figure 2.2) respectively. The side face consists of a 6-bar linkage connected by a spherical joint (D) and revolute joints (G, C, I, M and O). Similar joint designs are used for the third face. Notice that all the axes of the revolute joints at a vertex intersect at the vertex center point. Furthermore, $OA = CB = HF, OC = AB = DG, OD = CG, CH = BF$ (see Figure 3.11). The three actuators are fixed to the base. Then, the mechanism can be deformed with the faces remaining planar and can be used to position the end-effector.

In Case II, the bottom face consists of a spatial 8-bar linkage connected by spherical joint (A) and revolute joints (N, J, R, I, M, W and V). The side face consists of a 6-bar linkage connected by a spherical joint (D) and revolute joints (G, C, I, M, W and U). The third face also consists of a 6-bar linkage with a spherical joint (H) and revolute
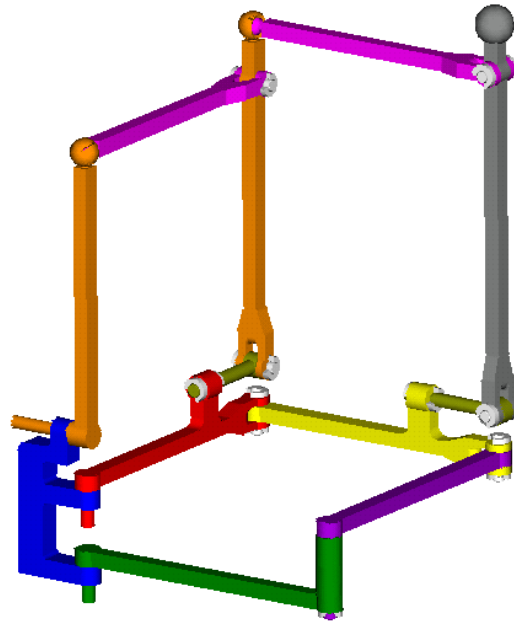
(a) CAD model.
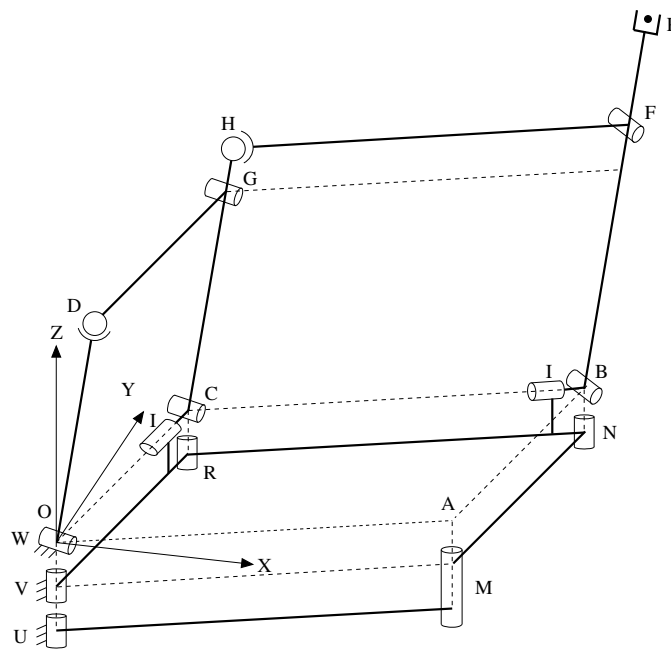
(b) Schematic representation.

Figure 3.11: CAD model and schematic representation of a practical implementation of 3-DOF parallelepiped mechanisms (Case I).
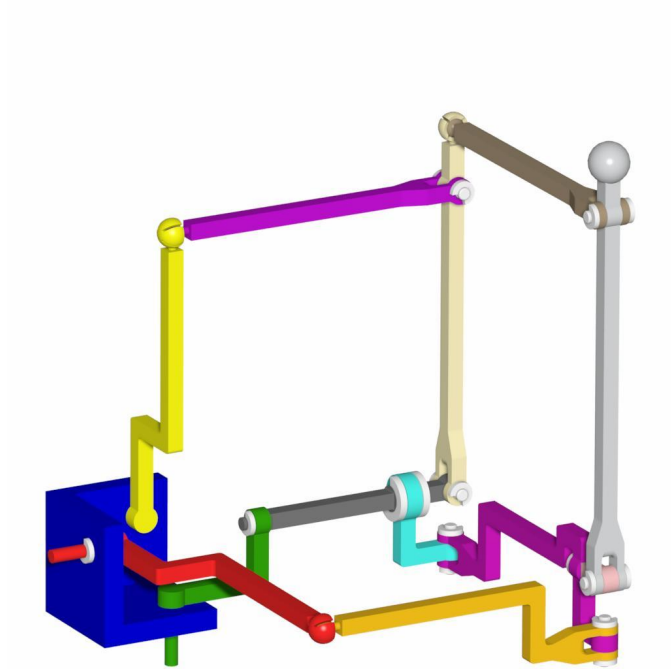
(a) CAD model.
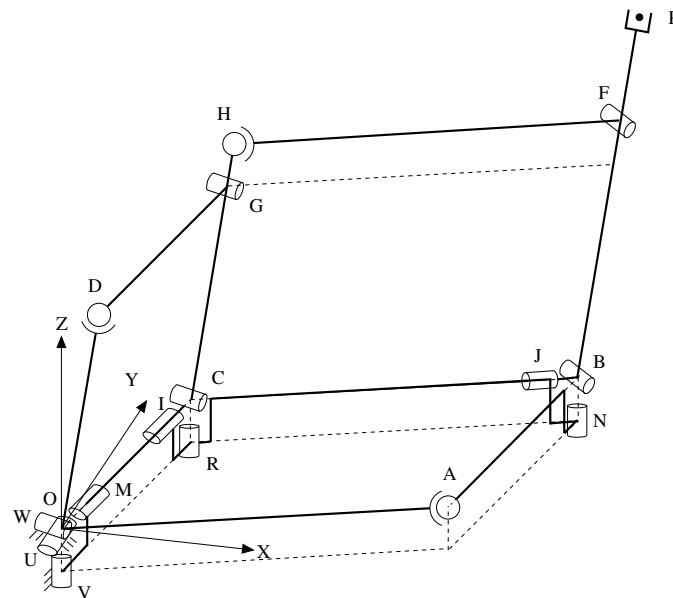
(b) Schematic representation.

Figure 3.12: CAD model and schematic representation of a practical implementation of 3-DOF parallelepiped mechanisms (Case II).
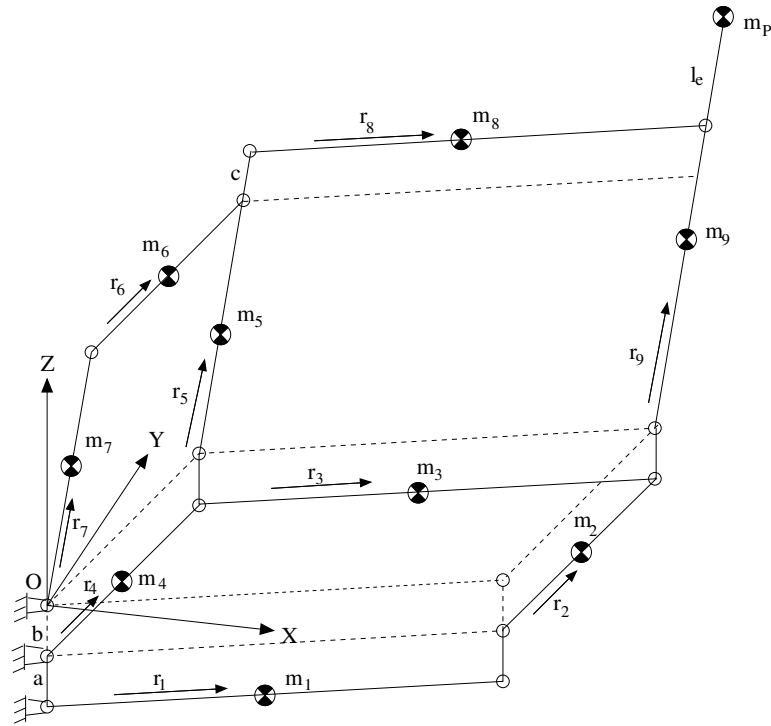
Figure 3.13: Schematic representation for the determination of the balancing conditions for the practical parallelepiped mechanisms (Case I).

joints (F, B, J, R and C). All the axes of the revolute joints at a vertex intersect at the vertex center point (e.g., the three actuated revolute joints (U, V, W) intersect at point O). Moreover, the equality of the length for the corresponding links are defined as in Case I. Then, the mechanism realizes the mobility and kinematics of the parallelepiped of Case II (Figure 2.2).

Clearly, the kinematics of practical parallelepiped mechanisms (Figure 3.11 and 3.12) is identical to that of parallelepiped mechanisms (Figure 2.2) for Case I and II respectively. Hence, all the results of the kinematic analysis obtained in Chapter 2 can be used for the practical parallelepiped mechanisms.

3.6.2 Reactionless Conditions for the Practical 3-DOF Parallelepiped Mechanisms

A schematic representation for the determination of the balancing conditions for the practical parallelepiped mechanism of Case I (Figure 3.11) is shown in Figure 3.13 where a and $(a + b)$ are the offsets of the moving plane of two actuators relative to the origin point O. The center of mass of each link is assumed to lie on the axis of the link. All the terms are defined as in Section 3.2.

From Figure 3.13, the position vector of the global center of mass of the parallelepiped mechanism, noted $\mathbf{r}$, can be written as

$$M\mathbf{r} = m_1(r_1\mathbf{e}_1 - (a + b)\mathbf{e}_z) + m_2(l_1\mathbf{e}_1 + r_2\mathbf{e}_2 - b\mathbf{e}_z) +$$
$$m_3(l_2\mathbf{e}_2 + r_3\mathbf{e}_1 - b\mathbf{e}_z) + m_4(r_4\mathbf{e}_2 - b\mathbf{e}_z) + m_5(l_2\mathbf{e}_2 + r_5\mathbf{e}_3) +$$
$$m_6((l_3 - c)\mathbf{e}_3 + r_6\mathbf{e}_2) + m_7r_7\mathbf{e}_3 + m_8(l_2\mathbf{e}_2 + l_3\mathbf{e}_3 + r_8\mathbf{e}_1) +$$
$$m_9(l_1\mathbf{e}_1 + l_2\mathbf{e}_2 + r_9\mathbf{e}_3) + m_p(l_1\mathbf{e}_1 + l_2\mathbf{e}_2 + (l_3 + l_e)\mathbf{e}_3) \tag{3.28}$$

where M is the total mass of the mechanism, i. e.,

$$M = \sum_{i=1}^{9} m_i + m_p \tag{3.29}$$

and vectors $\mathbf{e}_i$ are defined as follows:

$$\mathbf{e}_1 = \begin{bmatrix} \cos\theta_1 \\ \sin\theta_1 \\ 0 \end{bmatrix}, \quad \mathbf{e}_2 = \begin{bmatrix} \cos\theta_2 \\ \sin\theta_2 \\ 0 \end{bmatrix}, \quad \mathbf{e}_3 = \begin{bmatrix} 0 \\ \cos\theta_3 \\ \sin\theta_3 \end{bmatrix}, \quad \mathbf{e}_z = \begin{bmatrix} 0 \\ 0 \\ 1 \end{bmatrix} \tag{3.30}$$

Collecting terms in eq. (3.28), one obtains

$$M\mathbf{r} = (m_1r_1 + m_2l_1 + m_3r_3 + m_8r_8 + m_9l_1 + m_pl_1)\mathbf{e}_1 +$$
$$(m_2r_2 + m_3l_2 + m_4r_4 + m_5l_2 + m_6r_6 + m_8l_2 + m_9l_2 + m_pl_2)\mathbf{e}_2 +$$
$$(m_5r_5 + m_6(l_3 - c) + m_7r_7 + m_8l_3 + m_9r_9 + m_p(l_3 + l_e))\mathbf{e}_3 -$$
$$(m_1(a + b) + m_2b + m_3b + m_4b)\mathbf{e}_z \tag{3.31}$$

From eqs. (1.3) and (3.31), a set of sufficient conditions for force balancing of the mechanism can be written as follows:

$$m_1r_1 + m_3r_3 + m_8r_8 + (m_2 + m_9 + m_p)l_1 = 0 \tag{3.32}$$

$$m_2r_2 + m_4r_4 + m_6r_6 + (m_3 + m_5 + m_8 + m_9 + m_p)l_2 = 0 \tag{3.33}$$

$$m_5 r_5 + m_6(l_3 - c) + m_7 r_7 + m_8 l_3 + m_9 r_9 + m_p(l_3 + l_e) = 0 \qquad (3.34)$$

Under the above force balancing conditions, the global center of mass is fixed at

$$\mathbf{r} = \frac{m_1(a + b) + (m_2 + m_3 + m_4)b}{M} \mathbf{e}_z \qquad (3.35)$$

Moreover, the angular momentum of the mechanism can be written as

$$\mathbf{h}_o = \sum_{i=1}^{9}(\mathbf{h}_{gi} + \mathbf{r}_{gi} \times m_i \dot{\mathbf{r}}_{gi}) + \mathbf{r}_p \times m_p \dot{\mathbf{r}}_p - I_{cr1}\dot{\theta}_1 \mathbf{u}_1 - I_{cr2}\dot{\theta}_2 \mathbf{u}_4 - I_{cr3}\dot{\theta}_3 \mathbf{u}_7 \qquad (3.36)$$

where

$$\mathbf{h}_{gi} = m_i k_i^2 \dot{\theta}_i \mathbf{u}_i, \quad i = 1, \ldots, 9 \qquad (3.37)$$

$$\dot{\theta}_i = \dot{\theta}_1, \ \mathbf{u}_i = [\,0, 0, 1\,]^T, \quad i = 1, 3, 8;$$
$$\dot{\theta}_i = \dot{\theta}_2, \ \mathbf{u}_i = [\,0, 0, 1\,]^T, \quad i = 2, 4, 6;$$
$$\dot{\theta}_i = \dot{\theta}_3, \ \mathbf{u}_i = [\,1, 0, 0\,]^T, \quad i = 5, 7, 9$$

Hence, the angular momentum of the mechanism can be written in detail as follows:

$$\begin{aligned}
\mathbf{h}_o \ = \ & m_1 k_1^2 \dot{\theta}_1 \mathbf{u}_1 + m_1(r_1 \mathbf{e}_1 - (a + b)\mathbf{e}_z) \times r_1 \dot{\mathbf{e}}_1 + \\
& m_2 k_2^2 \dot{\theta}_2 \mathbf{u}_2 + m_2(l_1 \mathbf{e}_1 + r_2 \mathbf{e}_2 - b\mathbf{e}_z) \times (l_1 \dot{\mathbf{e}}_1 + r_2 \dot{\mathbf{e}}_2) + \\
& m_3 k_3^2 \dot{\theta}_1 \mathbf{u}_3 + m_3(l_2 \mathbf{e}_2 + r_3 \mathbf{e}_1 - b\mathbf{e}_z) \times (l_2 \dot{\mathbf{e}}_2 + r_3 \dot{\mathbf{e}}_1) + \\
& m_4 k_4^2 \dot{\theta}_2 \mathbf{u}_4 + m_4(r_4 \mathbf{e}_2 - b\mathbf{e}_z) \times r_4 \dot{\mathbf{e}}_2 + \\
& m_5 k_5^2 \dot{\theta}_3 \mathbf{u}_5 + m_5(l_2 \mathbf{e}_2 + r_5 \mathbf{e}_3) \times (l_2 \dot{\mathbf{e}}_2 + r_5 \dot{\mathbf{e}}_3) + \\
& m_6 k_6^2 \dot{\theta}_2 \mathbf{u}_6 + m_6((l_3 - c)\mathbf{e}_3 + r_6 \mathbf{e}_2) \times ((l_3 - c)\dot{\mathbf{e}}_3 + r_6 \dot{\mathbf{e}}_2) + \\
& m_7 k_7^2 \dot{\theta}_3 \mathbf{u}_7 + m_7 r_7 \mathbf{e}_3 \times r_7 \dot{\mathbf{e}}_3 + \\
& m_8 k_8^2 \dot{\theta}_1 \mathbf{u}_8 + m_8(l_2 \mathbf{e}_2 + l_3 \mathbf{e}_3 + r_8 \mathbf{e}_1) \times (l_2 \dot{\mathbf{e}}_2 + l_3 \dot{\mathbf{e}}_3 + r_8 \dot{\mathbf{e}}_1) + \\
& m_9 k_9^2 \dot{\theta}_3 \mathbf{u}_9 + m_9(l_1 \mathbf{e}_1 + l_2 \mathbf{e}_2 + r_9 \mathbf{e}_3) \times (l_1 \dot{\mathbf{e}}_1 + l_2 \dot{\mathbf{e}}_2 + r_9 \dot{\mathbf{e}}_3) + \\
& m_p(l_1 \mathbf{e}_1 + l_2 \mathbf{e}_2 + (l_3 + l_e)\mathbf{e}_3) \times (l_1 \dot{\mathbf{e}}_1 + l_2 \dot{\mathbf{e}}_2 + (l_3 + l_e)\dot{\mathbf{e}}_3) \\
& - I_{cr1}\dot{\theta}_1 \mathbf{u}_1 - I_{cr2}\dot{\theta}_2 \mathbf{u}_4 - I_{cr3}\dot{\theta}_3 \mathbf{u}_7 \qquad (3.38)
\end{aligned}$$

Furthermore, one has

$$\mathbf{e}_1 \times \dot{\mathbf{e}}_1 = \dot{\theta}_1 \begin{bmatrix} 0 \\ 0 \\ 1 \end{bmatrix}, \quad \mathbf{e}_2 \times \dot{\mathbf{e}}_2 = \dot{\theta}_2 \begin{bmatrix} 0 \\ 0 \\ 1 \end{bmatrix}, \quad \mathbf{e}_3 \times \dot{\mathbf{e}}_3 = \dot{\theta}_3 \begin{bmatrix} 1 \\ 0 \\ 0 \end{bmatrix},$$

$$\mathbf{e}_1 \times \dot{\mathbf{e}}_2 = \dot{\theta}_2 \begin{bmatrix} 0 \\ 0 \\ \cos(\theta_2 - \theta_1) \end{bmatrix}, \quad \mathbf{e}_2 \times \dot{\mathbf{e}}_1 = \dot{\theta}_1 \begin{bmatrix} 0 \\ 0 \\ \cos(\theta_2 - \theta_1) \end{bmatrix},$$

$$\mathbf{e}_1 \times \dot{\mathbf{e}}_3 = \dot{\theta}_3 \begin{bmatrix} \sin\theta_1 \cos\theta_3 \\ -\cos\theta_1 \cos\theta_3 \\ -\cos\theta_1 \sin\theta_3 \end{bmatrix}, \quad \mathbf{e}_3 \times \dot{\mathbf{e}}_1 = \dot{\theta}_1 \begin{bmatrix} -\cos\theta_1 \sin\theta_3 \\ -\sin\theta_1 \sin\theta_3 \\ \sin\theta_1 \cos\theta_3 \end{bmatrix},$$

$$\mathbf{e}_2 \times \dot{\mathbf{e}}_3 = \dot{\theta}_3 \begin{bmatrix} \sin\theta_2 \cos\theta_3 \\ -\cos\theta_2 \cos\theta_3 \\ -\cos\theta_2 \sin\theta_3 \end{bmatrix}, \quad \mathbf{e}_3 \times \dot{\mathbf{e}}_2 = \dot{\theta}_2 \begin{bmatrix} -\cos\theta_2 \sin\theta_3 \\ -\sin\theta_2 \sin\theta_3 \\ \sin\theta_2 \cos\theta_3 \end{bmatrix},$$

$$\mathbf{e}_z \times \dot{\mathbf{e}}_1 = \dot{\theta}_1 \begin{bmatrix} -\cos\theta_1 \\ -\sin\theta_1 \\ 0 \end{bmatrix}, \quad \mathbf{e}_z \times \dot{\mathbf{e}}_2 = \dot{\theta}_2 \begin{bmatrix} -\cos\theta_2 \\ -\sin\theta_2 \\ 0 \end{bmatrix} \tag{3.39}$$

The components of $\mathbf{h}_o$ can then be written as

$$\begin{aligned} h_{ox} &= A(\sin\theta_1 \cos\theta_3 \dot{\theta}_3 - \cos\theta_1 \sin\theta_3 \dot{\theta}_1) + B(\sin\theta_2 \cos\theta_3 \dot{\theta}_3 - \\ & \quad \cos\theta_2 \sin\theta_3 \dot{\theta}_2) + D\cos\theta_1 \dot{\theta}_1 + E\cos\theta_2 \dot{\theta}_2 + H\dot{\theta}_3 \end{aligned} \tag{3.40}$$

$$\begin{aligned} h_{oy} &= -A(\sin\theta_1 \sin\theta_3 \dot{\theta}_1 + \cos\theta_1 \cos\theta_3 \dot{\theta}_3) - B(\sin\theta_2 \sin\theta_3 \dot{\theta}_2 + \\ & \quad \cos\theta_2 \cos\theta_3 \dot{\theta}_3) + D\sin\theta_1 \dot{\theta}_1 + E\sin\theta_2 \dot{\theta}_2 \end{aligned} \tag{3.41}$$

$$\begin{aligned} h_{oz} &= A(\sin\theta_1 \cos\theta_3 \dot{\theta}_1 - \cos\theta_1 \sin\theta_3 \dot{\theta}_3) + B(\sin\theta_2 \cos\theta_3 \dot{\theta}_2 - \\ & \quad \cos\theta_2 \sin\theta_3 \dot{\theta}_3) + C\cos(\theta_2 - \theta_1)(\dot{\theta}_1 + \dot{\theta}_2) + F\dot{\theta}_1 + G\dot{\theta}_2 \end{aligned} \tag{3.42}$$

where

$$A = m_8 l_3 r_8 + m_9 l_1 r_9 + m_p l_1 (l_3 + l_e) \tag{3.43}$$

$$B = m_5 l_2 r_5 + m_6 (l_3 - c) r_6 + m_8 l_2 l_3 + m_9 l_2 r_9 + m_p l_2 (l_3 + l_e) \tag{3.44}$$

$$C = m_2 l_1 r_2 + m_3 l_2 r_3 + m_8 l_2 r_8 + m_9 l_1 l_2 + m_p l_1 l_2 \tag{3.45}$$

$$D = m_1 r_1 (a + b) + m_2 l_1 b + m_3 r_3 b \tag{3.46}$$

$$E = m_2 r_2 + m_3 l_2 + m_4 r_4 \tag{3.47}$$

$$\begin{aligned} F &= (m_2 + m_9 + m_p) l_1^2 + m_1 (k_1^2 + r_1^2) + m_3 (k_3^2 + r_3^2) + \\ & \quad m_8 (k_8^2 + r_8^2) - I_{cr1} \end{aligned} \tag{3.48}$$

$$\begin{aligned} G &= (m_3 + m_5 + m_8 + m_9 + m_p) l_2^2 + m_2 (k_2^2 + r_2^2) + \\ & \quad m_4 (k_4^2 + r_4^2) + m_6 (k_6^2 + r_6^2) - I_{cr2} \end{aligned} \tag{3.49}$$

$$\begin{aligned} H &= m_6 (l_3 - c)^2 + m_8 l_3^2 + m_p (l_3 + l_e)^2 + m_5 (k_5^2 + r_5^2) + \\ & \quad m_7 (k_7^2 + r_7^2) + m_9 (k_9^2 + r_9^2) - I_{cr3} \end{aligned} \tag{3.50}$$

From eqs. (1.4) and (3.40–3.42), a set of sufficient conditions for moment balancing of the mechanism can be written as $A = B = C = D = E = F = G = H = 0$, i. e.,

$$m_8 l_3 r_8 + m_9 l_1 r_9 + m_p l_1 (l_3 + l_e) = 0 \tag{3.51}$$

$$m_5 l_2 r_5 + m_6 (l_3 - c) r_6 + m_8 l_2 l_3 + m_9 l_2 r_9 + m_p l_2 (l_3 + l_e) = 0 \tag{3.52}$$

$$m_2 l_1 r_2 + m_3 l_2 r_3 + m_8 l_2 r_8 + m_9 l_1 l_2 + m_p l_1 l_2 = 0 \tag{3.53}$$

$$m_1 r_1 (a + b) + m_2 l_1 b + m_3 r_3 b = 0 \tag{3.54}$$

$$m_2 r_2 + m_3 l_2 + m_4 r_4 = 0 \tag{3.55}$$

$$(m_2 + m_9 + m_p) l_1^2 + m_1 (k_1^2 + r_1^2) + m_3 (k_3^2 + r_3^2) + m_8 (k_8^2 + r_8^2) - I_{cr1} = 0 \tag{3.56}$$

$$(m_3 + m_5 + m_8 + m_9 + m_p) l_2^2 + m_2 (k_2^2 + r_2^2) + m_4 (k_4^2 + r_4^2) + \\ m_6 (k_6^2 + r_6^2) - I_{cr2} = 0 \tag{3.57}$$

$$m_6 (l_3 - c)^2 + m_8 l_3^2 + m_p (l_3 + l_e)^2 + m_5 (k_5^2 + r_5^2) + m_7 (k_7^2 + r_7^2) + \\ m_9 (k_9^2 + r_9^2) - I_{cr3} = 0 \tag{3.58}$$

Hence, any mechanism of type I (Figure 3.11) satisfying eqs. (3.32–3.34) as well as eqs. (3.51–3.58) will be reactionless. The global center of mass will then be fixed as presented in eq. (3.35) and the angular momentum of the mechanism with respect to point O will be zero.

For the practical parallelepiped mechanism of Case II (Figure 3.12), a schematic representation of the mechanisms for the determination of the balancing conditions is shown in Figure 3.14. The center of mass of each link is also assumed to lie on the axis of the link.

From Figure 3.14, the position vector of the global center of mass of the parallelepiped mechanism, noted $\mathbf{r}$, can be written as

$$M\mathbf{r} = m_1 r_1 \mathbf{e}_1 + m_2 (l_1 \mathbf{e}_1 + r_2 \mathbf{e}_2) + m_3 (l_2 \mathbf{e}_2 + r_3 \mathbf{e}_1) + m_4 r_4 \mathbf{e}_2 + \\ m_5 (l_2 \mathbf{e}_2 + r_5 \mathbf{e}_3) + m_6 ((l_3 - c) \mathbf{e}_3 + r_6 \mathbf{e}_2) + m_7 r_7 \mathbf{e}_3 + m_8 (l_2 \mathbf{e}_2 + l_3 \mathbf{e}_3 + r_8 \mathbf{e}_1) +$$
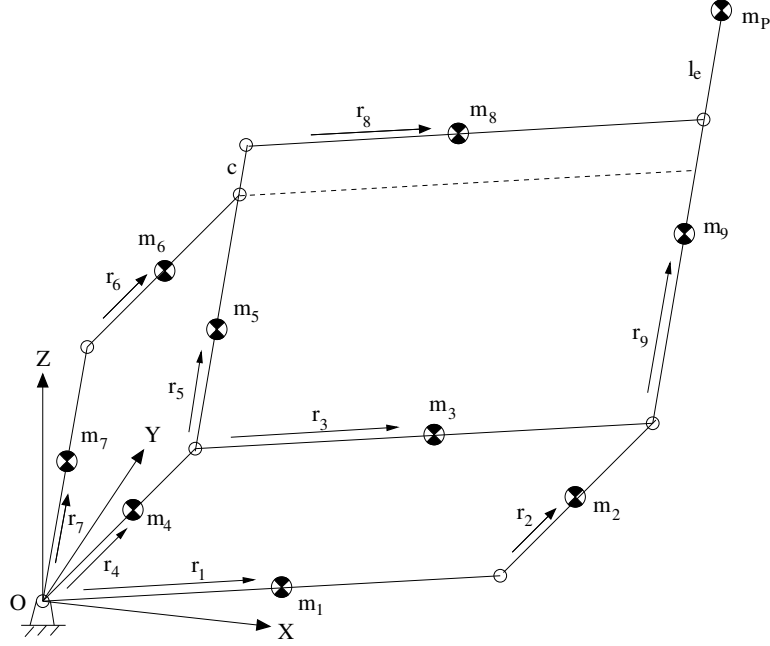
Figure 3.14: Schematic representation for the determination of the balancing conditions for the practical parallelepiped mechanisms (Case II).

$$m_9(l_1\mathbf{e}_1 + l_2\mathbf{e}_2 + r_9\mathbf{e}_3) + m_p(l_1\mathbf{e}_1 + l_2\mathbf{e}_2 + (l_3 + l_e)\mathbf{e}_3) \quad (3.59)$$

where vectors $\mathbf{e}_i$ are defined as follows:

$$\mathbf{e}_1 = \begin{bmatrix} \sin\theta_1 \\ 0 \\ \cos\theta_1 \end{bmatrix}, \ \mathbf{e}_2 = \begin{bmatrix} \cos\theta_2 \\ \sin\theta_2 \\ 0 \end{bmatrix}, \ \mathbf{e}_3 = \begin{bmatrix} 0 \\ \cos\theta_3 \\ \sin\theta_3 \end{bmatrix} \quad (3.60)$$

Collecting terms in eq. (3.59), one obtains

$$M\mathbf{r} = (m_1 r_1 + m_2 l_1 + m_3 r_3 + m_8 r_8 + m_9 l_1 + m_p l_1)\mathbf{e}_1 +$$
$$(m_2 r_2 + m_3 l_2 + m_4 r_4 + m_5 l_2 + m_6 r_6 + m_8 l_2 + m_9 l_2 + m_p l_2)\mathbf{e}_2 +$$
$$(m_5 r_5 + m_6(l_3 - c) + m_7 r_7 + m_8 l_3 + m_9 r_9 + m_p(l_3 + l_e))\mathbf{e}_3 \quad (3.61)$$

From eqs. (1.3) and (3.61), a set of sufficient conditions for force balancing of the mechanism can be written as follows:

$$m_1 r_1 + m_3 r_3 + m_8 r_8 + (m_2 + m_9 + m_p)l_1 = 0 \quad (3.62)$$

$$m_2 r_2 + m_4 r_4 + m_6 r_6 + (m_3 + m_5 + m_8 + m_9 + m_p)l_2 = 0 \quad (3.63)$$

$$m_5 r_5 + m_6(l_3 - c) + m_7 r_7 + m_8 l_3 + m_9 r_9 + m_p(l_3 + l_e) = 0 \quad (3.64)$$

Moreover, for case II, the angular momentum of the mechanism can be written as

$$\mathbf{h}_o = \sum_{i=1}^{9}(\mathbf{h}_{gi} + \mathbf{r}_{gi} \times m_i \dot{\mathbf{r}}_{gi}) + \mathbf{r}_p \times m_p \dot{\mathbf{r}}_p - I_{cr1}\dot{\theta}_1 \mathbf{u}_1 - I_{cr2}\dot{\theta}_2 \mathbf{u}_4 - I_{cr3}\dot{\theta}_3 \mathbf{u}_7 \qquad (3.65)$$

where the angular momentum $\mathbf{h}_{gi}$ of the ith link with respect to its center of mass can be written as

$$\mathbf{h}_{gi} = m_i k_i^2 \dot{\theta}_i \mathbf{u}_i, \quad i = 1, \ldots, 9 \qquad (3.66)$$

where

$$\dot{\theta}_i = \dot{\theta}_1, \ \mathbf{u}_i = [\,0, 1, 0\,]^T, \quad i = 1, 3, 8;$$
$$\dot{\theta}_i = \dot{\theta}_2, \ \mathbf{u}_i = [\,0, 0, 1\,]^T, \quad i = 2, 4, 6;$$
$$\dot{\theta}_i = \dot{\theta}_3, \ \mathbf{u}_i = [\,1, 0, 0\,]^T, \quad i = 5, 7, 9$$

Hence, the angular momentum of the mechanism can be written in detail as follows:

$$
\begin{aligned}
\mathbf{h}_o = \ & m_1 k_1^2 \dot{\theta}_1 \mathbf{u}_1 + m_1 r_1 \mathbf{e}_1 \times r_1 \dot{\mathbf{e}}_1 + \\
& m_2 k_2^2 \dot{\theta}_2 \mathbf{u}_2 + m_2 (l_1 \mathbf{e}_1 + r_2 \mathbf{e}_2) \times (l_1 \dot{\mathbf{e}}_1 + r_2 \dot{\mathbf{e}}_2) + \\
& m_3 k_3^2 \dot{\theta}_1 \mathbf{u}_3 + m_3 (l_2 \mathbf{e}_2 + r_3 \mathbf{e}_1) \times (l_2 \dot{\mathbf{e}}_2 + r_3 \dot{\mathbf{e}}_1) + \\
& m_4 k_4^2 \dot{\theta}_2 \mathbf{u}_4 + m_4 r_4 \mathbf{e}_2 \times r_4 \dot{\mathbf{e}}_2 + \\
& m_5 k_5^2 \dot{\theta}_3 \mathbf{u}_5 + m_5 (l_2 \mathbf{e}_2 + r_5 \mathbf{e}_3) \times (l_2 \dot{\mathbf{e}}_2 + r_5 \dot{\mathbf{e}}_3) + \\
& m_6 k_6^2 \dot{\theta}_2 \mathbf{u}_6 + m_6 ((l_3 - c)\mathbf{e}_3 + r_6 \mathbf{e}_2) \times ((l_3 - c)\dot{\mathbf{e}}_3 + r_6 \dot{\mathbf{e}}_2) + \\
& m_7 k_7^2 \dot{\theta}_3 \mathbf{u}_7 + m_7 r_7 \mathbf{e}_3 \times r_7 \dot{\mathbf{e}}_3 + \\
& m_8 k_8^2 \dot{\theta}_1 \mathbf{u}_8 + m_8 (l_2 \mathbf{e}_2 + l_3 \mathbf{e}_3 + r_8 \mathbf{e}_1) \times (l_2 \dot{\mathbf{e}}_2 + l_3 \dot{\mathbf{e}}_3 + r_8 \dot{\mathbf{e}}_1) + \\
& m_9 k_9^2 \dot{\theta}_3 \mathbf{u}_9 + m_9 (l_1 \mathbf{e}_1 + l_2 \mathbf{e}_2 + r_9 \mathbf{e}_3) \times (l_1 \dot{\mathbf{e}}_1 + l_2 \dot{\mathbf{e}}_2 + r_9 \dot{\mathbf{e}}_3) + \\
& m_p (l_1 \mathbf{e}_1 + l_2 \mathbf{e}_2 + (l_3 + l_e)\mathbf{e}_3) \times (l_1 \dot{\mathbf{e}}_1 + l_2 \dot{\mathbf{e}}_2 + (l_3 + l_e)\dot{\mathbf{e}}_3) \\
& - I_{cr1}\dot{\theta}_1 \mathbf{u}_1 - I_{cr2}\dot{\theta}_2 \mathbf{u}_4 - I_{cr3}\dot{\theta}_3 \mathbf{u}_7
\end{aligned}
\qquad (3.67)
$$

Furthermore, one has

$$\mathbf{e}_1 \times \dot{\mathbf{e}}_1 = \dot{\theta}_1 \begin{bmatrix} 0 \\ 1 \\ 0 \end{bmatrix}, \quad \mathbf{e}_2 \times \dot{\mathbf{e}}_2 = \dot{\theta}_2 \begin{bmatrix} 0 \\ 0 \\ 1 \end{bmatrix}, \quad \mathbf{e}_3 \times \dot{\mathbf{e}}_3 = \dot{\theta}_3 \begin{bmatrix} 1 \\ 0 \\ 0 \end{bmatrix},$$

$$\mathbf{e}_1 \times \dot{\mathbf{e}}_2 = \dot{\theta}_2 \begin{bmatrix} -\cos\theta_1 \cos\theta_2 \\ -\cos\theta_1 \sin\theta_2 \\ \sin\theta_1 \cos\theta_2 \end{bmatrix}, \quad \mathbf{e}_2 \times \dot{\mathbf{e}}_1 = \dot{\theta}_1 \begin{bmatrix} -\sin\theta_1 \sin\theta_2 \\ \sin\theta_1 \cos\theta_2 \\ -\cos\theta_1 \sin\theta_2 \end{bmatrix},$$

$$\mathbf{e}_1 \times \dot{\mathbf{e}}_3 = \dot{\theta}_3 \begin{bmatrix} \cos\theta_1 \sin\theta_3 \\ -\sin\theta_1 \cos\theta_3 \\ -\sin\theta_1 \sin\theta_3 \end{bmatrix}, \quad \mathbf{e}_3 \times \dot{\mathbf{e}}_1 = \dot{\theta}_1 \begin{bmatrix} -\sin\theta_1 \cos\theta_3 \\ \cos\theta_1 \sin\theta_3 \\ -\cos\theta_1 \cos\theta_3 \end{bmatrix},$$

$$\mathbf{e}_2 \times \dot{\mathbf{e}}_3 = \dot{\theta}_3 \begin{bmatrix} \sin\theta_2 \cos\theta_3 \\ -\cos\theta_2 \cos\theta_3 \\ -\cos\theta_2 \sin\theta_3 \end{bmatrix}, \quad \mathbf{e}_3 \times \dot{\mathbf{e}}_2 = \dot{\theta}_2 \begin{bmatrix} -\cos\theta_2 \sin\theta_3 \\ -\sin\theta_2 \sin\theta_3 \\ \sin\theta_2 \cos\theta_3 \end{bmatrix} \tag{3.68}$$

The components of $\mathbf{h}_o$ can then be written as

$$
\begin{aligned}
h_{ox} &= A(\cos\theta_1 \sin\theta_3 \dot{\theta}_3 - \sin\theta_1 \cos\theta_3 \dot{\theta}_1) + B(\sin\theta_2 \cos\theta_3 \dot{\theta}_3 - \\
&\quad \cos\theta_2 \sin\theta_3 \dot{\theta}_2) - C(\sin\theta_1 \sin\theta_2 \dot{\theta}_1 + \cos\theta_1 \cos\theta_2 \dot{\theta}_2) + H\dot{\theta}_3 \qquad (3.69)
\end{aligned}
$$

$$
\begin{aligned}
h_{oy} &= A(\cos\theta_1 \sin\theta_3 \dot{\theta}_1 - \sin\theta_1 \cos\theta_3 \dot{\theta}_3) - B(\sin\theta_2 \sin\theta_3 \dot{\theta}_2 + \cos\theta_2 \cos\theta_3 \dot{\theta}_3) + \\
&\quad \cos\theta_2 \cos\theta_3 \dot{\theta}_3) + C(\sin\theta_1 \cos\theta_2 \dot{\theta}_1 - \cos\theta_1 \sin\theta_2 \dot{\theta}_2) + F\dot{\theta}_1 \qquad (3.70)
\end{aligned}
$$

$$
\begin{aligned}
h_{oz} &= -A(\cos\theta_1 \cos\theta_3 \dot{\theta}_1 + \sin\theta_1 \sin\theta_3 \dot{\theta}_3) + B(\sin\theta_2 \cos\theta_3 \dot{\theta}_2 - \\
&\quad \cos\theta_2 \sin\theta_3 \dot{\theta}_3) + C(\sin\theta_1 \cos\theta_2 \dot{\theta}_2 - \cos\theta_1 \sin\theta_2 \dot{\theta}_1) + G\dot{\theta}_2 \qquad (3.71)
\end{aligned}
$$

where

$$A = m_8 l_3 r_8 + m_9 l_1 r_9 + m_p l_1 (l_3 + l_e) \tag{3.72}$$

$$B = m_5 l_2 r_5 + m_6 (l_3 - c) r_6 + m_8 l_2 l_3 + m_9 l_2 r_9 + m_p l_2 (l_3 + l_e) \tag{3.73}$$

$$C = m_2 l_1 r_2 + m_3 l_2 r_3 + m_8 l_2 r_8 + m_9 l_1 l_2 + m_p l_1 l_2 \tag{3.74}$$

$$
\begin{aligned}
F &= (m_2 + m_9 + m_p) l_1^2 + m_1 (k_1^2 + r_1^2) + m_3 (k_3^2 + r_3^2) + \\
&\quad m_8 (k_8^2 + r_8^2) - I_{cr1} \qquad (3.75)
\end{aligned}
$$

$$
\begin{aligned}
G &= (m_3 + m_5 + m_8 + m_9 + m_p) l_2^2 + m_2 (k_2^2 + r_2^2) + \\
&\quad m_4 (k_4^2 + r_4^2) + m_6 (k_6^2 + r_6^2) - I_{cr2} \qquad (3.76)
\end{aligned}
$$

$$
\begin{aligned}
H &= m_6 (l_3 - c)^2 + m_8 l_3^2 + m_p (l_3 + l_e)^2 + m_5 (k_5^2 + r_5^2) + \\
&\quad m_7 (k_7^2 + r_7^2) + m_9 (k_9^2 + r_9^2) - I_{cr3} \qquad (3.77)
\end{aligned}
$$

From eq. (1.4) and (3.69–3.71), a set of sufficient conditions for moment balancing of the mechanism can be written as $A = B = C = F = G = H = 0$, i. e.,

$$m_8 l_3 r_8 + m_9 l_1 r_9 + m_p l_1 (l_3 + l_e) = 0 \tag{3.78}$$

$$m_5 l_2 r_5 + m_6 (l_3 - c) r_6 + m_8 l_2 l_3 + m_9 l_2 r_9 + m_p l_2 (l_3 + l_e) = 0 \tag{3.79}$$

$$m_2 l_1 r_2 + m_3 l_2 r_3 + m_8 l_2 r_8 + m_9 l_1 l_2 + m_p l_1 l_2 = 0 \tag{3.80}$$

Table 3.2: A numerical example of reactionless practical 3-DOF parallelepiped mechanisms (Case I).

Link i	m_i (kg)	r_i (mm)	k_i (mm)
1	0.056891	16.171	76.952
2	0.053846	167.085	115.601
3	0.133818	-78.690	95.906
4	2.0351	-14.284	13.976
5	0.054788	50.819	74.583
6	0.360865	-123.556	67.988
7	2.0425	-48.331	17.704
8	0.147928	-85.492	93.612
9	0.044532	105.0	60.622
	I_{cr1} ($kgmm^2$)	I_{cr2} ($kgmm^2$)	I_{cr3} ($kgmm^2$)
	8127.2	19911.6	21629.4

$$(m_2 + m_9 + m_p)l_1^2 + m_1(k_1^2 + r_1^2) + m_3(k_3^2 + r_3^2) + m_8(k_8^2 + r_8^2) - I_{cr1} = 0 \quad (3.81)$$

$$(m_3 + m_5 + m_8 + m_9 + m_p)l_2^2 + m_2(k_2^2 + r_2^2) + m_4(k_4^2 + r_4^2) +$$
$$m_6(k_6^2 + r_6^2) - I_{cr2} = 0 \quad (3.82)$$

$$m_6(l_3 - c)^2 + m_8 l_3^2 + m_p(l_3 + l_e)^2 + m_5(k_5^2 + r_5^2) + m_7(k_7^2 + r_7^2) +$$
$$m_9(k_9^2 + r_9^2) - I_{cr3} = 0 \quad (3.83)$$

Hence, any mechanism of type II (Figure 3.12) satisfying eqs. (3.62–3.64) as well as eqs. (3.78–3.83) will be reactionless. The global center of mass will then be fixed at $\mathbf{r} = \mathbf{0}$ and the angular momentum of the mechanism with respect to point O will be zero.

By comparing the two sets of dynamic balancing conditions for the practical parallelepiped mechanisms of Case I and Case II respectively, it is found that the force balancing conditions are identical for both cases while there are two more conditions (eqs. 3.54 and 3.55) for the moment balancing of Case I than that of Case II. Actually, the dynamic balancing conditions for Case II are a subset of those of Case I associated with the special case for which $a = b = 0$. This confirms that dynamic balancing of a

Table 3.3: A numerical example of reactionless practical 3-DOF parallelepiped mechanism (Case II).

Link i	m_i (kg)	r_i (mm)	k_i (mm)
1	2.0076	-8.712	13.486
2	0.0904736	-43.315	98.642
3	0.0318086	75.0	43.301
4	2.0432	-51.575	18.085
5	0.3748467	-143.3	86.522
6	0.0636172	187.5	116.678
7	0.0318086	75.0	43.301
8	0.1479276	-85.492	93.612
9	0.0445321	105.0	60.622
	I_{cr1} $(kgmm^2)$	I_{cr2} $(kgmm^2)$	I_{cr3} $(kgmm^2)$
	7296.2	24860.8	19830.4

mechanism is only dependent on the geometric and inertial parameters but not on the actuation schemes and the motion of the mechanism.

3.6.3 Verification of the Reactionless Property

After dynamic balancing conditions have been obtained for each case, optimization using the same algorithm and procedure as used in Section 3.3 will be performed in order to obtain solutions for the counterweights and counter-rotations. The geometry of the mechanisms has been chosen such that

$$l_1 = 150 \ mm, \ l_2 = 150 \ mm, \ l_3 = 180 \ mm, \ l_e = 30 \ mm$$

$$a = 40 \ mm, \ b = 24 \ mm, \ c = 30 \ mm, \ m_p = 0.05 \ kg$$

$$\rho_l = 0.211272 \ kg/m$$

and an optimization has been performed using the objective function of eq. (3.27) and the constraints of corresponding dynamic balancing conditions. The optimization results for Case I and Case II have been obtained as shown in Table 3.2 and Table 3.3

respectively. Apparently, the parameters in Table 3.2 also satisfy the dynamic balancing conditions of Case II (eqs. 3.62–3.64 and eqs. 3.78–3.83). In other words, the practical parallelepiped mechanism of Case II with parameters in Table 3.2 will be dynamically balanced.

For the above example mechanisms, simulation models for the mechanisms of Case I and Case II respectively are built using ADAMS (Figure 3.15). The mass, center of mass and moments of inertia of each link are specified interactively. The three counter-rotations are fixed on the base and connected respectively to the actuated links by gears. Simulations have been performed for several arbitrary trajectories. The resulting reaction forces and moments on the base of one simulation are illustrated in Figure 3.16. The results clearly demonstrate that the resulting reaction forces and moments on the base are very small compared to the joint forces and driving torques (with a ratio of 10^{-4} to 10^{-5}).

Hence, it is clearly shown that the practical 3-DOF parallelepiped mechanisms can be completely balanced.

Notice that all the above dynamically balanced parallelepiped mechanisms are obtained on the assumption that the center of mass of each link of the mechanisms is located on the axis of the corresponding link. Otherwise, we have found that the parallelepiped mechanisms cannot be dynamically balanced unless all links whose center of mass is not on the axis of the link undergo planar motion. Hence, in the future structure design of each link, we must ensure both of these requirements and the dynamic balancing conditions as shown in the tables for the example mechanisms.

3.7   Discussion

By investigation of the parallelepiped mechanisms of both cases, it is found that the mechanism of Case II has a larger workspace — without the consideration of joint limitation and link interference — and more maximum real solutions of inverse kinematics than the mechanism of Case I. Yet, the dynamic balancing of the mechanism of Case II can be obtained only on the assumption that the center of mass of each link is located on the corresponding link, while the dynamic balancing of Case I could obtained
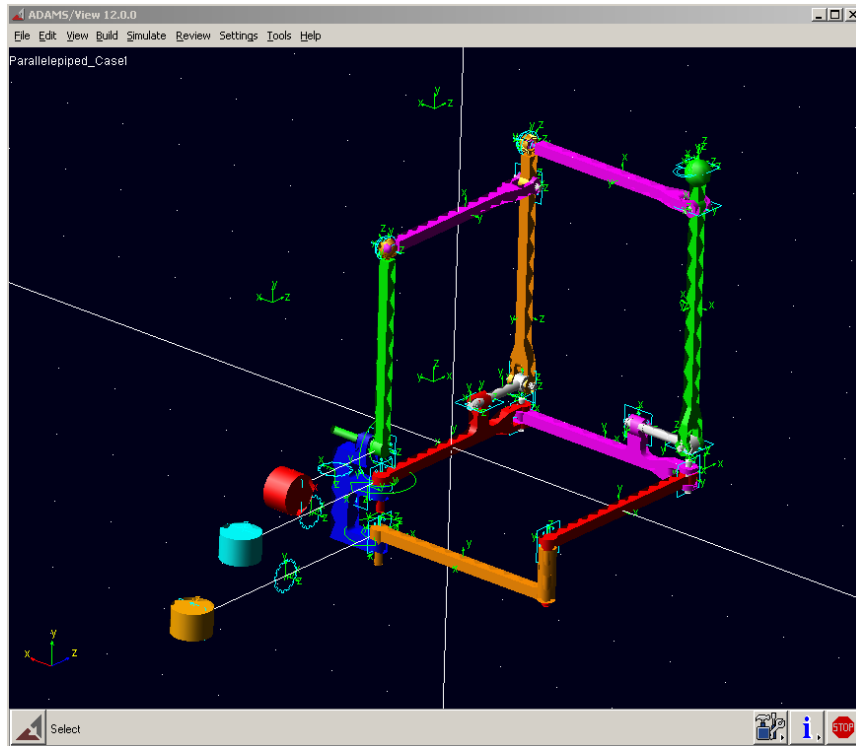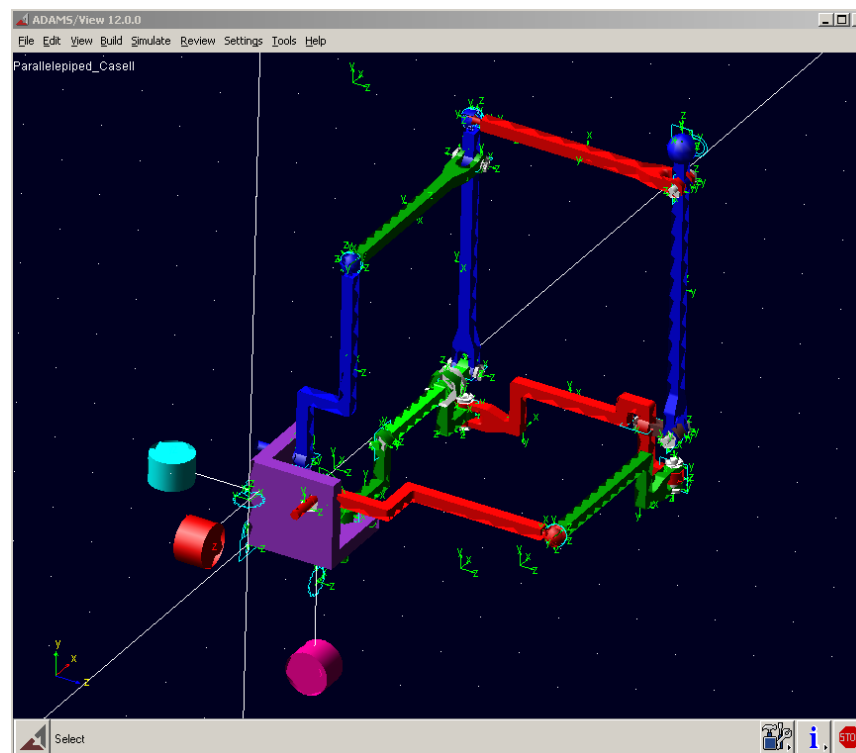
(a) Case I

(b) Case II

Figure 3.15: Simulation of practical 3-DOF parallelepiped mechanisms using ADAMS.
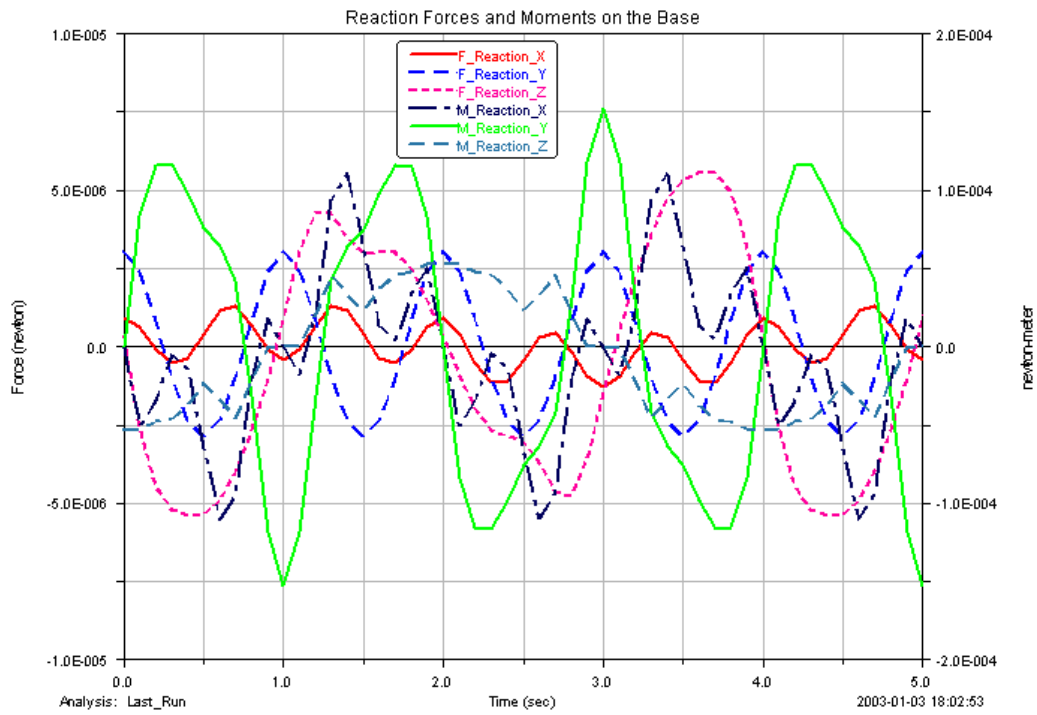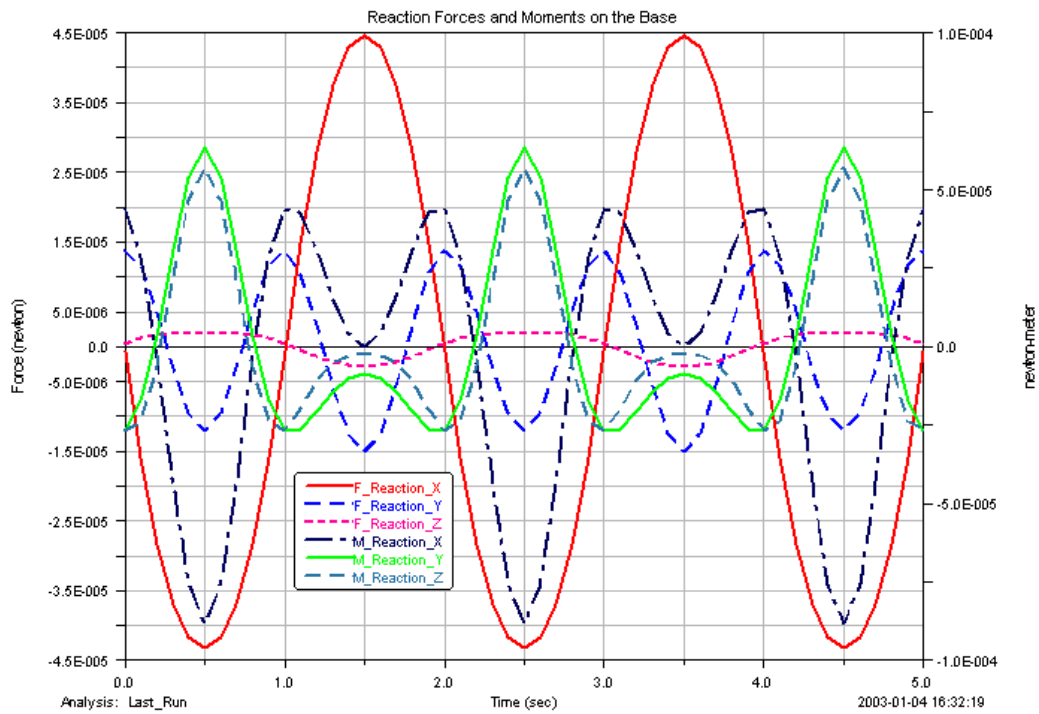
(a) Case I.

(b) Case II.

Figure 3.16: Verification of the reactionless property of practical 3-DOF parallelepiped mechanisms.

for a more general case. Which mechanism is better depends therefore on the design requirements and limitations of the practical applications.

From the above example mechanisms, we find that the reactionless 3-DOF parallelepiped mechanisms were achieved at the expense of a substantial increase of the masses of the moving links and the complexity of the mechanism. Let us take the practical 3-DOF parallelepiped mechanism (Case II; Table 3.3) as an example. The payload (point mass) is $0.05\,kg$, m_i and $r_i, i = 1, \ldots, 9$ are respectively the resulting mass and position of the center of mass of the combination of link i, the counterweight and the extension part for mounting the counterweight if applicable. The masses of the original links are $0.03817\,kg$ for link 5, $0.044532\,kg$ for link 9 and $0.0318086\,kg$ for other links. Actually, the counterweight and its position on link i are listed as follows:

$$m_{c1} = 1.9737,\ m_{c2} = 0.0277078,\ m_{c3} = 0,\ m_{c4} = 2.0,\ m_{c5} = 0.298506$$

$$m_{c6} = 0.0318086,\ m_{c7} = 0,\ m_{c8} = 0.0843104,\ m_{c9} = 0$$

$$r_{c1} = -10.0647,\ r_{c2} = -145.9847,\ r_{c3} = 0,\ r_{c4} = -53.7286,\ r_{c5} = -180$$

$$r_{c6} = 300.0,\ r_{c7} = 0,\ r_{c8} = -150.0,\ r_{c9} = 0$$

where masses are in kilograms and the lengths in millimeters. In order to balance the original mechanism, a total 4.5304518 (4.8358144-0.30536256) kg of mass has been added. Apparently, the total mass increases about 12.5 times (4.5304518/(0.05 + 0.30536256)). As mentioned before, a 3-DOF parallelepiped mechanism is kinematically equivalent to a spatial three-link serial chain (e.g., Figure 3.17). In order to balance this serial chain, an ordinary method can be used, i.e., at the extension part of each link a counterweight is added to locate the center of mass of the link at the joint for all motions (e.g., A, B, O). This results in zero linear momentum for whole mechanism, whereas adding a counter-rotation (or a combination of counterweight and a counter-rotation; not shown on the figure) leads to zero angular momentum. It is assumed that the three counterweights are mounted at the positions as: $r_{c1} = 10.0647$, $r_{c2} = 145.9847$, $r_{c9} = 50\,mm$, for comparison with the example above. Regardless of the mass of the extension part for simplicity, the three counterweight are finally determined as: $m_{c9} = (105m_{b9} + 210m_p)/r_{c9} = 0.3035172, m_A = m_{c9} + m_{b9} + m_p = 0.3980492, m_{c2} = (75m_{b2} + 150m_A)/r_{c2} = 0.425339265, m_B = m_{c2} + m_{b2} + m_A = 0.855197065, m_{c1} = (75m_{b1} + 150m_B)/r_{c1} = 15.1158\,kg$, where m_A and m_B are total mass of link 9 and link 2 respectively. Therefore, the total counterweight is $16.274516 kg$. The total mass increases $16.274516/(m_{b1} + m_{b2} + m_{b9}) = 150$ times. The shorter the length of r_{c1}, r_{c2}
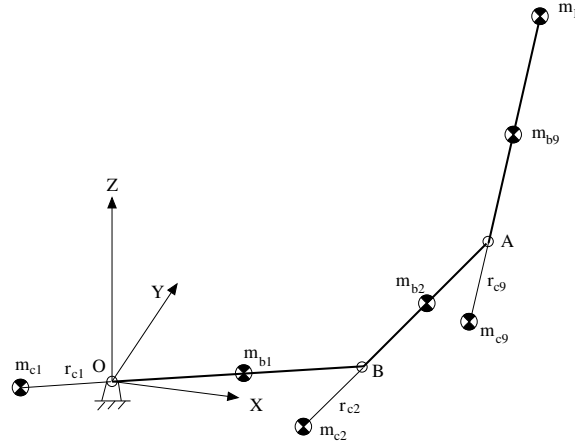
Figure 3.17: A three-link serial chain

or r_{c9}, the more the mass increase of the system. Clearly, for the dynamic balancing of the two mechanisms with the same payload, the parallelepiped mechanism can have much less mass increase of the system than that of the three-link serial chain. This result further confirms that the parallelograms can transmit the rotation of the moving mass to a link pivoted to the base, and results in adding less counterweight on this link for balancing the moving mass (Herder and Gosselin, 2003). A similar conclusion has been found for the three counter-rotations. All these results further demonstrate the advantage of lower inertia of the parallel mechanisms as compared to serial mechanisms.

3.8   Conclusion

The design and dynamic balancing of the novel 3-DOF parallelepiped mechanisms with general architecture and practical implementations have been addressed in this chapter. Two modes of actuation of the mechanisms are considered. The balancing equations have been derived by imposing that the center of mass of the mechanism is fixed and that the total angular momentum is constant with respect to a fixed point. A set of conditions on the link parameters for each case has thereby been obtained, which constitutes the balancing conditions. Counterweights and counter-rotations are used to dynamically balance the mechanism. Optimizations have been performed in order to obtain solutions for the counterweights and counter-rotations, based on the balancing conditions. The dynamic simulation software ADAMS has been used to simulate the motion of the novel 3-DOF parallelepiped mechanisms and to verify that

the mechanisms are reactionless at all times and for arbitrary trajectories. Several numerical examples of reactionless 3-DOF parallelepiped mechanisms have been given in this chapter and it has been shown that 3-DOF parallelepiped mechanisms can be completely balanced.

Chapter 4

Kinematic Analysis and Dynamic Balancing of 6-DOF Parallel Mechanisms Using Parallelepiped Mechanisms

This chapter deals with the synthesis, kinematic analysis and dynamic balancing of 6-DOF parallel mechanisms using parallelepiped mechanisms. The kinematic analysis including the inverse and direct kinematics as well as the determination of singularity loci and workspace of the 6-DOF parallel mechanisms are presented. The Jacobian matrix of the mechanisms associated with different actuation schemes are derived. A geometrical algorithm and a discretization method are respectively used for the determination of the workspace for both of the two cases of the mechanism. Then, the graphical representations that show the relationship between the singularity loci and the constant-orientation workspace of the mechanism are given. Finally, the dynamic equivalence between a platform and three point masses and the dynamic balancing of 6-DOF parallel mechanisms are addressed.

4.1 Introduction

The spatial 3-DOF parallelepiped mechanisms introduced in the preceding chapters can be used as legs to synthesize spatial multi-degree-of-freedom parallel mechanisms or manipulators, having up to 6-DOF. The end-effector point of the 3-DOF mechanism is attached to the mobile platform using either a spherical or a Hooke joint, depending on the number of legs used and the desired number of degrees of freedom for the mechanism. These factors also determine the number of joints to be actuated for each leg. The mobility l of the synthesized mechanism can be determined by the application of the general mobility criterion of Chebychev-Grbler-Kutzbach (Hunt, 1978), i.e.,

$$l = d(n - g - 1) + \sum_{i=1}^{g} f_i \tag{4.1}$$

where n is the number of links including the base, g is the number of joints, f_i is the degree of freedom of joint i, d is the dimension of the system under study (e.g., for a planar system $d = 3$, while for a spatial system $d = 6$). A 6-DOF parallel manipulator or mechanism can be obtained using only three legs and two actuators for each leg and spherical joints to connect the legs to the mobile platform. As mentioned before, the parallelepiped mechanism is kinematically equivalent to a spatial RRR serial chain. Hence, for the proposed mechanism, we have $d = 6$, $n = 11$, $g = 12$, and $\Sigma f_i = 18$, the mobility of the mechanism thus being equal to 6. In fact, for the synthesized manipulator, each leg has 6 degrees of freedom and does not exert any constraint on the platform.

For the dynamic balancing of a multi-degree-of-freedom parallel mechanism with several legs, the derivation of the balancing conditions is very complicated or even impossible to obtain using the approach used in the preceding chapters (eqs. (1.3) and (1.4)) for the whole mechanism where the mass and inertia of the moving platform and all the leg mechanisms need to be considered. One simple approach to this problem is to replace the moving platform with equivalent point masses located at the points of attachment of the legs to the platform. Ricard and Gosselin (2000) have used three point masses to replace the moving platform for the development of reactionless planar parallel manipulators.

In this chapter, after describing the synthesis of 6-DOF parallel mechanisms with three legs of parallelepiped mechanisms, the kinematic analysis including the inverse
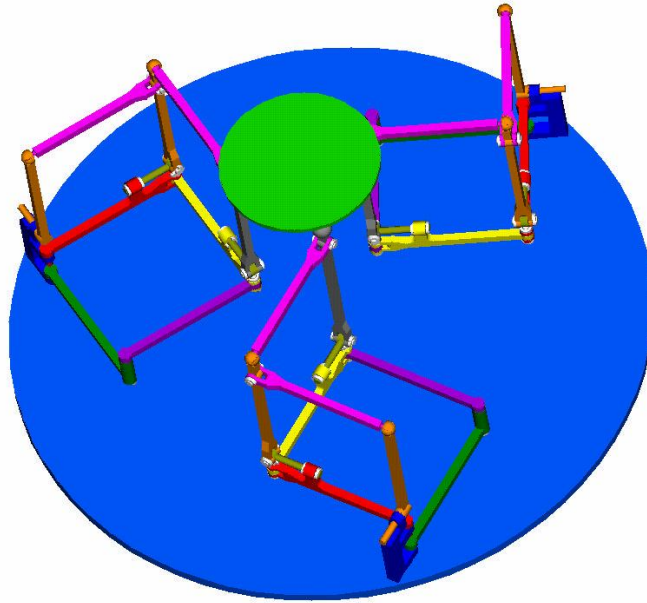
Figure 4.1: CAD model of a 6-DOF parallel mechanism (Case I).

and direct kinematics as well as the determination of singularity loci and workspace of the 6-DOF parallel mechanisms will be solved. The Jacobian matrix of the mechanisms associated with different actuation schemes are derived. A geometrical algorithm and a discretization method are used for the determination of the workspace for the mechanisms using two different cases of the leg mechanism denoted as Case I and Case II. The graphical representations that show the relationship between the singularity loci and the constant-orientation workspace of the mechanism are given. Finally, the dynamic equivalence between a platform and three point masses will be discussed and the dynamic balancing of 6-DOF parallel mechanisms will be addressed.

4.2   Geometric Description

The 6-DOF parallel mechanisms represented in Figures 4.1 and 4.2 are composed of a fixed base and a moving platform connected by three identical legs. The legs are symmetrically arranged and attached to the platform with spherical joints. Each of the three legs is a spatial 3-DOF parallelepiped mechanism. A schematic representation of
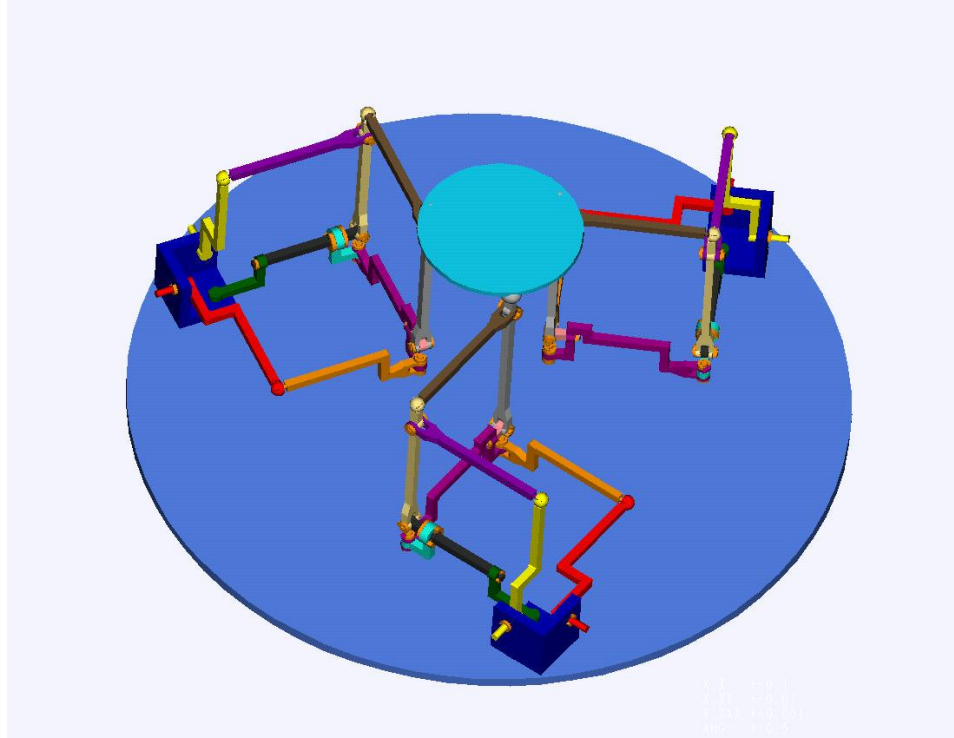
Figure 4.2: CAD model of a 6-DOF parallel mechanism (Case II).

one leg of the spatial 6-DOF parallel mechanism is shown in Figure 4.3. A fixed reference frame $O-xyz$ is attached to the base of the mechanism and a moving coordinate frame $O'-x'y'z'$ is attached to the mobile platform. Moreover, a local coordinate frame $\xi\eta\zeta$ is attached to the base at point B_i and its ξ-axis and η-axis coincide with the x-axis and y-axis of the parallelepiped mechanism (Figures 2.2, 3.11 and 3.12). Any two of the three links denoted by V_1, V_2 and V_3 respectively attached to the fixed base are actuated using fixed revolute actuators for each leg (Figure 4.3). Hence, totally 6 revolute actuators are used for the whole 6-DOF mechanism.

4.3 Inverse Kinematics

In Figure 4.3, the points of attachment of the three legs to the base are noted B_i, $i = 1, 2, 3$ and the points of attachment of all legs to the platform are noted P_i, $i = 1, 2, 3$. The mounting angle of the leg mechanism noted α_i is the angle of the ξ-axis of the

(a)

(b)
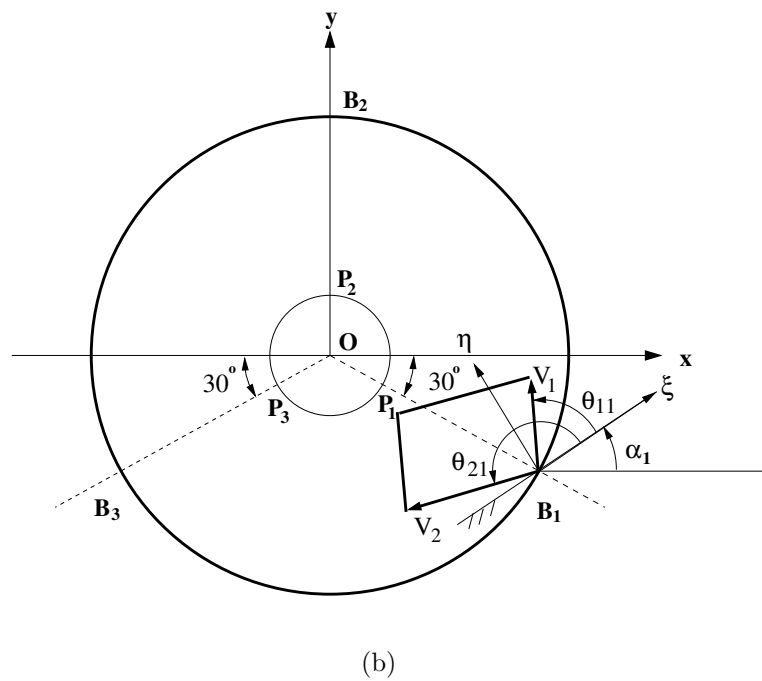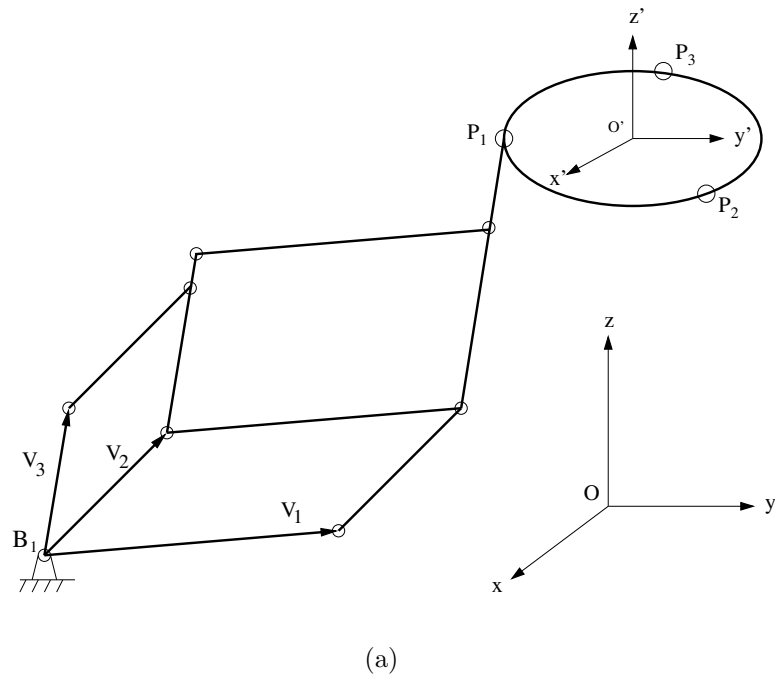
Figure 4.3: Schematic representation of one leg of the spatial 6-DOF parallel mechanism.

local frame with respect to the x-axis of the global frame. One can then write

$$\mathbf{p}_i = \mathbf{p} + \mathbf{Q}\mathbf{b}_i \tag{4.2}$$

where $\mathbf{p}_i$ and $\mathbf{p}$ are respectively the position vectors of point P_i and the centroid of the platform O' expressed in the fixed coordinate frame and $\mathbf{b}_i$ is the position vector of point P_i in the moving coordinate frame, i.e.,

$$\mathbf{p} = \begin{bmatrix} x \\ y \\ z \end{bmatrix}, \quad \mathbf{p}_i = \begin{bmatrix} x_i \\ y_i \\ z_i \end{bmatrix}, \quad \mathbf{b}_i = \begin{bmatrix} x'_i \\ y'_i \\ z'_i \end{bmatrix}, \quad i = 1, 2, 3 \tag{4.3}$$

Furthermore, $\mathbf{Q}$ is the rotation matrix corresponding to the orientation of the platform of the mechanism with respect to the base coordinate frame — usually written as a function of the three Euler angles representing the three degrees of freedom in rotation of the platform that are defined by first rotating the mobile frame about the base z-axis by angle ϕ, then about the mobile new x-axis by an angle θ, and finally about the mobile new y-axis by an angle ψ, i.e.,

$$
\begin{aligned}
\mathbf{Q} &= \mathbf{Q}_z(\phi)\mathbf{Q}_x(\theta)\mathbf{Q}_y(\psi) \\
&= \begin{bmatrix} \cos\phi\cos\psi - \sin\phi\sin\theta\sin\psi & -\sin\phi\cos\theta & \cos\phi\sin\psi + \sin\phi\sin\theta\cos\psi \\ \sin\phi\cos\psi + \cos\phi\sin\theta\sin\psi & \cos\phi\cos\theta & \sin\phi\sin\psi - \cos\phi\sin\theta\cos\psi) \\ -\cos\theta\sin\psi & \sin\theta & \cos\theta\cos\psi \end{bmatrix}
\end{aligned}
\tag{4.4}
$$

The computation of the joint coordinates of each leg is fully independent from the computation of the rest of the joint coordinates. For example, we take the ith leg into account. For a given position and orientation of the platform, the Cartesian coordinates of P_i in the fixed frame can be calculated from eq. (4.2). Then, the vector $\mathbf{s}_i$ from the base attachment point B_i (with position vector $\mathbf{p}_{0i}$) to the platform attachment point P_i in the global frame for each leg can be written as follows:

For Case I,

$$
\begin{aligned}
\mathbf{s}_i &= \mathbf{p}_i - \mathbf{p}_{0i} \\
&= \begin{bmatrix} l_1\cos(\theta_{1i} + \alpha_i) + l_2\cos(\theta_{2i} + \alpha_i) - (l_3 + l_e)\cos\theta_{3i}\sin\alpha_i \\ l_1\sin(\theta_{1i} + \alpha_i) + l_2\sin(\theta_{2i} + \alpha_i) + (l_3 + l_e)\cos\theta_{3i}\cos\alpha_i \\ (l_3 + l_e)\sin\theta_{3i} \end{bmatrix}
\end{aligned}
\tag{4.5}
$$

while for Case II,

$$\mathbf{s}_i = \mathbf{p}_i - \mathbf{p}_{0i}$$

$$= \begin{bmatrix} l_1 \cos \alpha_i \sin \theta_{1i} + l_2 \cos(\theta_{2i} + \alpha_i) - (l_3 + l_e) \cos \theta_{3i} \sin \alpha_i \\ l_1 \sin \alpha_i \sin \theta_{1i} + l_2 \sin(\theta_{2i} + \alpha_i) + (l_3 + l_e) \cos \theta_{3i} \cos \alpha_i \\ l_1 \cos \theta_{1i} + (l_3 + l_e) \sin \theta_{3i} \end{bmatrix} \quad (4.6)$$

where the first index of the subscript of joint coordinates (θ_{1i}, θ_{2i} and θ_{3i}) stands for ordered joint coordinate — as defined in Figures 2.5 and 2.6 — while the second index i represents the number of the leg. Then, the joint coordinates of the 3-DOF parallelepiped mechanisms, namely, the actuated joint coordinates of the 6-DOF parallel mechanism can be derived from eqs. (4.5) and (4.6) for Case I and Case II respectively.

Another solution to the inverse kinematic problem of the leg mechanisms is to substitute the components of vector $\mathbf{s}_i$ with respect to the local frame $B_i - \xi\eta\zeta$ to the components (x, y and z) of vector $\mathbf{p}$ in eqs. (2.3) and (2.7) respectively for Case I and Case II. Then, the solutions to eqs. (2.3) and (2.7) can be directly used for the inverse kinematics of the leg mechanisms.

4.4   Direct Kinematics

The direct kinematic problem of the 6-DOF parallel mechanisms using parallelepiped mechanisms can be shown to be equivalent to direct kinematics of the existing parallel mechanisms or manipulators — e.g., a mechanism with three prismatic legs (RRPS chains) and the TSSM mechanism — for which the solution has been shown to be reducible to a 16th-order polynomial equation (Merlet 1992a; Nanua *et al.* 1990; Ebert-Uphoff and Gosselin 1998).

4.5   Constant-Orientation Workspace

As we mentioned in Chapter 1, the constant-orientation workspace is the most common subset of the complete workspace for parallel mechanisms. In this section, both numerical and geometrical algorithms are used for the determination of the constant-orientation workspace of the 6-DOF parallel mechanisms.

Gosselin (1990) presented a geometrical algorithm for determining the constant-

orientation workspace of 6-DOF parallel manipulators. For Stewart platform manipulators, the workspace was obtained from the intersection of 6 regions, each of which being the difference between two concentric spheres. Similarly, if mechanical interferences are neglected for the 6-DOF parallel mechanism of this chapter, the workspace can be obtained from the intersection of three spatial regions. Each of these regions is the workspace of a parallelepiped leg as shown in Figures 2.14 and 2.15 for Case I and Case II, respectively, with respect to the local frame $B_i - \xi\eta\zeta$ and with its center of the workspace at the point with coordinates $(\mathbf{p}_{0i} - \mathbf{Q}\mathbf{b}_i)$ relative to the global frame.

Numerical algorithms (or discretization methods) are common and applicable to all parallel mechanisms, especially to some spatial complex ones. The constant-orientation workspace is the set of permissible positions — i.e., corresponding to real solutions of the inverse kinematic problem — for the center of the mobile platform while the platform is kept at a constant orientation if mechanical interferences are neglected. However, there are several real solutions to the inverse kinematics of the mechanism and only one real solution is used for the actuation of the practical mechanism. Therefore, we will also determine the constant-orientation workspace of the practical mechanism associated with the working mode (Chablat and Wenger, 1998) —the real solution of the inverse kinematics for the actuation of the joints.

Now, an example of the 6-DOF parallel mechanism is given, the geometry of the three leg mechanisms has been chosen such that

$$l_1 = 100 \ mm, \ l_2 = 50 \ mm, \ l_3 = 50 \ mm, \ l_e = 50 \ mm$$

and moreover, the radii — from the centroid to the attachment points — denoted by r and R of the mobile platform and the base are 60 mm and 171.8 mm, respectively, and the mounting angles of the leg mechanisms are chosen as

$$\alpha_1 = \frac{5\pi}{6} - \arctan(\frac{1}{2}), \ \alpha_2 = \alpha_1 + \frac{2\pi}{3}, \ \alpha_3 = \alpha_1 + \frac{4\pi}{3}$$

Then

$$\mathbf{b}_1 = \begin{bmatrix} r\cos\frac{\pi}{6} \\ -r\sin\frac{\pi}{6} \\ 0 \end{bmatrix}, \ \mathbf{b}_2 = \begin{bmatrix} 0 \\ r \\ 0 \end{bmatrix}, \ \mathbf{b}_3 = \begin{bmatrix} -r\cos\frac{\pi}{6} \\ -r\sin\frac{\pi}{6} \\ 0 \end{bmatrix} \tag{4.7}$$

$$\mathbf{p}_{01} = \begin{bmatrix} R\cos\frac{\pi}{6} \\ -R\sin\frac{\pi}{6} \\ 0 \end{bmatrix}, \ \mathbf{p}_{02} = \begin{bmatrix} 0 \\ R \\ 0 \end{bmatrix}, \ \mathbf{p}_{03} = \begin{bmatrix} -R\cos\frac{\pi}{6} \\ -R\sin\frac{\pi}{6} \\ 0 \end{bmatrix} \tag{4.8}$$
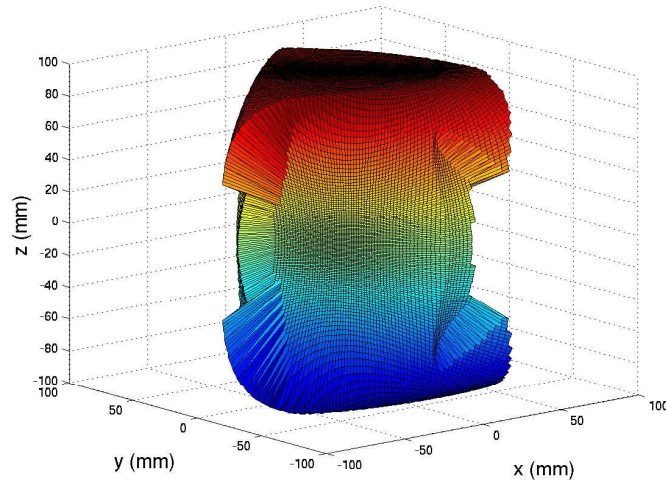
Figure 4.4: Constant-orientation workspace, $(\phi, \theta, \psi) = (0, 0, 0)$ (Case I).

Finally, a constant-orientation workspace of the example mechanism (Case I) associated with the Euler angles $(\phi, \theta, \psi) = (0, 0, 0)$ is obtained using a numerical method and is shown in Figure 4.4, while workspaces of the mechanism with orientation of $(\phi, \theta, \psi) = (0, 0, 0)$ and $(\phi, \theta, \psi) = (5°, 20°, 10°)$ of the platform associated with a specific working mode are shown in Figure 4.5. In order to show the difference between these two kinds of workspace, only one section (e.g., $z = 30mm$) of the workspaces is considered. The boundaries of the two kinds of workspace associated with this section are shown in Figure 4.6 where the outer thin curve represents the boundary of the constant-orientation workspace, while the inner thick curve stands for the workspace associated with the chosen working mode. The difference between the two boundaries is only apparent near the corners.

In order to better demonstrate the workspace of the example mechanism (Figure 4.4), different sections of the workspace are obtained and are shown in the left column of Figure 4.7 and 4.8.

Moreover, the workspace of the 3-DOF parallelepiped mechanism of Case I has been obtained using a geometrical method in Chapter 2 as shown in Figure 2.14. We can determine the workspace of the 6-DOF parallel mechanism (Case I) just from the intersection of these three workspaces of the leg mechanisms — each of which being with an orientation of the mounting angle α_i and with center at point of coordinates

(a) $(\phi, \theta, \psi)=(0, 0, 0)$

(b) $(\phi, \theta, \psi) = (5°, 20°, 10°)$
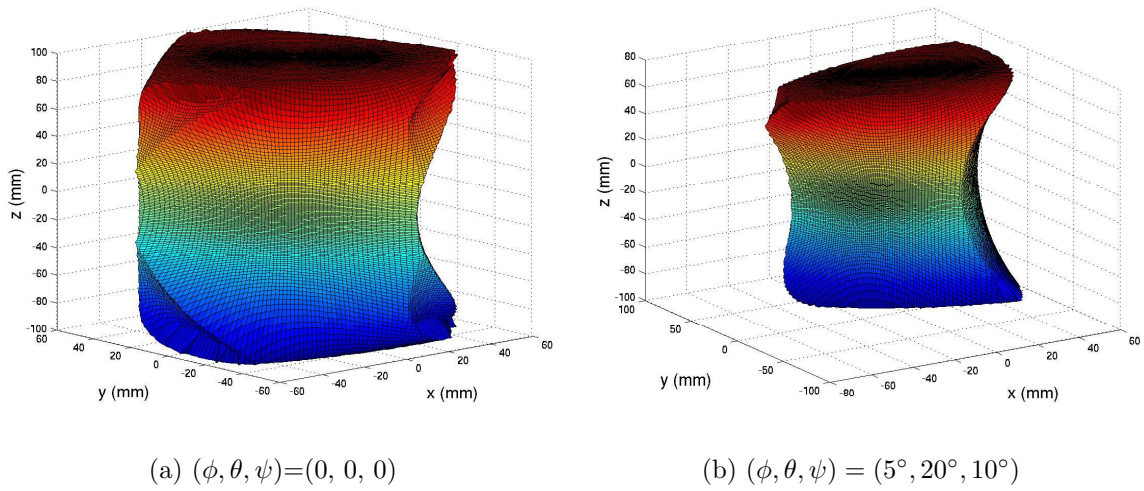
Figure 4.5: Constant-orientation workspaces associated with a specific working mode (Case I).
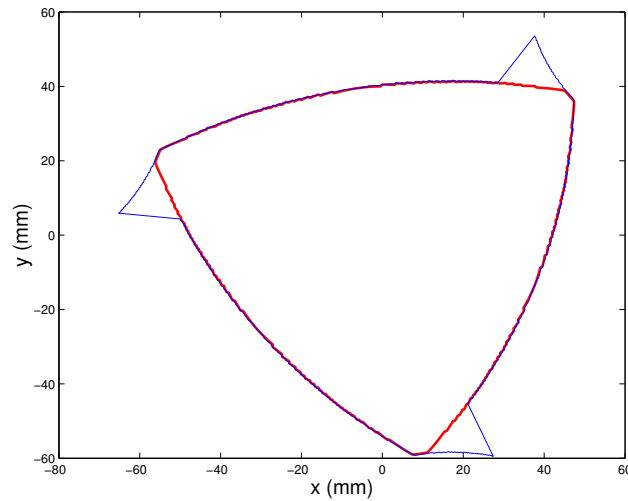
Figure 4.6: Comparison of constant-orientation workspaces associated with a specific working mode and all working modes respectively, $(\phi, \theta, \psi) = (0, 0, 0)$ (Case I).
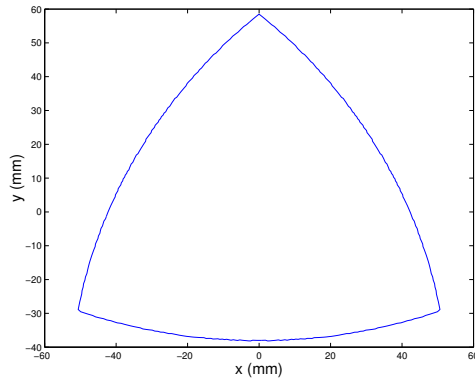
(a) $z = 100$ mm
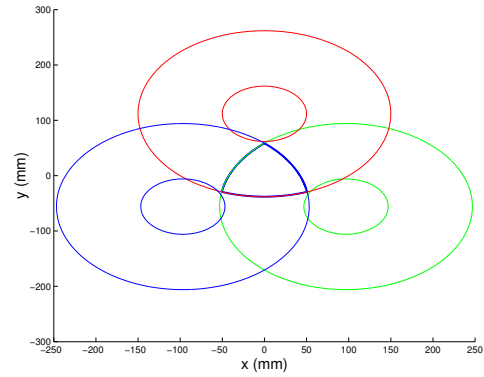
(b) $z = 100$ mm
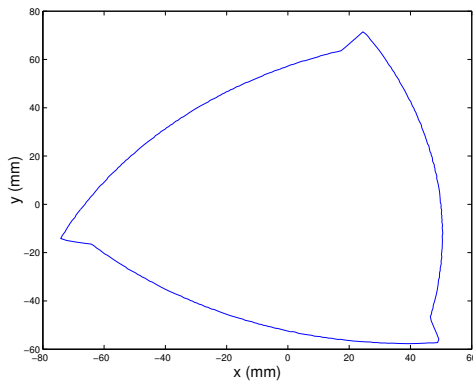
(c) $z = 90$ mm
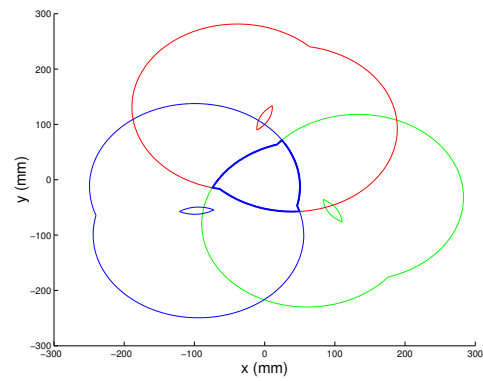
(d) $z = 90$ mm
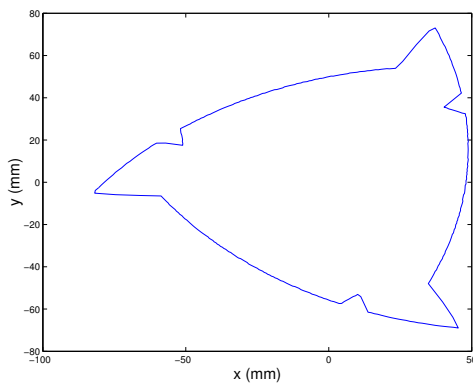
(e) $z = 70$ mm
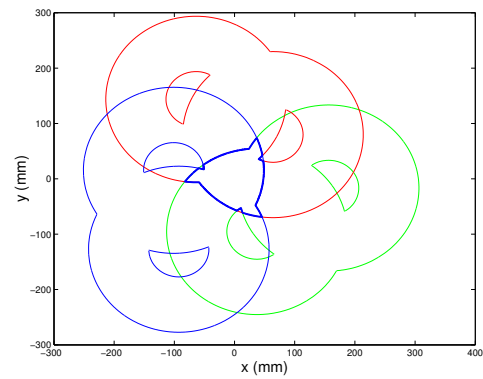
(f) $z = 70$ mm

Figure 4.7: Boundary of the workspace for different values of z, $(\phi, \theta, \psi) = (0, 0, 0)$ (Case I).
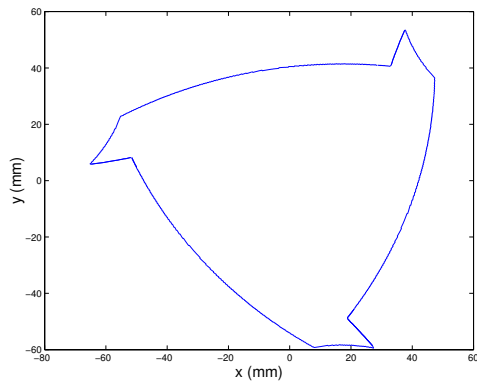
(a) $z = 30$ mm
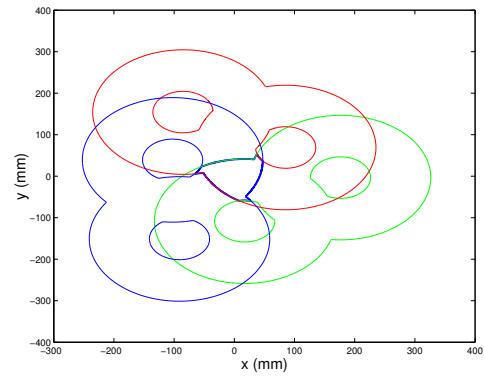
(b) $z = 30$ mm
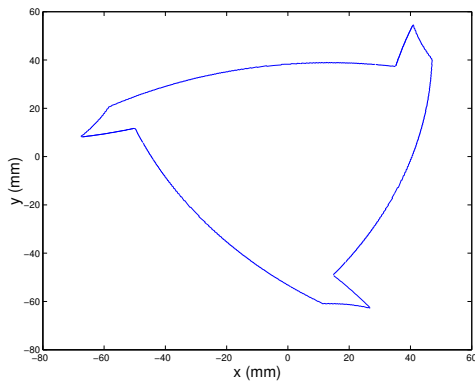
(c) $z = 0$ mm
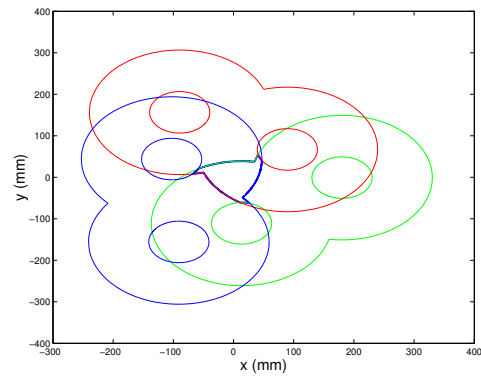
(d) $z = 0$ mm

Figure 4.8: Boundary of the workspace for different values of z, $(\phi, \theta, \psi) = (0, 0, 0)$ (Case I)(Cont.).
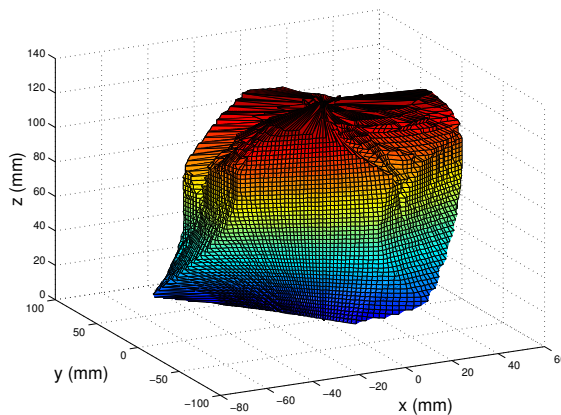
Figure 4.9: Constant-orientation workspace, $(\phi, \theta, \psi) = (0, 0, 0)$ (Case II).

$(\mathbf{p}_{0i} - \mathbf{Q}\mathbf{b}_i)$ relative to the global frame. Therefore, we can obtain the boundaries of the workspace of the 6-DOF parallel mechanism for a given section (i.e., a given value of z) from the corresponding boundaries of the workspace of the 3-DOF parallelepiped mechanism (Figure 2.14). Namely, after drawing the boundaries of the workspace of each leg mechanism in the global frame, by rotating the corresponding boundaries (Figure 2.14) with an angle α_i and putting the center at a point with the same x and y coordinates as the point $(\mathbf{p}_{0i} - \mathbf{Q}\mathbf{b}_i)$, the boundaries of the workspace of the 6-DOF parallel mechanism are obtained for the given section. The intersection (thick curves) of the three sets of boundaries just drawn are finally obtained as shown in the right column of Figures 4.7 and 4.8. By comparing the two columns in the figures, we can conclude that the constant-orientation workspaces determined respectively by the numerical algorithm and the geometrical method are completely coincident.

However, it is very difficult to determine the workspace of the 3-DOF parallelepiped mechanism of Case II by a geometrical method. Hence, a numerical algorithm is used for the determination of the constant-orientation workspace of the example 6-DOF parallel mechanism (Case II) with working mode. Figures 4.9 and 4.10 demonstrate respectively the workspace and its boundaries associated with different values of z.
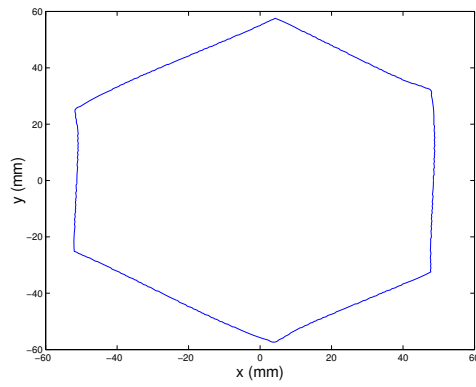
(a) $z = 70$ mm
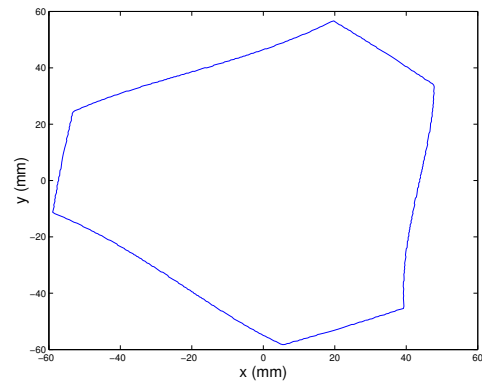
(b) $z = 50$ mm

(c) $z = 30$ mm
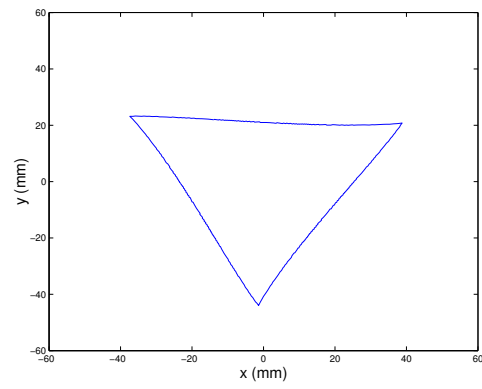
(d) $z = 10$ mm

Figure 4.10: Boundary of the workspace for different values of z (Case II).

4.6 Singularity Analysis

For Case I, differentiating eq. (4.5) with respect to time leads to

$$\dot{\mathbf{s}}_i = \mathbf{J}_i \dot{\boldsymbol{\theta}}_i, \ i = 1, 2, 3 \tag{4.9}$$

where $\dot{\boldsymbol{\theta}}_i = [\dot{\theta}_{1i} \ \dot{\theta}_{2i} \ \dot{\theta}_{3i}]^T$ and $\mathbf{J}_i$ is the Jacobian matrix of leg i, which can then be written as follows:

$$\mathbf{J}_i = \begin{bmatrix} -l_1 \sin(\theta_{1i} + \alpha_i) & -l_2 \sin(\theta_{2i} + \alpha_i) & (l_3 + l_e) \sin \alpha_i \sin \theta_{3i} \\ l_1 \cos(\theta_{1i} + \alpha_i) & l_2 \cos(\theta_{2i} + \alpha_i) & -(l_3 + l_e) \cos \alpha_i \sin \theta_{3i} \\ 0 & 0 & (l_3 + l_e) \cos \theta_{3i} \end{bmatrix}$$

The joint velocities $\dot{\boldsymbol{\theta}}_i$ can be obtained from the following inverse Jacobian matrix:

$$\mathbf{J}_i^{-1} = \begin{bmatrix} \frac{-\cos(\theta_{2i} + \alpha_i)}{l_1 \sin(\theta_{1i} - \theta_{2i})} & \frac{-\sin(\theta_{2i} + \alpha_i)}{l_1 \sin(\theta_{1i} - \theta_{2i})} & \frac{-\sin \theta_{2i} \sin \theta_{3i}}{l_1 \sin(\theta_{1i} - \theta_{2i}) \cos \theta_{3i}} \\ \frac{\cos(\theta_{1i} + \alpha_i)}{l_2 \sin(\theta_{1i} - \theta_{2i})} & \frac{\sin(\theta_{1i} + \alpha_i)}{l_2 \sin(\theta_{1i} - \theta_{2i})} & \frac{\sin \theta_{1i} \sin \theta_{3i}}{l_2 \sin(\theta_{1i} - \theta_{2i}) \cos \theta_{3i}} \\ 0 & 0 & \frac{1}{(l_3 + l_e) \cos \theta_{3i}} \end{bmatrix} \tag{4.10}$$

The Jacobian matrix $\mathbf{J}$ of the whole mechanism describes the relationship between the velocities of the actuated joints and the platform velocity in the form.

$$\dot{\boldsymbol{\theta}} = \mathbf{J} \begin{bmatrix} \dot{\mathbf{p}} \\ \boldsymbol{\omega} \end{bmatrix} \tag{4.11}$$

where $\dot{\boldsymbol{\theta}}$ contains the velocities of all actuated joints, $\dot{\mathbf{p}}$ is the velocity of the centroid of the platform and $\boldsymbol{\omega}$ is the angular velocity vector corresponding to the skew-symmetric matrix $\dot{\mathbf{Q}}\mathbf{Q}^T$, i. e.,

$$\boldsymbol{\omega} = \dot{\mathbf{Q}}\mathbf{Q}^T \tag{4.12}$$

The relationship between individual joint velocities $\dot{\theta}_{ji}$ and the vector $\dot{\mathbf{s}}_i$ can also be written as follows (Ebert-Uphoff and Gosselin 1998):

$$\dot{\theta}_{ji} = \mathbf{v}_{ji}^T \dot{\mathbf{s}}_i \tag{4.13}$$

where vector $\mathbf{v}_{ji}^T$ is actually one row of the leg inverse matrix in eq. (4.10). Moreover, one can write

$$\mathbf{s}_i = \mathbf{p} + \mathbf{Q}\mathbf{b}_i - \mathbf{p}_{0i} \tag{4.14}$$

Differentiating eq. (4.14) with respect to time yields

$$\dot{\mathbf{s}}_i = \dot{\mathbf{p}} + \boldsymbol{\omega} \times (\mathbf{Q}\mathbf{b}_i) \tag{4.15}$$

Substituting eq. (4.15) into eq. (4.13) leads to

$$\dot{\theta}_{ji} = [\, \mathbf{v}_{ji}^T \quad ((\mathbf{Q}\mathbf{b}_i) \times \mathbf{v}_{ji})^T \,] \begin{bmatrix} \dot{\mathbf{p}} \\ \boldsymbol{\omega} \end{bmatrix} \tag{4.16}$$

The above equation means that each actuated angle θ_{ji} generates one row in the Jacobian matrix $\mathbf{J}$ of the whole mechanism, i.e.,

$$\mathbf{J} = \begin{bmatrix} \mathbf{j}_1 \\ : \\ \mathbf{j}_6 \end{bmatrix} \tag{4.17}$$

with

$$\mathbf{j}_k = [\, \mathbf{v}_{ji}^T \quad ((\mathbf{Q}\mathbf{b}_i) \times \mathbf{v}_{ji})^T \,]_{1 \times 6} \tag{4.18}$$

where i is the leg in which the actuated joint associated with the kth row of the Jacobian is located and j is the actuated joint associated with this row.

It is now assumed that the revolute joints connected to the links V_1 and V_2 respectively are actuated for each leg. From eqs. (4.10), (4.11) and (4.18), one can then write the velocity equation in the form proposed in (Gosselin and Angeles, 1990), i. e.,

$$\mathbf{A}\dot{\mathbf{x}} = \mathbf{B}\dot{\boldsymbol{\theta}} \tag{4.19}$$

where

$$\dot{\mathbf{x}} = [\dot{\mathbf{p}}^T \boldsymbol{\omega}^T]^T \tag{4.20}$$

$$\dot{\boldsymbol{\theta}} = [\dot{\theta}_{11} \dot{\theta}_{12} \dot{\theta}_{13} \dot{\theta}_{21} \dot{\theta}_{22} \dot{\theta}_{23}] \tag{4.21}$$

$$\mathbf{A} = \begin{bmatrix} \mathbf{n}_{11}{}^T & ((\mathbf{Q}\mathbf{b}_1) \times \mathbf{n}_{11})^T \\ \mathbf{n}_{12}{}^T & ((\mathbf{Q}\mathbf{b}_2) \times \mathbf{n}_{12})^T \\ \mathbf{n}_{13}{}^T & ((\mathbf{Q}\mathbf{b}_3) \times \mathbf{n}_{13})^T \\ \mathbf{n}_{21}{}^T & ((\mathbf{Q}\mathbf{b}_1) \times \mathbf{n}_{21})^T \\ \mathbf{n}_{22}{}^T & ((\mathbf{Q}\mathbf{b}_2) \times \mathbf{n}_{22})^T \\ \mathbf{n}_{23}{}^T & ((\mathbf{Q}\mathbf{b}_3) \times \mathbf{n}_{23})^T \end{bmatrix} \tag{4.22}$$

$$\mathbf{B} = \mathrm{diag}(g_{11}, g_{12}, g_{13}, g_{21}, g_{22}, g_{23}) \tag{4.23}$$

$$\mathbf{n}_{1i} = \begin{bmatrix} -\cos(\theta_{2i} + \alpha_i) \cos\theta_{3i} \\ -\sin(\theta_{2i} + \alpha_i) \cos\theta_{3i} \\ -\sin\theta_{2i} \sin\theta_{3i} \end{bmatrix} \tag{4.24}$$

$$\mathbf{n}_{2i} = \begin{bmatrix} \cos(\theta_{1i} + \alpha_i) \cos\theta_{3i} \\ \sin(\theta_{1i} + \alpha_i) \cos\theta_{3i} \\ \sin\theta_{1i} \sin\theta_{3i} \end{bmatrix} \tag{4.25}$$

$$g_{1i} = l_1 \sin(\theta_{1i} - \theta_{2i}) \cos \theta_{3i} \tag{4.26}$$

$$g_{2i} = l_2 \sin(\theta_{1i} - \theta_{2i}) \cos \theta_{3i} \tag{4.27}$$

$$g_{3i} = (l_3 + l_e) \cos \theta_{3i} \tag{4.28}$$

According to the definition given by Gosselin and Angeles (1990), the singularities of Type I occur when

$$\det(\mathbf{B}) = 0 \tag{4.29}$$

i.e.,

$$\prod_{i=1}^{3} l_1 \sin(\theta_{1i} - \theta_{2i}) \cos \theta_{3i} \prod_{i=1}^{3} l_2 \sin(\theta_{1i} - \theta_{2i}) \cos \theta_{3i} = 0 \tag{4.30}$$

This equation leads to singular conditions which define the boundary of the constant-orientation workspace of the 6-DOF parallel mechanism as follows:

$$\theta_{1i} - \theta_{2i} = n\pi, \; n \in Z \tag{4.31}$$

$$\theta_{3i} = n\pi + \frac{\pi}{2}, \; n \in Z \tag{4.32}$$

where $Z = 0, \pm 1, \pm 2, \dots$. Actually, these conditions are the singular conditions of the parallelepiped mechanism of each leg as shown in Section 2.5.

The singularities of Type II occur when

$$\det(\mathbf{A}) = 0 \tag{4.33}$$

As mentioned before, however, the closed-form expression of the determinant of $\mathbf{A}$ depends both on the Cartesian and the joint coordinates and it is impossible to find the roots of such an expression analytically. Moreover, each row of matrix $\mathbf{A}$ associated with the actuated joint is a six-dimensional Plcker vector associated with a line in Cartesian space (Merlet, 1989; Monsarrat and Gosselin, 2001). Hence, totally six lines $l_{1i}, l_{2i}, i = 1, 2, 3$ can be obtained from vectors $\mathbf{n}_{1i}, \mathbf{n}_{2i}$. However, these lines are very complicated and cannot easily be represented in space. It will be very difficult to obtain singularity conditions using Grassmann line geometry. Here, a discretization method is also used to determine the singularity loci inside the constant-orientation workspace. Finally, the singularity locus and boundary of the workspace for different values of z for the example mechanism (Case I) are obtained as demonstrated in Figure 4.11, where the outer thick curve represents the boundary of the workspace while the inner thin curves stand for the singularity loci.
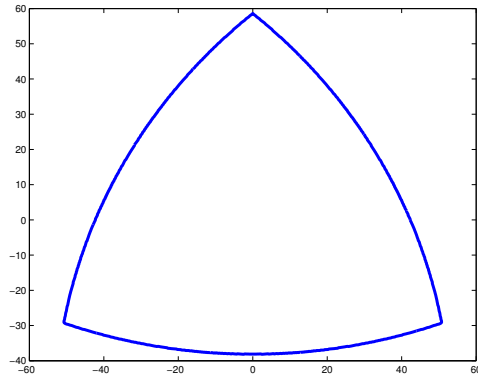
(a) $z = 100$ mm
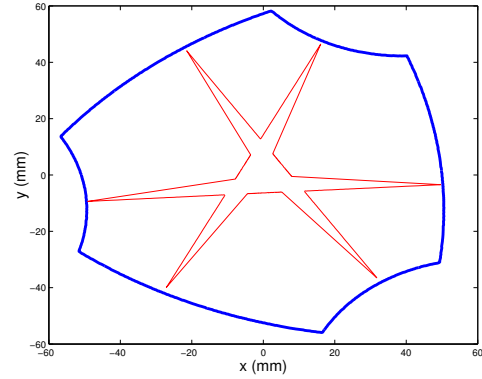
(b) $z = 90$ mm
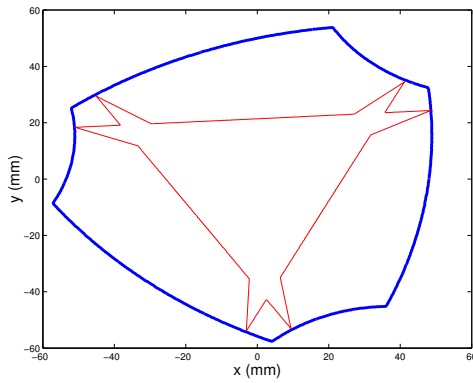
(c) $z = 70$ mm
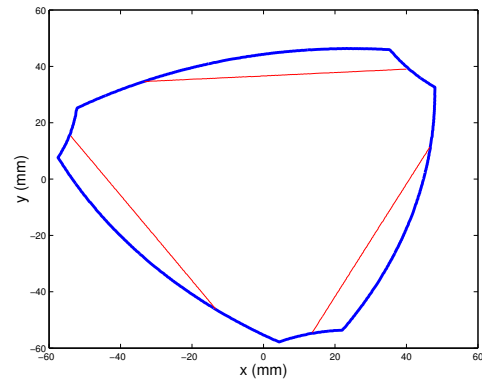
(d) $z = 50$ mm
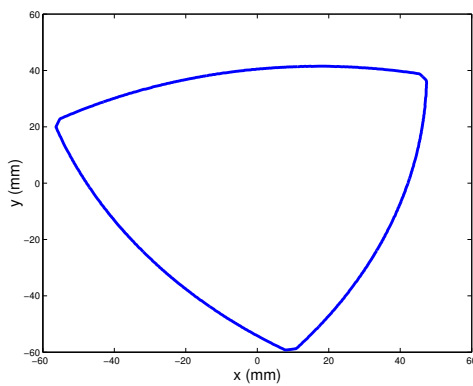
(e) $z = 30$ mm
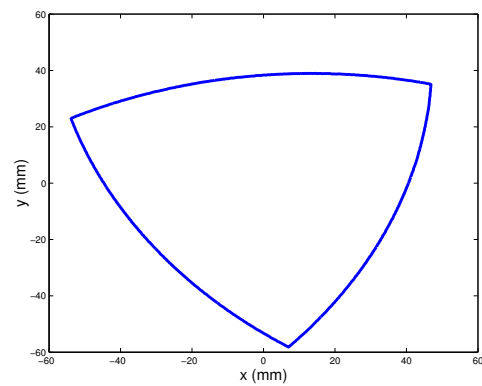
(f) $z = 0$ mm

Figure 4.11: Singularity locus and boundary of the workspace for different values of z, $(\phi, \theta, \psi) = (0, 0, 0)$ (Case I).
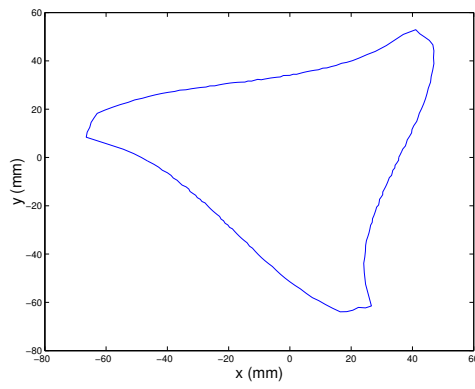
(a) $z = 70$ mm

(b) $z = 50$ mm

(c) $z = 30$ mm

(d) $z = 10$ mm
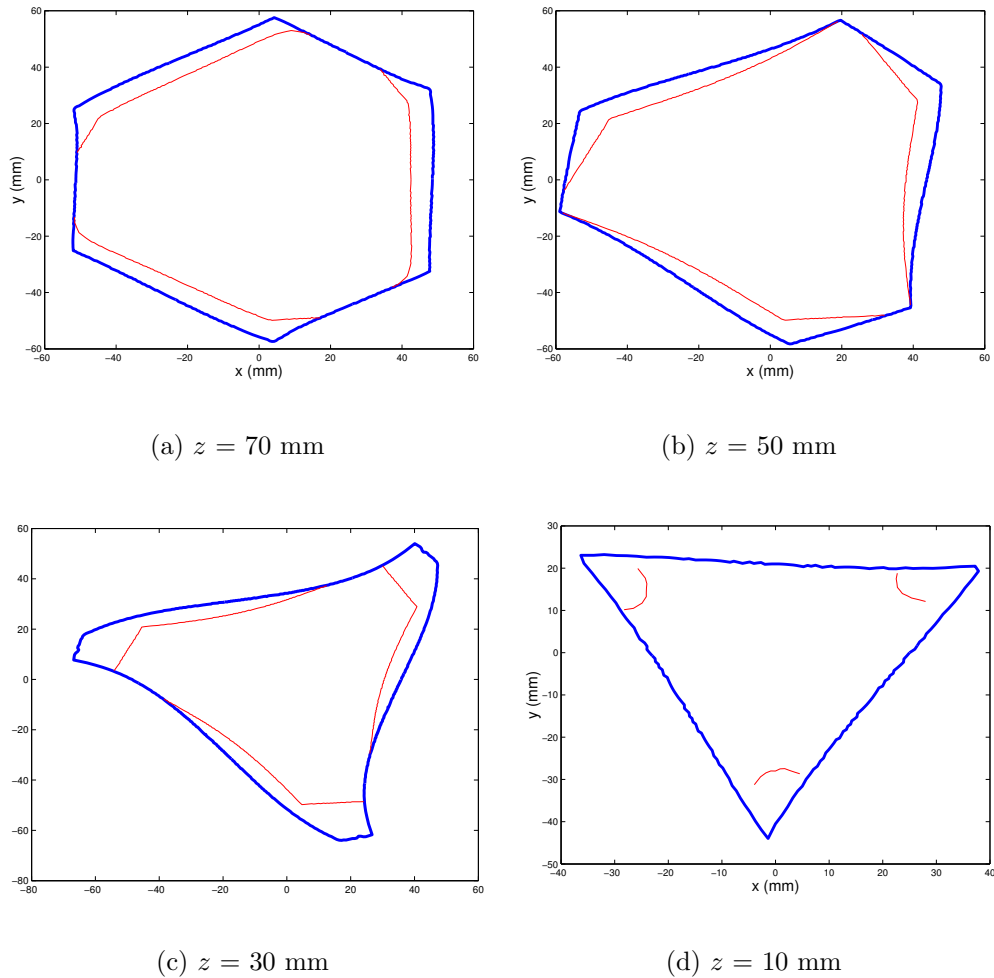
Figure 4.12: Singularity locus and boundary of the workspace for different values of z, $(\phi, \theta, \psi) = (0, 0, 0)$ (Case II).

For other types of actuation of the example mechanisms (Case I), the Jacobian matrices $\mathbf{A}$ and $\mathbf{B}$ can be obtained using vector $\mathbf{n}_{3i} = [0\ 0\ 1]^T$ and $g_{3i}, i = 1, 2, 3$ to replace the corresponding components in eqs. (4.23) and (4.24). For instance, if the revolute joints connected to the links V_1 and V_3 respectively are actuated for each leg, using vector $\mathbf{n}_{3i}$ and g_{3i} to replace $\mathbf{n}_{2i}$ and g_{2i} results in the Jacobian matrices $\mathbf{A}$ and $\mathbf{B}$ associated with this actuation. The singularity loci can then be obtained using the discretization method.

For the mechanisms of Case II, the Jacobian matrix of the leg parallelepiped mech-

anism is derived as follows:

$$\mathbf{J}_i = \begin{bmatrix} l_1 \cos \alpha_i \cos \theta_{1i} & -l_2 \sin(\theta_{2i} + \alpha_i) & (l_3 + l_e) \sin \alpha_i \sin \theta_{3i} \\ l_1 \sin \alpha_i \cos \theta_{1i} & l_2 \cos(\theta_{2i} + \alpha_i) & -(l_3 + l_e) \cos \alpha_i \sin \theta_{3i} \\ -l_1 \sin \theta_{1i} & 0 & (l_3 + l_e) \cos \theta_{3i} \end{bmatrix}$$

then, the inverse Jacobian matrix is written as

$$\mathbf{J}_i^{-1} = \begin{bmatrix} \frac{\cos(\theta_{2i}+\alpha_i)\cos\theta_{3i}}{l_1\delta_i} & \frac{\sin(\theta_{2i}+\alpha_i)\cos\theta_{3i}}{l_1\delta_i} & \frac{\sin\theta_{2i}\sin\theta_{3i}}{l_1\delta_i} \\ \frac{\cos\alpha_i\sin\theta_{1i}\sin\theta_{3i}-\sin\alpha_i\cos\theta_{1i}\cos\theta_{3i}}{l_2\delta_i} & \frac{\cos\alpha_i\cos\theta_{1i}\cos\theta_{3i}+\sin\alpha_i\sin\theta_{1i}\sin\theta_{3i}}{l_2\delta_i} & \frac{\cos\theta_{1i}\sin\theta_{3i}}{l_2\delta_i} \\ \frac{\sin\theta_{1i}\cos(\theta_{2i}+\alpha_i)}{(l_3+l_e)\delta_i} & \frac{\sin\theta_{1i}\sin(\theta_{2i}+\alpha_i)}{(l_3+l_e)\delta_i} & \frac{\cos\theta_{1i}\cos\theta_{2i}}{(l_3+l_e)\delta_i} \end{bmatrix}$$

$$(4.34)$$

where

$$\delta_i = \cos \theta_{1i} \cos \theta_{2i} \cos \theta_{3i} - \sin \theta_{1i} \sin \theta_{2i} \sin \theta_{3i} \tag{4.35}$$

For this case, it is assumed that the revolute joints connected to the links V_1 and V_3 respectively are actuated for each leg. The Jacobian matrices $\mathbf{A}$ and $\mathbf{B}$ can then be written as follows:

$$\mathbf{A} = \begin{bmatrix} \mathbf{n}_{11}{}^T & ((\mathbf{Qb}_1) \times \mathbf{n}_{11})^T \\ \mathbf{n}_{12}{}^T & ((\mathbf{Qb}_2) \times \mathbf{n}_{12})^T \\ \mathbf{n}_{13}{}^T & ((\mathbf{Qb}_3) \times \mathbf{n}_{13})^T \\ \mathbf{n}_{31}{}^T & ((\mathbf{Qb}_1) \times \mathbf{n}_{31})^T \\ \mathbf{n}_{32}{}^T & ((\mathbf{Qb}_2) \times \mathbf{n}_{32})^T \\ \mathbf{n}_{33}{}^T & ((\mathbf{Qb}_3) \times \mathbf{n}_{33})^T \end{bmatrix} \tag{4.36}$$

$$\mathbf{B} = \mathrm{diag}(g_{11}, g_{12}, g_{13}, g_{31}, g_{32}, g_{33}) \tag{4.37}$$

$$\mathbf{n}_{1i} = \begin{bmatrix} \cos(\theta_{2i} + \alpha_i) \cos \theta_{3i} \\ \sin(\theta_{2i} + \alpha_i) \cos \theta_{3i} \\ \sin \theta_{2i} \sin \theta_{3i} \end{bmatrix} \tag{4.38}$$

$$\mathbf{n}_{3i} = \begin{bmatrix} \cos(\theta_{2i} + \alpha_i) \sin \theta_{1i} \\ \sin(\theta_{2i} + \alpha_i) \sin \theta_{1i} \\ \cos \theta_{1i} \cos \theta_{2i} \end{bmatrix} \tag{4.39}$$

$$g_{1i} = l_1 \delta_i \tag{4.40}$$

$$g_{3i} = (l_3 + l_e) \delta_i \tag{4.41}$$

The singularities of Type I occur when

$$\cos \theta_{1i} \cos \theta_{2i} \cos \theta_{3i} - \sin \theta_{1i} \sin \theta_{2i} \sin \theta_{3i} = 0 \tag{4.42}$$
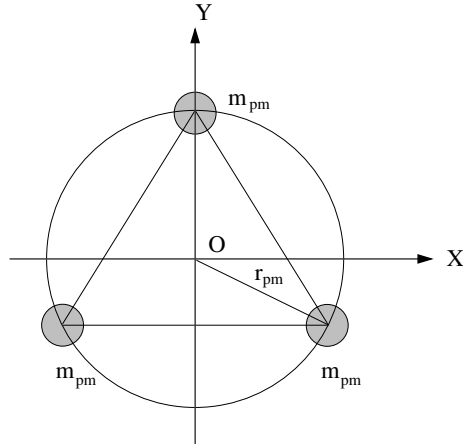
Figure 4.13: Determination of the three point masses.

This equation leads to singular conditions which define the boundary of the constant-orientation workspace of the mechanism.

Using a numerical method, the singularity locus (inner thin curves) of Type II and the boundary (outer thick curve) of the workspace for different values of z for the example mechanism (Case II) are demonstrated in Figure 4.12.

4.7 Dynamic Balancing of the 6-DOF Parallel Mechanisms

In order to simplify the dynamic balancing of multi-degree-of-freedom parallel mechanisms with several legs, the dynamic balancing for each detached leg mechanism is considered independently, if the mobile platform is replaced by point masses located at the points of attachment of the legs to the platform (see Appendix A). To ensure that the point masses are dynamically equivalent to the solid platform, three conditions must be satisfied (Ricard and Gosselin, 2000), namely: i) the sum of the masses of the point masses must be equal to the mass of the platform, ii) the center of mass of the point masses must be located at the center of mass of the platform and iii) the inertia tensor (or radius of gyration for planar motion) of the point masses must be the same as that of the platform with respect to any coordinate frame. For a platform undergoing planar motion, the radius of gyration should be equal to the distance between each of

the attachment points and the center of mass of the platform.

For the spatial 6-DOF parallel mechanism of this chapter, the mass and inertia of the platform are distributed among the attachment points of the legs to the platform and replaced by three identical point masses m_{pm} symmetrically arranged on a plane (Figure 4.13).

Clearly, the center of mass of the point masses is located at the center of mass of the platform if the latter is uniform. The conditions for dynamic equivalence can therefore be satisfied if the moments of inertia of the point masses and the platform are equal. These moments of inertia are given in the frame with the z' axis orthogonal to the plane and with the origin at the geometric center of the equilateral triangle — using the three points as its vertices — or the centroid of the platform. The moments of inertia of the three point masses relative to the frame can be written as follows:

$$I_{xx} = \frac{3}{2}m_{pm}r_{pm}^2 \tag{4.43}$$

$$I_{yy} = I_{xx} \tag{4.44}$$

$$I_{zz} = 3m_{pm}r_{pm}^2 \tag{4.45}$$

where r_{pm} is the distance between any point mass and the centroid of the platform. Since m_{pm} is equal to one third of the mass of platform m_{pl}, r_{pm} is equal to the radius of gyration of the platform with respect to the z' axis.

From eqs. (4.43) – (4.45), it can be found that any symmetric thin homogeneous platform (circular, square, equilaterally triangular, etc.) can satisfy the above conditions, which lead to $I_{xx} = I_{yy} = \frac{1}{2}I_{zz}$. Hence the platform can be replaced by three point masses. However, if the platform has a nonzero thickness or is not symmetric, the above conditions cannot be satisfied (Bedford and Fowler, 1996). In this case, the platform could be replaced by four non-coplanar point masses. Consequently, four legs could be used and the attachment points of the legs on the platform must not lie on one plane in order to obtain a reactionless 6-DOF parallel mechanism.

Once the equivalent point masses have been determined, each of the point masses is included in the corresponding 3-DOF leg and is considered in the balancing. By dynamically balancing each of the three legs individually — including the point mass — and attaching the legs — without the point masses — to a common platform satisfying the above conditions, a reactionless 6-DOF parallel mechanism will be obtained. This

result is correct because the redistribution of the internal forces due to the kinematic constraints induced by the platform do not affect the dynamic balancing. Indeed, the individual balancing of the legs is justified by the fact that dynamic balancing is a property associated with the moving masses and inertia. In other words, although the reaction forces and moments on the base of each leg may not be zero in the real system with the solid platform — because of the distribution of the internal forces — the net reactions on the base will be equal to zero.

For example, if the moving platform of the 6-DOF parallel mechanisms can be replaced by three point masses ($m_{pm} = 0.05\ kg$), numerical examples of the reactionless 3-DOF leg parallelepiped mechanisms associated with Case I and II can be given in Table 3.2 and Table 3.3 respectively and reactionless spatial 6-DOF parallel mechanisms can finally be obtained.

The verification of the reactionless property of the 6-DOF parallel mechanism has also been performed using ADAMS. Simulation models have been built using ADAMS (Figure 4.14). Simulations have been performed for several arbitrary trajectories. The resulting reaction forces and moments on the base are illustrated in Figure 4.15. The results clearly demonstrate that the resulting reaction forces and moments on the base are very small with respect to the joint forces and driving torques (with a ratio of 10^{-5} to 10^{-6}) due to small modeling errors. Hence, it is clearly demonstrated that the synthesized 6-DOF mechanisms are reactionless. These numerical simulation results support the approach of using point masses to replace a platform introduced in this chapter.

However, it is clear that replacing the platform by equivalent point masses may well yield balancing conditions that are more restrictive than those that would be obtained if the mechanism was balanced globally. Taking the 6-DOF parallel mechanism with 3 legs as an example, dynamic balancing of each 3-DOF leg mechanism independently is equivalent to dynamically balancing a system with in total 9 degrees of freedom (i.e., 9 counter-rotations have to be added), while dynamic balancing of the 6-DOF mechanism globally may be achieved using only 6 counter-rotations due to the constraints of the moving platform.
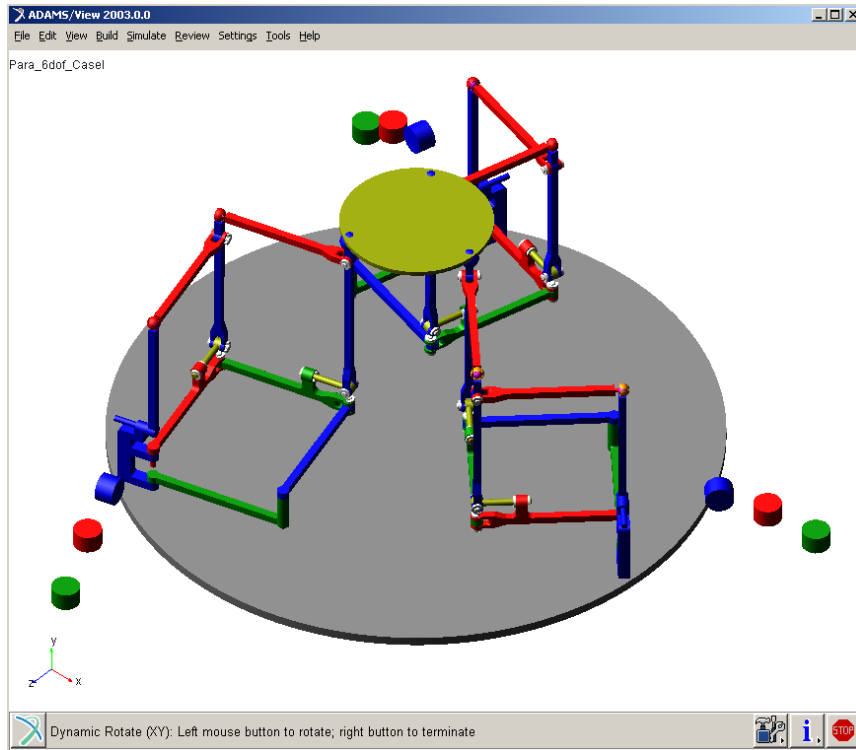
(a) Case I
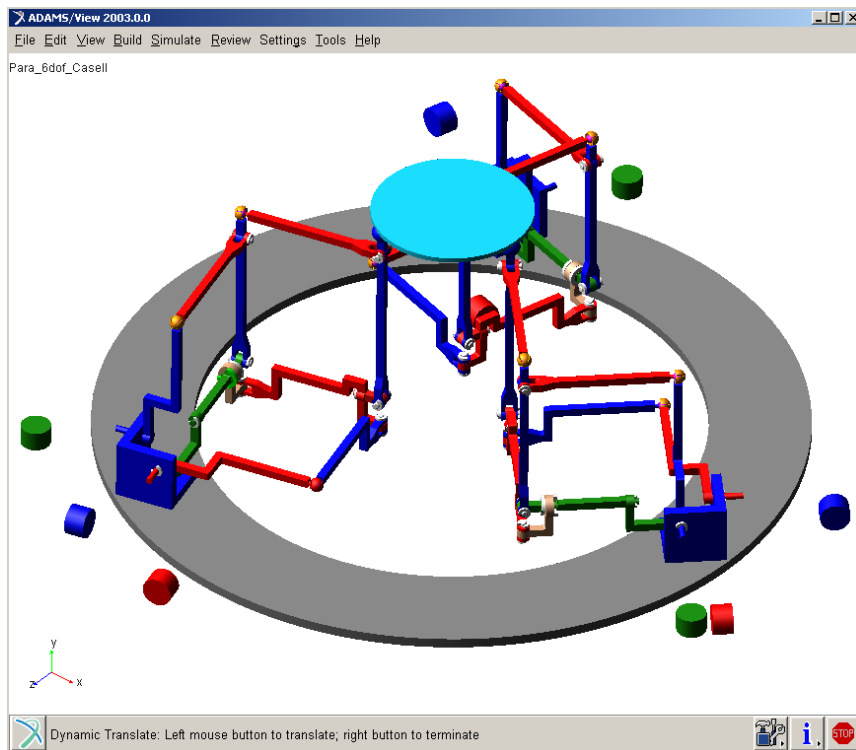
(b) Case II

Figure 4.14: Simulation of the 6-DOF parallel mechanisms using ADAMS.
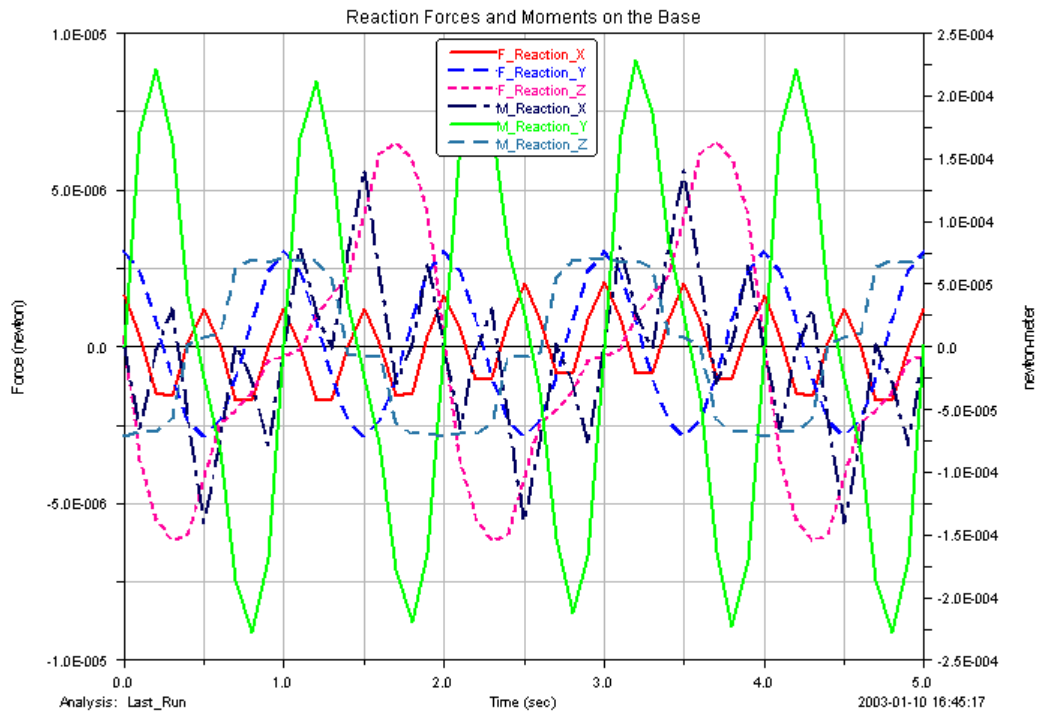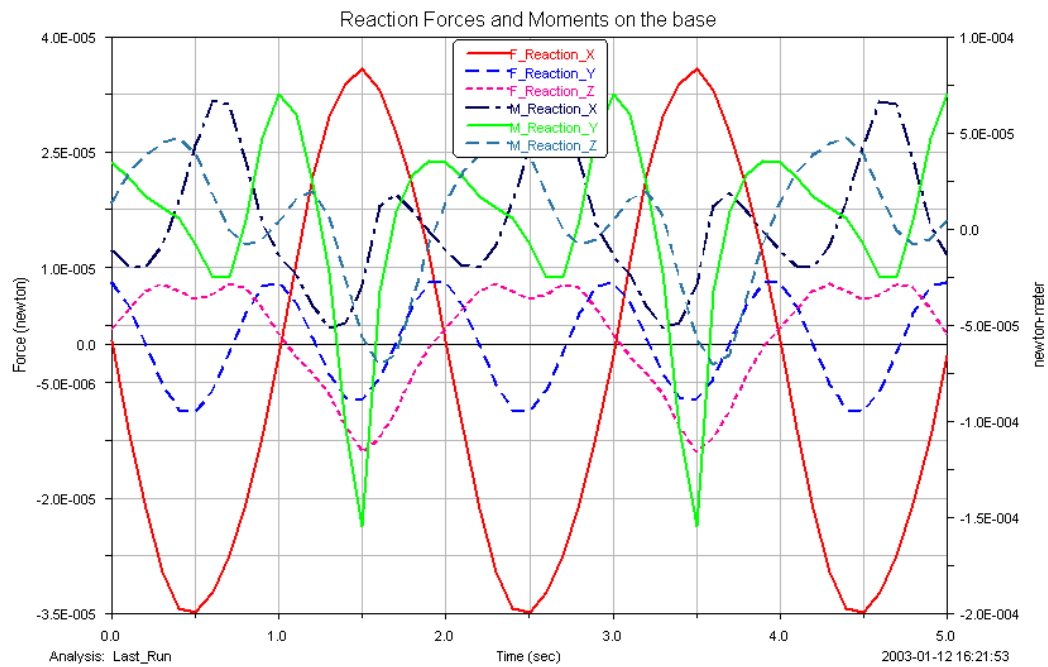
(a) Case I.

(b) Case II.

Figure 4.15: Verification of the reactionless property of the 6-DOF parallel mechanisms.

4.8   Conclusion

This chapter presented the kinematic analysis and dynamic balancing of 6-DOF parallel mechanisms using parallelepiped mechanisms. After describing the synthesis of 6-DOF parallel mechanisms with three legs composed of parallelepiped mechanisms, the kinematic analysis including the inverse and direct kinematics as well as the determination of singularity loci and workspace of the 6-DOF parallel mechanisms have been solved. The Jacobian matrix of the mechanisms associated with different actuation schemes have been derived. A geometrical algorithm and a discretization method have been used for the determination of the workspace and singularity loci for the two cases of the mechanism. The graphical representations that show the relationship between the singularity loci and the constant-orientation workspace of the mechanisms have been given. Finally, the dynamic equivalence between a platform and three point masses has been discussed and the dynamic balancing of 6-DOF parallel mechanisms has also been addressed. Numerical examples of reactionless 6-DOF mechanisms have been given and, with the help of the dynamic simulation software ADAMS, it has been shown that the mechanisms are reactionless for arbitrary trajectories.

Chapter 5

Synthesis of Reactionless Spatial 3-DOF and 6-DOF Mechanisms Using Planar Four-bar Linkages

This chapter presents the synthesis of novel reactionless spatial 3-DOF and 6-DOF mechanisms without any separate counter-rotation, using four-bar linkages. Based on the conditions of dynamic balancing of a single planar four-bar linkage developed elsewhere, the spatial problem is shown to be equivalent to ensuring that the inertia tensor of reactionless four-bar linkages remains constant when the planar mechanism(s) is(are) moving. The reactionless conditions for planar four-bar linkages undergoing spatial motion are first given. Then, reactionless spatial 3-DOF mechanisms using four-bar linkages are synthesized. A numerical example of the reactionless spatial 3-DOF mechanism is given and, with the help of the dynamic simulation software ADAMS, it is shown that the mechanism is reactionless for arbitrary trajectories. Finally, this mechanism is used to synthesize 6-DOF reactionless parallel mechanisms.

5.1   Introduction

In the preceding two chapters, the dynamic balancing of spatial 3-DOF parallelepiped mechanisms and 6-DOF parallel mechanisms synthesized with parallelepiped mechanisms have been achieved using counterweights and counter-rotations with fixed axis and inertia. Actually, in order to obtain dynamically balanced mechanisms, most of the authors in the literature on dynamic balancing have used additional counter-rotations. However, adding counter-rotations to a mechanism increases its complexity and brings some side effects, and then reduces its practicality significantly, especially in multi-degree-of-freedom systems. Ricard and Gosselin (2000) have focused on the planar four-bar linkage and obtained the complete balancing of the linkage in the plane as a set of constraints on the geometric and inertial parameters of the links but without separate counter-rotations. These dynamically balanced four-bar linkages have been stacked up to synthesize reactionless planar 3-DOF parallel mechanisms (Ricard and Gosselin 2000) and reactionless spatial 3-DOF parallel mechanisms (Vollmer and Gosselin, 2000; Gosselin et al., 2002). However, since the reactionless four-bar linkages are balanced only in the plane, the stacked reactionless 2-DOF mechanisms — used as legs to synthesize planar or spatial 3-DOF mechanisms — can only move in the plane. Hence, these reactionless four-bar linkages cannot be directly used to synthesize reactionless spatial 6-DOF mechanisms. Obtaining dynamically balanced four-bar linkages which can move spatially (out of the plane) is a more challenging problem and is necessary for the development of spatial reactionless multi-degree-of-freedom mechanisms or manipulators having up to 6-DOF using four-bar mechanisms.

In this chapter, a general planar four-bar linkage is first considered in order to obtain the conditions for its spatial dynamic balancing. Based on the conditions for dynamic balancing of a planar four-bar linkage, it is shown that the spatial problem is equivalent to ensuring that the inertia tensor of planar reactionless four-bar linkages remains constant while the linkages are undergoing motion. Then, the reactionless conditions for planar four-bar linkages moving spatially are derived and reactionless spatial 3-DOF mechanisms using four-bar linkages without any separate counter-rotation are synthesized. Finally, the latter mechanisms are used to synthesize 6-DOF reactionless mechanisms which do not involve any separate counter-rotation.
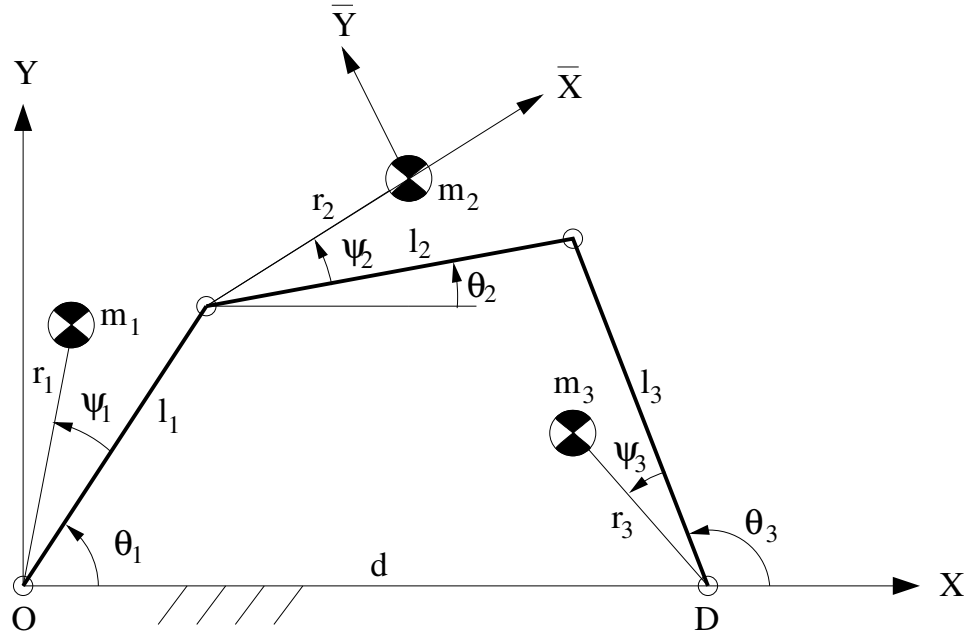
Figure 5.1: Planar four-bar linkage.

5.2 Reactionless Planar Four-Bar Linkages Without Separate Counter-rotations

A general planar four-bar linkage with fixed base is shown in Figure 5.1. As indicated in the figure, m_i and l_i are the mass and length, respectively, of the ith bar, and d is the distance between the two joints on the fixed base. The position of the center of mass of bar i is described by parameters r_i and ψ_i. Moreover, θ_i is the angular position of bar i with respect to the X axis. By imposing that the center of mass of the mechanism is fixed and that the total angular momentum is constant with respect to a fixed point — in order to obtain a dynamically balanced mechanism — Ricard and Gosselin (2000) have derived the dynamic balancing conditions for planar four-bar linkages and have identified three families (designated here as Case I, Case II and Case III respectively) of reactionless four-bar mechanisms. The mechanisms are represented schematically in Figure 5.2. In each case, there are no separate counter-rotations, and only counterweights are required for complete balancing.

For Case I, the balancing conditions are written as

$$\epsilon = \pm 1, \ \psi_1 = 0, \ \psi_2 = 0, \ \psi_3 = \pi, \ d = l_1, \ l_2 = l_3,$$
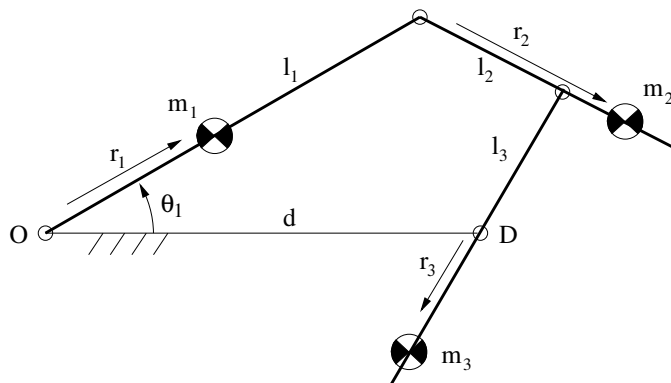
(a) Case I.
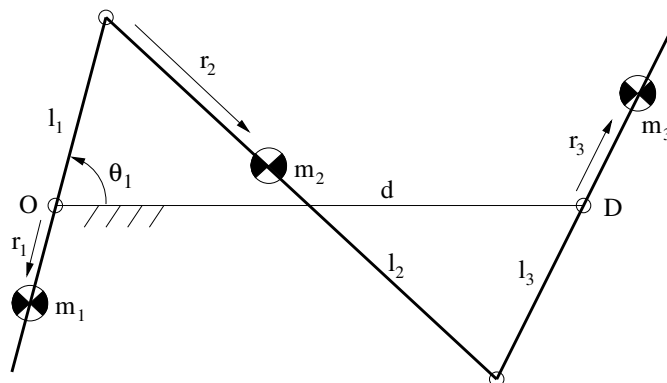
(b) Case II.
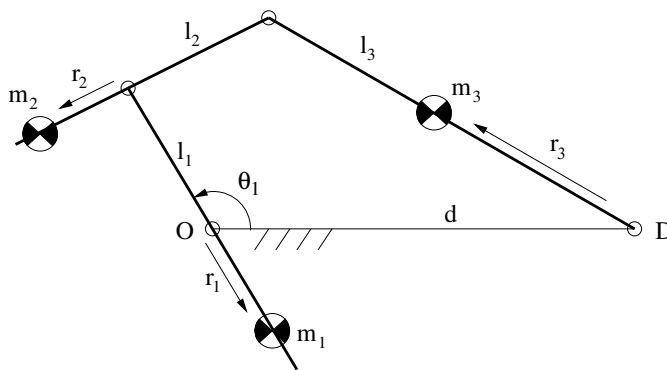
(c) Case III.

Figure 5.2: Three families of reactionless four-bar linkages.

$$r_2 = l_2(1 + \frac{m_1 r_1}{m_2 l_1}), \; k_2 = \sqrt{\frac{m_2 r_2(l_2 - r_2) - I_{c1}}{m_2}},$$

$$r_3 = \frac{m_2 r_2 l_3}{m_3 l_2}, \; k_3 = \sqrt{\frac{-m_3 r_3(l_3 + r_3) - I_{c1}}{m_3}} \tag{5.1}$$

for Case II,

$$\epsilon = -1, \; \psi_1 = \pi, \; \psi_2 = 0, \; \psi_3 = \pi, \; d = l_2, \; l_3 = l_1,$$

$$r_2 = l_2(1 - \frac{m_1 r_1}{m_2 l_1}), \; k_2 = \sqrt{\frac{m_2 r_2(l_2 - r_2) - I_{c1}}{m_2}},$$

$$r_3 = \frac{m_2 r_2 l_3}{m_3 l_2}, \; k_3 = \sqrt{\frac{-m_3 r_3(l_3 + r_3) + I_{c1}}{m_3}} \tag{5.2}$$

and, for Case III,

$$\epsilon = 1, \; \psi_1 = \pi, \; \psi_2 = \pi, \; \psi_3 = 0, \; d = l_3, \; l_2 = l_1,$$

$$r_2 = -l_1 + \frac{m_1 r_1}{m_2}, \; k_2 = \sqrt{\frac{I_{c1} - m_2 r_2(l_2 + r_2)}{m_2}},$$

$$r_3 = \frac{m_2 r_2 l_3}{m_3 l_2}, \; k_3 = \sqrt{\frac{m_3 r_3(l_3 - r_3) - I_{c1}}{m_3}} \tag{5.3}$$

where $\epsilon(= \pm 1)$ is the branch index (assembly mode of the four-bar linkage), i.e., the sign used in the quadratic equation in the determination of θ_2 and θ_3 for a given θ_1 (Appendix B), k_i is the radius of gyration of the ith bar with respect to its center of mass and $I_{c1} = m_1 k_1^2 + m_1(r_1^2 - r_1 l_1 \cos \psi_1)$. It is pointed out that the above balancing conditions impose strict constraints on the dimensional parameters of the linkage (and on the assembly mode for Cases II and III). These dimensional constraints make all three types of linkages "foldable", i.e., all the bars can be aligned on the base. Therefore, these mechanisms are generally not suitable for machinery where the input link must be driven through full rotations. However, for multi-degree-of-freedom applications (e.g. robotic applications), the above linkages can be considered as one-dof components providing sufficient range of motion for many practical purposes.

By inspection of the three families of reactionless four-bar linkages in Figure 5.2, it can be found that Case I and III are, structurally speaking, completely the same. They are classified as two separate cases due to the difference in the mounting mode as well as the actuation (i.e., the first link as input link). Nevertheless, for Case II, any of the other two links except for the base link and the second link can be considered as input link in eq. (5.2).
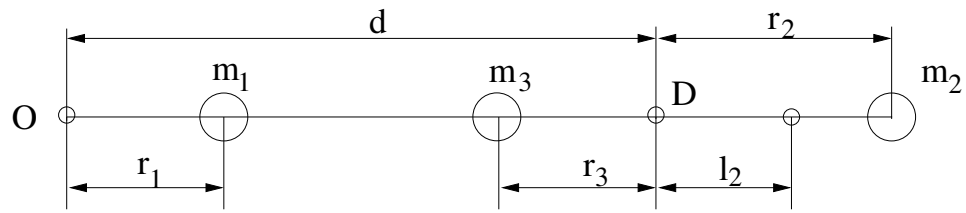
(a) Case I
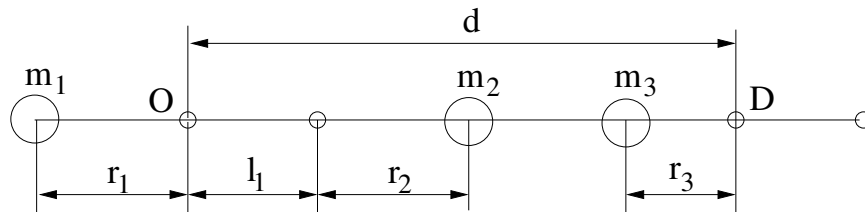
(b) Case II
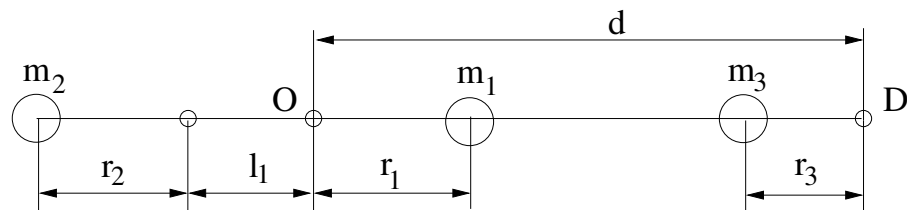
(c) Case III

Figure 5.3: Determination of the center of mass and radius of gyration of four-bar linkages.
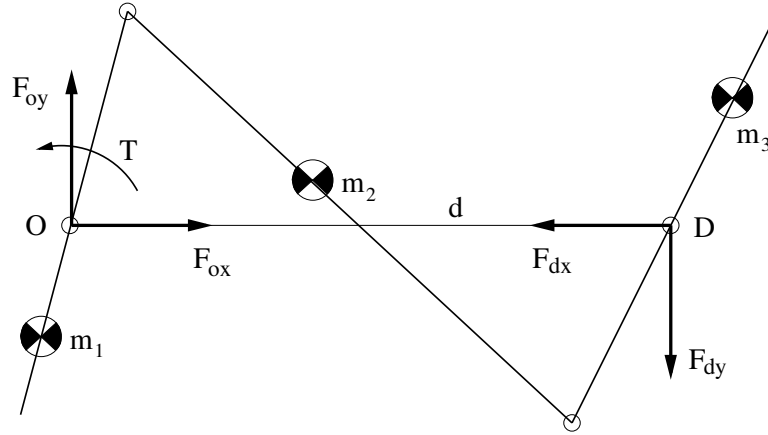
Figure 5.4: Reactionless property of a dynamically balanced four-bar linkage.

Since the center of mass remains fixed for any configuration in a reactionless mechanism, the position of the center of mass of any mechanism in Figure 5.2 can be determined by considering a flat configuration (one in which all bars are aligned as shown in Figure 5.3). Therefore, the center of mass lies on the base line OD at a distance $\bar{r}$ from joint O. This distance can be obtained for each of the three cases as follows:

for Case I,

$$\bar{r} = \frac{m_2 l_1 + m_1 r_1 + m_3 l_1}{m_t} \tag{5.4}$$

while for Cases II and III,

$$\bar{r} = \frac{d(m_2 l_1 - m_1 r_1 + m_3 l_1)}{l_1 m_t} \tag{5.5}$$

where $m_t = m_1 + m_2 + m_3$. The radius of gyration k_t for the whole mechanism with respect to its center of mass can be written as follows:

$$k_t = \sqrt{\frac{I_g + I_d - m_t \bar{r}^2}{m_t}} \tag{5.6}$$

where

$$\begin{aligned} I_g &= m_1 k_1^2 + m_2 k_2^2 + m_3 k_3^2 \\ I_d &= m_1 r_1^2 + m_2 (l_1 + r_2)^2 + m_3 (d - r_3)^2 \end{aligned} \tag{5.7}$$

Any planar four-bar mechanism satisfying one of the three sets of conditions given above (eq. (5.1), (5.2) or (5.3)) will be reactionless and will behave, globally, as a rigid

body in the plane — fixed center of mass and constant radius of gyration — when undergoing planar motion. In other words, any motion of the linkage will induce zero reaction force and moment on the base when the latter is fixed. Conversely, it is not possible to induce internal motion of the mechanism by imparting linear and/or angular accelerations to the base. Taking a dynamically balanced mechanism of Case II as an example, there is no shaking force and shaking moment on the base due to its fixed center of mass and zero angular momentum. Clearly, the resulting external force and moment of the mechanism are zero. If we consider the balanced four-bar linkage as a system isolated from the base (Figure 5.4), the external forces and moment are the joint forces ($\mathbf{F}_{ox}, \mathbf{F}_{oy}, \mathbf{F}_{dx}, \mathbf{F}_{dy}$) and the actuator driving torque $\mathbf{T}$ acting on the system (gravity is excluded and friction is neglected). Although the direction and magnitude of the forces and torque depend on which motion is applied, the zero reaction force and moment on the base always come from: $F_{ox} = F_{dx}, F_{oy} = F_{dy}$ and $T = dF_{dy}$ and their opposite directions. In other words, the reactions of the individual joint forces act on the base and generate a couple to cancel the actuator reaction torque for any motion. If the frictional torques are considered on the joints, the actuator driving torque and the joint forces will be changed. But the resulting reaction moment on the base is still $T - M_f - dF_{dy} = 0$ (where M_f is the sum of frictional torques on joints O and D). Namely, friction does not affect the results of dynamic balancing. Note that in a real prototype the actuator inertia must be considered as part of the inertia of the input link.

Notice that the above dynamic balancing conditions were derived on the assumption that each link of the planar four-bar linkage is symmetric about the motion plane, i.e., the products of inertia I_{xz}, I_{yz} of each link relative to its center of mass are zero. Moreover, any mechanism behaving as a rigid body in the plane (i.e., fixed center of mass and constant I_{zz}) and having zero products of inertia (I_{xz}, I_{yz}) can be mounted on the moving link (the first or third link) of the planar four-bar linkage to synthesize a reactionless mechanism with more degrees of freedom as long as the resulting parameters of the moving link meet the corresponding dynamic balancing conditions (eq. (5.1), (5.2) or (5.3)).

By inspection of eqs. (5.1–5.3), it is clear that infinitely many solutions exist and hence each of the three families includes infinitely many linkages. However, the parameters cannot be chosen arbitrarily since the expressions appearing under the square roots in the balancing conditions must be positive. Vollmer and Gosselin (2000) have
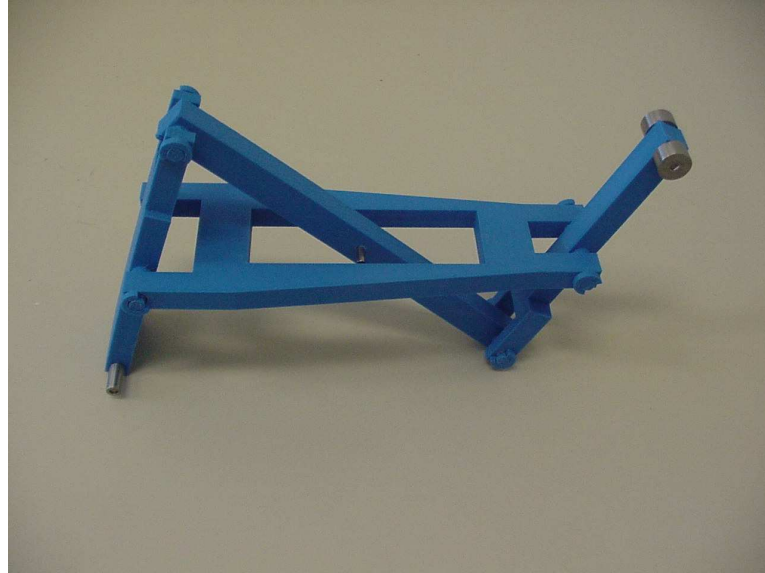
Figure 5.5: Prototype of a reactionless four-bar linkage (Courtesy of Gabriel Côté).

investigated the feasibility domain in the design space and found that Case II provides the widest range of feasible values of design parameters and better compactness properties. Hence, Case II is chosen for the design of reactionless four-bar linkages (Figure 5.5) and the synthesis of reactionless multi-degree-of-freedom parallel mechanisms in Vollmer and Gosselin (2000) and in this chapter.

The manipulation of a reactionless four-bar linkage of Case II shown in Figure 5.5 also provides a convincing demonstration of the reactionless property. When holding the base of the mechanism in one's hand, it is not possible to induce motion of the four-bar mechanism by imparting linear or angular accelerations to the base. By removing some of the metal cylinders and hence creating some unbalance, this property is lost and the result is clearly observable. Also, when holding the base in one hand and using the other hand to push the mechanism to one of its limits, it is clearly felt that there is no resulting reaction on the base when the mechanism hits its physical limit. Again, comparing with the unbalanced mechanism, the illustration is convincing.

5.3 Synthesis of Reactionless Planar and Spatial 3-DOF Parallel Mechanisms with Planar Motion of Legs

Since a reactionless four-bar linkage behaves as a rigid body moving in a plane, it can be mounted on the moving links of another planar four-bar linkage to synthesize a 2-DOF reactionless planar mechanism. In this case, the "distal" four-bar linkage is first balanced and then, its mass and inertia are added to the link on which it is attached to perform the balancing of the "proximal" four-bar linkage. By repeating this procedure, a multi-degree-of-freedom planar mechanism can be obtained simply by stacking the four-bar linkages on each other.

An example of a planar 2-DOF mechanism obtained with this approach is shown schematically in Figure 5.6 where the first index of the subscript stands for the number of the link, while the second index stands for the number of the mechanism. Figure 5.6(a) shows the first dynamically balanced four-bar linkage (a point mass has been considered at the end-effector if applicable but is not shown on the figure). The base link of the first mechanism and the third link of the second four-bar mechanism are the same link (the so-called common link). The global mass m_m, center of mass (position A) and radius of gyration of the first mechanism excluding the common link can be calculated from eqs. (5.5) and (5.6). Figure 5.6(b) shows the second four-bar linkage to be dynamically balanced. The center of mass of the common link with "naked" mass m_{3wm}, namely, without the first mechanism attached on it is located at position B. Figure 5.6(c) shows the synthesized mechanism. The mass and inertia of the first mechanism should be added to the common link. Hence, if the resulting mass m_3, center of mass r_3 (position C) and radius of gyration with respect to C of the common link and the attached first mechanism satisfy the balancing conditions of eqs. (5.2), the second four-bar linkage will be dynamically balanced, i.e., the synthesized 2-DOF mechanism will be reactionless. Note that all the centers of mass (i.e., A, B and C) should be on the axis of the common link. The 2-DOF reactionless mechanism can be used to synthesize reactionless 3-DOF parallel mechanisms. This can be achieved by using the 2-DOF mechanism as a leg for the 3-DOF mechanism. By connecting three such legs to a common platform, a 3-DOF reactionless mechanism can be obtained as shown in Figure 5.7 (Vollmer and Gosselin, 2000).
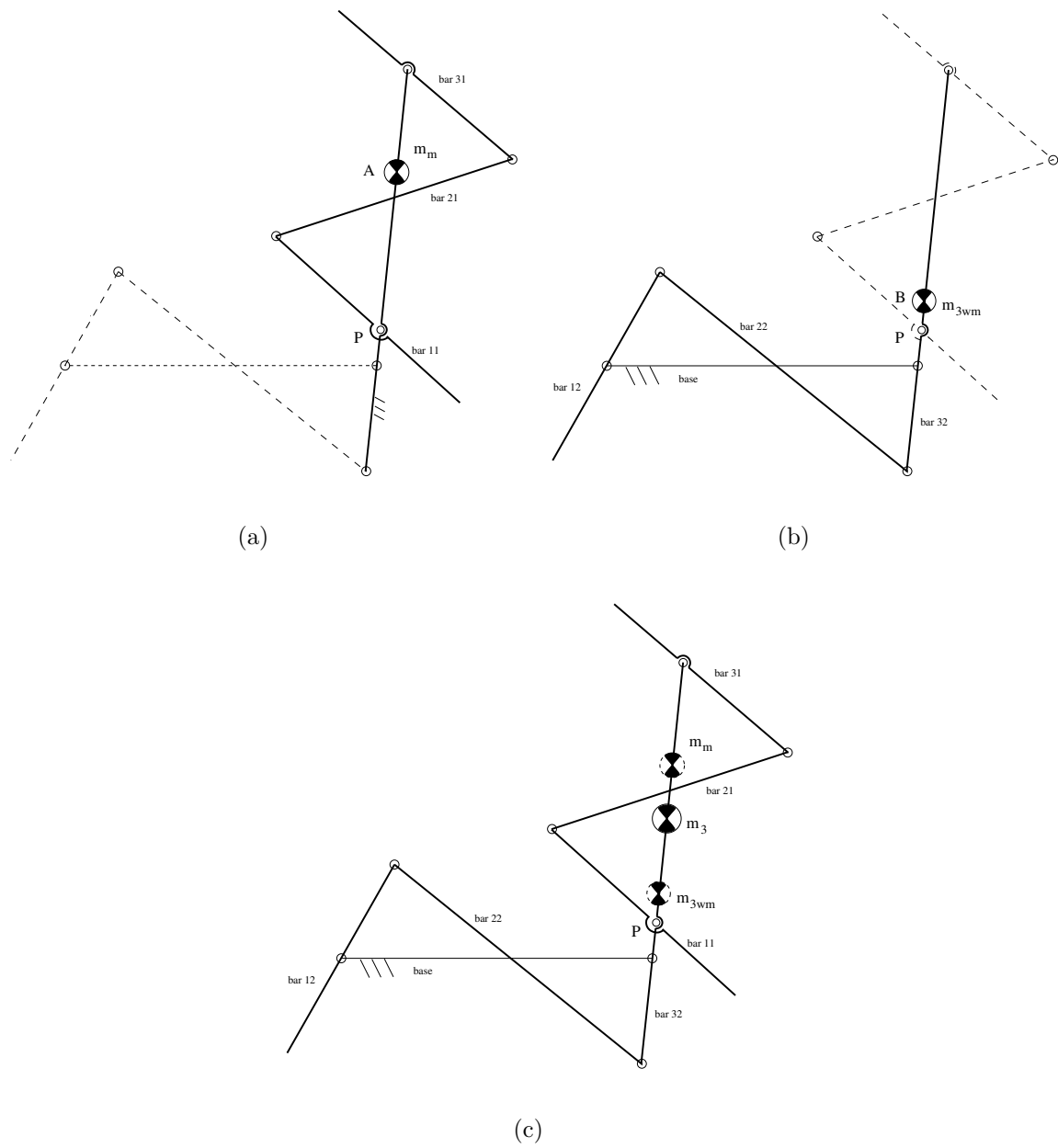
Figure 5.6: Sketch of the synthesis of a reactionless planar 2-DOF mechanism.
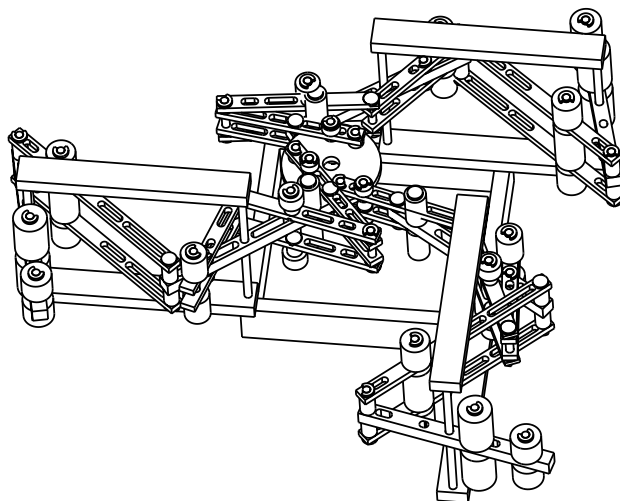
(a) Planar 3-DOF mechanism
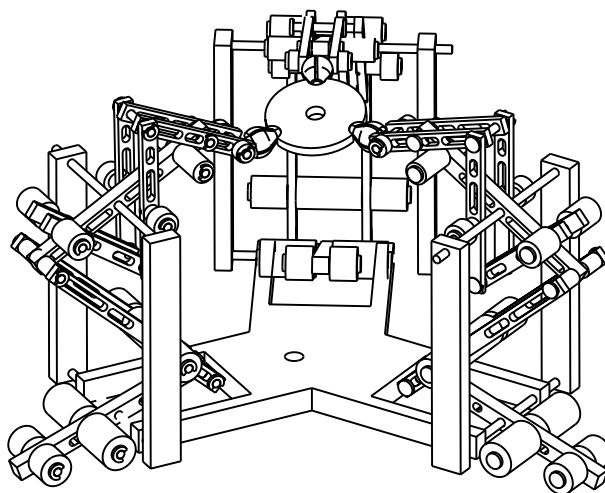
(b) Spatial 3-DOF mechanism.

Figure 5.7: Prototypes of reactionless 3-DOF parallel mechanisms (from Vollmer and Gosselin, 2000).

5.4   Reactionless Conditions for Planar Four-Bar Linkages Undergoing Spatial Motion

A reactionless mechanism behaves, globally, as a single rigid body. Hence, a fixed center of mass and a time-invariant inertia tensor are necessary conditions for the dynamic balancing of a mechanism undergoing general spatial motion.

Moreover, since a reactionless planar four-bar linkage behaves as a rigid body moving in the plane, it can be mounted on the third (or first) link of another four-bar linkage to synthesize a reactionless planar 2-DOF mechanism. By repeating this procedure, a reactionless planar multi-degree-of-freedom mechanism can be obtained simply by stacking the four-bar linkages on each other. However, the stacked reactionless mechanisms can only move in the plane. In order to obtain a 2-DOF mechanism using two four-bar linkages which undergoes spatial motion for further synthesis of spatial multi-degree-of-freedom mechanisms, the attached four-bar linkage must be mounted on the third link of the base four-bar linkage in such a way that the motion plane of the former mechanism is not coplanar to that of the latter mechanism. Therefore, if the attached mechanism behaves as a rigid body in space and the above synthesis and balancing conditions are satisfied, the synthesized spatial mechanism will be reactionless. Yet, there is no guarantee that a reactionless planar four-bar linkage (Figure 5.2) undergoing spatial motion will continue to behave as a rigid body in space. In order to address the balancing for spatial motion, the inertia tensor of a general planar four-bar linkage is now studied.

5.4.1   Determination of the Inertia Tensor of a Planar Four-Bar Linkage

From Figure 5.1, the inertia tensors $\mathbf{I}_{bi}$ of the three mobile bars ($i = 1, 2, 3$) of a planar four-bar linkage with respect to the local frames with origin at O — parallel to their corresponding local frame $\overline{X}, \overline{Y}$ — are written as follows:

$$\mathbf{I}_{b1} = \begin{bmatrix} I_{xx1} & -I_{xy1} & 0 \\ -I_{xy1} & I_{yy1} + m_1 r_1^2 & 0 \\ 0 & 0 & I_{zz1} + m_1 r_1^2 \end{bmatrix} \tag{5.8}$$

$$\mathbf{I}_{b2} = \begin{bmatrix} I_{xxb2} & -I_{xyb2} & 0 \\ -I_{xyb2} & I_{yyb2} & 0 \\ 0 & 0 & I_{zzb2} \end{bmatrix} \tag{5.9}$$

$$\mathbf{I}_{b3} = \begin{bmatrix} I_{xxb3} & -I_{xyb3} & 0 \\ -I_{xyb3} & I_{yyb3} & 0 \\ 0 & 0 & I_{zzb3} \end{bmatrix} \tag{5.10}$$

with

$$
\begin{aligned}
I_{xxb2} &= I_{xx2} + m_2 l_1^2 \sin^2 \theta_a \\
I_{xyb2} &= I_{xy2} + m_2 l_1 \sin \theta_a (r_2 + l_1 \cos \theta_a) \\
I_{yyb2} &= I_{yy2} + m_2 (r_2 + l_1 \cos \theta_a)^2 \\
I_{zzb2} &= I_{zz2} + m_2 (l_1^2 + r_2^2 + 2l_1 r_2 \cos \theta_a) \\
I_{xxb3} &= I_{xx3} + m_3 d^2 \sin^2 \theta_b \\
I_{xyb3} &= I_{xy3} - m_3 d(r_3 + d \cos \theta_b) \sin \theta_b \\
I_{yyb3} &= I_{yy3} + m_3 (r_3 + d \cos \theta_b)^2 \\
I_{zzb3} &= I_{zz3} + m_3 (d^2 + r_3^2 + 2dr_3 \cos \theta_b) \\
\theta_a &= \theta_1 - \theta_2 - \psi_2 \\
\theta_b &= \theta_3 + \psi_3
\end{aligned}
$$

where I_{xxi}, I_{yyi}, I_{zzi} and I_{xyi}, $i = 1, 2, 3$ are the moments and product of inertia of the ith bar relative to the local frame $\overline{X}, \overline{Y}$ with origin at the center of mass of the bar. Moreover, $I_{zzi} = m_i k_i^2$. Since a planar four-bar linkage is symmetric about the plane of motion, the products of inertia (I_{xzi}, I_{yzi}) of the ith bar are assumed to be zero.

The rotation matrix $\mathbf{Q}_i$ giving the orientation of the local frame $\overline{X}, \overline{Y}$ relative to the global frame X, Y can be given by

$$\mathbf{Q}_i = \begin{bmatrix} \cos(\theta_i + \psi_i) & -\sin(\theta_i + \psi_i) & 0 \\ \sin(\theta_i + \psi_i) & \cos(\theta_i + \psi_i) & 0 \\ 0 & 0 & 1 \end{bmatrix}, \quad i = 1, 2, 3 \tag{5.11}$$

Then, the total inertia tensor $\mathbf{I}$ of the four-bar linkage relative to the global frame is written as

$$\mathbf{I} = \sum_{i=1}^{3} \mathbf{Q}_i \mathbf{I}_{bi} \mathbf{Q}_i^T$$

$$= \begin{bmatrix} I_{xx} & -I_{xy} & -I_{xz} \\ -I_{xy} & I_{yy} & -I_{yz} \\ -I_{xz} & -I_{yz} & I_{zz} \end{bmatrix} \tag{5.12}$$

where all the components of the inertia tensor are functions of the parameters of the four-bar linkage and will be discussed in the following sections.

5.4.2   Conditions for Obtaining a Planar Four-Bar Linkage with a Constant Moment of Inertia I_{zz}

In this subsection, the component of the inertia tensor associated with the moment of inertia in a direction orthogonal to the plane of motion is first investigated.

In eq. (5.12), the total moment of inertia relative to the Z axis is found as

$$I_{zz} = I_c + 2m_2 l_1 r_2 \cos(\theta_1 - \theta_2 - \psi_2) + 2m_3 d r_3 \cos(\theta_3 + \psi_3) \tag{5.13}$$

with

$$I_c = I_{zz1} + I_{zz2} + I_{zz3} + m_1 r_1^2 + m_2 l_1^2 + m_2 r_2^2 + m_3 d^2 + m_3 r_3^2 \tag{5.14}$$

Substituting the cosine and sine of θ_2 and θ_3 expressed in terms of θ_1 (Appendix B) into eq. (5.13) gives

$$I_{zz} = I_c + A \cos \psi_2 + B \sin \psi_2 + C \cos \psi_3 + D \sin \psi_3 \tag{5.15}$$

where

$$A = \frac{m_2 r_2 (2 l_1^2 d^2 \cos^2 \theta_1 - (3 l_1^2 + l_{23}^2 + d^2) l_1 d \cos \theta_1 + l_1^2 (l_1^2 + l_{23}^2 + d^2) - \epsilon \Delta d^4)}{(2 l_1 d \cos \theta_1 - l_1^2 - d^2) l_2}$$

$$\tag{5.16}$$

$$B = \frac{m_2 r_2 d(-2 l_1^2 d \cos^3 \theta_1 - (l_1^2 + l_{23}^2 + d^2) l_1 \sin^2 \theta_1 + (2 l_1^2 + \epsilon \Delta d^2) d \cos \theta_1 - \epsilon \Delta l_1 d^2)}{(2 l_1 d \cos \theta_1 - l_1^2 - d^2) l_2 \sin \theta_1}$$

$$\tag{5.17}$$

$$C = \frac{m_3 r_3 (2 l_1^2 d^2 \cos^2 \theta_1 - (l_1^2 - l_{23}^2 + 3 d^2) l_1 d \cos \theta_1 + d^2 (l_1^2 - l_{23}^2 + d^2) - \epsilon \Delta d^4)}{(2 l_1 d \cos \theta_1 - l_1^2 - d^2) l_3}$$

$$\tag{5.18}$$

$$D = \frac{m_3 r_3 d (2l_1^3 d \cos^3 \theta_1 + (l_1^2 - l_{23}^2 + d^2) l_1^2 \sin^2 \theta_1 - (2l_1^2 + \epsilon \Delta d^2) l_1 d \cos \theta_1 + \epsilon \Delta d^4)}{(2l_1 d \cos \theta_1 - l_1^2 - d^2) l_1 l_3 \sin \theta_1}$$

(5.19)

$$l_{23}^2 = l_2^2 - l_3^2$$

(5.20)

where ϵ and Δ are defined in Appendix B.

Clearly, it is impossible for coefficients A, B, C and D to be all zero for any value of θ_1. By inspection of eqs. (5.15), (5.17) and (5.19), it is found that $\sin \psi_2$ and $\sin \psi_3$ must be zero in order to obtain a constant value (zero) of the fraction $B \sin \psi_2 + D \sin \psi_3$ due to the existence of the cosine and sine of θ_1 in both the numerator and denominator of the fraction.

Letting $T = A \cos \psi_2 + C \cos \psi_3$, then one has

$$T = \frac{B_2 \cos^2 \theta_1 + B_1 \cos \theta_1 + B_0}{(2l_1 d \cos \theta_1 - l_1^2 - d^2) l_2 l_3}$$

(5.21)

where B_i is a function of the constant parameters of the four-bar linkage, calculated from eqs. (5.16) and (5.18).

Suppose that eq. (5.21) can be decomposed as follows

$$T = (A_2 \cos \theta_1 + A_1) + \frac{A_0}{(2l_1 d \cos \theta_1 - l_1^2 - d^2)}$$

(5.22)

By comparing the coefficients of the polynomials in $\cos \theta_1$ in eqs. (5.21) and (5.22), one has the following linear system of equations.

$$\begin{bmatrix} 1 & -(l_1^2 + d^2) & 0 \\ 0 & 2l_1 d & -(l_1^2 + d^2) \\ 0 & 0 & 2l_1 d \end{bmatrix} \begin{bmatrix} A_0 \\ A_1 \\ A_2 \end{bmatrix} = \frac{1}{l_2 l_3} \begin{bmatrix} B_0 \\ B_1 \\ B_2 \end{bmatrix}$$

(5.23)

Then, $\begin{bmatrix} A_0 & A_1 & A_2 \end{bmatrix}^T$ can be obtained as follows:

$$A_0 = \frac{(m_2 r_2 l_3 \cos \psi_2 + m_3 r_3 l_2 \cos \psi_3)(l_1^2 l_2^2 - l_1^2 l_3^2 + l_3^2 d^2 - l_2^2 d^2 - 2\epsilon \Delta d^4)}{2l_2 l_3}$$

(5.24)

$$A_1 = \frac{m_2 r_2 l_3 \cos \psi_2 (l_3^2 - 2l_1^2 - l_2^2) + m_3 r_3 l_2 \cos \psi_3 (l_2^2 - 2d^2 - l_3^2)}{2l_2 l_3}$$

(5.25)

$$A_2 = \frac{l_1 d(m_2 r_2 l_3 \cos\psi_2 + m_3 r_3 l_2 \cos\psi_3)}{l_2 l_3} \tag{5.26}$$

From eq. (5.22), it can be found that only if $A_0 = A_2 = 0$ then T (and hence I_{zz}) will be constant, namely,

$$m_2 r_2 l_3 \cos\psi_2 + m_3 r_3 l_2 \cos\psi_3 = 0 \tag{5.27}$$

Since $\sin\psi_2$ and $\sin\psi_3$ must be zero, as found previously, the values of $\cos\psi_2$ and $\cos\psi_3$ in eq. (5.27) must be opposite due to the positive geometric parameters. Hence, over the interval $[0, 2\pi[$, one can finally obtain

$$\psi_2 = 0, \quad \psi_3 = \pi \tag{5.28}$$

or

$$\psi_2 = \pi, \quad \psi_3 = 0 \tag{5.29}$$

and

$$r_3 = \frac{m_2 r_2 l_3}{m_3 l_2} \tag{5.30}$$

Then

$$I_{zz} = I_c \pm \frac{m_2 r_2 (l_3^2 - l_1^2 - l_2^2 + d^2)}{l_2} \tag{5.31}$$

Hence, eqs. (5.28) (for Case I and Case II of Figure 5.2) or (5.29) (for Case III) and (5.30) are the conditions for a planar four-bar linkage to have a constant moment of inertia relative to the Z axis.

By comparing the two sets of conditions with eqs. (5.1–5.3), it is found that the conditions for constant moment of inertia (I_{zz}) are a subset of the dynamic balancing conditions in the plane, as it should be.

5.4.3 Conditions for Constant Moments of Inertia (I_{xx}, I_{yy}) of a Planar Four-Bar Linkage

In this section the possibility of obtaining constant moments of inertia relative to the X and Y axes (I_{xx}, I_{yy}) for a single planar four-bar linkage with constant I_{zz} will be investigated.

The moment of inertia I_{xx} is first studied. Suppose that all the bars are symmetric, namely, the inertia products are zero, i.e., $I_{xyi} = I_{xzi} = I_{yzi} = 0$. Also, from eqs. (5.1–5.3), we know that $\psi_1 = 0$ (for Case I) or $\psi_1 = \pi$ (for Case II). Substituting eqs. (5.28) and (5.30) into eq. (5.12), one can finally obtain

$$I_{xx} = \frac{B_4 \cos^4 \theta_1 + B_3 \cos^3 \theta_1 + B_2 \cos^2 \theta_1 + B_1 \cos \theta_1 + B_0}{(2l_1 d \cos \theta_1 - l_1^2 - d^2)^2} \tag{5.32}$$

where B_i is a function of the constant parameters of the four-bar linkage (Appendix C).

Suppose that eq. (5.32) can be decomposed as follows

$$I_{xx} = (A_4 \cos^2 \theta_1 + A_3 \cos \theta_1 + A_2) + \frac{A_1}{(2l_1 d \cos \theta_1 - l_1^2 - d^2)} + $$
$$\frac{A_0}{(2l_1 l_2 \cos \theta_1 - l_1^2 - d^2)^2} \tag{5.33}$$

By comparing the coefficients of the polynomials in $\cos \theta_1$ in eqs. (5.32) and (5.33), one has the following linear system of equations.

$$\begin{bmatrix} 1 & -V & V^2 & 0 & 0 \\ 0 & 2U & -4UV & V^2 & 0 \\ 0 & 0 & 4U^2 & -4UV & V^2 \\ 0 & 0 & 0 & 4U^2 & -4UV \\ 0 & 0 & 0 & 0 & 4U^2 \end{bmatrix} \begin{bmatrix} A_0 \\ A_1 \\ A_2 \\ A_3 \\ A_4 \end{bmatrix} = \begin{bmatrix} B_0 \\ B_1 \\ B_2 \\ B_3 \\ B_4 \end{bmatrix} \tag{5.34}$$

where $U = l_1 d$, $V = l_1^2 + d^2$.

Then, $\begin{bmatrix} A_0 & A_1 & A_2 & A_3 & A_4 \end{bmatrix}^T$ can be obtained (Appendix C). From eq. (5.33), it is clear that only if $A_0 = A_1 = A_3 = A_4 = 0$ then I_{xx} could be constant, i.e., $I_{xx} = A_2$.

Finally, the conditions for constant I_{xx} — the three independent solutions of $A_0 = A_1 = A_3 = A_4 = 0$ — are derived as

$$I_{xx1} - I_{yy1} = \frac{m_1 r_1^2 l_2 + m_2 l_1^2 l_2 - m_2 r_2 l_1^2}{l_2} \tag{5.35}$$

$$I_{xx2} - I_{yy2} = m_2 r_2^2 - m_2 r_2 l_2 \tag{5.36}$$

$$I_{xx3} - I_{yy3} = \frac{m_2^2 r_2^2 l_3^2 + m_2 m_3 r_2 l_2 l_3^2}{m_3 l_2^2} \tag{5.37}$$

Furthermore, substituting eqs. (5.35–5.37) into (5.12) leads to a constant and principal inertia tensor. In other words, the three principal moments of inertia are all constant and all the products of inertia are zero.

Similarly, for Case III, suppose that $I_{xyi} = I_{xzi} = I_{yzi} = 0$ and $\psi_1 = \pi$, substituting eqs. (5.29) and (5.30) into eq. (5.12) and using the same procedure as above leads to the following set of conditions for constant I_{xx} and I_{yy} for this case.

$$I_{xx1} - I_{yy1} = m_1 r_1^2 + m_1 r_1 l_1 \tag{5.38}$$

$$I_{xx2} - I_{yy2} = \frac{m_1^2 r_1^2 - m_1 m_2 r_1 l_1}{m_2} \tag{5.39}$$

$$I_{xx3} - I_{yy3} = m_3 r_3^2 - m_3 r_3 l_3 \tag{5.40}$$

Given the above results, it may seem possible for a single planar four-bar linkage to have a constant spatial inertia tensor while moving. However, from the balancing conditions (5.2) for Case II where $r_2 < l_2$ and eq. (5.36), one can write

$$|I_{xx2} - I_{yy2}| - I_{zz2} = I_{c1} = I_{zz1} + m_1(r_1^2 + r_1 l_1) > 0 \tag{5.41}$$

i.e.,

$$|I_{xx2} - I_{yy2}| > I_{zz2} \tag{5.42}$$

Clearly, this is impossible since the difference between any two components must be smaller than or equal to the third one for the three principal moments of inertia of any rigid body (Appendix D).

It has also been proved, with the help of the corresponding balancing conditions of the discussed case — as in Case II — that condition (5.35) of Case I and condition (5.40) of Case III cannot be satisfied. This means that it is impossible for a single planar dynamically balanced four-bar linkage without separate counter-rotation to have constant moments of inertia I_{xx} and I_{yy} while moving. In other words, a single planar four-bar linkage can only behave as a rigid body in the plane but not for a spatial motion. Hence, it cannot be dynamically balanced for spatial motion.

5.4.4   Synthesis of a Constant Inertia Tensor Mechanism Using a Pair of Planar Four-bar Linkages

Since it is impossible for a single planar dynamically balanced four-bar linkage to maintain a constant inertia tensor when undergoing spatial motion, the possibility for a

mechanism composed of a pair of planar dynamically balanced four-bar linkages is investigated in this section. Figure 5.8 is a schematic representation of this composition. The two dynamically balanced four-bar linkages are arranged perpendicularly. The base links and the input links of the two mechanisms are fixed perpendicularly respectively. Hence, the two mechanisms move simultaneously (namely with same values of θ_1, θ_2 and θ_3) if the lengths of the corresponding bars of the two mechanisms are equal or have the same ratio. This composite mechanism has one degree of freedom. The idea of using such a mechanism arose from the observation that the sum of the moments of inertia I_{xx} and I_{yy} of a single dynamically balanced four-bar linkage is constant for any value of θ_1. Hence, the composite mechanism emerges from the conjecture that by placing the mechanisms orthogonally, the components of the inertia tensor will be functions that may remain constant. This conjecture will now be verified. In the notation of Figure 5.8, the first index of the subscript is used for the number of the link, while the second index represents the number of the mechanism. Moreover, subscript b stands for base links. The pair of four-bar mechanisms used here are of type II. However, mechanisms of type I or III could also be used. Indeed, it has been proved that the planar dynamically balanced four-bar linkages of the other two cases (Case I and III) can also be synthesized as constant inertia tensor mechanisms for spatial motion. However, it has been found that there are more possibilities of interference in the synthesis for the latter two cases. Furthermore, there is much more freedom in the choice of the design parameters in Case II than in the other two cases (Gosselin *et al.* 2002). Therefore, the four-bar linkages of Case II are taken as components to synthesize reactionless multi-degree-of-freedom mechanisms in the present work.

First, assume that the base links of the two four-bar linkages are fixed and u and v represent respectively the ratios of the lengths and masses of the corresponding bars of the two mechanisms, i.e.,

$$l_{i2} = ul_{i1} \tag{5.43}$$

$$m_{i2} = vm_{i1} \tag{5.44}$$

After obtaining each inertia tensor $\mathbf{I}_i$ of the four-bar linkages, the total inertia tensor $\mathbf{I}_{twb}$ — where the subscript t means total while wb means without base links — of the composite mechanism with respect to the global frame X, Y can be written as

$$\mathbf{I}_{twb} = \mathbf{I}_1 + \mathbf{Q}_4 \mathbf{I}_2 \mathbf{Q}_4^T \tag{5.45}$$

where

$$\mathbf{Q}_4 = \begin{bmatrix} 0 & 1 & 0 \\ -1 & 0 & 0 \\ 0 & 0 & 1 \end{bmatrix} \tag{5.46}$$

Finally from eq. (5.45) it is found that to obtain a composite mechanism with constant inertia tensor the relationship between u and v should be as follows:

$$v = \frac{1}{u^2} \tag{5.47}$$

This result implies that the principal moments of inertia of the corresponding bars of the two mechanisms relative to their centers of mass should be equal.

After substituting eq. (5.47) into (5.45), the following constant and principal inertia tensor can be obtained.

$$\mathbf{I}_{twb} = \begin{bmatrix} I_{xxtwb} & 0 & 0 \\ 0 & I_{yytwb} & 0 \\ 0 & 0 & I_{zztwb} \end{bmatrix} \tag{5.48}$$

where

$$I_{xxtwb} = I_{yytwb} = [(m_{21} + m_{31})m_{21}^2 l_{11}^4 - 2m_{11}m_{21}^2 l_{11}^3 r_{11} + m_{21}m_{31}l_{11}^2(I_{xx11} +$$
$$I_{yy11} + I_{xx21} + I_{yy21} + I_{xx31} + I_{yy31} + m_{11}r_{11}^2 + m_{21}l_{21}^2 + m_{31}l_{21}^2) +$$
$$m_{11}^2 m_{21} l_{11}^2 r_{11}^2 - 2m_{11}m_{21}m_{31}l_{11}l_{21}^2 r_{11} + m_{11}^2 m_{31}l_{21}^2 r_{11}^2]/(m_{21}m_{31}l_{11}^2) \tag{5.49}$$

$$I_{zztwb} = 2I_{zz} \tag{5.50}$$

Then, assume that the base links are mobile and symmetric with masses m_{b1} and m_{b2}, hence the total mass M and center of mass — described by a distance r_t and an angle β in Figure 5.8 — of the composite mechanism can be written as

$$M = m_{t1} + m_{t2} \tag{5.51}$$

$$r_t = \frac{\sqrt{(m_{t1}x_{g1})^2 + (m_{t2}y_{g2})^2}}{M} \tag{5.52}$$

$$\tan \beta = \frac{m_{t2}y_{g2}}{m_{t1}x_{g1}} \tag{5.53}$$
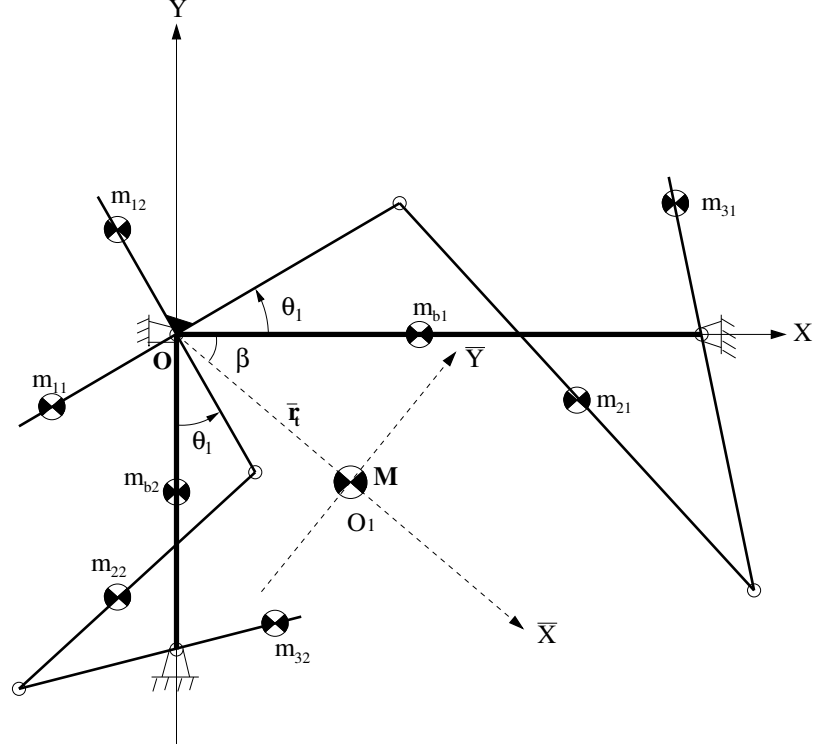
Figure 5.8: Synthesis of a constant inertia tensor mechanism.

with

$$m_{t1} = m_{11} + m_{21} + m_{31} + m_{b1} \tag{5.54}$$

$$m_{t2} = m_{12} + m_{22} + m_{32} + m_{b2} \tag{5.55}$$

$$x_{g1} = \frac{l_{21}(m_{21}l_{11} - m_{11}r_{11} + m_{31}l_{11}) + m_{b1}l_{11}r_{b1}}{m_{t1}l_{11}} \tag{5.56}$$

$$y_{g2} = \frac{l_{22}(m_{22}l_{12} - m_{12}r_{12} + m_{32}l_{12}) + m_{b2}l_{12}r_{b2}}{m_{t2}l_{12}} \tag{5.57}$$

where r_{bi} is the distance from joint O to the center of mass of the ith base link while x_{g1} and y_{g2} are the coordinates of the corresponding center of mass of the individual four-bar linkages including base links. It is apparent that the center of mass of a four-bar linkage including the base link is situated on its base line, namely on the axis of the frame. The total inertia tensor of the two base links relative to global frame X, Y is written as

$$\mathbf{I}_{tb} = \begin{bmatrix} I_{xxtb} & 0 & 0 \\ 0 & I_{yytb} & 0 \\ 0 & 0 & I_{zztb} \end{bmatrix} \tag{5.58}$$

with

$$I_{xxtb} = I_{xxb1} + I_{yyb2} + m_{b2}r_{b2}^2 \tag{5.59}$$

$$I_{yytb} = I_{yyb1} + I_{xxb2} + m_{b1}r_{b1}^2 \tag{5.60}$$

$$I_{zztb} = I_{zzb1} + I_{zzb2} + m_{b1}r_{b1}^2 + m_{b2}r_{b2}^2 \tag{5.61}$$

where I_{xxbi}, I_{yybi} and I_{zzbi} are moments of inertia of the base link of the ith four-bar linkage relative to the center of mass of the base link.

Finally, the inertia tensor of the composite mechanism relative to the local frame $\overline{X}, \overline{Y}$ — with origin O_1 at the center of mass of the total mechanism and the $\overline{X}$ axis passing through joint O and the center of mass — can be obtained as

$$\begin{aligned} \mathbf{I}_{tg} &= \mathbf{Q}_5(\mathbf{I}_{twb} + \mathbf{I}_{tb})\mathbf{Q}_5^T - \mathbf{R} \\ &= \begin{bmatrix} I_{xxtg} & -I_{xytg} & 0 \\ -I_{xytg} & I_{yytg} & 0 \\ 0 & 0 & I_{zztg} \end{bmatrix} \end{aligned} \tag{5.62}$$

where

$$\mathbf{Q}_5 = \begin{bmatrix} \cos\beta & -\sin\beta & 0 \\ \sin\beta & \cos\beta & 0 \\ 0 & 0 & 1 \end{bmatrix} \tag{5.63}$$

$$\mathbf{R} = \begin{bmatrix} 0 & 0 & 0 \\ 0 & Mr_t^2 & 0 \\ 0 & 0 & Mr_t^2 \end{bmatrix} \tag{5.64}$$

$$I_{xxtg} = I_{yytwb} + I_{xxtb}\cos^2\beta + I_{yytb}\sin^2\beta \tag{5.65}$$

$$I_{yytg} = I_{xxtwb} + I_{xxtb}\sin^2\beta + I_{yytb}\cos^2\beta - Mr_t^2 \tag{5.66}$$

$$I_{zztg} = I_{zztwb} + I_{zztb} - Mr_t^2 \tag{5.67}$$

$$I_{xytg} = \sin\beta\cos\beta(I_{yytb} - I_{xxtb}) \tag{5.68}$$

From eqs. (5.59), (5.60), (5.62) and (5.68), it is clear that a principal inertia tensor $\mathbf{I}_{tg}$ can be obtained only if I_{xytg} is equal to zero, i.e.,

$$I_{yytb} = I_{xxtb} \tag{5.69}$$

or

$$I_{yyb2} = I_{yyb1} - I_{xxb1} + I_{xxb2} + m_{b1}r_{b1}^2 - m_{b2}r_{b2}^2 \tag{5.70}$$

This condition can be satisfied by properly choosing the mass and inertia of the base links of the two four-bar linkages.
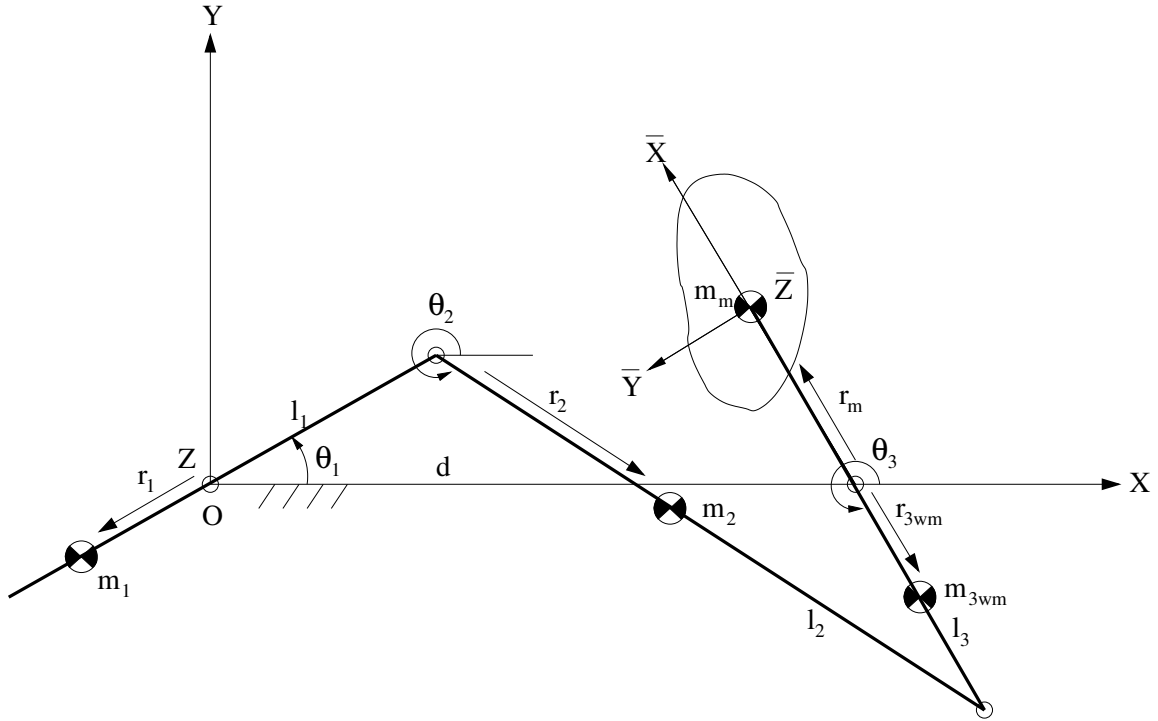
Figure 5.9: Synthesis of reactionless multi-degree-of-freedom mechanisms.

5.4.5 Synthesis of Reactionless Multi-degree-of-freedom Mechanisms

A planar dynamically balanced four-bar linkage can be considered as a rigid body when moving in the plane while the composite mechanism discussed in the preceding subsection can be regarded as a rigid body when moving spatially. Therefore, they can be attached on the third bar of another four-bar linkage to synthesize reactionless 2-DOF mechanisms.

A schematic representation of the synthesis principle is shown in Figure 5.9. A mechanism of mass m_m, behaving as a rigid body as mentioned above is attached on the third bar with mass m_{3wm} of a planar four-bar linkage with a fixed base. The center of mass of the attached mechanism is located on the axis of the third bar. A global frame X, Y, Z with origin at the fixed point O and a local frame $\overline{X}, \overline{Y}, \overline{Z}$ with origin at the center of mass of the attached mechanism and with $\overline{X}$ direction along the axis of the third bar are shown in the figure. The subscript wm stands for without attached mechanism while m stands for the attached mechanism.

The resulting parameters of the third bar and the attached mechanism which include the resulting mass m_3, center of mass r_3 and radius of gyration k_3 relative to the resulting center of mass can be written as

$$m_3 = m_{3wm} + m_m \tag{5.71}$$

$$r_3 = \frac{m_m r_m - m_{3wm} r_{3wm}}{m_3} \tag{5.72}$$

$$I_{zz3} = m_3 k_3^2 = I_{zz3wm} + m_{3wm}(r_{3wm} + r_3)^2 + I_{zzm} + m_m(r_m - r_3)^2. \tag{5.73}$$

If the attached mechanism is a planar four-bar linkage — mounted in the motion plane of the base mechanism — clearly I_{xzm} and I_{yzm} are zero. Whereas if the attached mechanism is the composite mechanism which is mounted on a plane orthogonal to the motion plane of the base mechanism and with the same $\overline{X}$ direction as in Figure 5.8 (i.e., the $\overline{Z}$ direction is identical to the $\overline{Y}$ direction in Figure 5.8) — then I_{xzm} and I_{yzm} are zero since the inertia tensor of the composite mechanism relative to its local frame (Figure 5.8) is principal under the condition of eq. (5.69) or (5.70). Clearly, if the resulting parameters (eq. (5.71–5.73)) and other parameters of the base mechanism meet the balancing conditions in eq. (5.2), the synthesized mechanism will then be reactionless. This result will be confirmed by the calculation of the linear momentum and angular momentum of the synthesized mechanism.

Apparently, the synthesized mechanism has a fixed center of mass (see eq. (5.5)), i.e., zero linear momentum. Moreover, the angular momentum with respect to the fixed point O and the global frame of the synthesized mechanism can be written as

$$\mathbf{h}_o = \sum_{i=1}^{2}(\mathbf{h}_{gi} + \mathbf{r}_{gi} \times m_i \dot{\mathbf{r}}_{gi}) + \mathbf{h}_{g3wm} + \mathbf{r}_{g3wm} \times m_{3wm} \dot{\mathbf{r}}_{g3wm} +$$
$$\mathbf{Q}_6 \mathbf{I}_{gm} \mathbf{Q}_6^T \dot{\boldsymbol{\theta}}_m + \mathbf{r}_{gm} \times m_m \dot{\mathbf{r}}_{gm} \tag{5.74}$$

with

$$\mathbf{r}_{g1} = \begin{bmatrix} r_1 \cos(\theta_1 + \pi) \\ r_1 \sin(\theta_1 + \pi) \\ 0 \end{bmatrix}, \ \mathbf{r}_{g2} = \begin{bmatrix} l_1 \cos\theta_1 + r_2 \cos\theta_2 \\ l_1 \sin\theta_1 + r_2 \sin\theta_2 \\ 0 \end{bmatrix}$$

$$\mathbf{r}_{g3wm} = \begin{bmatrix} d + r_{3wm} \cos\theta_3 \\ r_{3wm} \sin\theta_3 \\ 0 \end{bmatrix}, \ \mathbf{r}_{gm} = \begin{bmatrix} d + r_m \cos(\theta_3 - \pi) \\ r_m \sin(\theta_3 - \pi) \\ 0 \end{bmatrix}$$

$$\mathbf{h}_{gi} = \begin{bmatrix} 0 \\ 0 \\ I_{zzi}\dot{\theta}_i \end{bmatrix}, \ \mathbf{h}_{g3wm} = \begin{bmatrix} 0 \\ 0 \\ I_{zz3wm}\dot{\theta}_3 \end{bmatrix}, \ \dot{\boldsymbol{\theta}}_m = \begin{bmatrix} 0 \\ 0 \\ \dot{\theta}_3 \end{bmatrix}$$

$$\mathbf{Q}_6 = \begin{bmatrix} \cos(\theta_3 - \pi) & -\sin(\theta_3 - \pi) & 0 \\ \sin(\theta_3 - \pi) & \cos(\theta_3 - \pi) & 0 \\ 0 & 0 & 1 \end{bmatrix}$$

$$\mathbf{I}_{gm} = \begin{bmatrix} I_{xxm} & -I_{xym} & -I_{xzm} \\ -I_{xym} & I_{yym} & -I_{yzm} \\ -I_{xzm} & -I_{yzm} & I_{zzm} \end{bmatrix}$$

where $\mathbf{I}_{gm}$ is the inertia tensor of the attached mechanism relative to the local frame ($I_{xym} = 0$ if the attached is a composite mechanism) while $\mathbf{Q}_6$ is the rotation matrix of the local frame with respect to the global frame.

Substituting all the above parameters into eq. (3.9), one has

$$\mathbf{h}_o = \begin{bmatrix} 0 \\ 0 \\ h_{oz} \end{bmatrix}, \tag{5.75}$$

where

$$\begin{aligned} h_{oz} &= [I_{zz1} + m_1 r_1^2 + m_2(r_2 l_1 \cos(\theta_2 - \theta_1) + l_1^2)]\dot{\theta}_1 + \\ &\quad [I_{zz2} + m_2(r_2 l_1 \cos(\theta_2 - \theta_1) + r_2^2)]\dot{\theta}_2 + \\ &\quad [I_{zz3wm} + I_{zzm} + m_{3wm} r_{3wm}(d \cos\theta_3 + r_{3wm}) - \\ &\quad m_m r_m(d \cos\theta_3 - r_m)]\dot{\theta}_3 \end{aligned} \tag{5.76}$$

Substituting eqs. (5.2), (5.71–5.73) and (B.3–B.4) into (5.76) leads to $h_{oz} = 0$. i.e., $\mathbf{h}_o = 0$. Hence, the synthesized mechanism has a fixed center of mass and zero angular momentum, namely, the mechanism is dynamically balanced.

Since the synthesized mechanism is reactionless, it still behaves as a rigid body moving in the plane of the base four-bar linkage. Hence, the synthesized mechanism can be attached on the third bar of another planar dynamically balanced four-bar linkage in order to obtain spatial reactionless mechanisms with more degrees of freedom.

5.5 Synthesis of Reactionless Spatial 3-DOF Mechanisms

Now that two basic mechanisms — a single planar dynamically balanced four-bar linkage and a planar composite mechanism with a pair of four-bar linkages — have been
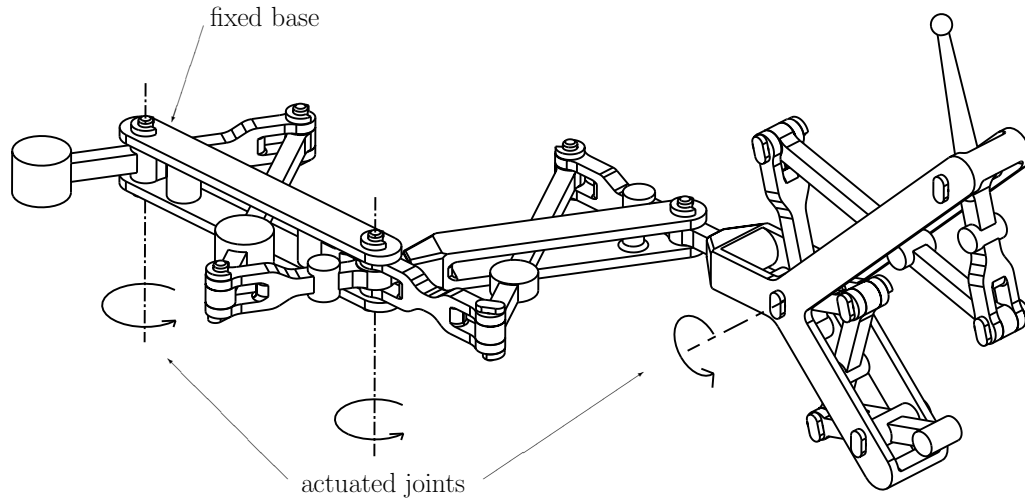
Figure 5.10: Conceptual CAD model of a reactionless spatial 3-DOF mechanism.

obtained, reactionless multi-degree-of-freedom mechanisms can be synthesized according to the synthesis principles and constraint conditions discussed in the above sections. Figure 5.10 schematically shows the synthesis of a reactionless spatial 3-DOF mechanism composed of these two basic mechanisms (counterweights are not shown on the figure). Two planar four-bar linkages are stacked in the horizontal plane, while a composite mechanism is rigidly attached on the third bar of the second planar four-bar linkage in the vertical plane. The numbering of the four-bar mechanisms starts from that with a fixed base link. Since a reactionless 6-DOF parallel manipulator using four-bar linkages will be constructed in the next section, a point mass is considered here at the end-effector. Indeed, the 6-DOF manipulator will be composed of three legs connecting the base to a common thin platform. Each of the three legs will consist of the reactionless 3-DOF mechanism shown in Figure 5.10. The mass and inertia of the platform are distributed among the attachment points of the legs and replaced by three point masses m_p. Hence, starting from this point mass, all the parameters of the bars of the four-bar mechanisms are chosen or calculated using the reactionless conditions. Finally a numerical example of this reactionless 3-DOF mechanism is given in Table 5.1 (point mass $m_p = 0.1143kg$). Note that if a point mass, a four-bar linkage or a combination of mechanisms is attached on one element of another four-bar linkage, the parameters of the latter element in the table are actually the resulting parameters of the element and the attached mechanisms. For example, the parameters (m_{32}, r_{32}, k_{32}) in the table are resulting quantities of the third bar of the second four-bar linkage and the composite mechanism.

Table 5.1: A numerical example of the reactionless spatial 3-DOF mechanism.

Parameters	1st Four-bar	2nd Four-bar	Composite Mechanism	
			3rd Four-bar	4th Four-bar
m_{1j} (kg)	16.386	5	0.7	2.8
m_{2j} (kg)	30.178	5	0.5	2.0
m_{3j} (kg)	21.475	10.875	0.775	3.1
m_{bj} (kg)			0.4	0.2
l_{1j} (mm)	1608	812	500	250
l_{2j} (mm)	5000	2500	1000	500
l_{3j} (mm)	1608	812	500	250
l_{bj} (mm)			1000	500
r_{1j} (mm)	804	285	174.46	87.23
r_{2j} (mm)	3642.55	1622.54	511.5	255.75
r_{3j} (mm)	1646.19	242.3	165	82.5
r_{bj} (mm)			500	250
k_{1j} (mm)	2673.709	636.766	197.312	98.656
k_{2j} (mm)	100	840	175	87.5
k_{3j} (mm)	1255.93	273.337	178.106	89.053

Furthermore, from eqs. (5.2), (5.49–5.70), it is found that besides the parameters given in the table, some additional parameters of the composite mechanism (i.e., the third and fourth four-bar mechanisms) have an influence on the dynamic balancing. These parameters are as follows, namely, $I_{yyb3} = 3.3 \times 10^4 kg \cdot mm^2$, $I_{xx1j} = I_{xx2j} = I_{xx3j} = I_{xxbj} = 6kg \cdot mm^2$, $I_{yy1j} = I_{zz1j} = m_{1j}k_{1j}^2$, $I_{yy2j} = I_{zz2j} = m_{2j}k_{2j}^2$, $I_{yy3j} = I_{zz3j} = m_{3j}k_{3j}^2$, $j = 3, 4$.

The verification of the reactionless property is performed using ADAMS. For the above example mechanism, a simulation model is built using ADAMS. Simulations have been performed for several arbitrary trajectories. The resulting reaction forces and moments on the base are illustrated in Figure 5.11. The results clearly demonstrate that the resulting reaction forces and moments on the base are very small with respect to the joint forces and driving torques (with a ratio of 10^{-5} to 10^{-6}). Indeed, the reaction forces and moments obtained are most likely due to small modeling errors. Hence, it is clearly shown that the synthesized spatial 3-DOF mechanisms can be completely
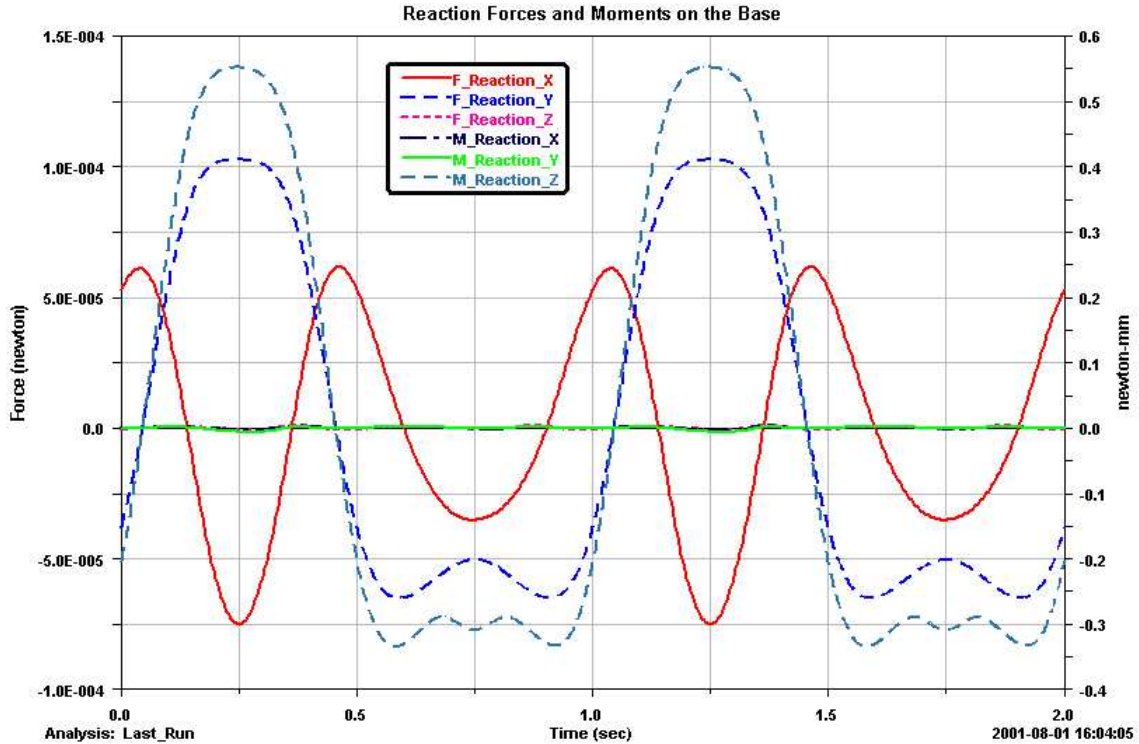
Figure 5.11: Verification of the reactionless property of the 3-DOF mechanism.

balanced. In other words, there are no reaction forces and moments on the base at all times, for arbitrary trajectories.

Note that the parameters of the example reactionless mechanism (Table 5.1) were not determined by optimization due to the complexity of the optimization for whole system. As was the case with other dynamically balanced mechanisms, this reactionless 3-DOF mechanism was achieved at the expense of a substantial mass increase of the system and complexity of the mechanism. The total masses of the composite mechanism, the second and the first mechanisms are 9.875, 20.875 and 68.039 kg respectively. We can approximately express this mass relationship with 1:2:7. Kinematically, this mechanism can be regarded as a spatial three-link serial chain. The mass variation of the distal link produces great influence for the balancing of the successive links. Hence, if we can decrease the mass of the composite mechanism, the total system mass will decrease greatly. For instance, if we choose the same link lengths for both four-bar linkages in the composite mechanism (i.e., $u = 1$), the same link masses can then be determined for both four-bar linkages (i.e., $v=1$). Therefore, if the total mass of the composite mechanism is decreased from 9.875 to 3.95, then, the total mass of the system

will be about 27.65 kg by multiplying 3.95 with 7 according to the above mass relationship. Moreover, there are some other possibilities to further decrease the system mass and shrink the reactionless 3-DOF mechanism. For example, changing the position of the attachment point of two four-bar linkages (e.g., from point P to P' in Figure 5.12) leads to the decrease of r_3 and k_3, then m_1, m_2 as well as the lengths of all links of the fixed four-bar linkage. Similarly, decreasing the length of the extension part of the link connected to the end-effector (or platform) can also lead to the similar results for the successive four-bar mechanisms. Moreover, an optimization for the whole mechanism with the considerations of the above factors and detailed parameters using dimensional variables specifically tailored to the link geometry will definitely decrease the system mass and shrink the whole reactionless 3-DOF mechanism.

Compared with a three-link serial chain dynamically balanced using the conventional method (Section 3.7), the reactionless 3-DOF mechanism with four-bar linkages has more moving links and larger system size for the same payload. However, this does not necesarily imply greater system mass because neither system has been optimized yet. Moreover, three separate counter-rotations have to be used for dynamically balancing the three-link serial chain. The design of separate counter-rotations is normally complicated (Figure 1.5) relative to the initial mechanism. Furthermore, using counter-rotations like gear inertia counterweights under cyclic torque variation may generate noise rattling (Esat and Bahai, 1999). Additionally, adding an actuator, a counterweight and a counter-rotation in each pivot of the serial chain is a difficult design. Therefore, the most important advantage of the reactionless 3-DOF mechanism presented in this chapter is that the use of additional separate counter-rotations and their side effects are avoided. Moreover, it is easy to design and manufacture a practical dynamically balanced system with only counterweights and revolute joints.

5.6 Synthesis of Reactionless Spatial 6-DOF Parallel Mechanisms

The spatial 3-DOF mechanism mentioned above can be used as a leg to synthesize spatial multi-degree-of-freedom — having up to 6-DOF — parallel mechanisms or manipulators. As discussed in Chapter 4, a 6-DOF parallel mechanism can be obtained
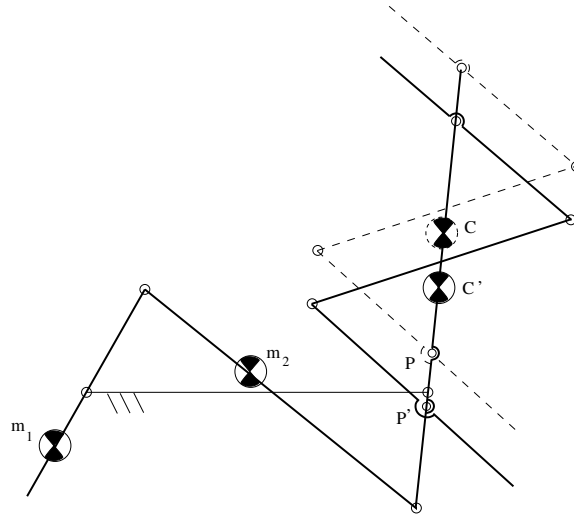
Figure 5.12: Attachment point of two four-bar linkages.

using only three such legs and two actuators for each leg and spherical joints to connect legs to the mobile platform. The spatial 6-DOF parallel mechanism schematically represented in Figure 5.13 (counterweights are not shown on the figure) is composed of three identical legs symmetrically connecting the fixed base to a common thin platform. Each of the three legs is a spatial 3-DOF mechanism (Figure 5.10).

In order to simplify the dynamic balancing for spatial multi-degree-of-freedom parallel mechanisms with several legs, as addressed in Chapter 4, the dynamic balancing for each detached leg mechanism is considered independently, if the mobile platform is replaced by point masses located at the points of attachment of the legs to the platform. For the spatial 6-DOF parallel mechanism of this chapter, the mass and inertia of the thin platform can be replaced by three identical point masses m_{pm} on the attachment points symmetrically arranged on a plane.

When the equivalent point masses have been determined according to eqs. (4.43–4.45), each of the point masses is included in the corresponding 3-DOF leg mechanism and is considered in the balancing. By dynamically balancing each of the three legs individually — including the point mass — and attaching the legs, without the point masses, to a common platform satisfying the above conditions, a reactionless 6-DOF parallel mechanism will be obtained. Hence starting from this point mass, all the parameters of the bars of the four-bar mechanisms are chosen or calculated under the reactionless conditions. For example, if a mobile platform can be replaced by three point masses ($m_{pm} = 0.1143kg$) a numerical example of the reactionless 3-DOF
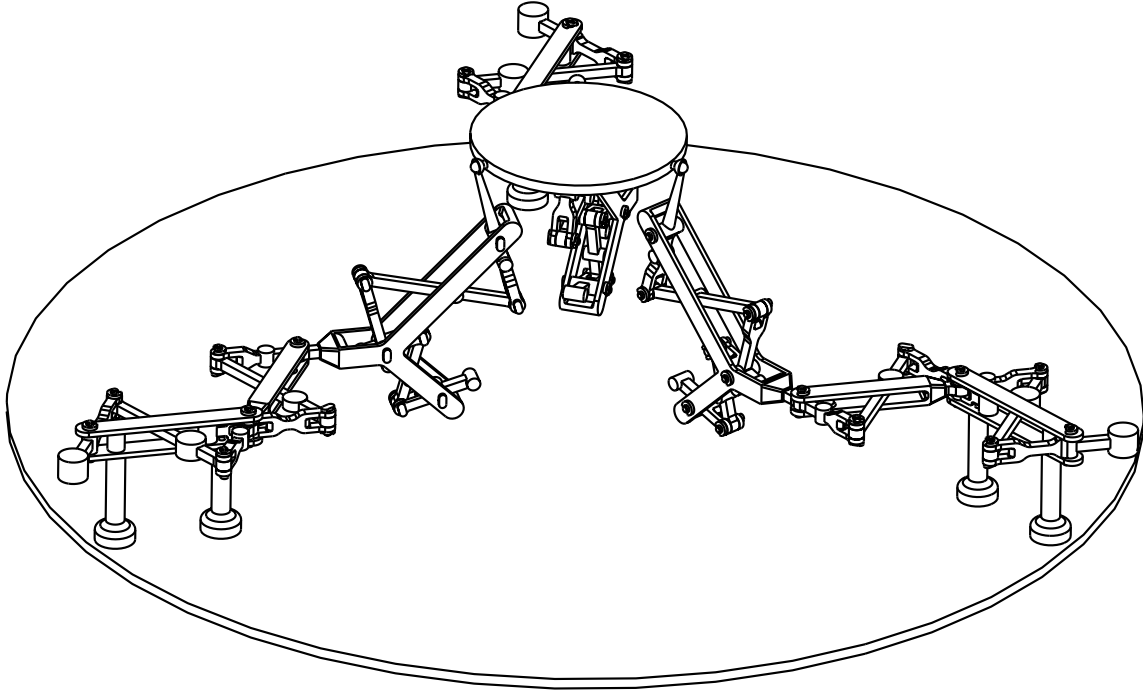
Figure 5.13: Conceptual CAD model of a reactionless spatial 6-DOF parallel mechanism.

leg mechanism can be given in Table 5.1 and a reactionless spatial 6-DOF parallel mechanism can finally be obtained.

The verification of the reactionless property of the spatial 6-DOF parallel mechanism is also performed using ADAMS. For the above example mechanism, a simulation model is built using ADAMS (Figure 5.14). Simulations have been performed for several arbitrary trajectories. The resulting reaction forces and moments on the base are illustrated in Figure 5.15. The results clearly demonstrate that the resulting reaction forces and moments on the base are very small with respect to the joint forces and driving torques (with a ratio of 10^{-5} to 10^{-6}) due to small modeling errors. Hence, it is clearly demonstrated that the synthesized spatial 6-DOF mechanisms are reactionless. These numerical simulation results support the formal mathematical proof and the algorithm using point masses to replace a platform used in this thesis.
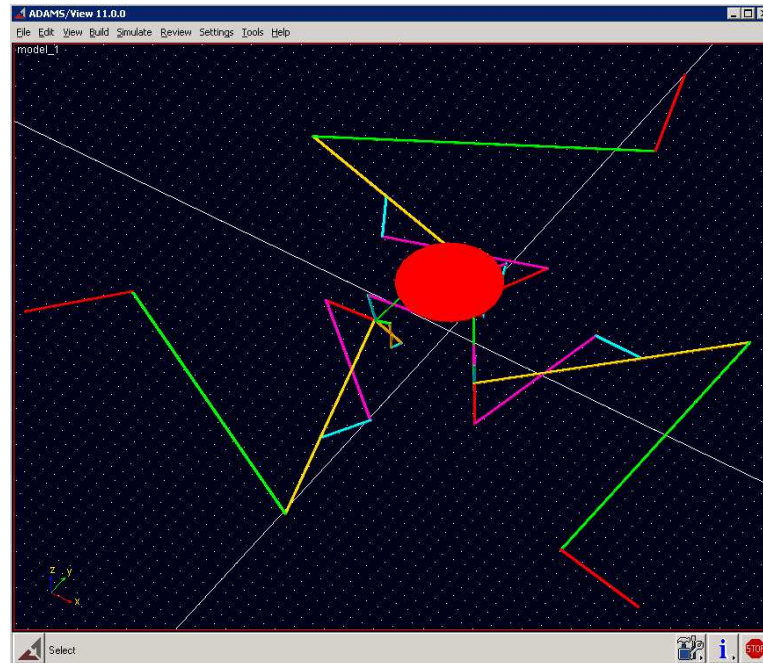
Figure 5.14: Modeling of reactionless 6-DOF mechanisms using ADAMS.
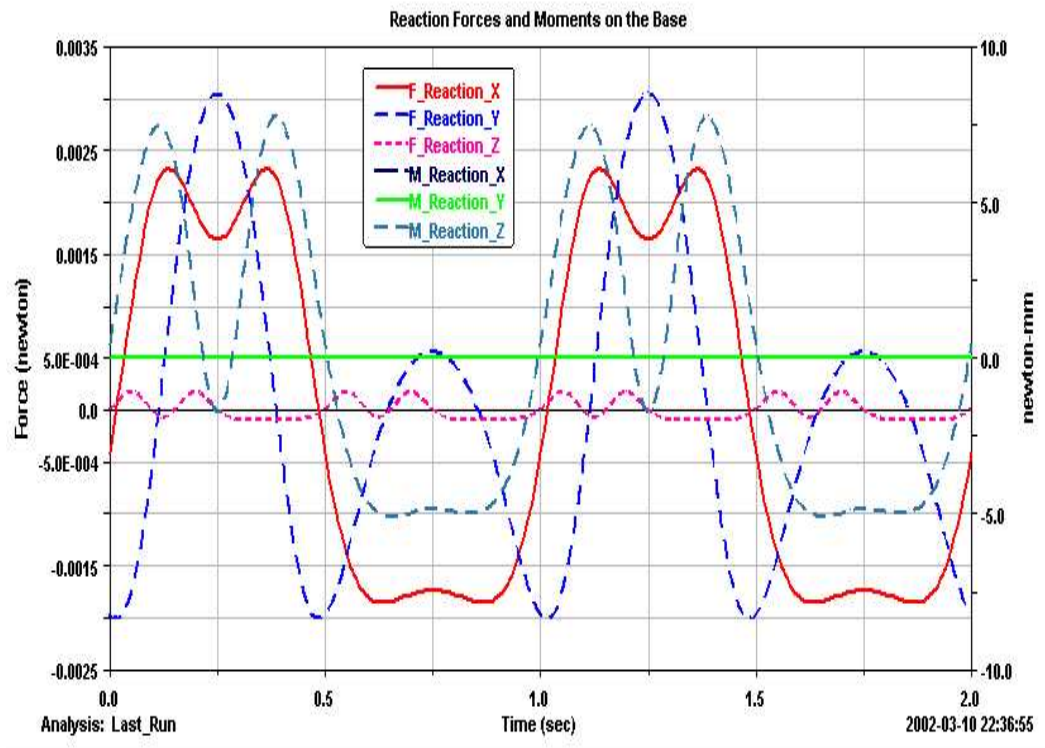
Figure 5.15: Verification of the reactionless property of the 6-DOF mechanisms.

5.7   Conclusion

The reactionless conditions for planar four-bar linkages moving spatially and the synthesis of novel reactionless spatial 3-DOF and 6-DOF mechanisms using four-bar linkages without additional counter-rotations have been addressed in this chapter. Based on the conditions of dynamic balancing of a single planar four-bar linkage moving in the plane, the spatial problem has been addressed. It has been shown that a single planar four-bar linkage cannot be dynamically balanced when moving spatially. However, it has been found that a mechanism composed of a pair of connected planar reactionless four-bar linkages has the property of a rigid body — a fixed center of mass and a constant inertia tensor — and can be dynamically balanced in space by being attached on another four-bar linkage undergoing planar motion in a plane perpendicular to the composite pair of four-bar linkages under the condition of the principal inertia tensor of the composite mechanism and the balancing conditions for a planar four-bar linkage. Then, reactionless spatial 3-DOF mechanisms using four-bar linkages have been synthesized. A numerical example of a reactionless spatial 3-DOF mechanism has been given and, with the help of the dynamic simulation software ADAMS, it has been shown that the mechanism is reactionless for arbitrary trajectories. Finally, a 6-DOF reactionless parallel mechanism has been synthesized. It is remarkable that such reactionless mechanisms can be synthesized without introducing any separate counter-rotation.

Chapter 6

Kinematic Analysis of a Reactionless Spatial 6-DOF Parallel Mechanism Using Planar Four-bar Linkages

In this chapter, the inverse kinematics and singularity analysis of a novel reactionless 6-DOF parallel mechanism using four-bar linkages are presented. Three types of actuation schemes of the mechanism are considered. The Jacobian matrix of the mechanism is first derived and the six lines defined by the Plücker vectors associated with the six actuated joints of the architecture are given. The linear dependencies between the corresponding lines are studied using Grassmann line geometry, and the singular configurations are presented using simple geometric rules. The expressions describing all the corresponding singularities are obtained and the graphical representations that show the relationship between the singularity loci and the constant-orientation workspace of the mechanism are given.

6.1   Introduction

For a novel 6-DOF parallel mechanism, kinematic analysis is a critical issue in the context of design and control. For the singularity analysis, as we mentioned in the Introduction, an efficient approach is based on the roots of the determinant of the Jacobian matrix (Gosselin and Angeles, 1990; Mayer St-Onge and Gosselin, 2000). However, in some cases the closed-form expression of the determinant depends on the Cartesian and the joint coordinates and is then of a very complex form. It is impossible to find the roots of such an expression analytically. Another useful approach is based on Grassmann line geometry (Merlet, 1989; Mouly and Merlet, 1992; Monsarrat and Gosselin, 2001). The procedure leads to an exhaustive list of geometric conditions that correspond to singularities.

In this chapter, the inverse kinematics of the reactionless 6-DOF parallel mechanism synthesized in Chapter 5 will be solved. The Jacobian matrices of the mechanism associated with different actuation schemes are derived and the corresponding lines defined by the Plücker vectors will be given. The line geometry method is used here to determine the conditions associated with the singular configurations. Finally, the graphical representations that show the relationship between the singularity loci and the constant-orientation workspace of the mechanism are given.

6.2   Geometric Description

The reactionless 6-DOF parallel mechanism schematically represented in Figure 5.13 is composed of a fixed base and a very thin moving platform connected by three identical legs. The legs are symmetrically arranged and are attached to the platform with spherical joints. Each of the three legs is a spatial 3-DOF mechanism in which two planar dynamically balanced four-bar linkages are stacked in the horizontal plane, while a planar composite mechanism — a pair of planar dynamically balanced four-bar linkages arranged perpendicularly with one-degree-of-freedom— is rigidly attached on the third bar of the second planar four-bar linkage in the vertical plane. A reactionless spatial 6-DOF parallel mechanism without separate counter-rotations is achieved under certain conditions as discussed in the preceding chapter. A schematic representation of
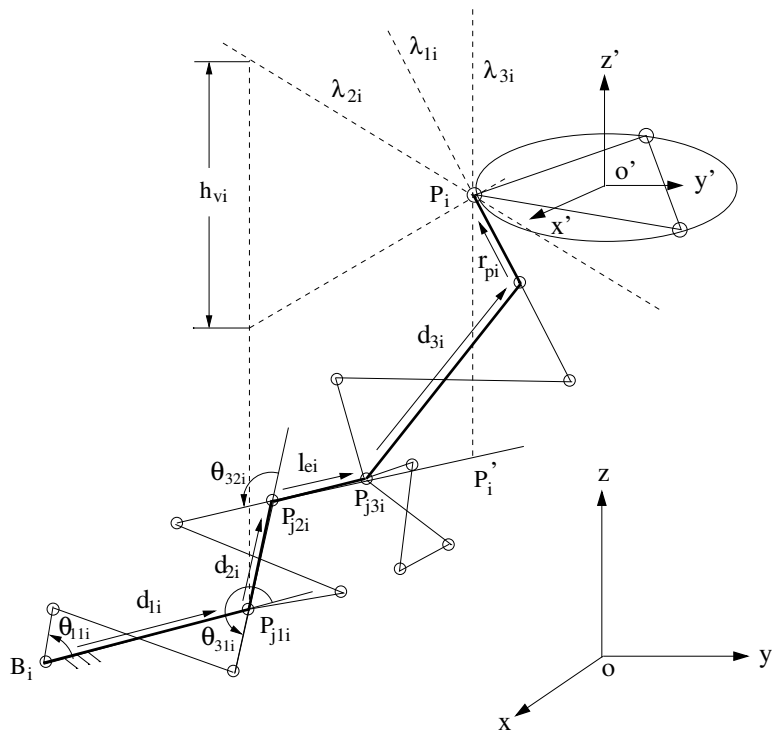
(a) General schematic
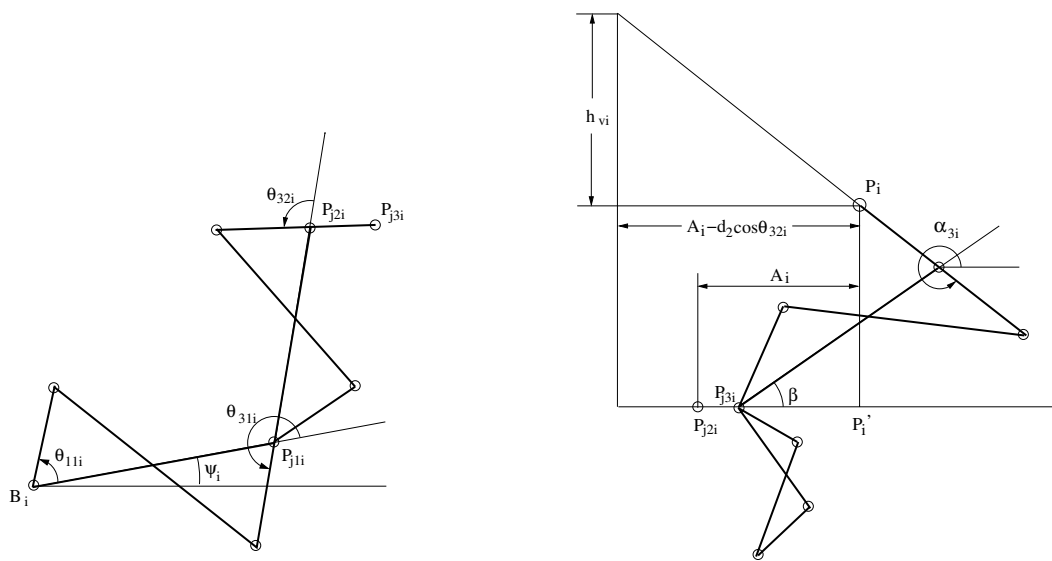
(b) Four-bar linkages in horizontal and vertical planes

Figure 6.1: Kinematic chain of one leg.

the kinematic chain of one leg of the mechanism is shown in Figure 6.1. Any two of the three revolute joints between the first bar and the base link of each four-bar linkage can be actuated for each leg. Globally, six revolute joints are actuated for the whole 6-DOF mechanism. Three types of actuation schemes of the mechanism designated as Case I, II and III respectively are considered in this thesis. In Case I, the first and second four-bar linkages (numbered from the base to the end-effector in Figure 6.1a) in the horizontal plane are actuated, while the first and third four-bar linkages as well as the second and third one are actuated in Case II and III respectively. In order to obtain a workspace as large as possible, for each leg, the attachment point on the base B_i, the projection point P_i' of point P_i on the base and point O are collinear in the initial configuration of the mechanism.

A fixed reference frame $O - xyz$ is attached to the base platform of the mechanism and a moving coordinate frame $O' - x'y'z'$ is attached to the moving platform. The nomenclature of Chapter 4 is used here, namely, vectors $\mathbf{p}_{0i}, \mathbf{p}_i, \mathbf{b}_i, \mathbf{Q}$ and $\mathbf{s}_i$ are used. The mounting angle of the leg mechanism noted ψ_i is defined as the angle made by the base link of the first four-bar linkage of the leg with respect to the x-axis of the global frame.

6.3 Inverse Kinematics

As mentioned in Chapter 4, for a given position and orientation of the moving platform, the position vectors of attachment point P_i, i=1, 2, 3 expressed in the fixed coordinate frame can be obtained from eq. (4.2).

Considering the ith leg mechanism, one can then write from the kinematic chain of the leg

$$\mathbf{s}_i = \mathbf{p}_i - \mathbf{p}_{0i} = \mathbf{d}_{1i} + \mathbf{d}_{2i} + \mathbf{l}_{ei} + \mathbf{d}_{3i} + \mathbf{r}_{pi} \tag{6.1}$$

with

$$\mathbf{p}_{0i} = \begin{bmatrix} x_{0i} \\ y_{0i} \\ z_{0i} \end{bmatrix}, \quad \mathbf{d}_{1i} = \begin{bmatrix} d_1 \cos \psi_i \\ d_1 \sin \psi_i \\ 0 \end{bmatrix}, \quad \mathbf{d}_{2i} = \begin{bmatrix} -d_2 \cos \alpha_{1i} \\ -d_2 \sin \alpha_{1i} \\ 0 \end{bmatrix}$$

$$\mathbf{l}_{ei} = \begin{bmatrix} l_e \cos \alpha_{2i} \\ l_e \sin \alpha_{2i} \\ 0 \end{bmatrix}, \quad \mathbf{d}_{3i} = \begin{bmatrix} d_3 \cos \beta \cos \alpha_{2i} \\ d_3 \cos \beta \sin \alpha_{2i} \\ d_3 \sin \beta \end{bmatrix}$$

$$\mathbf{r}_{pi} = \begin{bmatrix} -r_p \cos \alpha_{3i} \cos \alpha_{2i} \\ -r_p \cos \alpha_{3i} \sin \alpha_{2i} \\ -r_p \sin \alpha_{3i} \end{bmatrix} \tag{6.2}$$

where

$$\alpha_{1i} = \theta_{31i} + \psi_i \tag{6.3}$$

$$\alpha_{2i} = \theta_{31i} + \theta_{32i} + \psi_i \tag{6.4}$$

$$\alpha_{3i} = \theta_{33i} + \beta \tag{6.5}$$

where β is the angular position of the center of mass of the composite mechanism shown in Figure 5.8, namely, the angle between the base link of the third four-bar linkage and the base plane in the 6-DOF mechanism (Figure 6.1). The first index of the subscript of a variable with three subscripts (e.g., θ_{11i}) stands for the number of the bar, the second index for the number of the four-bar linkage and the third one for the number of the leg. Moreover, all variables (e.g., θ_{11i}, d_{1i}) are defined as in Chapter 5, simply by adding one index i for the leg (i. e., θ_{11}, d_1 become θ_{11i}, d_{1i}).

Substituting all the vectors in eq. (6.2) and eqs. (6.3) – (6.5) into eq. (6.1) leads to

$$\begin{bmatrix} d_1 \cos \psi_i - d_2 \cos \alpha_{1i} + A_i \cos \alpha_{2i} \\ d_1 \sin \psi_i - d_2 \sin \alpha_{1i} + A_i \sin \alpha_{2i} \\ d_3 \sin \beta - r_p \sin \alpha_{3i} \end{bmatrix} = \begin{bmatrix} x_i - x_{0i} \\ y_i - y_{0i} \\ z_i - z_{0i} \end{bmatrix} \tag{6.6}$$

where

$$A_i = l_e + d_3 \cos \beta - r_p \cos \alpha_{3i} \tag{6.7}$$

From eq. (6.6), two solutions for α_{3i}, i.e., θ_{33i} — obtained from the z component — and four solutions for α_{1i} and α_{2i} respectively, i.e., θ_{31i} and θ_{32i} are obtained.

Moreover, from Figure 5.1 and Appendix A, the relationship between the input joint angle θ_1 and output joint angle θ_3 for a four-bar mechanism of Type II ($\epsilon = -1$ in Appendix A) can be written as follows

$$\cos \theta_1 = \frac{(l_1^2 + l_2^2) \cos \theta_3 + 2l_1 l_2}{l_1^2 + 2l_1 l_2 \cos \theta_3 + l_2^2} \tag{6.8}$$

$$\sin \theta_1 = \frac{(l_1^2 - l_2^2) \sin \theta_3}{l_1^2 + 2l_1 l_2 \cos \theta_3 + l_2^2} \tag{6.9}$$

Hence, four solutions for θ_{11i} and θ_{12i} and two solutions for θ_{13i} — the joint coordinates of the first bars of the three four-bar linkages in the ith leg — are finally obtained.

6.4 Direct Kinematics

The direct kinematic problem of the 6-DOF parallel mechanism using planar four-bar linkages can also be shown to be equivalent to the direct kinematics of existing parallel mechanisms or manipulators for which the solution has been shown to be reducible to a 16th-order polynomial equation (Merlet 1992a; Nanua *et al.* 1990; Ebert-Uphoff and Gosselin 1998).

6.5 Singularity Analysis

6.5.1 Jacobian Matrix

Differentiating eq. (6.1) with respect to time leads to

$$\dot{\mathbf{s}}_i = \mathbf{J}_i \dot{\boldsymbol{\theta}}_i \tag{6.10}$$

where $\dot{\boldsymbol{\theta}}_i = (\dot{\theta}_{11i}, \dot{\theta}_{12i}, \dot{\theta}_{13i})^T$ and $\mathbf{J}_i$ is the Jacobian matrix of leg i, which can be written as follows

$$\mathbf{J}_i = \begin{bmatrix} B_{1i}(d_2 \sin\alpha_{1i} - A_i \sin\alpha_{2i}) & -A_i B_{2i} \sin\alpha_{2i} & r_p B_{3i} \cos\alpha_{2i} \sin\alpha_{3i} \\ B_{1i}(-d_2 \cos\alpha_{1i} + A_i \cos\alpha_{2i}) & A_i B_{2i} \cos\alpha_{2i} & r_p B_{3i} \sin\alpha_{2i} \sin\alpha_{3i} \\ 0 & 0 & -r_p B_{3i} \cos\alpha_{3i} \end{bmatrix} \tag{6.11}$$

and

$$B_{ji} = \frac{\sin(\theta_{1ji} - \theta_{2ji})}{\sin(\theta_{3ji} - \theta_{2ji})}, \quad j = 1, 2, 3 \tag{6.12}$$

The joint velocities $\dot{\boldsymbol{\theta}}_i$ can be obtained from the following inverse Jacobian matrix.

$$\mathbf{J}_i^{-1} = \begin{bmatrix} \frac{-\cos\alpha_{2i}\cos\alpha_{3i}}{g_{1i}} & \frac{-\sin\alpha_{2i}\cos\alpha_{3i}}{g_{1i}} & \frac{-\sin\alpha_{3i}}{g_{1i}} \\ \frac{A_i\cos\alpha_{2i}-d_2\cos\alpha_{1i}}{g_{2i}} & \frac{A_i\sin\alpha_{2i}-d_2\sin\alpha_{1i}}{g_{2i}} & \frac{(A_i-d_2c\theta_{32i})\tan\alpha_{3i}}{g_{2i}} \\ 0 & 0 & \frac{-1}{g_{3i}} \end{bmatrix} \tag{6.13}$$

where

$$g_{1i} = B_{1i}d_2\sin\theta_{32i}\cos\alpha_{3i} \tag{6.14}$$

$$g_{2i} = A_iB_{2i}d_2\sin\theta_{32i} \tag{6.15}$$

$$g_{3i} = B_{3i}r_p\cos\alpha_{3i} \tag{6.16}$$

The Jacobian matrix $\mathbf{J}$ of the whole mechanism, which describes the relationship between the velocities of the actuated joints and the platform velocity can be derived in the same form and following the same procedure as in Chapter 4. One can write

$$\mathbf{J} = \begin{bmatrix} \mathbf{j}_1 \\ : \\ \mathbf{j}_6 \end{bmatrix} \tag{6.17}$$

with

$$\mathbf{j}_k = \begin{bmatrix} \mathbf{v}_{ji}^T & ((\mathbf{Q}\mathbf{b}_i)\times\mathbf{v}_{ji})^T \end{bmatrix}_{1\times6}, \; k=1,...,6 \tag{6.18}$$

where vector $\mathbf{v}_{ji}^T$ is actually the corresponding row of the leg inverse matrix in eq. (6.13). For example, for the first type of actuation (Case I) — the first and second four-bar linkages are actuated for each leg — the first and second rows of the matrix in eq. (6.13) are taken as $\mathbf{v}_{ji}, j=1,2$ to constitute the global Jacobian matrix $\mathbf{J}$ (eqs. (6.17) and (6.18)). One can finally write the the following velocity equation:

$$\mathbf{A}\dot{\mathbf{x}} = \mathbf{B}\dot{\boldsymbol{\theta}} \tag{6.19}$$

where

$$\dot{\mathbf{x}} = [\dot{\mathbf{p}}^T\boldsymbol{\omega}^T]^T \tag{6.20}$$

$$\dot{\boldsymbol{\theta}} = [\dot{\theta}_{111}\dot{\theta}_{112}\dot{\theta}_{113}\dot{\theta}_{121}\dot{\theta}_{122}\dot{\theta}_{123}] \tag{6.21}$$

$$\mathbf{A} = \begin{bmatrix} \mathbf{n}_{11}^T & ((\mathbf{Q}\mathbf{b}_1)\times\mathbf{n}_{11})^T \\ \mathbf{n}_{12}^T & ((\mathbf{Q}\mathbf{b}_2)\times\mathbf{n}_{12})^T \\ \mathbf{n}_{13}^T & ((\mathbf{Q}\mathbf{b}_3)\times\mathbf{n}_{13})^T \\ \mathbf{n}_{21}^T & ((\mathbf{Q}\mathbf{b}_1)\times\mathbf{n}_{21})^T \\ \mathbf{n}_{22}^T & ((\mathbf{Q}\mathbf{b}_2)\times\mathbf{n}_{22})^T \\ \mathbf{n}_{23}^T & ((\mathbf{Q}\mathbf{b}_3)\times\mathbf{n}_{23})^T \end{bmatrix} \tag{6.22}$$

$$\mathbf{B} = \operatorname{diag}(-g_{11}, -g_{12}, -g_{13}, g_{21}, g_{22}, g_{23}) \tag{6.23}$$

$$\mathbf{n}_{1i} = \begin{bmatrix} \cos\alpha_{3i}\cos\alpha_{2i} \\ \cos\alpha_{3i}\sin\alpha_{2i} \\ \sin\alpha_{3i} \end{bmatrix} \tag{6.24}$$

$$\mathbf{n}_{2i} = \begin{bmatrix} A_i\cos\alpha_{2i} - d_2\cos\alpha_{1i} \\ A_i\sin\alpha_{2i} - d_2\sin\alpha_{1i} \\ (A_i - d_2\cos\theta_{32i})\tan\alpha_{3i} \end{bmatrix} \tag{6.25}$$

The singularities of Type I occur when $\det(\mathbf{B}) = 0$, i. e.,

$$\prod_{i=1}^{3} B_{1i} d_2 \sin\theta_{32i} \cos\alpha_{3i} \prod_{i=1}^{3} A_i B_{2i} d_2 \sin\theta_{32i} = 0 \tag{6.26}$$

This equation leads to singular conditions as follows

$$\theta_{1ji} - \theta_{2ji} = n\pi, \; n \in Z, \; j = 1, \; 2 \tag{6.27}$$

$$\theta_{32i} = n\pi, \; n \in Z \tag{6.28}$$

$$\alpha_{3i} = n\pi + \frac{\pi}{2}, \; n \in Z \tag{6.29}$$

$$\alpha_{3i} = 2n\pi \pm \arccos(\frac{l_e + d_3\cos\beta}{r_p}), \; n \in Z \tag{6.30}$$

Furthermore, the singularity of the ith leg mechanism can be obtained from the Jacobian matrix $\mathbf{J}_i$ (eq. (6.11)) of the leg, namely,

$$\det(\mathbf{J}_i) = 0 \tag{6.31}$$

then,

$$r_p d_2 A_i B_{1i} B_{2i} B_{3i} \theta_{32i} \cos\alpha_{3i} = 0 \tag{6.32}$$

This equation leads to singular conditions which define the boundary of the constant-orientation workspace of the 6-DOF parallel mechanism as shown in eq. (6.27–6.30) plus an additional singular condition, i. e.,

$$\theta_{13i} - \theta_{23i} = n\pi, \; n \in Z \tag{6.33}$$

As shown by Zlatanov, Fenton and Benhabib (1995), the existence of invertible 6×6 Jacobian matrices $\mathbf{A}$ and $\mathbf{B}$ is not a sufficient condition for nonsingularity unless the velocity equations between the active and passive joint velocities are defined. The 6-DOF parallel mechanism of this chapter is an example of this situation. In other words,

(a) $(\phi, \theta, \psi) = (5°, 0, 0)$, (r, R)=(800, 6200) mm

(b) $(\phi, \theta, \psi) = (15°, 20°, 15°)$, (r, R)=(200, 5600) mm
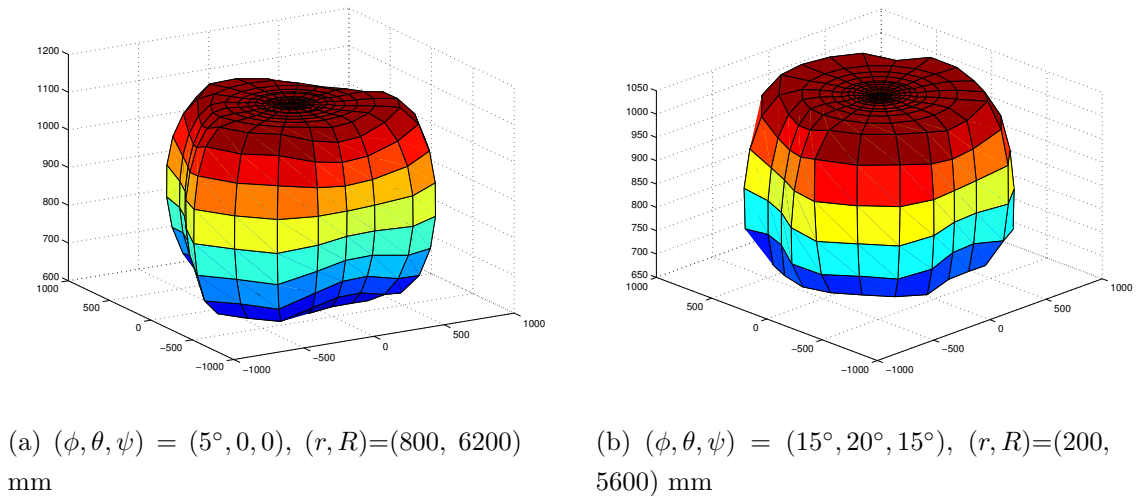
Figure 6.2: Constant-orientation workspace (Case I).

although the Jacobian matrices $\mathbf{A}$ and $\mathbf{B}$ are invertible, the singular configuration occurs when the additional condition (eq. (6.33)) is satisfied.

For other types of actuations (Case II and III), the Jacobian matrices $\mathbf{A}$ and $\mathbf{B}$ can be obtained by using vector $\mathbf{n}_{3i} = [0\ 0\ 1]^T$ and g_{3i} to replace the corresponding components. The singularities of Type I as well as the additional singular conditions associated with Case II and III can also be obtained.

For the singularities of Type II, the closed-form expression of the determinant of $\mathbf{A}$ is of a very complex form and it is impossible to find the the roots of such an expression analytically. Hence, a discretization method is first used to determine the singularity loci and the constant-orientation workspace. An example of the 6-DOF parallel mechanism is given, the geometry of the three leg mechanisms has been chosen in Section 5.5 and the mounting angles $(3°, 123°$ and $243°)$ of the leg mechanisms as well as two sets of radii (r, R) — $(800, 6200)$ mm and $(200, 5600)$ mm — of the mobile platform and the base respectively are chosen. The position vectors $\mathbf{p}_{0i}$ and $\mathbf{b}_i$ can be calculated from eqs. (4.7–4.8).

Figure 6.2 demonstrates the constant-orientation workspace of the example mechanism (Case I). Due to the limitation of workspace of the legs, the obtainable orientations for the example mechanism with larger platform is very limited. By contrast, the orientation workspace for the mechanism with smaller platform is considerable. The

(a) $z = 900$ mm   (b) $z = 700$ mm
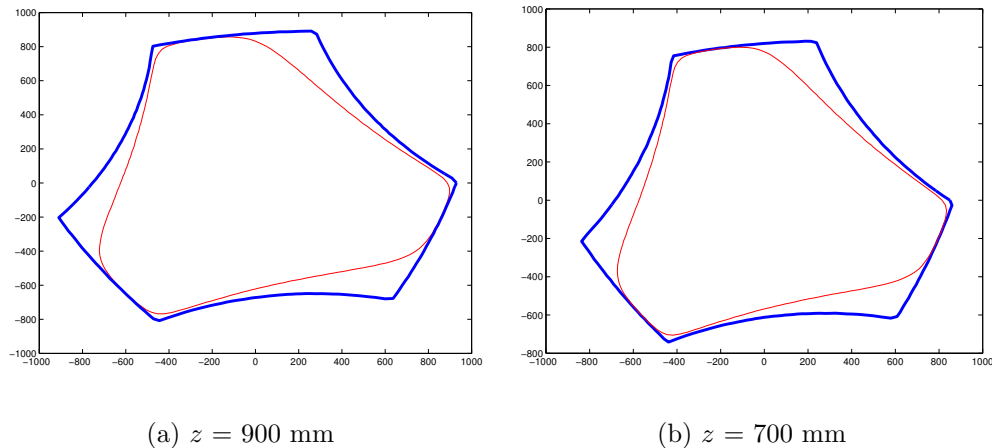
Figure 6.3: Singularity locus and boundary of the workspace for different values of z (Case I), $(\phi, \theta, \psi) = (5°, 0, 0)$, $(r, R) = (800, 6200)$ mm.

singularity locus (inner thin curve) of Type II and the boundary (outer thick curve) of the constant-orientation workspace for different values of z are shown in Figure 6.3.

6.5.2   Linear Dependencies of the Set of Lines for Case I

A geometric approach will now be used for the determination of the singularities of Type II in the following sections. As we mentioned before, a line can be defined by its Plücker vector (Merlet, 1989). Let two points on the line λ be M_1 and M_2. For any reference frame, let $\mathbf{a}$ be the vector from point M_1 to point M_2, and let $\mathbf{b}$ be the vector from the origin of the frame to point M_1. The corresponding six-dimensional Plücker vector $\mathbf{P}_\lambda$ is then defined by

$$\mathbf{P}_\lambda = \left[\mathbf{a}^T \left(\mathbf{b} \times \mathbf{a}\right)^T\right]^T \tag{6.34}$$

Actually, each row of matrix $\mathbf{A}$ associated with the actuated angle is a Plücker vector associated with a line. Hence, three lines $\lambda_{1i}, \lambda_{2i}, \lambda_{3i}$ for each leg can be obtained from vectors $\mathbf{n}_{1i}, \mathbf{n}_{2i}, \mathbf{n}_{3i}$ as shown in Figure 6.1. All the lines pass through the attachment point P_i. Line λ_{1i} is along the third bar of the third four-bar linkage, line λ_{3i} is parallel to the z axis of the fixed frame, while line λ_{2i} passes through P_i and a point which lies on the vertical line through point P_{j1i} and with a distance h_{vi} over the horizontal plane through point P_i. The distance h_{vi} can be calculated in the plane of the composite mechanism. For the case of actuation study, only two of the three lines for each leg and

(a) $(\phi, \theta, \psi) = (15°, 20°, 15°)$ (b) $(\phi, \theta, \psi) = (20°, 35°, 25°)$
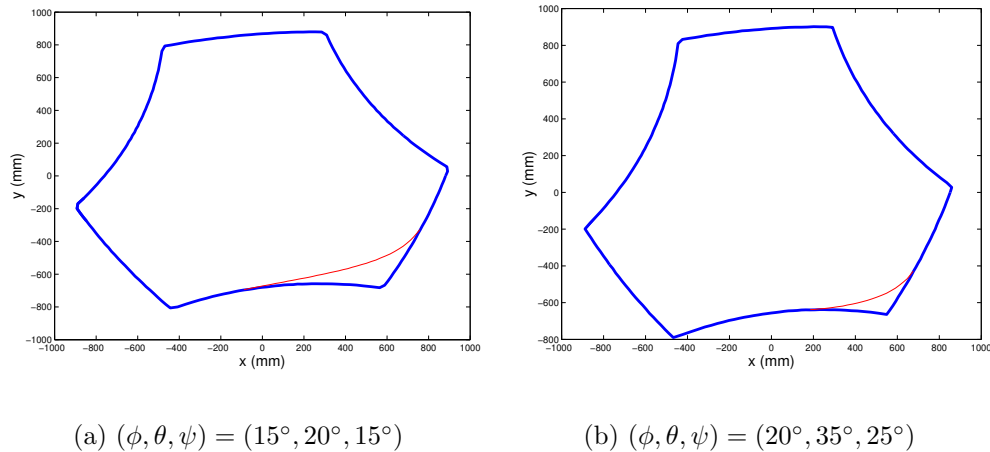
Figure 6.4: Singularity locus and boundary of the workspace for different orientations (Case I), (r, R)=(200, 5600) mm and z=900 mm.

globally 6 lines for the whole mechanism will be considered for the singularity analysis of Type II.

The 6-DOF parallel mechanism is in a singular configuration of Type II if and only if one of the Plücker vectors associated with a line is linearly dependent on the other Plücker vectors in the Jacobian matrix $\mathbf{A}$, namely, there is a subset spanned by n of its lines having a rank less than n. For Case I, the first and second four-bar linkages are actuated. Then, the corresponding lines λ_{1i} and λ_{2i} which define a plane $\triangle_i, i = 1, 2, 3$ are considered. The methodology and the notation used here are the same as those used in (Merlet, 1989). The detailed classification of the linear varieties by rank is shown in Figure 6.5 where a little black ball stands for the intersection of two lines, while a parallelogram for a plane. To study the singularities of the 6-DOF parallel mechanism with six lines, we have to consider the linear varieties of rank 1 to 5.

6.5.2.1 Subset of Two Lines

Condition 1. When two lines $\lambda_{ji}(i = 1, 2, 3; j = 1, 2)$ are collinear, a singular configuration is obtained. For the mechanism under study, the set of two lines can be of two types.

1. The two lines are associated with the same leg i. A singularity occurs when the two lines of the ith leg are aligned. The closed-form expression of the singularity locus
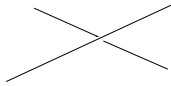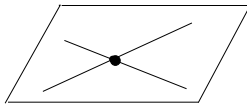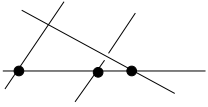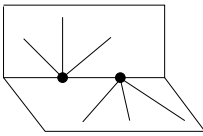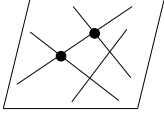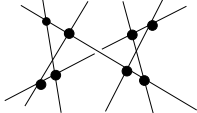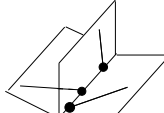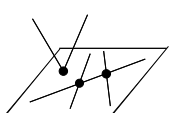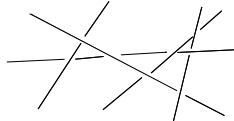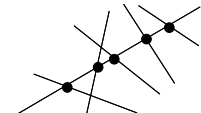
Figure 6.5: Linear Varieties by Rank.

for this case is the same as the one of Type I.

2. The two lines belong to different planes $\triangle_i$. Singular configurations occur only if two corresponding planes are coincident.

6.5.2.2 Subset of Three Lines

Condition 2. The lines belong to a flat pencil of lines: the three lines are coplanar and all intersect at a same point. Singularities arise in the following two sub-cases.

1. Two of the three lines belong to the same plane $\triangle_i$ and the other line in leg j passes through P_i and lies on the plane $\triangle_i$.

2. One line of each leg intersects at a common point lying on the plane of the mobile platform.

6.5.2.3   Subset of Four Lines

Condition 3b. The lines belong to two flat pencils having a common line but lying in two distinct planes and with distinct centers. We consider two sub-cases.

 1. Two pairs of lines have a common point each at P_i (e.g., P_1, P_2) and the common line of the two flat pencils passes through the points P_1 and P_2.

 2. Only one pair of the four lines has a common point (e.g., $\lambda_{11}, \lambda_{21}, \lambda_{i2}$ and λ_{i3}). The two lines λ_{i2} and λ_{i3} must be coplanar. Let P_{23} be the intersection point. The common line between the two flat pencils is the line going through P_1 and P_{23}.

Condition 3c. All the four lines pass through the same point but are not coplanar. In this case, only one pair of the four lines (e.g., $\lambda_{11}, \lambda_{21}, \lambda_{i2}$ and λ_{i3}) has a common point (P_1) and the lines λ_{i2} and λ_{i3} pass through the common point.

Condition 3d. The four lines are coplanar but do not belong to a flat pencil of lines. Two sub-cases are to be considered.

 1. Two pairs of lines have a common point each at P_i (e.g., $\lambda_{11}, \lambda_{21}, \lambda_{12}$ and λ_{22}). Such a case is obtained when the two planes are coincident.

 2. Only one pair of the four lines has a common point. In that case, all the lines must be coplanar with the moving platform.

6.5.2.4   Subset of Five Lines

Condition 4b. The five lines intersect two skew lines. Without loss of generality, let us consider the lines $\lambda_{11}, \lambda_{21}, \lambda_{12}, \lambda_{22}$, and $\lambda_{i3}, i = 1$ or 2. We first define a set of two skew lines s_1 and s_2 that intersect four lines in two different ways.

 1. $s_1 \in \triangle_1$ and crosses P_2, and $s_2 \in \triangle_2$ and crosses P_1. A singular configuration occurs if line λ_{i3} intersects the two skew lines s_1 and s_2 but does not lie in the mobile plane and the planes $\triangle_1$ and $\triangle_2$.

 2. $s_1 \in \triangle_1 \cap \triangle_2$ and s_2 is the line that passes through P_1 and P_2. A singular

configuration occurs if line λ_{i3} intersects s_1 and s_2.

Condition 4c. The five lines define three flat pencils having one line in common but lying in distinct planes and with distinct centers. We consider the five lines $\lambda_{11}, \lambda_{21}, \lambda_{12}, \lambda_{22}$, and $\lambda_{i3}, i = 1$ or 2. The former four lines belong to two flat pencils having the line $d \in \triangle_1 \cap \triangle_2$ in common with centers at P_1 and P_2. The singularity of condition 4c is obtained if and only if the line λ_{i3} intersects the line d, i.e., the three planes $\triangle_i, i = 1, 2, 3$ all intersect the line d.

Condition 4d. All the five lines belong to the same plane or pass through a unique point in that plane. There are three possible sub-cases.

1. Lines $\lambda_{11}, \lambda_{21}, \lambda_{12}$ belong to the same plane, λ_{22} and λ_{13} pass through the same point.

2. Lines $\lambda_{11}, \lambda_{21}, \lambda_{13}$ belong to the same plane as the platform, λ_{21} and λ_{22} pass through the same point.

3. Lines $\lambda_{11}, \lambda_{21}$ belong to the same plane and the other lines pass through the same point.

6.5.2.5 Subset of Six Lines

Condition 5a. The variety spanned by the six lines is a general linear complex. All coplanar lines of the complex intersect a common point. This can occur if the three lines belonging respectively to the three flat pencils defined by lines (λ_{1i} and $\lambda_{2i}, i = 1, 2, 3$) and lying on the moving platform plane intersect at the same point.

Condition 5b. All the six lines intersect the same line. There are two sub-cases for this singularity.

1. The common line passes through P_i and P_j. This singularity occurs if the plane $\triangle_k$ and the platform plane are coincident.

2. The common line is the line of intersection between planes $\triangle_i$ and $\triangle_j$. This singularity occurs when vertex P_k lies on the intersection line.
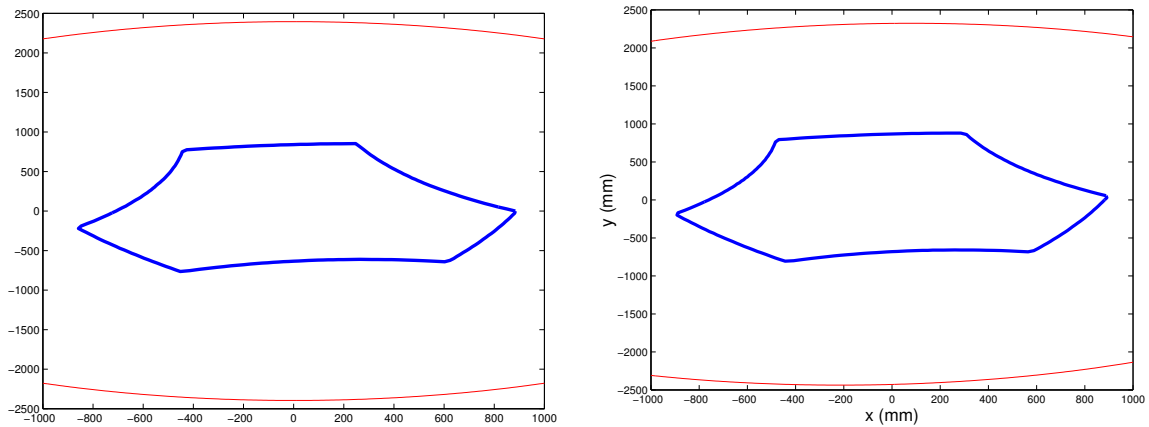
(a) $(\phi, \theta, \psi) = (5°, 0, 0)$, $(r, R, z)=(800, 6200, 1000)$ mm

(b) $(\phi, \theta, \psi) = (15°, 20°, 15°)$, $(r, R, z)=(200, 5600, 900)$ mm

Figure 6.6: Singularity loci and boundary of the constant-orientation workspace (Case III).

Now, all the singular configurations have been presented using geometric rules. The expressions describing the corresponding singularities can then be obtained. For example, only the expressions for the first sub-case of Condition 3b are derived and given here.

According to the condition and geometric rules one can write

$$(\mathbf{n_{11}} \times \mathbf{n_{21}}) \cdot \mathbf{p}_{12} \quad = \quad 0 \tag{6.35}$$

$$(\mathbf{n_{12}} \times \mathbf{n_{22}}) \cdot \mathbf{p}_{12} \quad = \quad 0 \tag{6.36}$$

where $\mathbf{p}_{12}$ is the vector connecting P_1 to P_2.

Finally, one can deduce two equations representing the singularity loci of this sub-case with the following form:

$$f_1(\alpha_{11}, \alpha_{21}, x, y, z, \phi, \theta, \psi) = 0 \tag{6.37}$$

$$f_2(\alpha_{12}, \alpha_{22}, x, y, z, \phi, \theta, \psi) = 0 \tag{6.38}$$

6.5.3 Expressions of the Singularity Loci for Cases II and III

For Cases II and III the six lines are λ_{1i} and λ_{3i} and λ_{2i} and λ_{3i} respectively. Moreover, the planes $\triangle_i, i = 1, 2, 3$ defined by the lines λ_{1i} and λ_{3i} (or λ_{2i} and λ_{3i}) are always perpendicular to the base plane of the mechanism. Following the same procedure as in Case I, it is found that all the singular configurations of the mechanism can be reduced to the generation of a general linear complex except for the first sub-case of 3b ($\theta = \pm\frac{\pi}{2}$ is a singular condition) (Monsarrat and Gosselin, 2001). In singular configurations, the three planes $\triangle_i$ are normal to the plane of the base and intersect one common line being perpendicular to that plane. Hence, for a given orientation of the moving platform, the cross section of the singularity surface is the same for any z coordinate. Let $d_i, i = 1, 2, 3$ be the three intersection lines between the planes $\triangle_i$ and the plane of base. In the plane, the three lines intersect the same point. We define the point P_i' as the projection of point P_i on the base plane, i.e., $\mathbf{p}_i' = \begin{bmatrix} p_{ix} & p_{iy} & 0 \end{bmatrix}^T$. Then, we determine the equations of the three lines d_i that pass through the points P_{j1i} and P_i' for Case III, i.e.,

$$(p_{j1iy} - p_{iy})u + (p_{ix} - p_{j1ix})v + p_{\delta i} = 0, i = 1, 2, 3 \tag{6.39}$$

where $p_{\delta i} = p_{j1ix}p_{iy} - p_{j1iy}p_{ix}$.

All the three lines intersect a common point only if the following determinant vanishes, i.e.,

$$\begin{vmatrix} p_{j11y} - p_{1y} & p_{j12y} - p_{2y} & p_{j13y} - p_{3y} \\ p_{1x} - p_{j11x} & p_{2x} - p_{j12x} & p_{3x} - p_{j13x} \\ p_{\delta 1} & p_{\delta 2} & p_{\delta 3} \end{vmatrix} = 0 \tag{6.40}$$

Substituting the components of vector $\mathbf{p}_{j1i}$ and $\mathbf{p}_i$ leads to

$$C_1 x^2 + C_2 y^2 + C_3 xy + C_4 x + C_5 y + C_6 = 0 \tag{6.41}$$

where the coefficients $C_i, i = 1, ..., 6$ are the function of the geometric parameters of the mechanism and the orientation $\mathbf{Q}$ of the mobile platform. Furthermore, the nature of the above curve depends on the following quantity:

$$\delta = C_1 C_2 - \frac{C_3^2}{4} \tag{6.42}$$

The curve will be a circle ($\delta = 1$), an ellipse ($\delta > 0$), a parabola ($\delta = 0$) or a hyperbola ($\delta < 0$). Figure (6.6) demonstrates the section of the constant-orientation workspace

(a) $(\phi, \theta, \psi) = (5°, 0, 0)$, (r, R, z)=(800, 6200, 900) mm.

(b) $(\phi, \theta, \psi) = (25°, 35°, 15°)$, (r, R, z)=(200, 5600, 900) mm.
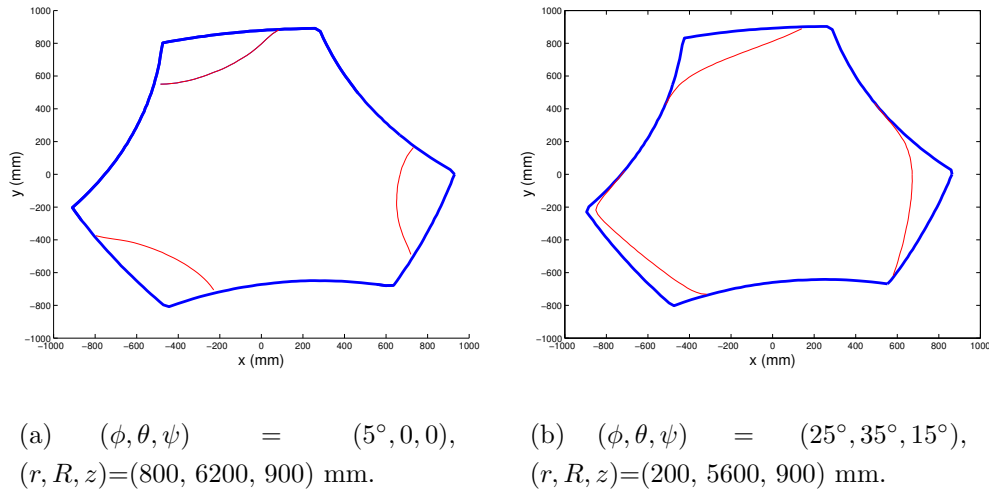
Figure 6.7: Singularity locus and boundary of the workspace (Case II).

and the singularity surface for a given coordinate z. It is found that there is no singularity inside the workspace for the mechanisms of Case III. This result is confirmed using the discretization method.

For Case II, we should replace the coordinates of point P_{j1i} with those of point P_{j2i} in eq. (6.40). However, the coefficients C_i include the joint coordinates of the first four-bar linkages. This implies that we cannot obtain a fixed singularity locus for a given orientation of the platform as shown for Case III. Figure 6.7 illustrates the singularity locus (inner thin curves) and the boundary (outer thick curve) of the constant-orientation workspace for the example mechanism which is obtained using a discretization method.

6.6   Conclusions

The inverse kinematics and singularity analysis of a novel reactionless 6-DOF parallel mechanism have been addressed in this chapter. Three types of actuation schemes of the mechanism were considered. The Jacobian matrix of the mechanism was first derived and the six lines defined by the Plücker vectors associated with the six input angles of the architecture have been given. The linear dependencies between the corresponding lines were studied using Grassmann line geometry, and the singular configurations were

presented using simple geometric rules. The expressions describing the corresponding singularities have been obtained and the graphical representations that show the relationship between the singularity loci and the constant-orientation workspace of the mechanism have been given.

All the results presented in this chapter will be of great help during the design process and for the control of the new type of parallel mechanism introduced in Chapter 5.

Chapter 7

Conclusions and Future Work

In order to eliminate the excitation of the base in high speed machinery and in large-scale precision devices or the disturbance of the free-floating base in space robotics and telescope mechanisms, thereby to significantly improve the general performance, the development of reactionless mechanisms and manipulators (including spatial ones having up to 6-DOF) has become an increasingly challenging and promising research subject in the field of parallel mechanisms and motivates researchers to study it. A systematic study of the synthesis and kinematic analysis of reactionless spatial multi-degree-of-freedom parallel mechanisms has been performed in this thesis. This study includes the conceptual design of 3-DOF leg mechanisms, the synthesis of 6-DOF parallel mechanisms, the geometric description and kinematic analysis of these mechanisms as well as their dynamic balancing. Some results of this study have been presented in international conferences or will appear in journal papers (Wu and Gosselin, 2002a, 2002b, 2002c, 2003a, 2003b; Gosselin and Wu, 2002). In this chapter, a number of

conclusions are highlighted, some results are discussed, and research issues for further studies are given.

7.1 Summary

This thesis set out to investigate the dynamic balancing of elementary linkages. The balancing equations are derived by imposing that the center of mass of the mechanism is fixed and that the total angular momentum is constant with respect to a fixed point. Counterweights and counter-rotations were added for dynamic balancing. A 1-DOF link was extended to a dynamically balanced 2-DOF serial chain. Two of these were used to synthesize a planar 2-DOF parallel mechanism. This allowed the simplification of the dynamic balancer. By adding another link that can move out of the plane of the 2-DOF mechanism, a new kind of 3-DOF parallel mechanism referred to as a parallelepiped mechanism has been presented and a practical design has been implemented in this thesis. The 3-DOF parallelepiped mechanism may be regarded as a three-link serial chain since the kinematic analyses of the two kinds of mechanisms are completely the same. On the other hand, the parallelepiped mechanism may be also considered as a "truly parallel" deformable truss, i.e., a multi-dof truss-type mechanism in which all actuators are mounted in parallel on the base. The mechanism has lower inertia and a higher stiffness compared to the three-link serial chain where two of three actuators are mounted on the moving links so that the mass and inertia of the actuators must be considered in the balancing. Optimizations were used to determine the counterweights and counter-rotations, based on the balancing conditions. The dynamic simulation software ADAMS has been used to simulate the motion of the 3-DOF parallelepiped mechanisms and to verify that the mechanisms are reactionless at all times and for arbitrary trajectories. Furthermore, compared to the dynamic balancing for the three-link serial chain by adding a counterweight at the extension of each link, it has been found that reactionless 3-DOF parallelepiped mechanism can be obtained at a lower expense of the addition of counterweights due to the parallelograms which can transmit the rotation of the moving mass to a link pivoted to the base and result in adding less counterweights on this link. Finding simple mechanisms which can be dynamically balanced and then serve as legs to construct multi-degree-of-freedom parallel mechanisms is crucial for the synthesis of reactionless parallel mechanisms of the desired degrees of freedom.

The reactionless conditions for planar four-bar linkages moving spatially and the synthesis of novel reactionless spatial 3-DOF using four-bar linkages without additional counter-rotations have been addressed in this thesis. Based on the conditions of dynamic balancing of a single planar four-bar linkage moving in the plane, the spatial problem has been addressed. It has been shown that a single planar four-bar linkage cannot be dynamically balanced when moving spatially. However, it has been found that a mechanism composed of a pair of orthogonally connected planar reactionless four-bar linkages has the property of a rigid body, i. e., the composite mechanism has a fixed center of mass and a constant inertia tensor. Therefore, it can be attached to any other mechanism provided its mass and inertia comply with the balancing conditions of this other mechanism. In this thesis, such a composite mechanism was attached to a serial chain of dynamically balanced four-bar linkages undergoing planar motion in a plane perpendicular to the composite mechanism, in such a way that the inertia tensor of the composite mechanism is constant and that the balancing conditions of the planar serial chain are satisfied. Thus, reactionless spatial 3-DOF mechanisms using four-bar linkages have been synthesized. The reactionless property of this 3-DOF mechanism has been verified by a numerical example using ADAMS. The most important advantage of the kind of reactionless mechanism is that the use of additional separate counter-rotations and their side effects are avoided. Moreover, it is easy to design and manufacture a practical dynamically balanced system with only counterweights and revolute joints.

Reactionless spatial 6-DOF parallel mechanisms using parallelepiped mechanisms and a reactionless spatial 6-DOF parallel mechanism using four-bar linkages have been synthesized in this thesis. These are the first completely balanced spatial 6-DOF parallel mechanisms we have seen in the literature. An algorithm using point masses located at the points of attachment of the legs to the platform to replace a moving platform has been derived in this thesis in order to simplify the dynamic balancing for planar and spatial multi-degree-of-freedom parallel mechanisms with several legs. It has been shown that a reactionless spatial parallel mechanism can be obtained by dynamically balancing each detached leg mechanism independently instead of dynamically balancing the whole mechanism. It has been found that for planar parallel mechanisms a uniform platform with any thickness while for spatial parallel mechanisms only symmetric thin homogeneous platforms can meet the requirement of dynamic equivalence derived in this thesis. Although there is still some skepticism about this algorithm, numerical examples and their simulations using ADAMS have verified the reactionless properties

of the balanced mechanisms as well as the correctness and efficiency of this algorithm. The approach of dynamically balancing each leg independently can be applied to the dynamic balancing of any multi-degree-of-freedom parallel mechanisms if the moving platform can be replaced by corresponding point masses.

The kinematic analyses including the inverse and direct kinematics as well as the determination of singularity loci and workspace of both the 3-DOF leg mechanisms and the 6-DOF parallel mechanisms have been solved in this thesis. For novel manipulators, it is necessary to find out the inherent characteristics of the mechanisms in the context of design and control of the mechanisms. The Jacobian matrices of the mechanisms associated with different actuation schemes have been derived. Geometrical algorithms and discretization methods are used for the determination of the workspace for the corresponding mechanisms. Also, analytic methods based on the determinant of the Jacobian matrix and discretization methods have been utilized for the singularity analysis. Especially, a geometrical algorithm based on Grassmann line geometry has been used for the singularity analysis of such a complex mechanism as the reactionless 6-DOF parallel mechanism using four-bar linkages. Finally, the graphical representations that show the relationship between the singularity loci and the constant-orientation workspace of the mechanisms were given. Each approach has its own advantages and is suitable to different applications. In addition, some important results of kinematic analysis have been obtained. For instance, by suitable design of the parameters of the 6-DOF parallel mechanism using four-bar linkages (Case III), singularities can be avoided inside its workspace.

A general procedure for the synthesis of reactionless multi-degree-of-freedom parallel mechanism has been developed in this thesis. Essentially, this procedure is based on stationary global center of mass and constant angular momentum. This classic approach was extended by the notion that dynamically balanced mechanisms, globally behaving as rigid bodies, can be attached to a rigid link in any other dynamically balanced mechanism. Thereby, the number of degrees of freedom can be expanded (Figure 5.8). This was proved to be a useful tool in the design of multi-dof dynamically balanced mechanisms. The procedure includes the design of a simple mechanism, derivation of balancing conditions of the mechanism, optimization for determination of counterweights and/or counter-rotations, synthesis of multi-degree-of-freedom parallel mechanism, dynamically balancing each leg mechanism independently, simulation using ADAMS with numerical examples, verification of reactionless property, kinematic

analysis with suitable algorithm, characteristics verification of the mechanism with the design criteria. This procedure is very helpful in both the conceptual design and detailed design stages.

Reactionless spatial multi-degree-of-freedom mechanisms have great potential applications such as space robots, telescope mirror mechanisms and some industrial high speed devices. All the results of kinematic analysis will be of great help during the design process and for the control of the mechanisms presented in this thesis.

7.2 Discussion and Future Work

Many dynamic balancing approaches and balanced mechanisms have been proposed in the literature. However, the practical application of the proposed balancing techniques is questionable. The price paid for balancing includes extra additional masses, complex balancing devices, increase of joint forces and driving torques and even unrealistic configurations. Most of the mentioned problems are common to many balancing techniques and undesirable but unavoidable, just as an ancient Chinese proverb says "one cannot get something without paying anything in return".

As we have discussed in the respective chapters in this thesis, the development of reactionless multi-degree-of-freedom robotic systems was achieved also at the expense of a substantial increase of the masses of the moving links and the complexity of the mechanism. However, we have shown the advantage of the two kinds of reactionless 3-DOF mechanisms proposed in this thesis as compared to three-link serial chains. The reactionless 3-DOF mechanism using four-bar linkages has 11 moving links, 2 more than that (9) of the reactionless 3-DOF parallelepiped mechanism, and hence may have a greater mass increase of the system for the same payload. Apparently, the former mechanism looks larger and more complicated than the latter mechanism. However, three counter-rotations have to be used for the latter mechanism. Moreover, the design of separate counter-rotations is normally complicated relative to the initial mechanism especially for the design near a pivot on the base with counterweights and counter-rotations as well as actuators, a challenging issue for future work. Furthermore, using counter-rotations like gear inertia counterweights may generate noise and vibrations. Hence, the disadvantages of the complexity and larger mass of the reactionless 3-DOF

mechanism using four-bar linkages may be overcome by its merit of avoiding separate counter-rotations in high speed applications. For a completely new design of reactionless 3-DOF mechanism or 6-DOF parallel mechanism, the two kinds of syntheses using parallelepiped mechanism or using four-bar linkages respectively are both good candidates. Which one is better depends on the design requirements and limitations.

Another challenge in the future is the simplification of the designs proposed in this thesis in order to decrease the total system mass and render them more suitable for practical application as the launch cost is a crucial consideration for space robots. As mentioned before, for instance, there are some possibilities to shrink the reactionless 3-DOF mechanism using four-bar linkages such as changing the position of the attachment point of two four-bar linkages (point P in Figure 5.6), decreasing the length r_p (eq. 6.2) of the extension part of the link connected to the platform, using the same size for the two four-bar linkages of the composite mechanism and so on. Many solutions are no more than proof-of-principle. For instance, optimization has been used to find a solution from infinitely many, but selecting different object functions or boundaries of optimum variables may well yield much better performance. An optimization for the whole mechanism with the considerations of the above factors and detailed parameters using dimensional variables specifically tailored to the link geometry will definitely decrease the mass of the mechanism. Following the general procedure and using the kinematic analysis algorithm as well as the corresponding codes developed in this thesis, finally, a more practical design of the reactionless mechanism can be obtained. Future work also includes the applications of the approaches presented in this thesis to other mechanisms as well as the design and fabrication of balanced prototypes of the reactionless spatial 3-DOF mechanisms and spatial 6-DOF reactionless parallel manipulators.

Some of the procedures used in this thesis may be generalized. For example, in the parallelepiped mechanism of Case I, the assumption that the center of mass of each link is located on the link axis may be generalized.

To find out the dynamic equivalence between a moving platform and four point masses is an imperative research issue for future work. We have shown that a very thin uniform moving platform can be dynamically replaced by three point masses. However, if the platform has a nonzero thickness or is not symmetric, the dynamic equivalence conditions cannot be satisfied. In this case, the platform could be replaced by four non coplanar point masses. Subsequently, four legs could be used and the attachment points

of the legs on the platform do not lie on one plane in order to obtain a reactionless 6-DOF parallel mechanism. It is worth while to derive these conditions such that the approach of dynamically balancing each leg mechanism independently for the dynamic balancing of whole mechanism can be applied to more parallel mechanisms.

The dynamic balancing of mechanisms has received considerable attention for several decades and many dynamic balancing approaches and balanced mechanisms have been proposed. However, so far, very few have been put into practical applications due to the high cost for the balancing. The potential applications have attracted researchers to continue working on this subject and new approaches and solutions are constantly being reported. To develop a perfect reactionless parallel mechanism which will finally be used in space robots or telescopes is our dream, but there is still a long way to go.

Bibliography

Agrawal, S. K., and Shirumalla, S., 1995, "Planning motions of a dual-arm free-floating manipulator keeping the base inertially fixed", *Mechanism and Machine Theory*, Vol. 30, No. 1, pp. 59–70.

Angeles, J., Nahon, M. A., and Thümmel, T., 1992, "Active control for the complete dynamic balancing of linkages", *in DE Flexible Mechanisms, Dynamics, and Analysis, 22nd ASME Biennial Mechanisms Conference*, DE–Vol. 47, pp. 305–310.

Arakelian, V. H., and Smith, M. R., 1999, "Complete shaking force and shaking moment balancing of linkages", *Mechanism and Machine Theory*, Vol. 34, No. 8, pp. 1141–1153.

Arun, V., Reinholtz ,C. F., and Watson, L. T., 1990, "Enumeration and analysis of variable geometry truss manipulators", *Proceedings of the 1990 ASME Design Technical Conference*, DE-Vol. 26, Chicago, USA.

Bagci, C., 1982, "Complete shaking force and shaking moment balancing of link mechanisms using balancing idler loops", *ASME Journal of Mechanical Design*, Vol. 104, pp. 482–493.

Bagci, C., 1983, "Complete balancing of space mechanisms – shaking force balancing", *ASME Journal of Mechanisms, Transmissions, and Automation in Design*, Vol. 105, pp. 609–616.

Bagci, C., 1992, "Complete balancing of linkages using complete dynamical equivalents of floating links: CDEL method", *in DE Flexible Mechanisms, Dynamics, and Analysis, 22nd ASME Biennial Mechanisms Conference*, DE–Vol. 47, pp. 477–488.

Benea, R., 1996, "Contribution à l'étude des robots pleinement parallèles de type 6 R-RR-S," *Ph.D. Thesis*, Université de Savoie, Annecy, France, December.

Bedford, A., and Fowler, W., 1996, Appendix, *Engineering Mechanics: Dynamics*, Addison-Wesley.

Berkof, R. S., and Lowen, G.G., 1969, "A new method for completely force balancing simple linkages", *ASME Journal of Engineering for Industry*, Vol. 91, No. 1, pp. 21–26.

Berkof, R. S., and Lowen, G.G., 1971, "Theory of shaking moment optimization of force-balanced four-bar linkages", *ASME Journal of Engineering for Industry*, Vol. 93, No. 1, pp. 53–60.

Berkof, R. S., 1973, "Complete force and moment balancing of inline four-bar linkages", *Mechanism and Machine Theory*, Vol. 8, pp. 397–410.

Bonev, I. A., 2002a, "Geometric analysis of parallel mechanisms", *Ph.D thesis*, Université Laval, Québec, Canada.

Bonev, I. A., and Gosselin, C. M., 2002b, "Geometric algorithms for the computation of the constant-orientation workspace and singularity surfaces of a special 6-RUS parallel manipulator", *Proceedings of the ASME 2002 Design Engineering Technical Conference*, Montreal, Canada, September 30–October 2.

Bonev, I. A., 2003, "The true origins of parallel robots" (**http://www.parallemic.org/Reviews/Review007.html**).

Chen, N. X., 1984, "The complete shaking force balancing of a spatial linkage, *Mechanism and Machine Theory*, Vol. 19, No. 3, pp. 243–255.

Chablat, D., and Wenger, P., 1998, "Working modes and aspects in fully parallel manipulators", *Proceedings of the 1998 IEEE International Conference on Robotics and Automation*, Leuven, Belgium, May, pp. 1994—1969.

Clavel, R., 1988, "DELTA, a fast robot with parallel geometry", *18th International Symposium on industrial robots*, pp. 91–100, Lausanne, Avril 26-28.

Collins, C. L., and Long, G. L., 1994, "Line geometry and the singularity analysis of an in-parallel hand controller for force-reflected teleoperation", *Robotics: Kinematics, Dynamics and Controls in Proceedings of the 1994 ASME Design Technical Conference*, DE-Vol. 72, Minneapolis, USA.

Collins, C. L., and McCarthy, J .M, 1998, "The quartic singularity surfaces of planar platforms in the Clifford algebra of the projective plane", *Mechanism and Machine Theory*, Vol. 33, No. 7, pp. 931–944.

Di Gregorio, R., and Parenti-Castelli, V., 1998, "A translational 3-DOF parallel manipulator", *Advances in Robot Kinematics: Analysis and Control*, Kluwer Academic Publishers, The Netherlands, pp. 49–58.

Dresig, H., *et al.* (VDI), 1998, "Dynamics of mechanisms – Rigid body mechanisms", Richtlinien 2149 Part 1, Verein Deutscher Ingenieure.

Dresig, H., Rockhausen, L., Naake, S., 1992, "Balancing conditions for planar mechanisms", *Proceedings of the 22nd Bieenial Mechanisms Conference, Flexible Mechanisms, Dynamics, and Analysis*, DE-VOl. 47, ASME, pp. 67–73.

Dubowsky, S., and Torres, M. A., 1991, "Path planning for space manipulators to minimize spacecraft attitude disturbances", *Proceedings of the 1991 IEEE International Conference on Robotics and Automation*, Sacramento CA, pp. 2522–2528.

Ebert-Uphoff, I., and Gosselin, C. M., 1998, "Kinematic study of a new type of spatial parallel platform mechanism", *Proceedings of the ASME 1998 Design Engineering Technical Conference*, Atlanta, Georgia, September 13–16.

Esat, I., and Bahai, H., 1999, "A theory of complete force and moment balancing of planer linkage mechanisms", *Mechanism and Machine Theory*, Vol. 34, No. 6, pp. 903–922.

Foucault, S., and Gosselin, C. M., 2002, "On the development of a planar 3-DOF reactionless paralle mechanism", *Proceedings of the ASME 2002 Design Engineering Technical Conference*, Montreal, Quebec, September 30-Octobor 2.

Gao, F., 1989, "Complete shaking force and shaking moment balancing of four types of six-bar linkages", *Mechanism and Machine Theory*, Vol. 24, No. 4, pp. 275–287.

Gao, F., 1990, 'Complete shaking force and shaking moment balancing of 26 types of four-,five- and six-bar linkages with prismatic pairs', *Mechanism and Machine Theory*, Vol. 25, No. 2, pp. 183–192.

Gao, F., 1991, "Complete shaking force and shaking moment balancing of 17 types of eight-bar linkages only with revolute pairs", *Mechanism and Machine Theory*, Vol. 26, No. 2, pp. 197–206.

Gosselin, C. M., and Angeles, J., 1989, "The optimum kinematic design of a spherical three-degree-of-freedom parallel manipulator", *ASME Journal of Mechanisms, Transmissions, and Automation in Design*, Vol. 111, No. 2, pp. 202–207.

Gosselin, C. M., and Angeles, J., 1990, "Singularity analysis of closed-loop kinematic chains", *IEEE Transaction on Robotics and Automation*, Vol. 6, No. 3, pp. 281–290.

Gosselin, C. M., 1990, "Determination of the workspace of 6-DOF parallel manipulators", *ASME Journal of Mechanical Design*, Vol. 112, September, pp. 331–336.

Gosselin, C. M., Lavoie, E., and Toutant, P., 1992, "An efficient algorithm for the graphical representation of the three-dimensional workspace of parallel manipulators", *Proceedings of the ASME 22nd Biennial Mechanisms Conference*, Scottsdale, AZ, USA, Vol. 45, pp. 323–328.

Gosselin, C. M., and Sefrioui, J., 1992, "Determination of the singularity loci of spherical three-degree-of-freedom parallel manipulators", *Robotics, Spatial Mechanisms and Mechanical Systems*, Vol. 45, pp. 329–336.

Gosselin, C. M., and Jean, M., 1995, "Determination of the workspace of planar parallel manipulators with joint limits", *Journal of Robotics and Autonomous Systems* Vol. 17, No. 3, pp. 129–138.

Gosselin, C. M., and Wang, J., 1997, "Singularity loci of planar parallel manipulators with revolute actuators", *Robotics and Autonomous Systems*, Vol. 21, pp. 377-398.

Gosselin, C. M., Wang, J., Laliberté, T., and Ebert-Uphoff, I. 1999, "On the design of a statically balanced 6-DOF parallel manipulator", *Proceedings of the IFToMM Tenth World Congress on the Theory of Machines and Mechanism*, Oulu, Finland, June 20-24, pp. 1045-1050.

Gosselin, C. M., and Wang, J., 2000, "Static balancing of spatial six-degree-of-freedom parallel mechanisms with revolute actuators", *Journal of Robotic Systems*, Vol. 17, No. 3, pp. 159–170.

Gosselin, C. M., and Wu, Y., 2002, "On the development of reactionless spatial 3-DOF parallelepiped mechanisms", *Proceedings of the ASME 2002 Design Engineering Technical Conference*, Montreal, Quebec, September 30-Octobor 2.

Gosselin, C. M., Vollmer, F., Côté, G., and Wu, Y., 2003, "Synthesis and Design of Reactionless Three-degree-of-freedom Parallel Mechanisms", To appear in *IEEE Transactions on Robotics and Automation.*

Gough, V. E.,and Whitehall, S.G., 1962, "Universal tyre test machine", *Proceedings of the FISITA Ninth International Technical Congress*, pp. 117–137, May.

Hamlin, G. J., and Sanderson, A. C., 1994, "A novel concentric multilink spherical joint with parallel robotics applications", *Proceedings of the 1994 IEEE International Conference on Robotics and Automation*, San Diego, USA, May 8-13, pp. 1267–1272.

Hertz, R. B., Hughes, P. C., 1994, "Kinematic analysis of a class of spatial parallel manipulators with three degrees of freedom", *Proceedings of the 1994 ASME Design Technical Conference*, DE-Vol. 72, Minneapolis, USA.

Herder, J. L., 2001, *Energy-free system. Theory, conception and design of statically balanced spring mechanisms*, Ph.D. Thesis, Delft University of Technology, The Netherlands, ISBN 90-370-0192-0.

Herder, J. L., and Gosselin, C. M., 2003, "Reaction-free systems. Principles, conception and design of dynamically balanced mechanisms", *Technical Report*, Université Laval, Quebec, Canada

Huang, Z., Liu, D. Y., 1986, "Shaking moment balancing of force-balanced six-bar linkages", *Proceedings of the 1986 ASME Design Technical Conference*, Columbus, Ohio, Oct. 5-8.

Hunt, K. H, 1978, *Kinematic Geometry of Mechanisms*, Oxford University Press.

Kaufman, R. E., and Sandor, G. N., 1971, "Complete force balancing of spatial linkages", *ASME Journal of Engineering for Industry*, Vol. 93, pp. 620–626.

Kochev, I. S., 1987, "General method for full force balancing of spatial and planar linkages by internal mass redistribution", *Mechanism and Machine Theory*, Vol. 22, No. 4, pp. 333–341.

Kochev, I. S.,1990a, "General method for active balancing of combined shaking moment and torque fluctuations in planar linkages", *Mechanism and Machine Theory*, Vol. 25, No. 6, pp. 679–687.

Kochev, I. S., 1990b, "Full shaking moment balancing of planar linkages by a prescribed input speed fluctuation", *Mechanism and Machine Theory*, Vol. 25, No. 4, pp. 459–466.

Kochev, I. S., 1991, "Contribution to the theory of torque, shaking force and shaking moment balancing of planar linkages", *Mechanism and Machine Theory*, Vol. 26, No. 3, pp. 275–284.

Kochev, I. S., 1992a, "Active balancing of the frame shaking moment in high speed planar machines", *Mechanism and Machine Theory*, Vol. 27, No. 1, pp. 53–57.

Kochev, I. S., 1992b, "Qualitative theory of the reactions and stresses in high speed planar linkages", *Mechanism and Machine Theory*, Vol. 27, No. 1, pp. 59–68.

Kochev, I. S., 2000, "General theory of complete shaking moment balancing of planar linkages: a critical review", *Mechanism and Machine Theory*, Vol. 35, No. 11, pp. 1501–1514.

Kong, X. W., and Yang, T. L., 1998, "Extensions to the mass moment substitution method for complete shaking force balancing of spatial linkages", *Proceedings of the ASME 1998 Design Engineering Technical Conference*, Atlanta, GA, September 13–16, DETC/MECH-5846.

Kong, X. W., 2002, "Type synthesis and kinematics of analytic and general parallel mechanisms", *Ph.D thesis*, Université Laval, Québec, Canada.

Lee, K.M., and Shah, D.K., 1988, "Kinematic analysis of a three-degree-of-freedom in-parallel actuated manipulator", *IEEE Transactions on Robotics and Automation*, Vol. 4, No. 3, pp. 354–360.

Legnani, G., Zappa, B. Adamini, R., and Casolo, F., 1999, "A contribution to the dynamics of free-flying space manipulators", *Mechanism and Machine Theory*, Vol. 34, No. 3, pp. 359–372.

Lowen, G. G., and Berkof, R. S., 1968, "Survey of Investigations into the balancing of linkages", *J. Mechanisms*, Vol. 3, pp. 221–231.

Lowen, G. G., Tepper, F. R., and Berkof, R. S., 1983, "Balancing of linkages – an update", *Mechanism and Machine Theory*, Vol. 18, No. 3, pp. 213–220.

Ma, O., and Angeles, J., 1991, "Architecture singularities of platform manipulators", *Proceedings of the 1991 IEEE International Conference on Robotics and Automation*, Sacramento, CA, April, pp. 1542–1547.

Masory, O., and Wang, J., 1992, "Workspace evaluation of Stewart platforms", *Robotics, Spatial Mechanisms, and Mechanical Systems, 22nd ASME Biennial Mechanisms Conference*, DE–Vol. 45, pp. 337–346.

Mayer St-onge, B., and Gosselin, C. M., 2000, "Singularity analysis and representation of the general Gough-Stewart platform", *The International Journal of Robotics Research*, Vol. 19, No. 3, pp. 271-288.

Meriam, J. L., and Kraige, L. G., 1993, Chapter 7, *Engineering Mechanics: Dynamics*, John Wiley & Sons, Inc.

Monsarrat, B., and Gosselin, C. M., (2001), "Singularity analysis of a three-leg six-degree-of-freedom parallel platform mechanism based on Grassmann line geometry", *The International Journal of Robotics Research*, Vol. 20, No. 4, pp. 312–326.

Merlet, J-P., 1988, "Parallel manipulator, Part 2: Singular configurations and Grassmann geometry", INRIA Research Report No. 791.

Merlet, J-P., 1989, "Singular configurations of parallel manipulators and Grassmann geometry", *International Journal of Robotics Research*, Vol. 8, No. 5, pp. 45–56.

Merlet, J-P., and Gosselin, C. M., 1991, "Nouvelle architecture pour un manipulateur parallèle à 6 degrés de liberté", *Mechanism and Machine Theory*, Vol. 2, No. 26, pp. 77–90.

Merlet, J-P., 1992a, "Direct kinematics and assembly modes of parallel manipulators", *International Journal of Robotics Research*, Vol. 11, No. 2, pp. 150–162.

Merlet, J-P., 1992b, "On the infinitesimal motion of a parallel manipulator in singular configurations", *Proceedings of the 1992 IEEE International Conference on Robotics and Automation*, Nice, France, pp. 320–325.

Merlet, J-P., 1994, "Détermination de l'espace de travail d'un robot parallèle pour une orientation constante," *Mechanism and Machine Theory*, Vol. 29, No. 8, pp. 1099–1113.

Mouly, N., Merlet, J-P., "Singular configurations and direct kinematics of a new parallel manipulator", *Proceedings of the 1992 IEEE International Conference on Robotics and Automation*, Nice, France, pp. 338-343

Nanua, P., Waldron, K. J., and Murthy, V., 1990, "Direct kinematic solution of a Stewart platform", *IEEE Transaction on Robotics and Automation*, Vol. 6, No. 4, pp. 438–444.

Notash, L., 1998, "Uncertainty configurations of parallel manipulators" *Mechanism and Machine Theory*, Vol. 33, No. 1/2, pp. 123-138.

Oldham, K., and Walker, M. J., 1978, "A procedure for force-balancing planar linkages using counterweights", *Journal of Mechanical Engineering Science*, Vol. 20, No. 4, pp. 177–182.

Papadopoulos, E., and Dubowsky, S., 1991, "Coordinated manipulator/spacecraft motion control for space robotic systems", *Proceedings of the 1991 IEEE International Conference on Robotics and Automation*, Sacramento CA, pp. 1696–1701.

Papadopoulos, E., and Abu-Abed, A., 1996, "On the design of zero reaction manipulators", *ASME Journal of Mechanical Design*, Vol. 118, No. 3, pp. 372–376.

Reinholtz, C. F., and Gokhale, D., 1987, "Design and analysis of variable geometry truss robots", *Proceedings of the 9th Applied Mechanisms Conference*, New Orleans, USA.

Ricard, R., and Gosselin, C. M., 2000, "On the development of reactionless parallel manipulators", *Proceedings of the ASME 2000 Design Engineering Technical Conference*, Baltimore, MA, September 10–13.

Salerno, R. J., Reinholtz, C. F., 1994, "A modular, long-reach, truss-type manipulator for waste storage tank remediation", *Proceedings of the 1994 ASME Design Technical Conference*, DE-Vol. 72, Minneapolis, USA.

Sefrioui, J., and Gosselin, C. M., 1995, "On the quadratic nature of the singularity curves of planar three-degree-of-freedom parallel manipulators", *Mechanism and Machine Theory*, Vol. 30, No. 4, pp. 533–551.

Siciliano, B., 1999, "The tricept robot: inverse kinematics, manipulability analysis and closed-loop direct kinematics algorithm", *Robotica*, Vol. 17, pp. 437–445.

Smith, M. R., 1975, "Optimal balancing of planar multi-bar linkages", *Proceedings of the 5th World Congress on the Theory of Machines and Mechanisms*, New-Castle-Upon-Tyne, pp. 142–149.

Stevensen, E. N. Jr., 1973, "Balancing of machines", *ASME Journal of Engineering for Industry*, Vol. 95, No. 2, pp. 650–656.

Stewart, D., 1965-1966, "A platform with six degrees of freedom", *Proceedings of the IMechE*, Vol. 180, Pt. 1, No. 15, pp. 371–385.

Shin, E., and Streit, D. A., 1991, "Spring equilibrator theory for static balancing of planar pantograph linkages" *Mechanism and Machine Theory*, Vol. 26, No. 7, pp. 645–657.

Tepper, F. R., and Lowen, G. G., 1972, "General theorems concerning full force balancing of planar linkages by internal mass redistribution", *ASME Journal of Engineering for Industry*, Vol. 94B, No. 3, pp. 789–796.

Tricamo, S. J., and Lowen, G. G., 1981, "A new concept for force balancing machines for planar linkages. Part 2: Application to four-bar linkages experiment", *ASME Journal of Mechanical Design*, Vol. 103, No. 4, pp. 784–792.

Tsai, L. W., 1999, *Robot analysis: the mechanics of serial and parallel manipulators*, New York, John Wiley & Sons.

Tsai, L. W., and Joshi, S., (2000), "Kinematics and optimization of a spatial 3-UPU parallel manipulator", *ASME Journal of Mechanical Design*, Vol. 122, No. 4, pp. 439–446.

Vollmer, F., Gosselin, C. M., 2000, "Analysis and design of reactionless 3-DOF parallel mechanisms", *Technical Report*, Université Laval, Quebec, Canada.

Waler, M. J., and Oldhan, K., 1978, "General theory of force balancing using counterweights", *Mechanism and Machine Theory*, Vol. 13, pp. 175–185.

Waler, M. J., and Oldhan, K., 1979, "Extensions to the theory of balancing forces in planar linkages", *Mechanism and Machine Theory*, Vol. 14, No. 3, pp. 201–207.

Wang, J., 1998, "Kinematic analysis, dynamic analysis and static balancing of planar and spatial parallel mechanisms or manipulators with revolute actuators", *Ph.D thesis*, Université Laval, Québec, Canada.

Weisstein, E. W., 2002, "Bohemian Dome," *Eric Weisstein's World of Mathematics*, (**http://mathworld.wolfram.com/BohemianDome.html**).

Wu, Y., and Gosselin, C. M., 2002b, "Kinematic Analysis of Spatial 3-DOF Parallelepiped Mechanisms" *Advances in Robot Kinematics*, J. Lenarčič and F. Thomas (eds.), Kluwer Academic Publishers, The Netherlands, pp. 423–432.

Wu, Y., and Gosselin, C. M., 2002c, "On the synthesis of reactionless spatial 3-DOF mechanisms using planar four-bar linkages", *Proceedings of the ASME 2002 Design Engineering Technical Conference*, Montreal, Canada, September 30–October 2.

Wu, Y., and Gosselin, C. M., 2002d, "On the synthesis of a reactionless 6-DOF parallel mechanism using planar four-bar linkages", *Proceedings of the Workshop on Fundamental Issues and Future Research Directions for Parallel Mechanism and Manipulators*, Quebec, Canada, October 3–4.

Wu, Y., and Gosselin, C. M., 2003, "Singularity analysis of a reactionless 6-DOF parallel mechanism", *Proceedings of the 11th World Congress in Mechanism and Machine Science*, Tianjin, China.

Wu, Y., and Gosselin, C. M., 2003b, "Synthesis of reactionless spatial 3-DOF and 6-DOF mechanisms without counter-rotations", Submitted to *International Journal of Robotics Research*.

Yang, T. L., Zhang, M., Xu, Z., 2000, "A comparative study on some different methods for complete balancing of shaking force and moment of linkages using force counterweights and inertia counterweights", *Proceedings of the ASME 2000 Design Engineering Technical Conference*, Baltimore, MA, September 10–13, DETC/MECH-14074.

Yao, J., and Smith, M. R., 1993, "An improved complex mass method for force balancing of planar linkages", *Mechanism and Machine Theory*, Vol. 29, No. 5, pp. 701–712.

Ye, Z., and Smith, M. R., 1994, "Complete balancing of planar linkages by an equivalence method", *Mechanism and Machine Theory*, Vol. 29, No. 5, pp. 701–712.

Yu, Y. Q., 1987a, "Research on complete shaking force and shaking moment balancing of spatial linkages", *Mechanism and Machine Theory*, Vol. 22, No. 1, pp. 27–37.

Yu, Y. Q., 1987b, "Optimum shaking force and shaking moment balancing of the RSS'R spatial linkage", *Mechanism and Machine Theory*, Vol. 22, No. 1, pp. 39–45.

Yu, Y. Q., 1988, "Complete shaking force and shaking moment balancing of spatial irregular force transmission mechanisms using additional links", *Mechanism and Machine Theory*, Vol. 23, No. 4, pp. 279–285.

Zlatanov, D., Fenton, R. G., and Benhabib, B., 1994, "Singularity analysis of mechanisms and robots via a motion-space model of the instantaneous kinematics," *Proceedings of the 1994 IEEE International Conference on Robotics and Automation*, San Diego, CA, USA, May 8-13, pp. 980–985.

Zlatanov, D., Fenton, R. G., and Benhabib, B., 1995, "A unifying framework for classification and interpretation of mechanism singularities" *ASME Journal of Mechanical Design*, Vol. 117, No. 4, pp. 566–572.

Appendix A

Dynamic Balancing of a Spatial Parallel Mechanism with Multiple Legs

Figure A.1 shows a spatial multi-degree-of-freedom parallel mechanism with k legs. Assume that each leg has n links. A fixed and a moving coordinate frame and some nomenclatures are defined as in Section 4.2 and 4.3. The angular momentum of the k point masses with respect to the fixed point O and the fixed frame can be written as follows:

$$
\begin{aligned}
\mathbf{h}_{kp} &= \sum_{i=1}^{k} \mathbf{p}_i \times m_{pi} \dot{\mathbf{p}}_i \\
&= \sum_{i=1}^{k} (\mathbf{p} + \mathbf{Q}\mathbf{b}_i) \times m_{pi} (\dot{\mathbf{p}} + \dot{\mathbf{Q}}\mathbf{b}_i)
\end{aligned}
$$
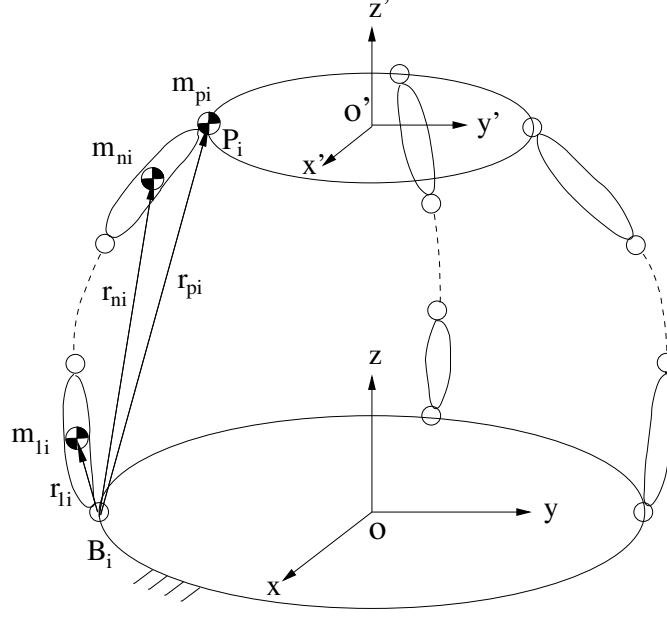
Figure A.1: A spatial parallel mechanism with multiple legs.

$$
\begin{aligned}
= \quad & \mathbf{p} \times (\sum_{i=1}^{k} m_{pi})\dot{\mathbf{p}} + \mathbf{p} \times \dot{\mathbf{Q}}(\sum_{i=1}^{k} m_{pi}\mathbf{b}_i) + \mathbf{Q}(\sum_{i=1}^{k} m_{pi}\mathbf{b}_i) \times \dot{\mathbf{p}} + \\
& \sum_{i=1}^{k} \mathbf{Q}\mathbf{b}_i \times m_{pi}(\boldsymbol{\omega} \times \mathbf{Q}\mathbf{b}_i),
\end{aligned}
\tag{A.1}
$$

where $\boldsymbol{\omega}$ is the angular velocity of the moving platform.

If the center of mass of the point masses coincides with that of the platform (i.e., O'), then $\Sigma m_{pi}\mathbf{b}_i = 0$ and eq. (A.1) becomes

$$
\mathbf{h}_{kp} \quad = \quad \mathbf{p} \times (\sum_{i=1}^{k} m_{pi})\dot{\mathbf{p}} + \sum_{i=1}^{k} \mathbf{Q}\mathbf{b}_i \times m_{pi}(\boldsymbol{\omega} \times \mathbf{Q}\mathbf{b}_i).
\tag{A.2}
$$

Moreover, the second term in eq. (A.2) stands for the angular momentum of the point masses relative to their center of mass O'. We express the angular velocity of the platform $\boldsymbol{\omega}$ and the position of the point masses relative to their center of mass O' in the fixed frame (i.e., $\mathbf{Q}\mathbf{b}_i$) as

$$
\boldsymbol{\omega} = \begin{bmatrix} \omega_x \\ \omega_y \\ \omega_z \end{bmatrix}, \quad \mathbf{Q}\mathbf{b}_i = \begin{bmatrix} x_{bi} \\ y_{bi} \\ z_{bi} \end{bmatrix},
\tag{A.3}
$$

then the angular momentum of the point masses relative to their center of mass O' can

be obtained as

$$\mathbf{h}_{o'} = \begin{bmatrix} \Sigma m_{pi}(y_{bi}^2 + z_{bi}^2)\omega_x - \Sigma m_{pi}x_{bi}y_{bi}\omega_y - \Sigma m_{pi}x_{bi}z_{bi}\omega_z \\ -\Sigma m_{pi}y_{bi}x_{bi}\omega_x + \Sigma m_{pi}(x_{bi}^2 + z_{bi}^2)\omega_y - \Sigma m_{pi}y_{bi}z_{bi}\omega_z \\ -\Sigma m_{pi}z_{bi}x_{bi}\omega_x - \Sigma m_{pi}z_{bi}y_{bi}\omega_y + \Sigma m_{pi}(x_{bi}^2 + y_{bi}^2)\omega_z \end{bmatrix}. \tag{A.4}$$

Using the definition of the moments and products of inertia (Bedford and Fowler 1996), eq. (A.4) leads to

$$\mathbf{h}_{o'} = \begin{bmatrix} I_{xx} & -I_{xy} & -I_{xz} \\ -I_{yx} & I_{yy} & -I_{yz} \\ -I_{zx} & -I_{zy} & I_{zz} \end{bmatrix} \begin{bmatrix} \omega_x \\ \omega_y \\ \omega_z \end{bmatrix} = \mathbf{I_{kp}}\boldsymbol{\omega}, \tag{A.5}$$

then

$$\mathbf{h}_{kp} = \mathbf{p} \times (\sum_{i=1}^{k} m_{pi})\dot{\mathbf{p}} + \mathbf{I_{kp}}\boldsymbol{\omega}. \tag{A.6}$$

From eq. (A.6), it is found that if the k point masses are dynamically equivalent to the platform — namely with the same mass ($m_{pl} = \Sigma m_{pi}$), the same center of mass (O') and the same inertia tensor ($\mathbf{I_{pl}} = \mathbf{I_{kp}}$) — the angular momentum of the point masses is identical to that of the platform. Therefore, by using the point masses to replace the platform, the angular momentum of the complete mechanism relative to the fixed point O and expressed in the fixed frame can be written as

$$\begin{aligned} \mathbf{h}_o &= \sum_{i=1}^{k}(\mathbf{h}_{g1i} + (\mathbf{r}_{1i} + \mathbf{a}_i) \times m_{1i}\dot{\mathbf{r}}_{1i} + \ldots + \mathbf{h}_{gni} + (\mathbf{r}_{ni} + \mathbf{a}_i) \times m_{ni}\dot{\mathbf{r}}_{ni} + \\ &\quad (\mathbf{r}_{pi} + \mathbf{a}_i) \times m_{pi}\dot{\mathbf{r}}_{pi}) \\ &= \sum_{i=1}^{k}(\mathbf{h}_{g1i} + \mathbf{r}_{1i} \times m_{1i}\dot{\mathbf{r}}_{1i} + \ldots + \mathbf{h}_{gni} + \mathbf{r}_{ni} \times m_{ni}\dot{\mathbf{r}}_{ni} + \mathbf{r}_{pi} \times m_{pi}\dot{\mathbf{r}}_{pi}) + \\ &\quad \sum_{i=1}^{k}\mathbf{a}_i \times (m_{1i}\dot{\mathbf{r}}_{1i} + \ldots + m_{ni}\dot{\mathbf{r}}_{ni} + m_{pi}\dot{\mathbf{r}}_{pi}), \end{aligned} \tag{A.7}$$

where $\mathbf{h}_{gji}, j = 1 \ldots n$ is the angular momentum of the corresponding link relative to its center of mass. If each leg mechanism including the point mass is dynamically balanced, then the center of mass of the leg is fixed and the angular momentum of the leg with respect to the fixed point B_i is zero, namely, the sums in both parentheses in eq. (A.7) are zero respectively. Hence, $\mathbf{h}_o = 0$ and the global center of mass of the complete mechanism is fixed, i.e., the whole system is reactionless. Furthermore, from eq. (A.7) the same conclusion can be obtained even if the leg mechanisms of the system are not identical, namely with different number of links.

Appendix B

Determination of the Dependent Variables in Planar Four-bar Linkages

The kinematic constraint equations can be written from Figure 5.1 as

$$l_1\cos\theta_1 + l_2\cos\theta_2 = d + l_3\cos\theta_3 \tag{B.1}$$

$$l_1\sin\theta_1 + l_2\sin\theta_2 = l_3\sin\theta_3 \tag{B.2}$$

Differentiating eqs. $(B.1)$ and $(B.2)$ with respect to time, $\dot\theta_2$ and $\dot\theta_3$ can be found as:

$$\dot\theta_2 = \frac{l_1\sin(\theta_1-\theta_3)}{l_2\sin(\theta_3-\theta_2)}\dot\theta_1 \tag{B.3}$$

$$\dot\theta_3 = \frac{l_1\sin(\theta_1-\theta_2)}{l_3\sin(\theta_3-\theta_2)}\dot\theta_1 \tag{B.4}$$

Also, from eqs. $(B.1)$ and $(B.2)$, $\cos\theta_3$ and $\sin\theta_3$ can be written as

$$\cos\theta_3 = (l_1\cos\theta_1 + l_2\cos\theta_2 - d)/l_3 \qquad (B.5)$$

$$\sin\theta_3 = (l_1\sin\theta_1 + l_2\sin\theta_2)/l_3 \qquad (B.6)$$

Substituting eqs. (B.5) and (B.6) into the trigonometric identity $\cos\theta_i^2 + \sin\theta_i^2 = 1$, one has

$$\sin\theta_2 = \frac{(d - l_1\cos\theta_1)l_2\cos\theta_2 - H}{l_1 l_2 \sin\theta_1} \qquad (B.7)$$

and

$$\cos\theta_2 = \frac{-A_1 + Y_1}{2A_2} \qquad (B.8)$$

with

$$Y_1 = \epsilon\sqrt{A_1^2 - 4A_2 A_0} = \epsilon\Delta$$

$$H = \frac{1}{2}(l_1^2 + l_2^2 - l_3^2 + d^2) - dl_1\cos\theta_1$$

$$A_0 = H^2 - l_1^2 l_2^2 \sin^2\theta_1$$

$$A_1 = -2l_2 H(d - l_1\cos\theta_1)$$

$$A_2 = l_1^2 l_2^2 + d^2 l_2^2 - 2dl_1\cos\theta_1$$

$$\epsilon = \pm 1$$

Then, θ_2, θ_3 and their derivatives can be obtained using the above formulae for given θ_1 and $\dot{\theta}_1$.

Appendix C

Coefficients B_i and A_i of the Polynomials in $\cos\theta_1$ in eqs. (5.32) and (5.33)

C.1 Coefficients B_i in $\cos\theta_1$ in eq. (5.32)

$$
\begin{aligned}
B_0 = & \; (-I_{yy3}m_3l_2^6d^2 - I_{yy3}m_3l_2^2d^6 - m_2^2l_3^2r_2^2d^6 - m_2^2l_3^6r_2^2d^2 + I_{xx2}m_3l_3^2d^6 + I_{xx2}m_3l_3^6d^2 + \\
& I_{xx3}m_3l_2^2d^6 + I_{xx3}m_3l_2^6d^2 - I_{yy2}m_3l_3^2d^6 - I_{yy2}m_3l_3^6d^2 + 2I_{yy3}m_3l_2^4d^4 + 2m_2^2l_3^4r_2^2d^4 + \\
& 4m_2^2l_3^4r_2^2l_1^4 - 2I_{xx2}m_3l_3^4d^4 - 2I_{xx3}m_3l_2^4d^4 + 2I_{yy2}m_3l_3^4d^4 - m_2r_2^2m_3l_3^2d^2l_2^4 - \\
& m_2r_2^2m_3l_3^6d^2 - I_{yy3}m_3l_2^2\epsilon^2\Delta^2d^6 - I_{yy3}m_3l_2^2d^2l_3^4 - I_{yy3}m_3l_2^2d^2l_1^4 - \\
& m_2r_2^2m_3l_3^2d^2l_1^4 - m_2r_2^2m_3l_3^2\epsilon^2\Delta^2d^6 - m_2r_2^2m_3l_3^2d^6 - m_2^2l_3^2r_2^2\epsilon^2\Delta^2d^6 - \\
& m_2^2l_3^2r_2^2d^2l_2^4 - m_2^2l_3^2r_2^2d^2l_1^4 + I_{xx2}m_3l_3^2d^2l_2^4 + I_{xx2}m_3l_3^2d^2l_1^4 + I_{xx2}m_3l_3^2\epsilon^2\Delta^2d^6 -
\end{aligned}
$$

$$I_{yy2}m_3l_3^2d^2l_2^4 + I_{xx3}m_3l_2^2d^2l_1^4 + I_{xx3}m_3l_2^2d^2l_3^4 + I_{xx3}m_3l_2^2\epsilon^2\Delta^2d^6 - I_{yy2}m_3l_3^2d^2l_1^4 -$$
$$I_{yy2}m_3l_3^2\epsilon^2\Delta^2d^6 + 4m_2r_2l_2m_3l_3^4l_1^2d^2 - 4m_2r_2l_2m_3l_3^2l_1^6 - 4m_2r_2l_2^3m_3l_3^2l_1^4 -$$
$$2m_2r_2^2m_3l_3^2d^4l_2^2\epsilon + 2m_2r_2^2m_3l_3^4d^4\epsilon\Delta + 2m_2r_2^2m_3l_3^4d^4 + 2m_2r_2^2m_3l_3^2d^4l_2^2 +$$
$$2m_2r_2^2m_3l_3^4l_1^2d^2 - 8m_2r_2l_2m_3l_3^2d^2l_1^4 + 4m_2r_2l_2m_3l_3^2\epsilon\Delta d^6 - 4m_2r_2l_2^3m_3l_3^2l_1^2d^2 +$$
$$4m_2r_2l_2m_3l_3^2\epsilon\Delta d^4l_1^2 - 4m_2r_2l_2m_3l_3^2d^4l_1^2 + 4m_2r_2l_2m_3l_3^4l_1^4 + 2I_{yy3}m_3l_2^4l_1^2d^2 +$$
$$2I_{yy3}m_3l_2^4d^2l_3^2 + 2I_{yy3}m_3l_2^2d^4l_3^2 + 6I_{yy3}m_3l_2^2l_1^2l_3^2d^2 - 2I_{yy3}m_3l_2^2d^4l_1^2 +$$
$$2I_{yy3}m_3l_2^2\epsilon\Delta d^6 - 2I_{yy3}m_3l_2^4d^4\epsilon\Delta + 2I_{yy3}m_3l_2^2d^4l_3^2\epsilon\Delta + 2I_{yy3}m_3l_2^2\epsilon\Delta d^4l_1^2 -$$
$$2m_2r_2^2m_3l_3^2\epsilon\Delta d^6 + 6m_2r_2^2m_3l_3^2l_1^2l_2^2d^2 - 2m_2r_2^2m_3l_3^2d^4l_1^2 + 2m_2r_2^2m_3l_3^2d^2l_2^2 +$$
$$4I_{yy1}m_3l_2^2l_3^2l_1^4 + 8I_{yy1}m_3l_2^2l_3^2d^2l_1^2 + 4I_{yy1}m_3l_2^2l_3^2d^4 - 2m_2r_2^2m_3l_3^2\epsilon\Delta d^4l_1^2 +$$
$$4m_2r_2^2m_3l_2^2l_3^2l_1^4 + 4m_2l_1^6m_3l_2^2l_3^2 + 8m_2l_1^4m_3l_2^2l_3^2d^2 + 4m_2l_1^2m_3l_2^2l_3^2d^4 +$$
$$4I_{yy3}m_3l_2^2l_3^2l_1^4 + 4I_{yy2}m_3l_2^2l_3^2l_1^4 + 6I_{yy2}m_3l_2^2l_3^2d^2l_1^2 + 2I_{yy2}m_3l_2^2l_3^2d^4 +$$
$$2m_2^2l_3^2r_2^2\epsilon\Delta d^6 + 2m_2^2l_3^2r_2^2l_1^2l_2^2d^2 + 2m_2^2l_3^4r_2^2d^2l_2^2 + 2m_2^2l_3^4r_2^2d^4\epsilon\Delta +$$
$$2m_2^2l_3^2r_2^2d^4l_2^2 + 6m_2^2l_3^4r_2^2l_1^2d^2 - 2m_2^2l_3^2r_2^2d^4l_1^2 - 2m_2^2l_3^2r_2^2d^4l_2^2\epsilon\Delta +$$
$$2m_2^2l_3^2r_2^2\epsilon\Delta d^4l_1^2 + 2I_{xx2}m_3l_3^2d^4l_2^2\epsilon\Delta - 2I_{xx2}m_3l_3^4d^4\epsilon\Delta +$$
$$2I_{xx2}m_3l_3^2d^4l_2^2 - 2I_{xx2}m_3l_3^4l_1^2d^2 + 2I_{xx2}m_3l_3^2d^4l_1^2 + 2I_{xx2}m_3l_3^2\epsilon\Delta d^6 +$$
$$2I_{xx2}m_3l_3^2l_1^2l_2^2d^2 - 2I_{xx2}m_3l_3^4d^2l_2^2 + 4m_1r_1^2m_3l_2^2l_3^2d^4 - 2I_{yy2}m_3l_3^2d^4l_2^2\epsilon\Delta +$$
$$4m_1r_1^2m_3l_2^2l_3^2l_1^4 + 8m_1r_1^2m_3l_2^2l_3^2d^2l_1^2 + 2I_{yy2}m_3l_3^4d^4\epsilon\Delta + 2I_{yy2}m_3l_3^4l_1^2d^2 -$$
$$2I_{yy2}m_3l_3^2\epsilon\Delta d^4l_1^2 - 2I_{xx3}m_3l_2^2\epsilon\Delta d^6 - 2I_{xx3}m_3l_2^4l_1^2d^2 - 2I_{xx3}m_3l_2^4d^2l_3^2 -$$
$$2I_{xx3}m_3l_2^2\epsilon\Delta d^4l_1^2 + 2I_{xx3}m_3l_2^4d^4\epsilon\Delta - 2I_{xx3}m_3l_2^2d^4l_3^2\epsilon\Delta + 2I_{xx3}m_3l_2^2d^4l_3^2 +$$
$$2I_{xx3}m_3l_2^2l_1^2l_3^2d^2 + 2I_{xx3}m_3l_2^2d^4l_1^2 - 2I_{yy2}m_3l_3^2d^4l_1^2 - 2I_{yy2}m_3l_3^2\epsilon\Delta d^6 +$$
$$2I_{yy2}m_3l_3^4d^2l_2^2 + 2I_{xx2}m_3l_3^2\epsilon\Delta d^4l_1^2)/(4l_3^2m_3l_2^2)$$

$$B_1 = -l_1d(-m_2^2l_3^2r_2^2l_1^4 + 8I_{yy1}m_3l_2^2l_3^2l_1^2 + I_{xx2}m_3l_3^2l_2^2\epsilon\Delta d^2 - 2I_{xx2}m_3l_3^4l_2^2 -$$
$$m_2r_2^2m_3l_3^2l_2^2\epsilon\Delta d^2 - 4m_2r_2^2m_3l_3^2d^2l_1^2 - m_2r_2^2m_3l_3^2l_1^4 + 8I_{yy1}m_3l_2^2l_3^2d^2 +$$
$$2m_2^2l_3^4r_2^2l_2^2 - 4m_2^2l_3^2r_2^2d^2l_1^2 - 3m_2^2l_3^2r_2^2d^4 - 3m_2r_2^2m_3l_3^2d^4 + 2m_2r_2l_2m_3l_3^2l_1^2\epsilon\Delta d^2 +$$
$$4I_{yy2}m_3l_2^2l_3^2d^2 + 6I_{yy2}m_3l_2^2l_3^2l_1^2 + 6m_2r_2l_2m_3l_3^2\epsilon\Delta d^4 + 2I_{yy3}m_3l_2^4l_1^2 +$$
$$2m_2r_2^2m_3l_3^4l_1^2 - 3m_2r_2^2m_3l_3^2\epsilon\Delta d^4 - 3I_{yy2}m_3l_3^2\epsilon\Delta d^4 + m_2^2l_3^4r_2^2\epsilon\Delta d^2 - I_{yy2}m_3l_3^2l_2^4 -$$
$$I_{xx3}m_3l_2^2l_1^2\epsilon\Delta d^2 + 4I_{xx3}m_3l_2^2d^2l_1^2 + I_{xx3}m_3l_2^2l_1^4 + 2I_{yy2}m_3l_3^4l_1^2 - I_{yy2}m_3l_3^2l_1^4 +$$
$$3I_{xx2}m_3l_3^2d^4 + 8m_2l_1^2m_3l_2^2l_3^2d^2 + 6m_2r_2^2m_3l_3^2l_1^2l_2^2 + I_{xx2}m_3l_3^6 + 4I_{xx2}m_3l_3^2d^2l_1^2 +$$
$$I_{xx2}m_3l_3^2l_1^4 + 8m_2l_1^4m_3l_2^2l_3^2 + 4I_{xx2}m_3l_3^2d^2l_2^2 + I_{xx2}m_3l_3^2l_2^2 - I_{xx2}m_3l_3^2\epsilon\Delta d^2 -$$
$$m_2^2l_3^6r_2^2 + 4m_2^2l_3^2r_2^2d^2l_2^2 - m_2^2l_3^2r_2^2l_2^2\epsilon\Delta d^2 + 4m_2^2l_3^2r_2^2d^2 + 4I_{xx3}m_3l_2^2d^2l_3^2 +$$
$$4m_2r_2l_2m_3l_3^4l_1^2 - 4I_{yy2}m_3l_3^2d^2l_1^2 - I_{yy3}m_3l_3^4\epsilon\Delta d^2 + I_{xx3}m_3l_2^6 - m_2^2l_3^2r_2^2l_2^4 +$$
$$6m_2^2l_3^4r_2^2l_1^2 - 4I_{xx3}m_3l_2^4d^2 + 6I_{yy3}m_3l_2^2l_1^2l_3^2 + 4m_2r_2^2m_3l_3^2d^2l_2^2 + 2m_2r_2^2m_3l_3^4l_2^2 +$$
$$3I_{yy3}m_3l_2^2\epsilon\Delta d^4 + I_{yy3}m_3l_2^2l_1^2\epsilon\Delta d^2 + 2I_{yy3}m_3l_2^4l_3^2 + 3m_2^2l_3^2r_2^2\epsilon\Delta d^4 +$$
$$m_2^2l_3^2r_2^2l_1^2\epsilon\Delta d^2 - 4I_{yy3}m_3l_2^2d^2l_1^2 - I_{yy3}m_3l_2^2l_1^4 - 3I_{yy3}m_3l_2^2d^4 - I_{yy3}m_3l_2^2l_3^4 +$$
$$4I_{yy3}m_3l_2^4d^2 + I_{yy3}m_3l_2^2l_3^2\epsilon\Delta d^2 + 4I_{yy3}m_3l_2^2d^2l_3^2 + I_{yy2}m_3l_3^4\epsilon\Delta d^2 + 4m_2r_2^2m_3l_3^4d^2 +$$
$$m_2r_2^2m_3l_3^4\epsilon\Delta d^2 - m_2r_2^2m_3l_3^2l_1^2\epsilon\Delta d^2 - I_{yy3}m_3l_3^6 - I_{yy2}m_3l_3^6 + 3I_{xx3}m_3l_2^2d^4 +$$
$$I_{xx2}m_3l_3^2l_1^2\epsilon\Delta d^2 + 4I_{yy2}m_3l_3^4d^2 - I_{yy2}m_3l_3^2l_2^2\epsilon\Delta d^2 + 8m_1r_1^2m_3l_2^2l_3^2d^2 +$$
$$8m_1r_1^2m_3l_2^2l_3^2l_1^2 + 2I_{yy2}m_3l_3^4l_2^2 - I_{yy2}m_3l_3^2l_1^2\epsilon\Delta d^2 - 4I_{xx2}m_3l_3^4d^2 + 2I_{xx2}m_3l_3^2l_1^2l_2^2 -$$
$$4m_2r_2l_2^3m_3l_3^2l_1^2 - 2I_{xx2}m_3l_3^4l_1^2 + 2I_{xx3}m_3l_2^2l_1^2l_3^2 - 3I_{yy2}m_3l_3^2d^4 + I_{xx3}m_3l_2^2l_3^4 -$$

$$m_2 r_2^2 m_3 l_3^6 + 2m_2^2 l_3^2 r_2^2 l_1^2 l_2^2 - I_{xx3} m_3 l_2^2 l_3^2 \epsilon \Delta d^2 - 2I_{xx3} m_3 l_2^4 l_3^2 + 3I_{xx2} m_3 l_3^2 \epsilon \Delta d^4 -$$
$$3I_{xx3} m_3 l_2^2 \epsilon \Delta d^4 - m_2 r_2^2 m_3 l_2^2 l_3^4 + I_{xx3} m_3 l_2^6 \epsilon \Delta d^2 - 8m_2 r_2 l_2 m_3 l_3^2 d^2 l_1^2 -$$
$$8m_2 r_2 l_2 m_3 l_3^2 l_1^4 - 2I_{xx3} m_3 l_2^4 l_1^2)/(2l_3^2 m_3 l_2^2)$$

$$B_2 = -(-2I_{yy2} m_3 l_3^4 l_1^2 l_2^2 + m_2^2 l_2^6 r_2^2 l_1^2 + I_{yy3} m_3 l_2^2 l_1^6 + I_{yy2} m_3 l_3^2 l_1^6 + I_{yy2} m_3 l_3^6 l_1^2 +$$
$$m_2^2 l_2^2 l_3^2 r_2^2 l_1^6 - I_{xx2} m_3 l_3^6 l_1^2 + I_{yy3} m_3 l_2^6 l_1^2 - I_{xx2} m_3 l_3^2 l_1^6 - I_{xx3} m_3 l_2^2 l_1^6 -$$
$$I_{xx3} m_3 l_2^6 l_1^2 + 2m_2^2 l_3^4 r_2^2 l_1^4 - 2I_{yy3} m_3 l_2^4 l_1^4 + 2I_{xx3} m_3 l_2^4 l_1^4 + 2I_{xx2} m_3 l_3^4 l_1^4 -$$
$$2I_{yy2} m_3 l_3^4 l_1^4 + 10I_{yy3} m_3 l_2^2 d^2 l_1^4 + 10m_2 r_2^2 m_3 l_3^2 d^2 l_1^4 + 10m_2^2 l_3^2 r_2^2 d^2 l_1^4 -$$
$$10I_{xx2} m_3 l_3^2 d^2 l_1^4 - 10I_{xx3} m_3 l_2^2 d^2 l_1^4 + 10I_{yy2} m_3 l_3^2 d^2 l_1^4 + m_2^2 l_3^2 r_2^2 l_1^2 l_2^4 +$$
$$I_{yy3} m_3 l_2^2 l_1^2 l_2^4 + I_{yy2} m_3 l_3^2 l_1^2 l_2^4 + m_2 r_2^2 m_3 l_3^2 l_1^6 + m_2 r_2^2 m_3 l_3^6 l_1^2 +$$
$$m_2 r_2^2 m_3 l_3^2 l_1^2 l_2^4 - I_{xx2} m_3 l_3^2 l_1^2 l_2^4 - I_{xx3} m_3 l_2^2 l_1^2 l_2^4 + 4m_2 r_2 l_2 m_3 l_2^4 l_1^2 d^2 -$$
$$4m_2 r_2 l_2 m_3 l_3^2 l_1^6 - 4m_2 r_2 l_2^3 m_3 l_3^2 l_1^4 - 10m_2 r_2^2 m_3 l_3^4 l_1^2 d^2 + 8m_2 r_2 l_2 m_3 l_3^2 d^2 l_1^4 -$$
$$4m_2 r_2 l_2^3 m_3 l_3^2 l_1^2 d^2 - 8m_2 r_2 l_2 m_3 l_3^2 \epsilon \Delta d^4 l_1^2 - 4m_2 r_2 l_2 m_3 l_3^2 d^4 l_1^2 + 4m_2 r_2 l_2 m_3 l_3^2 l_1^4 -$$
$$10I_{yy3} m_3 l_2^4 l_1^2 d^2 - 6I_{yy3} m_3 l_2^2 l_1^2 l_3^2 d^2 + 13I_{yy3} m_3 l_2^2 d^4 l_1^2 - 4I_{yy3} m_3 l_2^2 \epsilon \Delta d^4 l_1^2 -$$
$$6m_2 r_2^2 m_3 l_3^2 l_1^2 l_2^2 d^2 + 13m_2 r_2^2 m_3 l_3^2 d^4 l_1^2 + 4I_{yy1} m_3 l_2^2 l_3^2 l_1^4 - 8I_{yy1} m_3 l_2^2 l_3^2 d^2 l_1^2 +$$
$$4I_{yy1} m_3 l_2^2 l_3^2 d^4 + 4m_2 r_2^2 m_3 l_3^2 \epsilon \Delta d^4 l_1^2 + 2m_2 r_2^2 m_3 l_2^2 l_3^2 l_1^4 + 4m_2 l_1^6 m_3 l_2^2 l_3^2 -$$
$$8m_2 l_1^4 m_3 l_2^2 l_3^2 d^2 + 4m_2 l_1^2 m_3 l_2^2 l_3^2 d^4 + 2I_{yy3} m_3 l_2^2 l_3^2 l_1^4 + 2I_{yy2} m_3 l_2^2 l_3^2 l_1^4 -$$
$$6I_{yy2} m_3 l_2^2 l_3^2 d^2 l_1^2 - 10m_2^2 l_3^2 r_2^2 l_1^2 l_2^2 d^2 - 6m_2^2 l_3^4 r_2^2 l_1^2 d^2 + 13m_2^2 l_3^2 r_2^2 d^4 l_1^2 -$$
$$4m_2^2 l_3^2 r_2^2 \epsilon \Delta d^4 l_1^2 + 10I_{xx2} m_3 l_3^4 l_1^2 d^2 - 13I_{xx2} m_3 l_3^2 d^4 l_1^2 - 10I_{xx2} m_3 l_3^2 l_1^2 l_2^2 d^2 +$$
$$4m_1 r_1^2 m_3 l_2^2 l_3^2 l_1^4 - 8m_1 r_1^2 m_3 l_2^2 l_3^2 d^2 l_1^2 + 4m_1 r_1^2 m_3 l_2^2 l_3^2 d^4 - 10I_{yy2} m_3 l_3^4 l_1^2 d^2 +$$
$$4I_{yy2} m_3 l_3^2 \epsilon \Delta d^4 l_1^2 + 10I_{xx3} m_3 l_2^4 l_1^2 d^2 + 4I_{xx3} m_3 l_2^2 \epsilon \Delta d^4 l_1^2 - 10I_{xx3} m_3 l_2^2 l_1^2 l_3^2 d^2 -$$
$$13I_{xx3} m_3 l_2^2 d^4 l_1^2 + 13I_{yy2} m_3 l_3^2 d^4 l_1^2 - 4I_{xx2} m_3 l_3^2 \epsilon \Delta d^4 l_1^2 - 2m_2 r_2^2 m_3 l_3^4 l_1^4 -$$
$$4I_{xx1} m_3 l_2^2 l_3^2 l_1^4 + 2I_{xx3} m_3 l_2^4 l_1^2 l_3^2 - 8I_{xx1} m_3 l_2^2 l_3^2 d^2 l_1^2 - 2I_{xx2} m_3 l_3^4 l_1^4 l_2^2 -$$
$$2m_2^2 l_3^4 r_2^2 l_1^2 l_2^2 + 2I_{xx2} m_3 l_3^4 l_1^2 l_2^2 - 4I_{xx1} m_3 l_2^2 l_3^2 d^4 - 2m_2^2 l_3^2 r_2^2 l_1^4 l_2^2 -$$
$$2I_{yy3} m_3 l_2^4 l_1^2 l_3^2 - 2m_2 r_2^2 m_3 l_3^4 l_1^2 l_2^2 - 2I_{xx3} m_3 l_2^2 l_1^4 l_2^2)/(4l_3^2 m_3 l_2^2)$$

$$B_3 = l_1 d(m_2^2 l_3^2 r_2^2 l_1^4 + 4I_{yy1} m_3 l_2^2 l_3^2 l_1^2 + 3m_2 r_2^2 m_3 l_3^2 d^2 l_1^2 + m_2 r_2^2 m_3 l_3^2 l_1^4 +$$
$$4I_{yy1} m_3 l_2^2 l_3^2 d^2 + 3m_2^2 l_3^2 r_2^2 d^2 l_1^2 + I_{yy2} m_3 l_2^2 l_3^2 l_1^2 - I_{yy3} m_3 l_2^4 l_1^2 -$$
$$m_2 r_2^2 m_3 l_3^4 l_1^2 - 3I_{xx3} m_3 l_2^2 d^2 l_1^2 - I_{xx3} m_3 l_2^2 l_1^4 - I_{yy2} m_3 l_3^4 l_1^2 +$$
$$I_{yy2} m_3 l_3^2 l_1^4 + 4m_2 l_1^2 m_3 l_2^2 l_3^2 d^2 + m_2 r_2^2 m_3 l_3^2 l_1^2 l_2^2 - 3I_{xx2} m_3 l_3^2 d^2 l_1^2 -$$
$$I_{xx2} m_3 l_3^4 l_1^4 + 4m_2 l_1^4 m_3 l_2^2 l_3^2 + 2m_2 r_2 l_2 m_3 l_3^4 l_1^2 + 3I_{yy2} m_3 l_3^2 d^2 l_1^2 +$$
$$m_2^2 l_3^4 r_2^2 l_1^2 + I_{yy3} m_3 l_2^2 l_1^2 l_3^2 + 3I_{yy3} m_3 l_2^2 d^2 l_1^2 + I_{yy3} m_3 l_2^2 l_1^4 +$$
$$4m_1 r_1^2 m_3 l_2^2 l_3^2 d^2 + 4m_1 r_1^2 m_3 l_2^2 l_3^2 l_1^2 - I_{xx2} m_3 l_3^2 l_1^2 l_2^2 - 2m_2 r_2 l_2^3 m_3 l_3^2 l_1^2 +$$
$$I_{xx2} m_3 l_3^4 l_1^2 - I_{xx3} m_3 l_2^2 l_1^2 l_3^2 - m_2^2 l_3^2 r_2^2 l_1^2 l_2^2 - 4m_2 r_2 l_2 m_3 l_3^2 d^2 l_1^2 -$$
$$4m_2 r_2 l_2 m_3 l_3^2 l_1^4 + I_{xx3} m_3 l_2^4 l_1^2 - 4I_{xx1} m_3 l_2^2 l_3^2 d^2 - 4I_{xx1} m_3 l_2^2 l_3^2 l_1^2)/(l_3^2 m_3 l_2^2)$$

$$B_4 = -l_1^2 d^2 (4m_1 r_1^2 m_3 l_2^2 l_3^2 + 4I_{yy1} m_3 l_2^2 l_3^2 + 4m_2 l_1^2 m_3 l_2^2 l_3^2 - 4m_2 r_2 l_2 m_3 l_3^2 l_1^2 +$$
$$m_2 r_2^2 m_3 l_3^2 l_1^2 + m_2^2 l_3^2 r_2^2 l_1^2 + I_{yy3} m_3 l_2^2 l_1^2 - 4I_{xx1} m_3 l_2^2 l_3^2 + I_{yy2} m_3 l_3^2 l_1^2 -$$
$$I_{xx3} m_3 l_2^2 l_1^2 - I_{xx2} m_3 l_3^2 l_1^2)/(l_3^2 m_3 l_2^2)$$

C.2 Coefficients A_i of the Polynomials in $\cos\theta_1$ in eq. (5.33)

$$
\begin{aligned}
A_0 \;=\; & (l_1^4 m_2^2 l_3^6 r_2^2 + l_1^4 I_{yy2} m_3 l_3^6 - l_1^4 I_{xx2} m_3 l_3^6 + l_1^4 I_{yy3} m_3 l_2^6 - l_1^4 I_{xx3} m_3 l_2^6 + \\
& 4d^6 I_{xx3} m_3 l_2^2 l_3^2 \epsilon \Delta - 2d^4 I_{yy2} m_3 l_3^4 l_2^2 + 2l_1^4 I_{xx3} m_3 l_2^4 l_3^2 - 2l_1^4 m_2^2 l_3^4 r_2^2 l_2^2 + \\
& 2l_1^4 I_{xx2} m_3 l_3^4 l_2^2 - 2l_1^4 I_{yy3} m_3 l_2^4 l_3^2 - 2l_1^4 m_2 r_2^2 m_3 l_3^4 l_2^2 - 2l_1^4 I_{yy2} m_3 l_3^4 l_2^2 + \\
& l_1^4 m_2^2 l_3^2 r_2^2 l_2^4 + l_1^4 I_{yy3} m_3 l_2^2 l_3^4 + l_1^4 I_{yy2} m_3 l_3^2 l_2^4 + l_1^4 m_2 r_2^2 m_3 l_3^6 + \\
& l_1^4 m_2 r_2^2 m_3 l_3^2 l_2^4 - l_1^4 I_{xx2} m_3 l_3^2 l_2^4 - l_1^4 I_{xx3} m_3 l_2^2 l_3^4 - 2l_1^2 d^2 m_2^2 l_3^2 r_2^2 l_2^4 - \\
& 2l_1^2 d^2 I_{yy3} m_3 l_2^2 l_3^4 - 2l_1^2 d^2 I_{yy2} m_3 l_3^2 l_2^4 - 2l_1^2 d^2 m_2 r_2^2 m_3 l_3^6 - 2l_1^2 d^2 m_2 r_2^2 m_3 l_3^2 l_2^4 + \\
& 2l_1^2 d^2 I_{xx2} m_3 l_3^2 l_2^4 + 2l_1^2 d^2 I_{xx3} m_3 l_2^2 l_3^4 + 4l_1^2 d^4 m_2^2 l_3^4 r_2^2 \epsilon \Delta - 4l_1^2 d^4 I_{xx2} m_3 l_3^4 \epsilon \Delta - \\
& 4l_1^2 d^4 m_2^2 l_3^2 r_2^2 l_2^2 \epsilon \Delta - 4l_1^2 d^4 I_{yy3} m_3 l_2^4 \epsilon \Delta + 4l_1^2 d^4 I_{yy3} m_3 l_2^2 l_3^2 \epsilon \Delta + \\
& 4l_1^2 d^4 I_{yy2} m_3 l_3^4 \epsilon \Delta + 4l_1^2 d^4 m_2 r_2^2 m_3 l_3^4 \epsilon \Delta - 4l_1^2 d^4 I_{yy2} m_3 l_3^2 l_2^2 \epsilon \Delta + \\
& 4l_1^2 d^4 I_{xx2} m_3 l_3^2 l_2^2 \epsilon \Delta - 4l_1^2 d^4 m_2 r_2^2 m_3 l_3^2 l_2^2 \epsilon \Delta - 2l_1^2 d^2 m_2^2 l_3^6 r_2^2 - \\
& 2l_1^2 d^2 I_{yy2} m_3 l_3^6 + 2l_1^2 d^2 I_{xx2} m_3 l_3^6 - 2l_1^2 d^2 I_{yy3} m_3 l_2^6 + 2l_1^2 d^2 I_{xx3} m_3 l_2^6 + \\
& 4l_1^2 d^2 I_{yy2} m_3 l_3^4 l_2^2 - 4l_1^2 d^4 I_{xx3} m_3 l_2^2 l_3^2 \epsilon \Delta + 4l_1^2 d^4 I_{xx3} m_3 l_2^4 \epsilon \Delta + \\
& 2d^4 I_{xx3} m_3 l_2^2 l_3^2 + d^4 m_2 r_2^2 m_3 l_3^2 l_2^4 + 4d^8 I_{yy3} m_3 l_2^2 \epsilon^2 \Delta^2 + d^4 I_{yy3} m_3 l_2^2 l_3^4 + \\
& 4d^8 m_2 r_2^2 m_3 l_3^2 \epsilon^2 \Delta^2 + 4d^8 m_2^2 l_3^2 r_2^2 \epsilon^2 \Delta^2 + d^4 m_2^2 l_3^2 r_2^2 l_2^4 - d^4 I_{xx2} m_3 l_3^2 l_2^4 - \\
& 4d^6 m_2 r_2^2 m_3 l_3^4 \epsilon \Delta - 2d^4 I_{yy3} m_3 l_2^4 l_3^2 + d^4 I_{yy3} m_3 l_2^6 + d^4 m_2^2 l_3^6 r_2^2 - d^4 I_{xx2} m_3 l_3^6 - \\
& d^4 I_{xx3} m_3 l_2^6 + d^4 I_{yy2} m_3 l_3^6 + 4l_1^2 d^2 m_2^2 l_3^4 r_2^2 l_2^2 - 4l_1^2 d^2 I_{xx2} m_3 l_3^4 l_2^2 + \\
& 4l_1^2 d^2 I_{yy3} m_3 l_2^4 l_3^2 + 4l_1^2 d^2 m_2 r_2^2 m_3 l_3^4 l_2^2 + 4d^6 I_{yy3} m_3 l_2^4 \epsilon \Delta - \\
& 4d^6 I_{yy3} m_3 l_2^2 l_3^2 \epsilon \Delta - 2d^4 m_2 r_2^2 m_3 l_3^4 l_2^2 - 4d^8 I_{xx2} m_3 l_3^2 \epsilon^2 \Delta^2 + \\
& d^4 I_{yy2} m_3 l_3^4 l_2^2 - d^4 I_{xx3} m_3 l_2^2 l_3^4 - 4d^8 I_{xx3} m_3 l_2^2 \epsilon^2 \Delta^2 + 4d^8 I_{yy2} m_3 l_3^2 \epsilon^2 \Delta^2 + \\
& d^4 m_2 r_2^2 m_3 l_3^6 - 2d^4 m_2^2 l_3^4 r_2^2 l_2^2 - 4d^6 m_2^2 l_3^4 r_2^2 \epsilon \Delta + 4d^6 m_2^2 l_3^2 r_2^2 l_2^2 \epsilon \Delta - \\
& 4d^6 I_{xx2} m_3 l_3^2 l_2^2 \epsilon \Delta + 4d^6 I_{xx2} m_3 l_3^4 \epsilon \Delta + 2d^4 I_{xx2} m_3 l_3^4 l_2^2 + 4d^6 I_{yy2} m_3 l_3^2 l_2^2 \epsilon \Delta - \\
& 4d^6 I_{yy2} m_3 l_3^4 \epsilon \Delta + 4d^6 m_2 r_2^2 m_3 l_3^2 l_2^2 \epsilon \Delta - 4l_1^2 d^2 I_{xx3} m_3 l_2^4 l_3^2 - \\
& 4d^6 I_{xx3} m_3 l_2^4 \epsilon \Delta)/(16 d^2 l_3^2 m_3 l_2^2)
\end{aligned}
$$

$$
\begin{aligned}
A_1 \;=\; & -(-I_{yy3} m_3 l_2^6 d^2 - 2I_{yy2} m_3 l_3^4 l_1^2 l_2^2 - 2d^4 m_2 r_2 l_2 m_3 l_3^4 + 2d^4 m_2 r_2 l_2^3 m_3 l_3^2 - m_2^2 l_3^6 r_2^2 d^2 + \\
& I_{xx2} m_3 l_3^6 d^2 + I_{xx3} m_3 l_2^6 d^2 - I_{yy2} m_3 l_3^6 d^2 + m_2^2 l_3^6 r_2^2 l_1^2 + I_{yy2} m_3 l_3^6 l_1^2 - I_{xx2} m_3 l_3^6 l_1^2 + \\
& I_{yy3} m_3 l_2^6 l_1^2 - I_{xx3} m_3 l_2^6 l_1^2 + I_{yy3} m_3 l_2^4 d^4 - m_2^2 l_3^4 r_2^2 d^4 - m_2^2 l_3^4 r_2^2 l_1^4 - I_{xx2} m_3 l_3^4 d^4 - \\
& I_{xx3} m_3 l_2^4 d^4 + I_{yy2} m_3 l_3^4 d^4 + I_{yy3} m_3 l_2^4 l_1^4 - I_{xx3} m_3 l_2^4 l_1^4 - I_{xx2} m_3 l_3^4 l_1^4 + I_{yy2} m_3 l_3^4 l_1^4 - \\
& m_2 r_2^2 m_3 l_3^2 d^2 l_2^4 - m_2 r_2^2 m_3 l_3^6 d^2 - I_{yy3} m_3 l_2^2 d^2 l_3^4 - m_2^2 l_3^2 r_2^2 d^2 l_2^4 + I_{xx2} m_3 l_3^2 d^2 l_2^4 - \\
& I_{yy2} m_3 l_3^2 d^2 l_2^4 + I_{xx3} m_3 l_2^2 d^2 l_3^4 + m_2^2 l_3^2 r_2^2 l_1^2 l_2^4 + I_{yy3} m_3 l_2^2 l_1^2 l_3^4 + I_{yy2} m_3 l_3^2 l_1^2 l_2^4 + \\
& m_2 r_2^2 m_3 l_3^6 l_1^2 + m_2 r_2^2 m_3 l_3^2 l_1^2 l_2^4 - I_{xx2} m_3 l_3^2 l_1^2 l_2^4 - I_{xx3} m_3 l_2^2 l_1^2 l_3^4 + 4m_2 r_2 l_2 m_3 l_3^4 l_1^2 d^2 + \\
& 2m_2 r_2 l_2^3 m_3 l_3^2 l_1^4 - 2m_2 r_2^2 m_3 l_3^2 d^4 l_2^2 \epsilon \Delta + 2m_2 r_2^2 m_3 l_3^4 d^4 \epsilon \Delta + m_2 r_2^2 m_3 l_3^4 d^4 - \\
& m_2 r_2^2 m_3 l_3^2 d^4 l_2^2 - 2m_2 r_2^2 m_3 l_3^4 l_1^4 d^2 + 4m_2 r_2 l_2 m_3 l_3^2 \epsilon \Delta d^6 - 4m_2 r_2 l_2^3 m_3 l_3^2 l_1^2 d^2 - \\
& 4m_2 r_2 l_2 m_3 l_3^2 \epsilon \Delta d^4 l_1^2 - 2m_2 r_2 l_2 m_3 l_3^4 l_1^4 - 2I_{yy3} m_3 l_2^4 l_1^2 d^2 + 2I_{yy3} m_3 l_2^4 d^2 l_3^2 - \\
& I_{yy3} m_3 l_2^2 d^4 l_3^2 + 2I_{yy3} m_3 l_2^2 l_1^2 l_3^2 d^2 + 2I_{yy3} m_3 l_2^2 \epsilon \Delta d^6 - 2I_{yy3} m_3 l_2^4 d^4 \epsilon \Delta + \\
& 2I_{yy3} m_3 l_2^2 d^4 l_3^2 \epsilon \Delta - 2I_{yy3} m_3 l_2^2 \epsilon \Delta d^4 l_1^2 - 2m_2 r_2^2 m_3 l_3^2 \epsilon \Delta d^6 +
\end{aligned}
$$

$$2m_2 r_2^2 m_3 l_3^2 l_1^2 l_2^2 d^2 + 2m_2 r_2^2 m_3 l_3^4 d^2 l_2^2 + 2m_2 r_2^2 m_3 l_3^2 \epsilon \Delta d^4 l_1^2 - m_2 r_2^2 m_3 l_2^2 l_3^2 l_1^4 -$$
$$I_{yy3} m_3 l_2^2 l_3^2 l_1^4 - I_{yy2} m_3 l_2^2 l_3^2 l_1^4 + 2I_{yy2} m_3 l_2^2 l_3^2 d^2 l_1^2 - I_{yy2} m_3 l_2^2 l_3^2 d^4 +$$
$$2m_2^2 l_3^2 r_2^2 \epsilon \Delta d^6 - 2m_2^2 l_3^2 r_2^2 l_1^2 l_2^2 d^2 + 2m_2^2 l_3^4 r_2^2 d^2 l_2^2 + 2m_2^2 l_3^4 r_2^2 d^4 \epsilon \Delta +$$
$$m_2^2 l_3^2 r_2^2 d^4 l_2^2 + 2m_2^2 l_3^4 r_2^2 l_1^2 d^2 - 2m_2^2 l_3^2 r_2^2 d^4 l_2^2 \epsilon \Delta - 2m_2^2 l_3^2 r_2^2 \epsilon \Delta d^4 l_1^2 +$$
$$2I_{xx2} m_3 l_3^2 d^4 l_2^2 \epsilon \Delta - 2I_{xx2} m_3 l_3^4 d^4 \epsilon \Delta + I_{xx2} m_3 l_3^2 d^4 l_2^2 + 2I_{xx2} m_3 l_3^4 l_1^2 d^2 +$$
$$2I_{xx2} m_3 l_3^2 \epsilon \Delta d^6 - 2I_{xx2} m_3 l_3^2 l_1^2 l_2^2 d^2 - 2I_{xx2} m_3 l_3^4 d^2 l_2^2 - 2I_{yy2} m_3 l_3^2 d^4 l_2^2 \epsilon \Delta -$$
$$2I_{yy2} m_3 l_3^4 d^4 \epsilon \Delta - 2I_{yy2} m_3 l_3^4 l_1^2 d^2 + 2I_{yy2} m_3 l_3^2 \epsilon \Delta d^4 l_1^2 - 2I_{xx3} m_3 l_2^2 \epsilon \Delta d^6 +$$
$$2I_{xx3} m_3 l_2^4 l_1^2 d^2 - 2I_{xx3} m_3 l_2^4 d^2 l_3^2 + 2I_{xx3} m_3 l_2^2 \epsilon \Delta d^4 l_1^2 + 2I_{xx3} m_3 l_2^4 d^4 \epsilon \Delta -$$
$$2I_{xx3} m_3 l_2^2 d^4 l_3^2 \epsilon \Delta + I_{xx3} m_3 l_2^2 d^4 l_3^2 - 2I_{xx3} m_3 l_2^2 l_1^2 l_3^2 d^2 - 2I_{yy2} m_3 l_3^2 \epsilon \Delta d^6 +$$
$$2I_{yy2} m_3 l_3^4 d^2 l_2^2 - 2I_{xx2} m_3 l_3^2 \epsilon \Delta d^4 l_1^2 + m_2 r_2^2 m_3 l_3^4 l_1^4 + 2I_{xx3} m_3 l_3^4 l_1^2 l_2^2 +$$
$$I_{xx2} m_3 l_3^2 l_1^4 l_2^2 - 2m_2^2 l_3^4 r_2^2 l_1^2 l_2^2 + 2I_{xx2} m_3 l_3^4 l_1^2 l_2^2 + m_2^2 l_3^2 r_2^2 l_1^4 l_2^2 -$$
$$2I_{yy3} m_3 l_2^4 l_1^2 l_3^2 - 2m_2 r_2^2 m_3 l_3^4 l_1^2 l_2^2 + I_{xx3} m_3 l_2^2 l_1^4 l_3^2)/(8d^2 l_3^2 m_3 l_2^2)$$

$$A_2 = (4m_2 r_2 l_2 m_3 l_3^4 d^2 - 4m_2 r_2 l_3^3 m_3 l_3^2 d^2 - 2I_{xx2} m_3 l_3^4 l_2^2 + 16I_{yy1} m_3 l_2^2 l_3^2 d^2 + 2m_2^2 l_3^4 r_2^2 l_2^2 -$$
$$4m_2^2 l_3^2 r_2^2 d^4 - 4m_2 r_2^2 m_3 l_3^2 d^4 + 10I_{yy2} m_3 l_2^2 l_3^2 d^2 + 2I_{yy2} m_3 l_2^2 l_3^2 l_1^2 + 8m_2 r_2 l_2 m_3 l_3^2 \epsilon \Delta d^4 -$$
$$2I_{yy3} m_3 l_2^4 l_1^2 - 2m_2 r_2^2 m_3 l_3^4 l_1^2 - 4m_2 r_2^2 m_3 l_3^2 \epsilon \Delta d^4 - 4I_{yy2} m_3 l_3^2 \epsilon \Delta d^4 -$$
$$I_{yy2} m_3 l_3^2 l_2^4 - 2I_{yy2} m_3 l_3^4 l_1^2 + 4I_{xx2} m_3 l_3^2 d^4 + 16m_2 l_1^2 m_3 l_2^2 l_3^2 d^2 + 2m_2 r_2^2 m_3 l_3^2 l_1^2 l_2^2 +$$
$$I_{xx2} m_3 l_3^6 + 6I_{xx2} m_3 l_3^2 d^2 l_2^2 + I_{xx2} m_3 l_3^2 l_2^4 - m_2^2 l_3^6 r_2^2 + 6m_2^2 l_3^2 r_2^2 d^2 l_2^2 + 10m_2^2 l_3^4 r_2^2 d^2 +$$
$$6I_{xx3} m_3 l_2^2 d^2 l_3^2 + 4m_2 r_2 l_2 m_3 l_3^4 l_1^2 + I_{xx3} m_3 l_2^6 - m_2^2 l_3^4 r_2^2 l_2^2 + 2m_2^2 l_3^4 r_2^2 l_1^2 - 6I_{xx3} m_3 l_2^4 d^2 +$$
$$2I_{yy3} m_3 l_2^2 l_1^2 l_3^2 + 10m_2 r_2^2 m_3 l_3^2 d^2 l_2^2 + 2m_2 r_2^2 m_3 l_3^4 l_2^2 + 4I_{yy3} m_3 l_2^2 \epsilon \Delta d^4 +$$
$$2I_{yy3} m_3 l_3^4 l_3^2 + 4m_2^2 l_3^2 r_2^2 \epsilon \Delta d^4 - 4I_{yy3} m_3 l_2^2 d^4 - I_{yy3} m_3 l_2^2 l_3^4 + 6I_{yy3} m_3 l_2^4 d^2 +$$
$$10I_{yy3} m_3 l_2^2 d^2 l_3^2 + 6m_2 r_2^2 m_3 l_3^4 d^2 - I_{yy3} m_3 l_2^6 - I_{yy2} m_3 l_3^6 + 4I_{xx3} m_3 l_2^2 d^4 + 6I_{yy2} m_3 l_3^4 d^2 +$$
$$16m_1 r_1^2 m_3 l_2^2 l_3^2 d^2 + 2I_{yy2} m_3 l_3^2 l_2^4 - 6I_{xx2} m_3 l_3^4 d^2 - 2I_{xx2} m_3 l_3^2 l_1^2 l_2^2 - 4m_2 r_2 l_2^3 m_3 l_3^2 l_1^2 +$$
$$2I_{xx2} m_3 l_3^4 l_1^2 - 2I_{xx3} m_3 l_2^2 l_1^2 l_3^2 - 4I_{yy2} m_3 l_3^2 d^4 + I_{xx3} m_3 l_2^2 l_3^4 - m_2 r_2^2 m_3 l_3^6 -$$
$$2m_2^2 l_3^2 r_2^2 l_1^2 l_2^2 - 2I_{xx3} m_3 l_2^4 l_3^2 + 4I_{xx2} m_3 l_3^2 \epsilon \Delta d^4 - 4I_{xx3} m_3 l_2^2 \epsilon \Delta d^4 -$$
$$m_2 r_2^2 m_3 l_3^2 l_2^2 - 16m_2 r_2 l_2 m_3 l_3^2 d^2 l_1^2 + 2I_{xx3} m_3 l_2^4 l_1^2)/(16d^2 l_3^2 m_3 l_2^2)$$

$$A_3 = l_1(2m_2 r_2^2 m_3 l_3^2 d^2 + 2m_2^2 l_3^2 r_2^2 d^2 + I_{yy2} m_3 l_2^2 l_3^2 - I_{yy3} m_3 l_2^4 - m_2 r_2^2 m_3 l_3^4 - 2I_{xx3} m_3 l_2^2 d^2 -$$
$$I_{yy2} m_3 l_3^4 + m_2 r_2^2 m_3 l_3^2 l_2^2 - 2I_{xx2} m_3 l_3^2 d^2 + 2m_2 r_2 l_2 m_3 l_3^4 + 2I_{yy2} m_3 l_3^2 d^2 + m_2^2 l_3^4 r_2^2 +$$
$$I_{yy3} m_3 l_2^2 l_3^2 + 2I_{yy3} m_3 l_2^2 d^2 - I_{xx2} m_3 l_3^2 l_2^2 - 2m_2 r_2 l_2^3 m_3 l_3^2 + I_{xx2} m_3 l_3^4 - I_{xx3} m_3 l_2^2 l_3^2 -$$
$$m_2^2 l_3^2 r_2^2 l_2^2 + I_{xx3} m_3 l_2^4)/(4d l_3^2 m_3 l_2^2)$$

$$A_4 = -(4m_1 r_1^2 m_3 l_2^2 l_3^2 + 4I_{yy1} m_3 l_2^2 l_3^2 + 4m_2 l_1^2 m_3 l_2^2 l_3^2 - 4m_2 r_2 l_2 m_3 l_3^2 l_1^2 + m_2 r_2^2 m_3 l_3^2 l_1^2 +$$
$$m_2^2 l_3^2 r_2^2 l_1^2 + I_{yy3} m_3 l_2^2 l_1^2 - 4I_{xx1} m_3 l_2^2 l_3^2 + I_{yy2} m_3 l_3^2 l_1^2 - I_{xx3} m_3 l_2^2 l_1^2 -$$
$$I_{xx2} m_3 l_3^2 l_1^2)/(4l_3^2 m_3 l_2^2)$$

Appendix D

Relationship between I_{xx}, I_{yy} and I_{zz}

The moments of inertia relative to any three coordinate axes for any rigid body can be written as (Bedford and Fowler, 1996)

$$
\begin{aligned}
I_{xx} &= \int (y^2 + z^2)\, dm \\
I_{yy} &= \int (x^2 + z^2)\, dm \\
I_{zz} &= \int (x^2 + y^2)\, dm
\end{aligned}
$$

where x, y and z are the coordinates of a differential mass dm of the body in the three-dimensional frame.

Clearly, the difference between any two moments of inertia must be smaller than or equal to the third one.